1

Foundations and Process Engineering

Freeze-drying or lyophilization is a drying process in which the solvent and/or the suspension medium is crystallized at low temperatures and thereafter sublimed from the solid state directly into the vapor phase.

Freeze-drying is mostly done with water as solvent. Figure 1.1 shows the phase diagram of water and the area in which this transfer from solid to vapor is possible.

Table 1.1 shows the relation of temperature (°C), mTorr, and mbar.

This step is relatively straightforward for pure water. If the product contains two or more components in true solutions or suspensions, the situation can become so complicated that simplified model substances have to be used to make the process more understandable. Such complex systems occur ubiquitously in biological substances.

The drying transforms the ice or water in an amorphous phase into vapor. Owing to the low vapor pressure of the ice, the vapor volumes become large, as can be seen in Figure 1.2. During the second step of the drying, the water adsorbed on the solids is desorbed.

The goal of freeze-drying is to produce a substance with good shelf stability and which is unchanged after reconstitution with water, although this depends also very much on the last step of the process: the packing and conditions of storage.

The advantages of freeze-drying can be summarized as follows:

- The drying at low temperatures reduces degradation of heat-sensitive products.
- The liquid product can be accurately dosed.
- The moisture content of the final product can be controlled during the process.
- The dry product can have an appealing physical form.
- The dry product with a high specific surface area is rapidly reconstituted.

The disadvantages are as follows:

- The high investment, operating and maintenance costs.
- The complexity of the process and the equipment requires a team of skilled and permanently trained collaborators.

COPYRIGHTED MATERIAL

Freeze-Drying, Third Edition. Peter Haseley and Georg-Wilhelm Oetjen.
© 2018 Wiley-VCH Verlag GmbH & Co. KGaA. Published 2018 by Wiley-VCH Verlag GmbH & Co. KGaA.

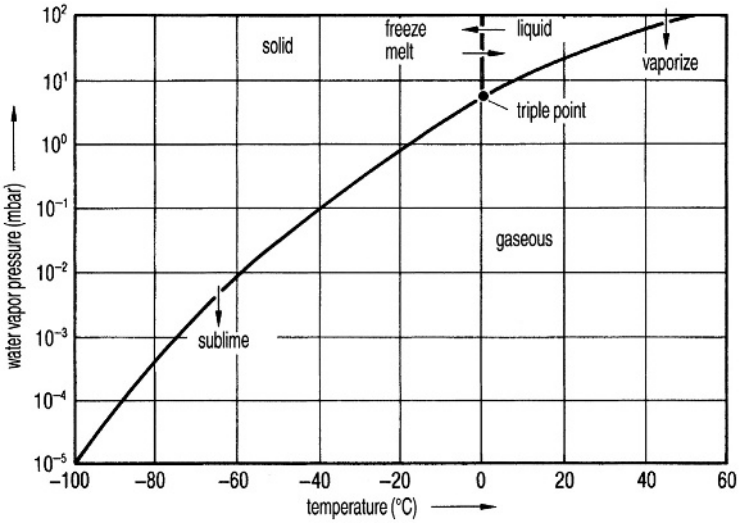

Figure 1.1 Phase diagram of water.

1.1 Freezing

To freeze a substance, it must be cooled to a temperature at which the water and the solids are fully crystallized or at which areas of crystallized ice and solids are enclosed in zones in which amorphous concentrated solids and water remain in a mechanically solid state (see Section 1.1.2). In the zone of freezing, the ice crystals first grow, thus concentrating the remaining solution, which can vary the pH value. In many substances an eutectic temperature can be determined, but in many others this value does not exist. The crystallization depends on several

Table 1.1 Vapor pressure of water.

Temperature (°C)	mTorr	mbar	Temperature (°C)	mTorr	mbar
0	4579	6.108	−40	96.6	0.1238
−4	3280	4.372	−44	60.9	0.0809
−8	2326	3.097	−48	37.8	0.0502
−12	1832	2.172	−52	23.0	0.0300
−16	1132	1.506	−56	13.8	0.0183
−20	930	1.032	−60	8.0	0.0107
−24	526	0.6985	−64	4.6	0.0061
−28	351	0.4669	−68	2.8	0.0034
−32	231	0.3079	−72	1.4	0.0018
−36	150	0.2020			

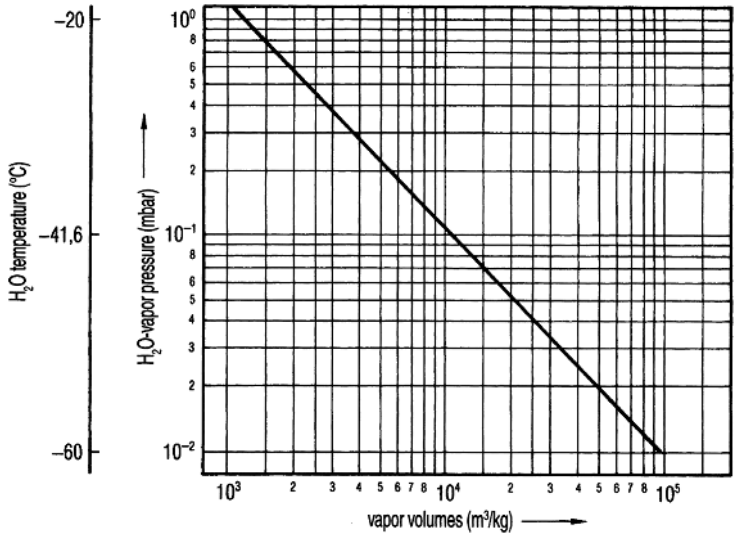

Figure 1.2 Specific volume of water vapor as a function of the water vapor pressure. The temperature of the vapor in this diagram is that of ice.

factors that influence each other: cooling rate, initial concentration, end temperature of cooling, and the time at this temperature. In several products, no crystallization takes place and the product remains in an amorphous, glass-like phase or a mixture of both occurs.

1.1.1 Amount of Heat, Heat Conductivity, Heat Transfer, and Cooling Rate

For pure water, the melting heat to be withdrawn for freezing (Q_{tot}) can be calculated by Eq. (1.1), if the starting and the desired final temperatures are known:

$$Q_{tot} = c_w(T_1 - T_0) + Q_e + c_e(T_0 - T_2) \quad \text{(kJ/kg)} \tag{1.1}$$

where

c_w = specific heat capacity of water;
Q_e = melting heat of ice;
c_e = specific heat capacity of ice;
T_0 = freezing temperature of ice;
T_1 = initial temperature of water;
T_2 = final temperature of ice.

The temperature dependences of c_w between +20 and 0 °C and c_e between 0 and −50 °C have to be adopted as average values.

For solutions and suspensions, the solid content has to be recognized. This is reflected in Eq. (1.2):

$$Q_{tot} = [(c_w x_w + c_{f'} x_f)(T_1 - T_0)] + x_w Q_e + [(c_e x_w + c_f x_{w'})(T_0 - T_2)] \tag{1.2}$$

where

x_w = part of water above 0 °C;
c_f = specific heat of solids, for example:
for animal products ≈ 1.47 kJ/kg °C
for plant products ≈ 1.34 kJ/kg °C
for some solids:
carbohydrates ≈ 1.42 kJ/kg °C
proteins ≈ 1.55 kJ/kg °C
fats ≈ 1.7 kJ/kg °C
salts ≈ 0.8 kJ/kg °C;
x_f = part of solids;
$x_{w'}$ = part of ice, which freezes until temperature T_2 is reached. If not all water is frozen at T_2, an additional term has to be introduced, which reflects the cooling of the unfrozen water.

Table 1.2 shows the unfreezable water (UFW) in various foods. The reasons and the consequences are described in Sections 1.1.3 and 1.1.4. In comparing these data with other publications, for example, Ref. [1], smaller values may be found. This can depend not only on the different raw materials and the history of the probe until measurement but also on the methods of measurement.

For meat with less than 4% fat content, Riedel [2] has published an enthalpy diagram (shown in Figure 1.3). For some other foods, Table 1.3 shows enthalpy data at various temperatures. At −40 °C the enthalpy is set at 0 kJ/kg.

Table 1.2 Percentage of water frozen out at various temperatures for some foods.

Product	Frozen out water at °C (% of the total water)				UFW (% of total water)
	– 10	– 15	– 20	– 30	
Lean beef	82	85	87	88	12
Haddock	84	87	89	91	9
Whole eggs, liquid	89	91	92	93	7
Yolk	85	86	87	87	13
Egg white	91	93	94		6
Yeast	80	85	88	89	11
Fruit juice	85	90	93	96	(3)
Peas	80	86	89	92	(7)

Part of Table 1.1 in Refs [2,3].

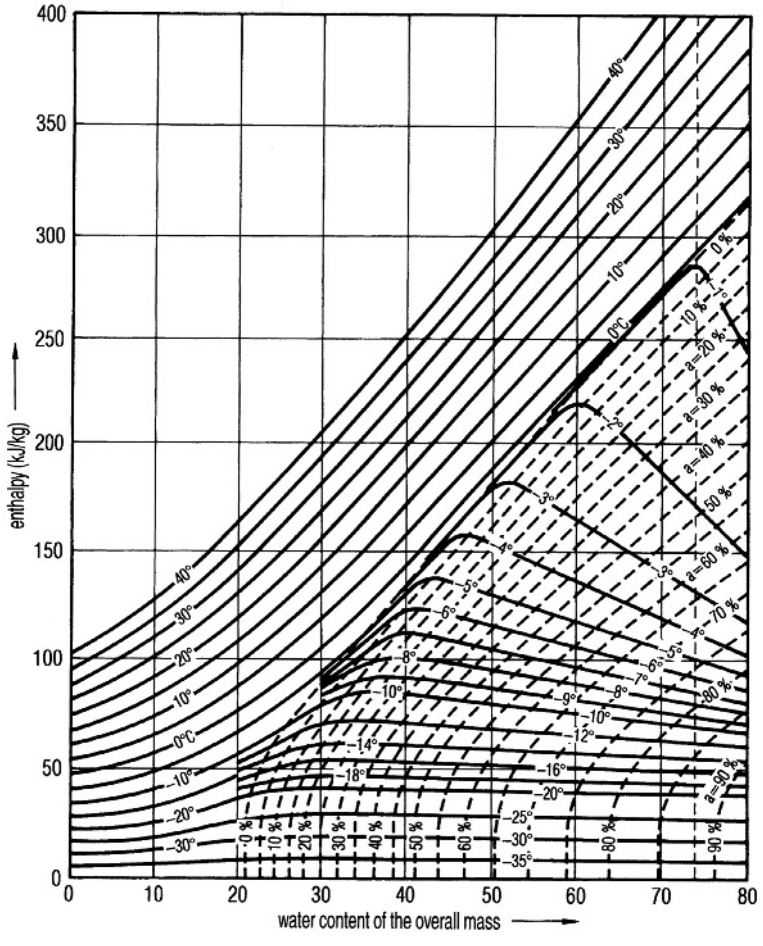

Figure 1.3 Enthalpy of lean beef meat as a function of its water content (0 kJ/kg at −40 °C). The temperatures at the beginning of cooling and the desired end temperatures for freezing are plotted as parameters. The dotted lines indicate the percentage of water frozen at the end temperatures (see also Figure 1 from Refs [2,3]). *Example*: Beef meat has 74% water. At +10 °C, the enthalpy is ~325 kJ/kg; at −20 °C, the enthalpy is ~40 kJ/kg; therefore, 285 kJ/kg have to be removed and 83% of the water frozen. The maximum possible (88%) (see Table 1.1) is reached at ≃30 °C.

In Table 1.4 the UFW data for products used in pharmaceuticals are listed in Ref. [6] of Chapter 3.

The transport of the calculated energy from the freezing zone of the product to the cooling medium can be described in a simplified way by the following steps: the product is an infinite plate, which is cooled from one site only, and the energy flows only perpendicular to its infinite expansion. The crystallization energy flows from the crystallization zone, through the already frozen ice, through the container bottom to a shelf, and finally into the cooling brine.

Table 1.3 Enthalpy of meat, fish, and egg products.

Product	Water content (weight %)	Enthalpy (kJ/kg) at a temperature of °C					
		−30	−20	−10	0	+5	+20
Beef, 8% fat	74.0	19.2	41.5	72.4	298.5	314.8	368.4
Cod	80.3	20.1	41.9	74.1	322.8	341.2	381.0
Egg white	86.5	18.4	38.5	64.5	351.3	370.5	427.1
Whole egg	74.0	18.4	38.9	66.2	308.1	328.2	386.9

Part of Table 1.3 in Refs [2,3].

The freezing time (t_e) is approximately given by Eq. (1.3) [4]:

$$t_e = \Delta J / \Delta T \rho_g (d^2/2\lambda_g + d/K_{su}) \tag{1.3}$$

$$t_e = \Delta J / \Delta T \rho_g (w + u) \tag{1.3a}$$

where

t_e = freezing time;
ΔJ = enthalpy difference between the initial freezing point and the final temperature;
ΔT = difference of temperature between the freezing point and the cooling medium;
D = thickness of the product parallel to direction of prevailing heat transfer;
ρ_g = density of the frozen product;
λ_g = thermal conductivity of the frozen product;
K_{su} = surface heat transfer coefficient between cooling medium and the freezing zone.

Table 1.4 Percentage of unfrozen water (UFW) , which cannot be frozen by lower temperature (see Figure 1.20).

Excipient	UFW (%)
Trehalose	16.7
Sorbitol	18.7
Maltose	20
Glycerin	27
Glucose	29.1
Sucrose	35.9
Lactose	40.8
Glycerol	45.9
Fructose	49.0

The thermal conductivity of ice and of dried products are relatively well known, but the surface heat transfer coefficient K_{su} during freezing and the total heat transfer coefficient K_{tot} during freeze-drying vary largely, as described in the various chapters. Table 1.5 gives a survey of some data of interest in freeze-drying.

The influence of the variables in Eq. (1.3) can be studied by an example. A slice of lean beef with a thickness that is small compared with its horizontal dimensions is to be frozen to −20 °C. The influences of the border of the slice are neglected. The thickness of the slice is $d = 2$ cm. As can be seen in Figure 1.3, the enthalpy difference for beef with 74% water is approximately 240 kJ/kg. If the freezing process starts between 0 and −3 °C and is mostly finished at −20 °C, the cooling medium has a temperature of −43 °C and an average $\lambda = 1.38 \times 10^{-2}$ J/°C cm s is used when the slice is in contact with a liquid, having a similar behavior to water at 20 °C, $K_{su} = 4.61 \times 10^{-2}$ J/°C cm^2 s can be used for the calculation. The freezing time is

$$t^{fl}_{e\,d20} = 5.4(0.725 \times 10^2 + 0.43 \times 10^2) \approx 12\ \text{min} \tag{1.4}$$

As shown in Eqs. (1.3) and (1.3a), the thickness d has a major influence if the conductivity term w, which includes d^2, is large compared with the transfer term u, which includes only d.

Table 1.5 Surface heat transfer coefficient, total heat transfer coefficient, and thermal conductivity.

K_{su}	From gases to a solid surface (kJ/m^2 h °C): free convection	17–21
	Laminar flow 2 m/s	50
	Laminar flow 5 m/s	100
K_{su}	Between the shelf of a freeze-drying plant and a product in vials or trays during freezing (kJ/m^2 h °C)	200–400
K_{su}	Between a liquid and a solid surface (kJ/m^2 h °C): oil in tubes, laminar	160–250
	LN_2 by drops on the product[a)]	900
	From liquids similar to water[b)]	1600
	From water at 1 bar, temperature difference <7 °C[c)]	3600
K_{tot}	Between the shelf of a freeze-drying plant and the sublimation front in the product contained in vials or trays under vacuum[d)] (kJ/m^2 h °C)	60–130
λ	Thermal conductivity (kJ/m^2 h °C)	
λ_g	Frozen product (ice)[e)]	5.9–6.3
λ_{tr}	Dry product[f)]	0.059–0.29

a) Reinsert, A.P.: Factors affecting the erythrocyte during rapid freezing and thawing. *Ann. N. Y. Acad. Sci.* **85**, 576–594, 1960.
b) From Ref. [3].
c) From VDI- = Wärmeatlas 5. Auflage, Bild 38, P. A 26, VDI-Verlag, Düsseldorf, 1988.
d) Figures 1.116 and 1.117.
e) From Ref. [3].
f) From Refs [5–8].

In Eq. (1.4), $w{:}u = 1.7{:}1$, showing that the influence of the conductivity is almost double that of the transfer. Assuming that d is only 0.2 cm, the freezing time falls to

$$t^{\mathrm{fl}}_{\mathrm{e\,d2}} = 5.4(0.725 + 4.35) \approx 28\ \mathrm{s} \tag{1.5}$$

In this case, $w{:}u = 1{:}6$ and the transfer term is overwhelming. The freezing time is neither reduced by d^2 nor by d, since the importance of w and u has changed. An increase in d by a factor of 3, to 6 cm, prolongs the freezing time:

$$t^{\mathrm{fl}}_{\mathrm{e\,d60}} \approx 70\ \mathrm{min} \tag{1.6}$$

Here $w{:}u = 5{:}1$, and the freezing time depends mostly on the heat conductivity of the material.

The freezing of a slice of beef in direct contact with a model liquid has been used to demonstrate the influence of the two terms w and u. To freeze a product for freeze-drying, two methods are mainly used: (i) freezing of the product in trays or in vials on cooled surfaces; or (ii) in a flow of cold air. If these methods do not result in a sufficient freezing rate, liquid nitrogen (LN_2) in direct contact with the vials is used (see Figures 2.2 and 2.3) or droplets of the product are sprayed into LN_2 (see Section 2.1.4).

The heat transfer coefficient K_{su} in air varies strongly with the gas velocity, surface conditions of the product, and the geometry of the installation. In practical operations, it will be difficult to achieve K_{su} values of $1.7–2.5 \times 10^{-3}$ J/cm^2 s °C or ~75 kJ/m^2 h °C and in many applications only half of this value (or less) may be possible. However, even with this high K_{su}, the above-discussed slice of beef (2 cm thick) has a freezing time

$$t^{\mathrm{lu}}_{\mathrm{e\,d20}} = 5.4(0.72 \times 10^2 + 9.5 \times 10^2) \approx 92\ \mathrm{min} \tag{1.7}$$

compared with 12 min when cooled by a liquid, since the K_{su} of a gas is ≤10% that of a liquid.

The time to reach a desired temperature level can be expressed as freezing rate v_{f}, the change in temperature per unit time, for example, °C/min. Thus, the results of Eqs. (1.4)–(1.7) are approximately as follows:

(4) $v_{\mathrm{f}} = 1.7$ °C/min (5) $v_{\mathrm{f}} = 43$ °C/min
(6) $v_{\mathrm{f}} = 0.3$ °C/min (7) $v_{\mathrm{f}} = 0.2$ °C/min

These data are calculated by using 0 °C as the start and −20 °C as the end temperature to show the relative data. The exact calculation requires more information, as given below.

Figure 1.4 is the cooling curve of vials filled with a solution of 4% solid content and 27 mm filling height. From the curve, v_{f} can be estimated:

0 to −10 °C	~0.15 °C/min
0 to −14° C	~0.18 °C/min
−14 to −30 °C	~0.73 °C/min
0 to −30 °C	~0.3 °C/min

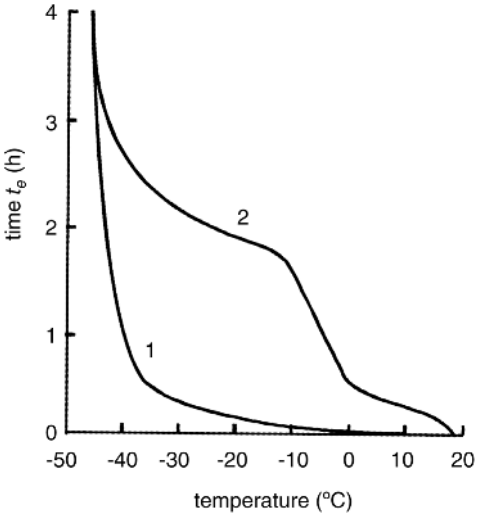

Figure 1.4 Temperatures during freezing as a function of time. 1, shelf temperature; 2, product temperatures in a product with $d = 2.7$ cm, solid content ~4%. (From Steris GmbH, 50354 Hürth, Germany.)

During the freezing of the main part of the water, v_T is only 25% compared with the value after most of the water is crystallized. Taking the average value between 0 and −30 °C can therefore be misleading: The intention to freeze at a rate of 0.3 °C/min has not occurred during an important part of the operation. The difference between 0.15 and 0.7 °C/min influences the structure of the product. How important the change is has to be checked from case to case, but the difference between 0.15 and 0.7 °C/min is most likely important.

With Eq. (1.3), it is also possible to estimate $K_{su.}$ The uncertainties are the differences between the freezing of the product around the temperature sensor and in the undisturbed product, the position of the sensors, the correlation between time and temperature, and occasionally also the actual amount of frozen water. From Figure 1.4, the estimated K_{su} is approximately 480 kJ/m^2 h °C with a possible error of ±10% and maximum error of ±20%. Such high values can only be expected if the vials are carefully selected for their uniformity, especially with respect to a very even and flat bottom. Otherwise, the K_{su} can be much smaller, for example, 230 kJ/m^2 h °C as calculated from data shown in Table 1.6.

If the vials are placed in trays and these are loaded on the shelves, K_{su} will be reduced, very likely to <100 kJ/m^2 h °C, with the consequence that the freezing time is twice or three times longer and freezing rates of 1 °C/min cannot be achieved.

Equation (1.3) can be used to estimate the influence of the variation of the layer thickness and the shelf temperature, if the K_{su} values are measured for the type of vials used.

As shown, for example, in Figures 1.5–1.7, the temperature as a function of time can vary. Therefore, the calculation of freezing rates and the resulting K_{su} contain a certain error. Table 1.7 shows a comparison of cooling rates [9]. Run 1 is from Figure 1.5, run 3 from Figure 1.6, and run 5 from Figure 1.7. The percentage indicates the maximum differences between the measurements with three temperature sensors in three vials.

Table 1.6 Cooling time and freezing rate as a function of layer thickness for well manufactured vials, not selected for the flatness of the bottom.

Layer (mm)	Time from 0 °C to – 10 °C (min)	Cooling rate (°C/min)	Time from – 10 °C to – 30 °C (min)[a)]	Cooling rate (°C/min)	Cooling rate from 0 °C to – 30 °C (°C/min)
6	14	0.71	9.3	2.1	1.29
12	32	0.31	12.9	1.6	0.67
20	60	0.17	19.0	1.1	0.38
30	105	0.095	28.3	0.7	0.23

a) In this time the cooling of the glass of the vials from 0 °C to −30 °C is included.

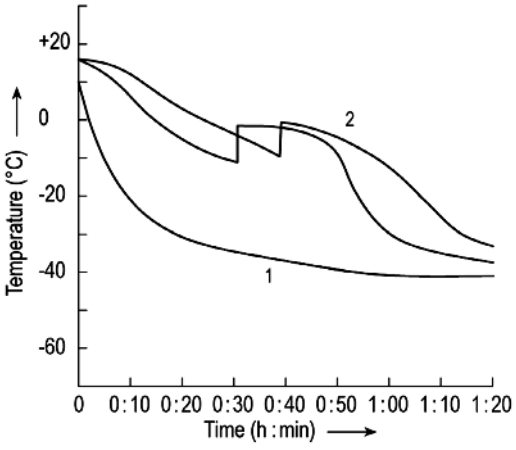

Figure 1.5 Temperatures during freezing as a function of time for two different runs in the same plant, with the same product, T_{sh} cooled as quickly as possible. 1, shelf temperature; 2, product temperature.

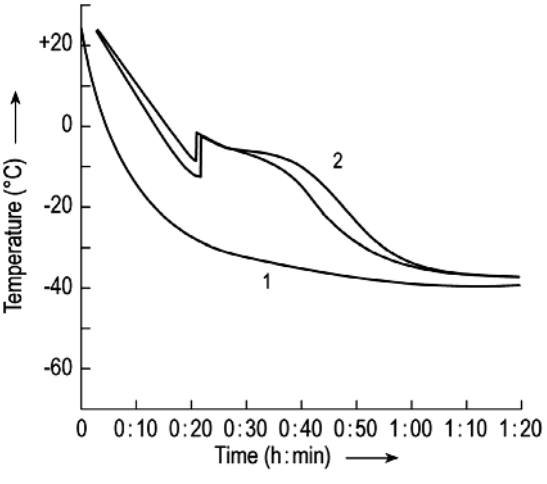

Figure 1.6 See Figure 1.5.

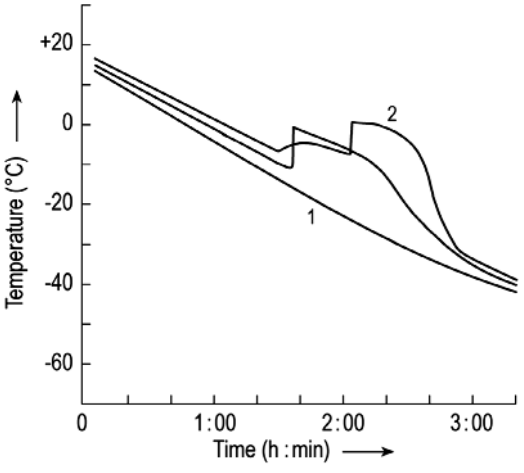

Figure 1.7 As Figure 1.5, but T_{sh} cooled controlled. (From Ref. [9].)

To increase v_t, the following possibilities can be used: (i) reducing d; (ii) reducing the shelf temperature; (iii) precooling of the vials, for example, to −80 °C, and filling the precooled product, for example, +4 °C, into the cold vials; (iv) cooling of the vials directly with LN_2; and (v) dropping the product into LN_2. With precooled vials, v_t can be on the order of 10–20 °C/min, and with direct cooling by LN_2 40–60 °C/min and more is possible. With droplet freezing, up to 1000 °C/min can be achieved.

For laboratory work, different cooling liquids can be used as shown in Table 1.8. However, these substances are not easy to use, they boil and are partially explosive. The cooling method shown in Figure 1.8 can be helpful. LN_2 is evaporated under vacuum, freezing part of the N_2 as a solid. In this mixture

Table 1.7 Comparison of cooling rates, measured in the same installation, with comparable vials and comparable d.

Run	Time from 0 °C to – 10 °C (min)	Cooling rate (°C/min)	Time from – 10 °C to – 30 °C (min)	Cooling rate (°C/min)
1	34 ± 5	0.29 ± 15%	13 ± 5	1.5 ± 38%
2	25	0.4	17	1.2
3	23 ± 1.5	0.4 ± 6%	15 ± 2	1.3 ± 13%
4[a)]	19 ± 2.5	0.5 ± 13%	21 ± 3.5	0.95 ± 17%
5[b)]	79 ± 7	0.13 ± 9%	38 ± 5	0.5 ± 13%

a) During the cooling phase −10 to −30 °C $\Delta T \approx 13$ °C instead of ≈ 20 °C in run 1–3; taking this into account, the value of 0.95 corresponds to 1.4 in run 1–3.

b) The shelf temperature was constantly lowered at ≈10 °C/30 min. Therefore, ΔT is only ≈ 8 °C during the freezing phase, compared with ≈ 30 °C in run 1–3. 0.13 °C/min therefore corresponds to ≈ 0.48 °C/min. The same applies to the 0.5 °C/min during the cooling phase, making it comparable to 1.3 °C/min.

Table 1.8 Physical data of cooling liquids.

Medium	Boiling point, T_s (°C)	c_p of liquid at T_s (kJ/kg °C)	λ of liquid at T_s (kJ/mh °C)	Heat of vaporization at T_s (kJ/kg)
Helium (He^4)	−268.9	4.41	0.098	20.5
Nitrogen	−195.8	2.05	0.506	197.6
Propane	−42.3	2.19		426.2
n-Pentane	+36.1	2.2		234.1
(Figure 2 from Umrath, W. Kurzbeitrag für die Tagung Raster-Elektronenmikroskopie in Medizin and Biologie, unpublished, Brühl.)				

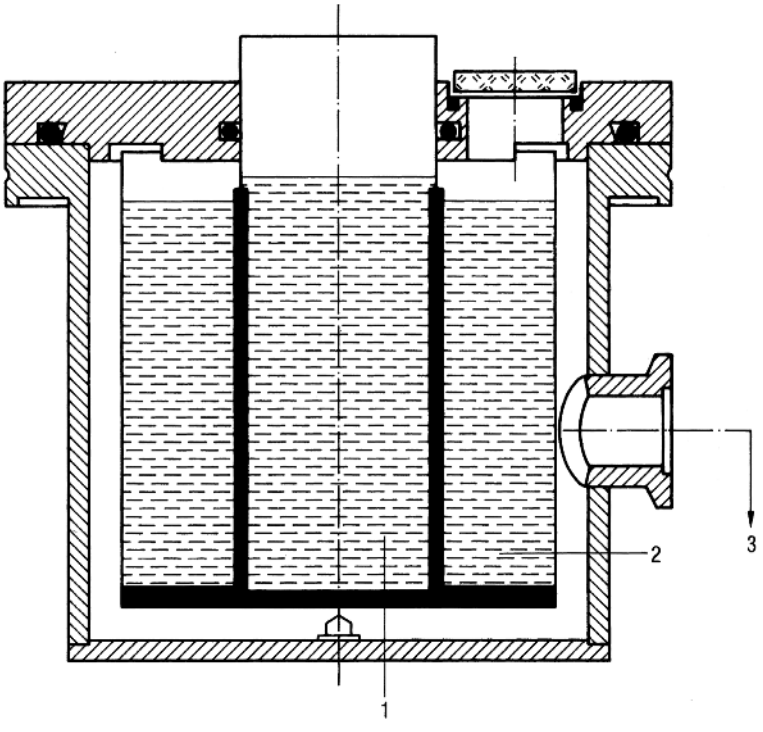

Figure 1.8 Apparatus to produce a mixture of liquid and solid nitrogen. 1, inner container with LN_2; 2, external container with LN_2 connected to a vacuum pump; 3, the container 2 is evacuated to ~124 mbar and kept at that pressure. The evaporating nitrogen reduces the temperature in 2 and thereby also in 1, since the two containers are in close thermal contact. A temperature of −210 °C is reached in container 1 after ~5 min. (From Umrath, 1974 [10]. Reproduced with permission of John Wiley & Sons.)

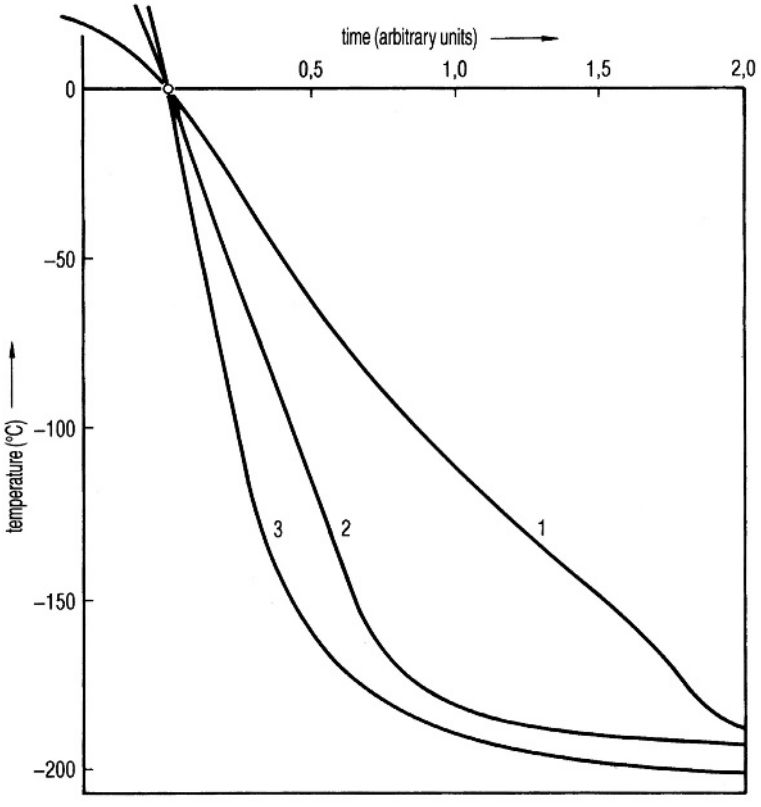

Figure 1.9 Relative cooling rate of a small sample in different forms of N_2. (The plot for LN_2 depends mostly on the successful removal of the nitrogen gas.) Melting solid nitrogen reduces the formation of gaseous N_2, since the crystallization energy melts the solid nitrogen and does not evaporate the liquid. (*Note*: Theoretically, cooling in solid N_2 would be the fastest method, but liquid N_2 will be formed and the heat transfer is not stable.) 1, LN_2; 2, LN_2 + solid N_2; 3, melting of solid N_2. (See also Umrath, W., unpublished results, Brühl.)

the solid melts, if energy is produced from cooling and crystallization. Thus, the formation of gaseous N_2 is greatly reduced, which otherwise limits the heat transfer. Figure 1.9 shows the relative cooling rates for different forms of N_2.

Riehle [11] has calculated the theoretically possible cooling velocities for small objects between 1 and 10^{-3} mm as shown in Figure 1.10. These calculations are made for a substance consisting of water only and K_{su} is assumed to be infinitely large for the geometric dimensions shown in (a) a sphere, (b) a square cylinder of infinite length, and (c) a plate of infinite length and the thickness X, cooled only from one side. For the plate (c), v_f is also calculated for three limited K_{su}: 10^3, 10^4, and 10^5 W/m^2 s (Chain lines). The purpose of this calculation is to show that freezing rates of 10^3–10^4 °C/s (6×10^4–6×10^5 °C/min) cannot be achieved. However, these rates are necessary to reduce the velocity of crystal growth in pure water sufficiently to obtain water in a glass-like phase with irregular particle size $<10^{-8}$ m.

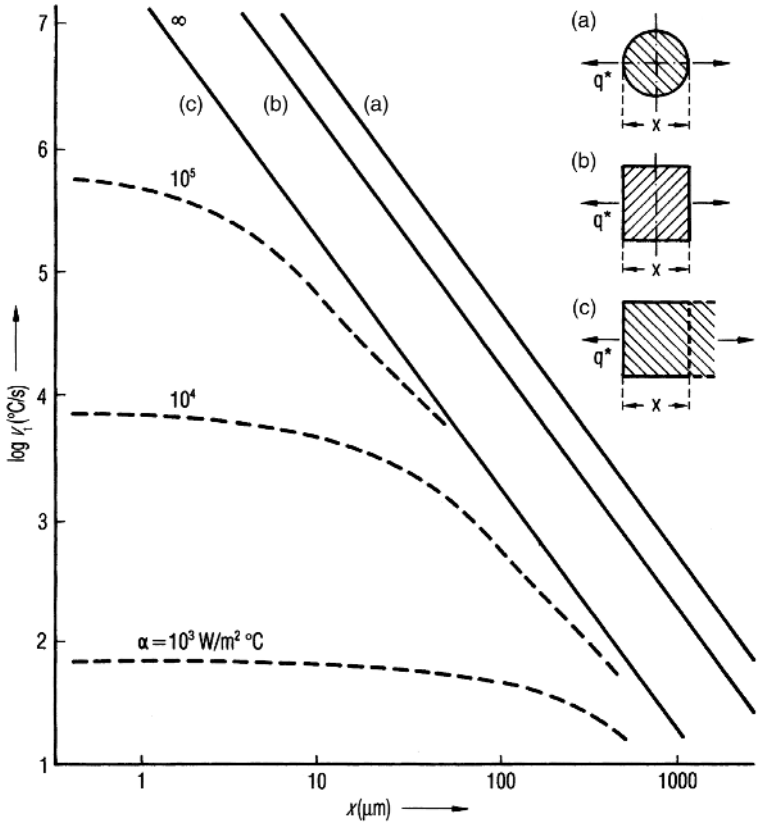

Figure 1.10 Maximum theoretical cooling rate for different geometric configurations (a–c) of water by cooling with LN_2, if α is assumed to be ∞. The dotted lines are calculated for three values: $\alpha = 10^3$, 10^4, 10^5 W/m^2 s. (From Riehle, 1986 [11]. Reproduced with permission of John Wiley & Sons.)

Riehle showed that such freezing rates can only be reached for layers of <0.1 mm under a pressure of 1.5–2.5 kbar.

A different way of obtaining short cooling and freezing times is to evaporate part of the water in the product under vacuum. The evaporation energy of water at 0 °C is approximately 2.5×10^3 kJ/kg. To cool 1 kg of beef from 0 to −20 °C, 240 kJ have to be removed, which corresponds to ~0.1 kg of water to be evaporated or 15% of the water in the beef. This quick evaporation will produce foam or bubbles in the product. This is unacceptable in most cases, since the original structure is changed and that part of the product that is vacuum dried will have different qualities to the freeze-dried part. Often the product frozen in this way cannot be freeze-dried at all.

1.1.2 Structure of Ice, Solutions, and Dispersions

The water molecule has a configuration as shown in Figure 1.11 [12], having a pronounced dipole moment, which produces the liquid phase at relatively high

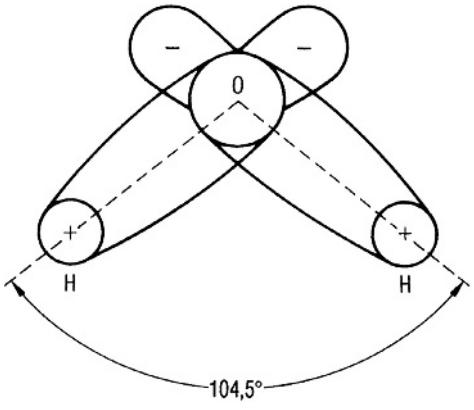

Figure 1.11 Configuration of the electrical charges in a water molecule. (From de Quervain, 1975 [12]. Reproduced with permission of Elsevier.)

temperatures and ensures a structure in the envelope of molecules that surrounds ions [13]. However, clusters are also in water without ions; these consist of approximately 10 water molecules in a tetrahedral geometry surrounded by O—H—O groups. The clusters are not stable units with always the same molecules and they are constantly exchanging molecules with their surroundings, having an average lifetime of between 10^{-10} and 10^{-1} s. The number of clusters decreases as the temperature is lowered until freezing occurs.

In water that is very well cleared of all foreign particles, the clusters begin to crystallize in the subcooled water at −39 °C; this is called homogeneous nucleation. Foreign, undissolved particles in water act as nuclei for the crystallization of ice and this is called heterogeneous nucleation. In normal water there exist approximately 10^6 particles per cm^3 and these act as nuclei for crystallization. They become increasingly effective if their structure is similar to that of water. If a nucleus has formed, it grows faster at the outside than at the inside, producing (depending on subcooling and cooling velocity) structures of ice stars (Figure 1.12). During further freezing, branches grow at an angle of 60°, well known as frost flowers. For a crystal of $1 \times 10^{-9}\,mm^3$, 2.7×10^{10} molecules have to be brought into position. It is difficult to visualize how such a crystal can be formed in a small fraction of a second, but it is obvious that the growth of such a crystal will be influenced or disturbed by many factors.

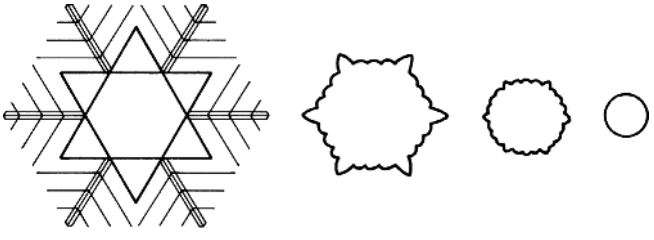

Figure 1.12 Growth of ice crystals in water. The subcooling is increased from left to right. (From de Quervain, 1975 [12]. Reproduced with permission of Elsevier.)

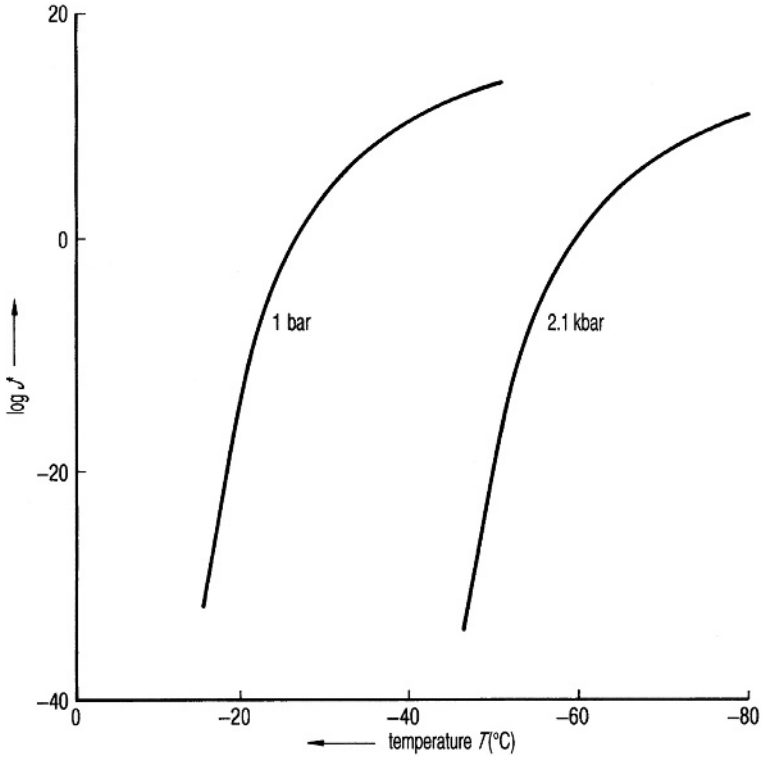

Figure 1.13 Nucleation rate J^* (nuclei/volume time) as a function of the temperature of the water–ice phase transformation. (From Riehle, 1986 [11]. Reproduced with permission of John Wiley & Sons.)

Figure 1.13 shows logJ^* (J^* = nuclei per unit time and volume) as a function of the temperature of the water–ice phase transition at different pressures of 1 and 2100 bar according to Riehle. At 2100 bar, J^* is comparable to J^* at an approximately 35 °C higher temperature. Under pressure, water can be subcooled further, with a delayed formation of nuclei.

The growth of crystals is determined by the diffusion of molecules to the surface of the nucleus, the finding of a proper place, and the distribution of the freed energy to the surroundings. Under normal conditions (cooling speed $v_f < 10^2$ °C/s and subcooling $T_{sc} < 10$ °C), Eq. (1.8) can be used:

$$v_k = \text{constant} \times T_{sc}^n \tag{1.8}$$

where $n = 1$ if the energy transport and $n = 1.7$ if the surface reactions are decisive (Hillig and Turnbull, *J. Chem. Physiol.*, **1956**, *24*, 914). If $T_{sc} > 10$ °C, the diffusion process has to be taken into account. Since v_k is furthermore dependent on the concentration, the calculation of v_k is insecure.

To summarize, the following can be stated:

To produce large crystals,

- the rate of nucleation should be small, therefore the subcooling should be small;
- the freezing should take place in a quasi-equilibrium situation between solution and crystals;
- the temperature should be as high as possible, since the crystals grow with the function $e^{-1/T}$;
- the time given for crystallization has to be increased, since v_K is inversely proportional to the size of the crystal.

To produce only very few or no crystals,

- freezing should take place under high pressure (Figure 1.13);
- the freezing rate should be as high as possible, to produce a large degree of subcooling.

As can be seen from Figure 1.14, in pure water Ic and the other phases can only be reached under high pressures.

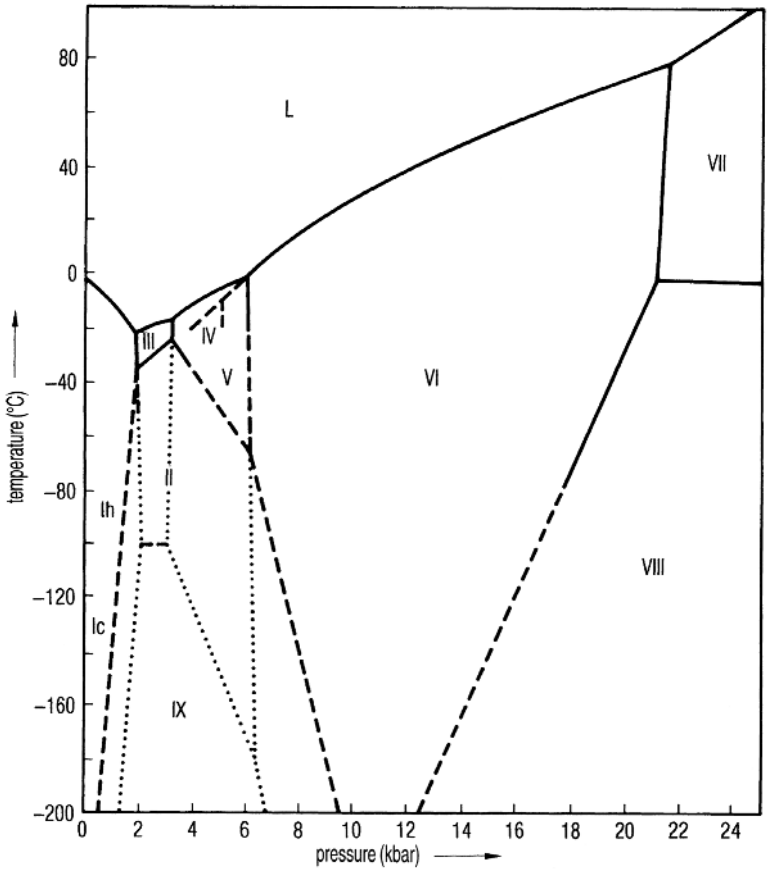

Figure 1.14 Phase diagram of water. L = liquid water; Ih = hexagonal ice; Ic = cubic ice; III–IX crystal configurations of ice. (From de Quervain, 1978 [12]. Reproduced with permission of Elsevier.)

Dowell and Rinfret [14] demonstrated that the phase at temperatures above −160 °C consists of small crystals ~400 Å in size and having cubic and pseudo-hexagonal structures.

Figure 1.15 shows the three phases of ice that exist under normal pressure as a function of temperature, indicating also the time it takes to change from one type to another. If water vapor is condensed on a cold surface in a very thin film, amorphous ice is formed and remains stable at −160 °C for a long time. As shown in Figure 1.15, the change from amorphous to cubic ice will take $\sim 5 \times 10^5$ min or more than a year. The rate of change depends very much on the temperature: at

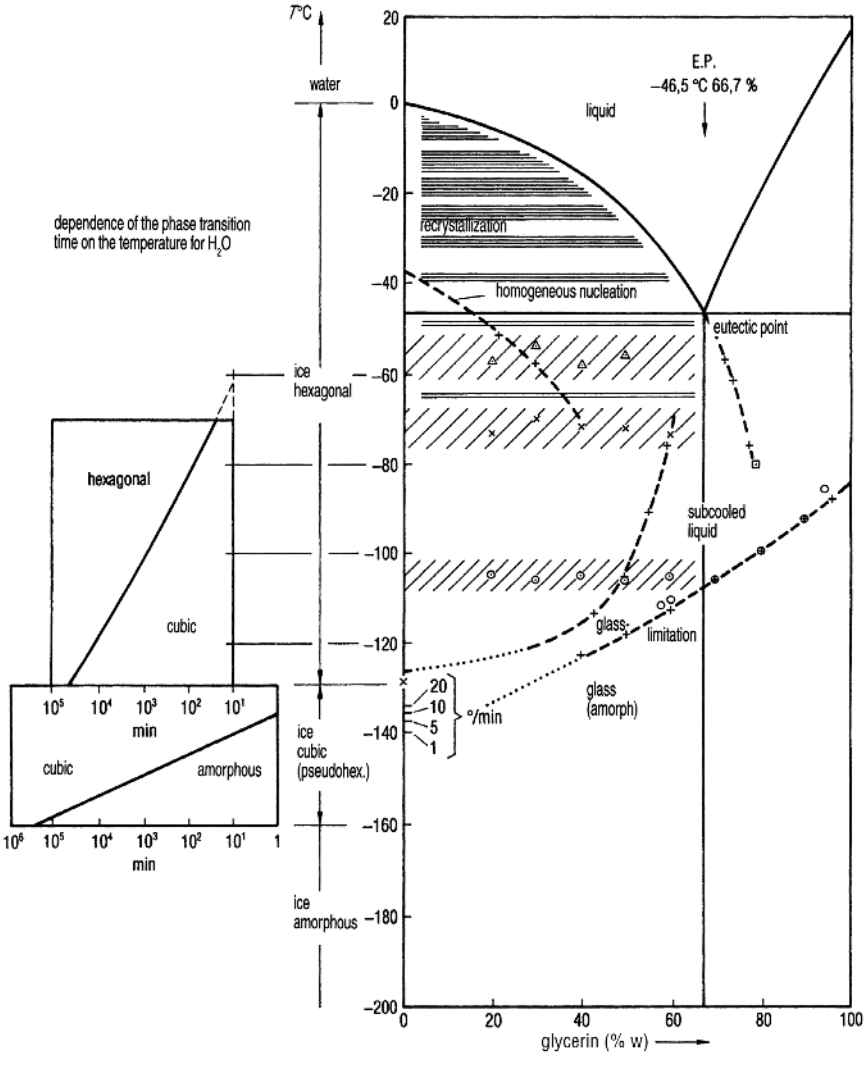

Figure 1.15 Water–glycerin phase diagram. On the left-hand side, the dependence of the phase transformation time on the ice temperature is shown: At −140 °C, amorphous ice transforms into cubic ice in ~10 min. (See also Figure 8 from Ref. (Umrath, W., Kurzbeitrag für die Tagung Raster-Elektronenmikroskopie in Medizin and Biologie, unpublished, Brühl.))

−135 °C the same change takes only 1 min. This change is called devitrification. At −125 °C the change from cubic to hexagonal ice takes ∼1000 h, while at −65 °C only hexagonal ice is stable.

To summarize, amorphous ice is stable below −160 °C, until −125 °C when cubic ice is formed irreversibly from the amorphous phase; above this temperature, hexagonal ice develops. Between −160 and −130 °C, cubic ice can be embedded in an amorphous surrounding. During warming, it is likely that some amorphous ice changes directly into the hexagonal form. Between −130 and −65 °C all three phases could be present, depending on the time–temperature function. This behavior of pure water changes if water solutions, suspensions in water, and mixtures with water are studied, as will be the case for virtually all products to be freeze-dried.

The freezing process will be discussed with model substances, which will be used as cryoprotective agents (CPAs). If a solution of water and glycerol is cooled quickly, a 10% solution in a layer of 3×10^{-3} mm and $\nu_f = 10^6$ °C/s can be vitrified ([11], p. 218), but in a 5% solution crystals of 1000 Å are formed. At high pressures (1.5–2.1 kbar), 4×10^3 °C/s is sufficient for a 10% solution and 2×10^4 C/s for a 5% solution to achieve vitrification. For these measurements, the absence of foreign particles must be presumed in order to use the subcooling effect fully. Foreign particles could also come from containers, holding devices, and so on.

Riehle has proved the existence of such vitrification by electron microscopy. With higher concentrations of glycerol, vitrification becomes simpler. Luyet [15] showed diagrammatically (Figure 1.16) how various phase changes take place at different glycerol concentrations. At 60% glycerol devitrification takes place at ≃115 °C and increases with increasing glycerol concentration to ≃85 °C. However, such high concentrations of glycerol can normally not be used to freeze-dry organic substances.

As shown for pure water, the phase transitions depend on the cooling rate, the end temperature of cooling, and the temperature and time of the treatment after cooling. The rate of rewarming is especially critical. One has to differentiate between quasi-static situations, which are independent of time and all other dynamic states, in which the history of the present situation and the rate of the further changes play an important role.

Freezing processes can be divided into two categories: one type is so slow that they run under almost equilibrium conditions; others are too fast to approach the equilibrium situation. Figures 1.17–1.19 show the effect of the freezing rate on the structure of the dried product. In Figure 1.17, milk has been frozen slowly (0.2–0.4 °C/min) in trays. In Figure 1.18, mannitol solution has been frozen in vials at a rate of ∼1 °C/min; the arch at the bottom represents the vial bottom. In Figure 1.19, γ-globulin has been frozen in LN_2 (∼10–15 °C/min). This shows only the upper part of the dry product. The cake has been frozen so quickly from the bottom and the walls that the concentrated liquid has been pushed to the center, where it has been pressed to form a cone. The cake is cut and in the center of the cone a channel can be seen, in which highly concentrated solution has been included, leaving a channel. Since the solids of this part are agglomerated to the surrounding areas, the structure of the channel is partially collapsed during drying.

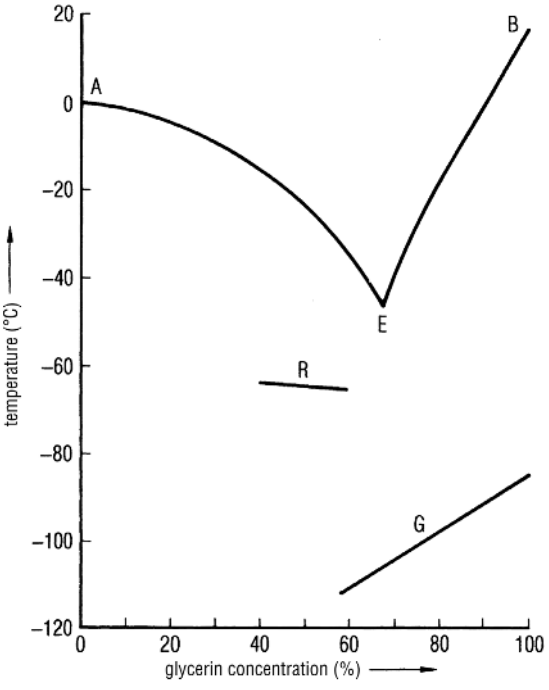

Figure 1.16 Temperature as a function of the concentration of water–glycerin mixture at which phase transformations occur. (Figure 14 from Ref. [15].) Definitions by Luyet: AE, formation of small crystals or molecular groups; E, eutectic point; EB, formation of clusters; R, eruptive recrystallization; G, glass transition.

The nonequilibrium status can be seen during a slow cooling of a water–glycerol solution. Starting with a 20% glycerol solution, pure ice crystals will first be formed until at −46.5 °C when the glycerol concentration has reached 66.7%. At this temperature, the eutectic should solidify. However, it is possible to reduce

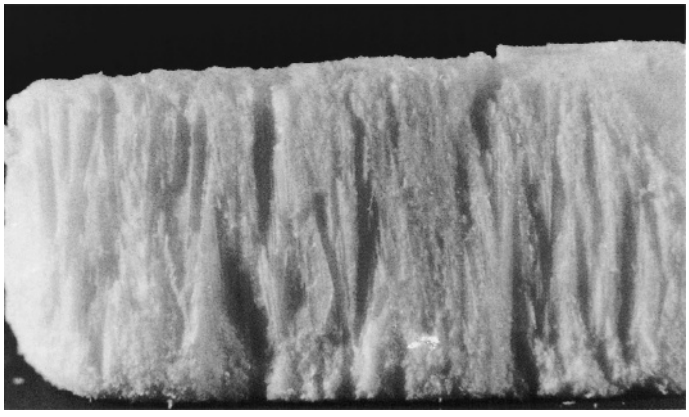

Figure 1.17 Milk frozen slowly (0.2–0.4 °C/min) in a tray. (Courtesy of Steris GmbH, Hürth, Germany.)

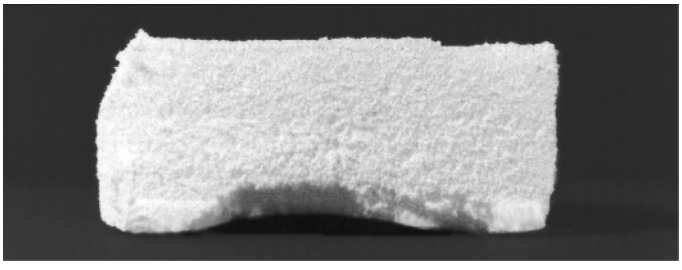

Figure 1.18 Mannitol solution frozen at ~1 °C/min in a vial on precooled shelf. (Courtesy of Steris GmbH, Hürth, Germany.)

the temperature to −58 °C with a glycerol concentration of 73%. A further decrease in temperature does not crystallize any more water. The solution is so highly concentrated and viscous and the mobility of the water molecules is so much reduced that the remaining water is unfreezable (UFW) in an amorphous state between the glycerol and ice molecules.

Figure 1.20 ([16], p. 286) shows diagrammatically at a given starting concentration which parts will be ice, unfrozen water, and glycerol at a freezing temperature actually used under equilibrium conditions. A solution of 20% initial glycerol contains, when cooled to −50 °C, 70% ice, 10% UFW, and 20% glycerol. At −58 °C, the line marked UFW is effective; 72% is glycerol and 27% UFW.

The fact that a certain amount of water cannot crystallize in a highly concentrated solution, and that the molecules cannot move any more to the existing crystals, is important during the freezing of biological substances. Tables 1.2 and 1.4 show this for some food products and CPAs.

The combination of this knowledge and the results of quick-freezing processes provide a theoretical opportunity to freeze products into a solid, amorphous state. If the freezing velocity is smaller than required for vitrification, but large enough to avoid an equilibrium state, an amorphous mixture will result of hexagonal ice, concentrated solids, and UFW.

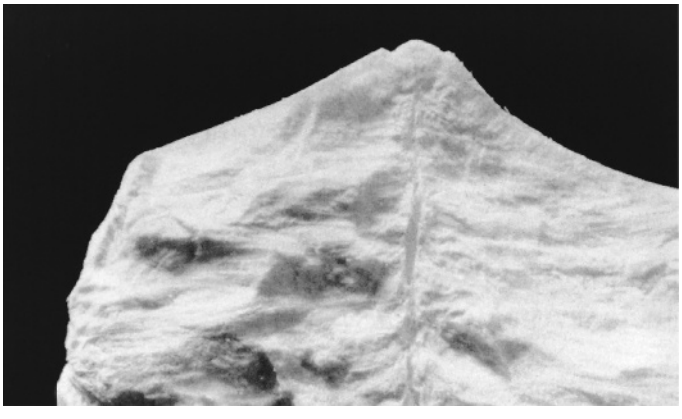

Figure 1.19 γ-Globulin solution frozen in a vial by LN_2 at ~10 °C/min (only the upper part of the product is shown). (Courtesy of Steris GmbH, Hürth, Germany.)

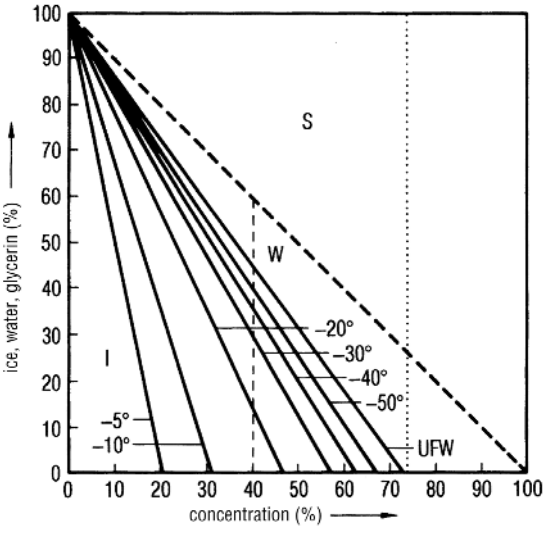

Figure 1.20 Rate of ice, water, and dissolved substance in the state of equilibrium of a glycerin–water solution as a function of the initial glycerin concentration, plotted at different freezing temperatures between −5 and −50 °C. A 40% glycerin solution frozen at −30 °C contains in the state of equilibrium ~32% ice, 30% water, and 38% glycerin. The line marked UFW represents the temperature at which the glycerin concentration becomes so high that no more water can be frozen (the water molecules become highly unmovable). The glycerin concentration is ~73% and the UFW concentration 27%. The diagram shows the equilibrium conditions, which may not exist during quick freezing. (See also Figure 1 from Ref. [16].)

1.1.3 Influence of Excipients

The freezing of complex organic solutions and suspensions is often difficult to predict theoretically. The methods to analyze the freezing process and the structure formed are described in Section 1.1.5. The freezing is influenced by several factors, which often act in opposing directions:

1) Freezing rate
   – slow: quasi-equilibrium
   – very fast: dynamically governed
2) Number and geometry of foreign particles, which influence the heterogeneous nucleation: the closer their structure is similar to the ice structure, the better is their effectiveness as nuclei.
3) The degree of subcooling, which depends on the substance, but is strongly influenced by the two points above.
4) The rate of growth of the ice crystals, which depends on temperature and the viscosity of the solution; the latter increases strongly with increasing concentration of the solution.
5) That part of the water that is not frozen due to high freezing rate forms highly viscous occlusions in between the ice crystals.
6) The crystallization of the solved substance(s) (or part of it) or the subcooling and the delay of this crystallization, which depends again not only on the temperature but also very much on the viscosity of mixture.

By adding excipients not only is it possible to influence the cooling and solidification processes, but also they may be necessary to obtain one or more of the following objectives:

- To grow stable structures if the amount of solids is small, for example, <3% in the solution, to prevent solid particles from being carried out of the vials by the water vapor stream (bulking agents).
- To adjust pH data (buffers).
- To avoid or induce crystallization.
- To protect the active constituent during freezing (cryoprotectants).
- To protect the active constituent during freeze-drying (lyoprotectants).
- To reduce changes of the active constituent during storage (e.g., unfolding or aggregation of proteins.

An example of avoiding crystallization of sucrose by adding polyvinylpyrrolidone (PVP) was given by Shamblin and Zografi [17] even if a significant level of absorbed water is present. Zeng *et al.* [18] described the effect of the molecular weight (MW) and the added amount of PVP on the glass transition temperature T_g and the crystallization of sucrose; 5% of PVP of MW 300 K increased T_g from 48.3 °C for freeze-dried sucrose alone to 58.8 °C; 2.5% of PVP of MW 24 K or 40 K showed smaller or no effects on T_g. Shalaev *et al.* [19] freeze-dried sucrose in the presence of citric acid (citric acid:sucrose 1: 10) to RM <0.1% w/w. At 50 °C, the sucrose undergoes significant inversion in spite of the low RM. The rate of inversion is directly related to the citric acid concentration in the solution before freeze-drying. The authors concluded that the freeze-drying of sucrose with acidic substances may lead to substances that could react with other ingredients. Kouassi and Roos [20] freeze-dried maltodextrin–sucrose (2: 1) and maltodextrin–lactose–sucrose solutions (1: 1: 1) with invertase (10 mg/17.2 g). Sorption isotherms and T_g values of the amorphous dried products were measured. Sucrose hydrolysis was observed significantly at 24 °C and 0.662 aw. Saleki-Gerhardt and Zografi [21] studied the crystallization of sucrose from the amorphous state, influenced by absorbed water and additives (lactose, trehalose, and raffinose). Table 1.9 shows the data for T_g and T_c with absorbed water, and Table 1.10 the respective data with additives.

Mannitol, a frequently used excipient, shows complexity in its application. Yu *et al.* [22] reported the formation of a metastable mannitol hydrate during freeze-drying. The amount of mannitol hydrate varies from vial to vial in one batch. It reduces the drying rate, it can be converted to anhydrous polymorphs, redistributing the residual hydrate water, and it shows varying moisture levels from vial to vial. Cannon and Trappler [23] found at least three different polymorphs of mannitol. Under all studied process conditions, all three polymorphs were present, but in different ratios, strongly dependent on the freezing technique.

Pyne and Suryanarayanan [24] followed the phase transitions of glycine during freeze-drying among other methods in the sample chamber of an X-ray diffractometer. Freezing rates of 20 and 2 °C/min of a 15% wt/wt glycin solution resulted in the crystallization of 2-glycin with an increasing amount after annealing to −10 °C. Glycin immersed in LN_2 formed an amorphous product. Upon heating to −65 °C, an unidentified crystalline phase of glycin was observed, which

Table 1.9 Glass transition temperature T_g and crystallization temperature T_c for amorphous sucrose, trehalose, lactose, raffinose, and amorphous sucrose in the presence of absorbed water.

Product	T_g (°C)	T_c (°C)
Sucrose	74	130
Sucrose, 0.99% H_2O	60	125
Sucrose, 1.47% H_2O	58	115
Sucrose, 1.98% H_2O	50	100
Sucrose, 3.13% H_2O	32	92
Trehalose	115	–[a)]
Lactose	108	185
Raffinose	102	–[a)]

a) Did not crystallize.
Table I and II from Ref. [23].

transformed at ≃55 °C to 2-glycin. After annealing, 3-glycin appeared to an extent that depended on the annealing temperature. Cooling rate, annealing, and the temperature during MD influence the solid state of glycin.

Hinrichs *et al.* [25] compared inulin of various degrees of polymerization with trehalose as glass-forming agents. Inulin above a certain degree of polymerization, $DP_n/DP_w > 5.5/6.0$ and trehalose stabilize alkaline phosphatase equally well. The T_g and T'_g values for inulin of <5.5/6.0 were higher than those for trehalose.

Glucose-6-phosphate dehydrogenase (G6PDH) freeze-dried with sucrose/raffinose at different mass ratios showed a higher T_g at higher mass ratios of raffinose than sucrose [26]. Different mass ratios did not influence the recovery of G6PDH after freeze-drying, but during storage low sucrose offered the best enzyme stability.

Fakes *et al.* [27] evaluated the moisture sorption behavior of mannitol, anhydrous lactose, sucrose, D-(+)-trehalose, dextran 40, and povidine (PVP K24) as bulking agents. Mannitol was found to be crystalline and nonhygroscopic

Table 1.10 Crystallization temperature of sucrose with various proportions of additives.

Additives (% w/w)	Crystallization temperature (°C)		
	Lactose	Trehalose	Raffinose
0.0	130	130	130
1.0	131	128	128
5.0	137	145	148
10.0	156	161	160

Table IV in Ref. [23].

Table 1.11 Size and number of pores in chicken meat as a function of freezing rate.

Freezing rate (°C/min)	Size of pores (μm)[a)]	Rate of pores (%)
0.5	≥10	95
9	≥10	65
230	≥10	25
0.5	≥30	85
9	≥30	22
230	≥30	12

a) $1\ \mu m = 10^{-3}\ mm = 10^{-6}\ m$.

before and after freeze-drying with RM 0.1–0.3% w/w at 25 °C and 10–60% RH. Anhydrous lactose, sucrose, and trehalose were crystalline and relatively non-hygroscopic with RM 0.86, 0.15, and 9.2%, respectively. After freeze-drying, they were amorphous with RM 1.6, 2.5, and 1.2%, respectively, and adsorbed moisture in an increasing RH atmosphere. Lactose adsorbed 10% water and formed its crystalline hydrate at 55% RH.

The cooling rate directly influences the size of the ice crystals, which can be measured after drying by the size of the pores in the product. Thijssen and Rulkens [28] gave the size of the pores in chicken meat (Table 1.11). Figure 1.21 shows the average size of pores in 20% dextrose solution as a function of the

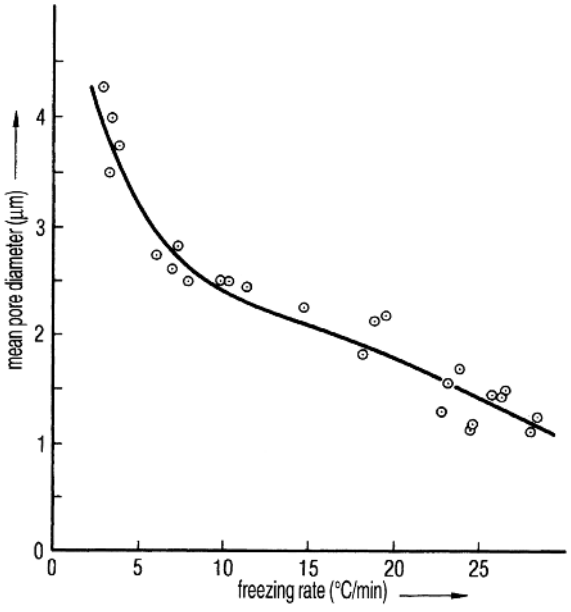

Figure 1.21 Pore diameter as a function of freezing rate in 20% dextran solution. (See also Figure 3 from Ref. [28].)

freezing rate. Godward *et al.* [29] used NMR to measure the pore size distribution in freeze-dried starch gels. They used the fact that starch surfaces change the relaxation for acetone proton transverse magnetization and recommended this method for pore size measurements in food systems. The pore size influences the drying rate and the retention of aroma (see Section 1.2.5).

Reid *et al.* [30] described the effect of the addition of 1% of certain polymers on the heterogeneous nucleation rate: At −18 °C, the rate was 30 times greater than in distilled, microfiltered water and at −15 °C, the factor was still 10-fold higher. All added polymers (1%) influenced the nucleation rate in a more or less temperature-dependent manner. However, the authors could not identify a connection between the polymer structure and nucleation rate. Nonetheless, it became clear that the growth of dendritic ice crystals depended on two factors: (i) the concentration of the solution (5–30% sucrose) and (ii) the rate at which the water–ice crystals phase boundary moved. However, the growth was found to be independent of the freezing rate. (*Note:* The freezing rate influences the rate of boundary movement.) The chances of a water molecule reaching dendritic ice decrease as sucrose concentration increases and the distance between the points of the ice stars increases. The addition of polymers reinforces this effect.

Burke and Lindow [31] showed that certain bacteria (e.g., *Pseudomonas syringae*) can act as nuclei for crystallization if their surface qualities and their geometric dimensions are close to those of ice. Rassmussen and Luyet [32] developed a connection for solutions of water with ethylene glycol (EG) , glycerol (GL) , and polyvinylpyrrolidone (PVP) between the subcooling to the heterogeneous and the homogeneous nucleation of ice.

The heterogeneous and homogeneous temperatures of nucleation during cooling (5 °C/min) and the melting temperatures during rewarming may be measured by differential thermal analysis (DTA). Figure 1.22 shows the resulting phase diagram for water–glycerol and Figure 1.23 for water–PVP. Glycerol reduces the temperature of homogeneous crystallization to a much greater extent than PVP; the melting temperatures follow the same tendency. Figures 1.22 and 1.23 also show the temperatures of devitrification: 50% PVP is sufficient to avoid crystallization at ≃68 °C, while 50% glycerol reaches this effect only at ≃132 °C.

PVP decreases the temperatures of crystallization less than GL, the temperatures of devitrification being higher with PVP than with GL. With GL, crystallization can be avoided until ≃70 °C, but PVP pushes devitrification in an amorphous product to higher temperatures.

Sutton [33] studied the question of how quickly solutions with certain CPAs (GL, dimethyl sulfoxide (DMSO) , and others) have to be cooled in order to avoid crystallization. At 100 °C/min, concentrations of 42.1% DMSO and 48.5% GL are necessary to achieve the glass phase. With a 32.5% solution of (2*R*,3*R*)-(−)-butane-2,3-diol, the same effect can be accomplished at ∼50 °C/min. Sutton showed (see Figure 1.24) that polyethylene glycol with a molecular weight of 400 (PEG 400) reduced the critical cooling rate to ∼25 °C/min. The addition of PEG 8000 [34] improved the protection of lactate dehydrogenase (LDH) by maltodextrins, if maltodextrins with low dextrose equivalents are used.

Levine and Slade [36] investigated the mechanics of cryostability by carbohydrates. Figure 1.25 shows an idealized phase diagram developed from differential

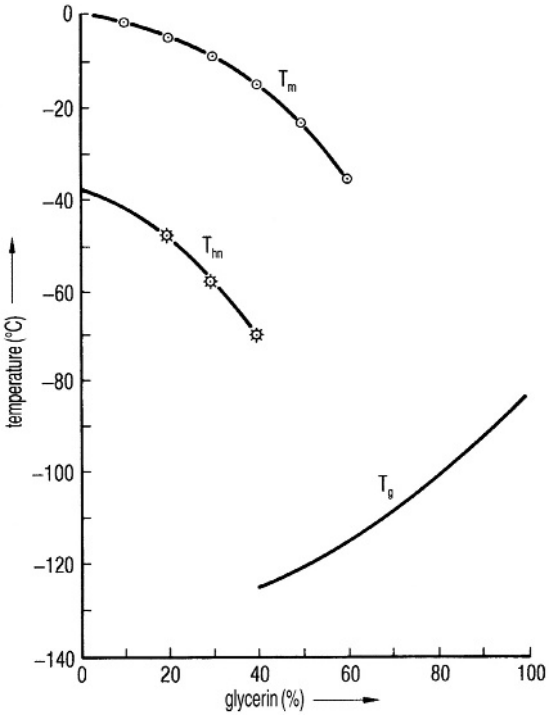

Figure 1.22 Phase diagram for glycerin–water. T_m, melting temperature; T_{hn}, temperature of homogeneous crystallization; T_g, devitrification temperature. (See also Figure 3 from Ref. [32].)

scanning calorimetry (DSC) measurements for hydrolyzed starch (MW >100) and for polyhydroxy combinations having a low molecular weight. With slow cooling (quasi-equilibrium conditions), no water crystallizes below the T_g curve.

The terms "antemelting" and "incipient melting" describe phenomena that occur at temperatures near T_g. Also the "eruptive" crystallization, during the main drying of the freeze-drying process, is the consequence of a collapse of the matrix, allowing the water molecules to diffuse to the ice crystals. This may also free volatile substances, enclosed in the amorphous phase. These phenomena can also occur only in a part of the product, especially if the temperature gradient in the product is substantial. Measurements of T_r and T_c by other authors agree well with T'_g measurements made by Levine and Slade [36], for example, for sucrose −32/−32 °C, for maltose −32.2/−29.5 °C, for lactose −32/−28 °C (Tables 5 and 6 in Ref. [36]). T'_g, c'_g, and g UFW/g carbohydrate are characteristic data for such solutions. Shalaev and Kaney [37] investigated the solid–liquid state diagram of the ternary system water–glycine–sucrose with DTA and X-ray diffraction. Figure 1.26 shows the isoplethal section of the solid–liquid state diagram for a glycine/sucrose ratio of $R = 0.1$. The line EE' divides the two-phase (ice + amorphous phase) and single-phase (amorphous phase) fields. The lines ABB' and CDD' subdivide the fields with different states of the amorphous phase. Below T'_g (line ABB), the amorphous phase is in a structural solid state and the translational

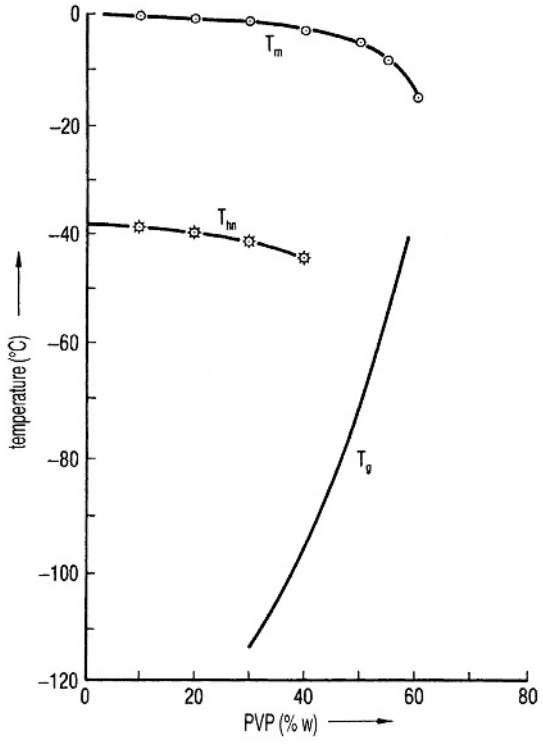

Figure 1.23 Phase diagram for polyvinylpyrrolidone (PVP)–water. For explanation, see Figure 1.22. (See also Figure 4 from Ref. [32].)

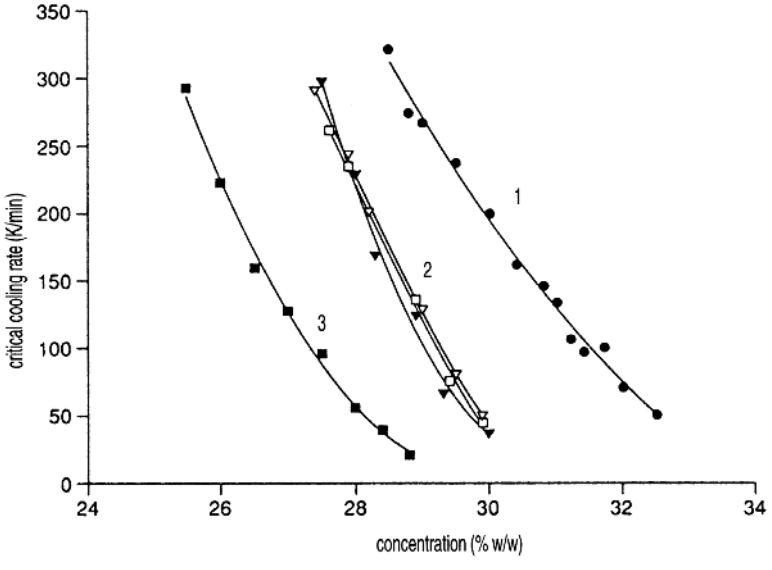

Figure 1.24 Critical cooling rates for butane-2,3-diol and dextran as a function of butane-2,3-diol concentration. 1, butane-2,3-diol; 2, butane-2,3-diol and dextran 20; 3, butane-2,3-diol and PEG 400. (From Sutton, 1992 [35]. Reproduced with permission of Elsevier.)

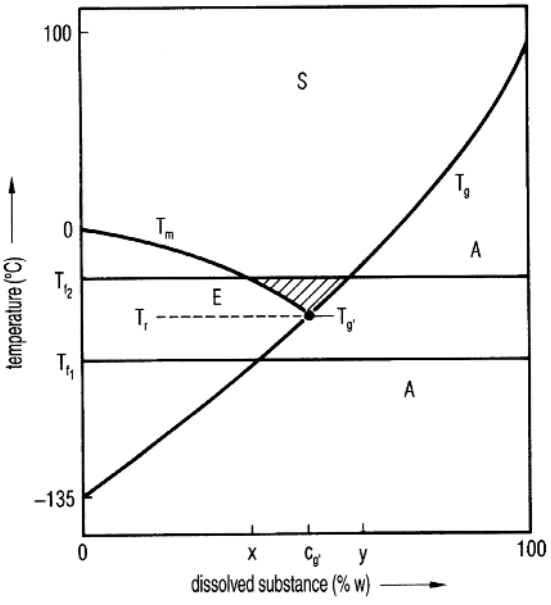

Figure 1.25 Idealized diagram to show generally the dependence of the phase on temperature and concentration. The dissolved, hypothetical substance consists of small carbohydrates as found in food. The figure illustrates the meaning of T'_g. If a temperature range between T_{f1} and T_{f2} is applied, the product can, above T'_g, recrystallize, start melting, or remain in the amorphous phase, depending on the concentration of the dissolved substance. Below T'_g and at concentrations lower than c'_g, crystallization is possible. A, amorphous solid; E, ice; S, solution area. (See also Figure 1 from Ref. [36].)

motion of the molecules is retarded. Above T'_g, the product transforms into a structural liquid state, but the sample keeps its form because the viscosity is so high. At $R = 1$, devitrification is observed at −30 °C and ≥50% water.

Jang *et al.* [38] investigated the glass transition temperature T'_g for FK 906 (a synthetic peptide) during rewarming from the frozen state and T_g of the dry product in the presence of sucrose, maltose, trehalose, and lactose and also polymers with different molecular weights and three salts. For the first group of disaccharides, the Gordon–Taylor equation [39] describes the glass transition temperatures as a function of the FK906 content if the T_g of each component is known. The three salts have approximate eutectic temperatures of NaCl −21 °C, NaBr −31 °C, and KCl −11 °C, and FK 906 −19 °C. NaCl (0.1–0.3%) lowers the T'_g of a 10% FK 906 solution from −19 to −27 °C. NaBr (0.1–1%) solutions have approximately the same effect, while KCl induces a small decrease from −19 to −23 °C at concentrations of 0.1–0.2% in 10% FK 906 solution. However, on increasing the concentration to 1.5%, T_g increases by approximately 2 °C. The glass transition temperature of the freeze-dried product is not changed by NaCl contents up to 0.6%. Nicolajsen and Hvidt [40] described a similar effect of NaCl in the trehalose–NaCl–water system. At trehalose concentrations above 3.5% frozen to −70 °C and heated at 2 °C/min, no eutectic transition was found, indicating that all the NaCl is trapped in the glass phase. However, the lower the

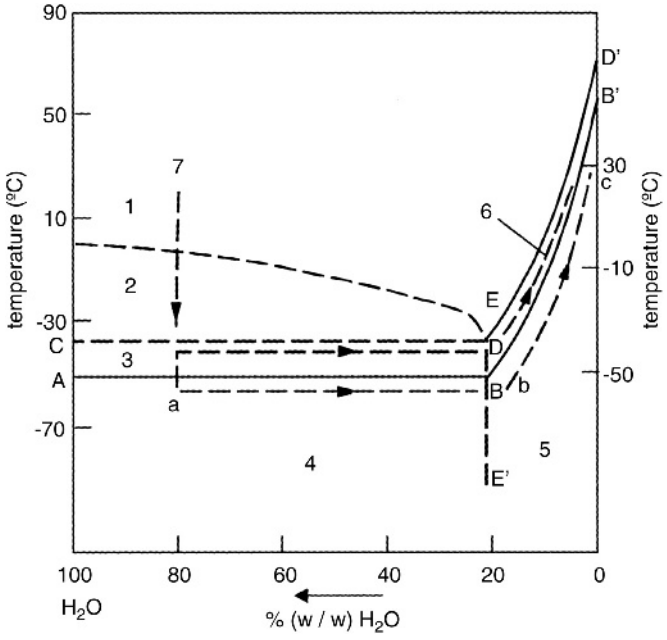

Figure 1.26 Isoplethal section of the solid–liquid state diagram for $R = 0.1$. Section fields: 1, solution (viscous-flow state); 2, ice; 3, ice and amorphous phase (mechanical properties of a solid); 4, ice + glass; 5, glass; 6, amorphous phase (mechanical properties of a solid); 7, freeze-drying pathway. (From Shalaev, 1994 [37]. Reproduced with permission of Elsevier.)

glass transition temperature, the larger the % NaCl/% trehalose ratio. NaCl appears to be a destabilizing factor in the glass phase.

As shown in Section 1.1.5, DSC, MDSC, and TMDSC have provided a better understanding of changes in glass, amorphous, and crystalline phases.

For freeze-drying, one can summarize as follows:

- If the product temperature approaches T'_g from lower temperatures, the viscosity changes rapidly (within a few degrees) by several decimal powers. Since the product temperature can also be measured only with a certain accuracy (see Section 1.2.3), one has to account for both uncertainties. It is recommended that the maximum product temperature during main drying be chosen 3–5 °C below T'_g.
- The addition of certain carbohydrates increases, by varying degrees, the values and decreases the amount of UFW. These stabilize the glass phase to higher temperatures and permit higher drying temperatures. They can also bind volatile components.

Carpenter *et al.* [41] showed that the stabilization of proteins, using the enzymes phosphofructokinase (PFK) and lactate dehydrogenase (LDH) as models, during freezing and thawing and freeze-drying is based on two different mechanisms. In Table 1.12, nine substances provide relatively good protection against denaturation during freezing and thawing (40–85% of the activity

Table 1.12 Activity of lactate dehydrogenase after freezing and thawing in the presence of dissolved substances, which are mostly repelled by proteins.

Dissolved substance	Highest tested concentration (mol/L)	Remaining activity (%)
None	0.0	21.5
Sucrose	1.0	85.4
Lactose	0.5	74.2
Glucose	1.0	60.2
Glycerin	1.0	71.4
Sorbitol	1.0	75.3
Mannitol	1.0	67.3
Glycine	2.0	39.1
Sodium acetate	2.0	81.2
$MgSO_4$	2.0	61.7
NaCl	3.0	20.7

See also Table III in Ref. [41].

remains). This does not apply for 3 mol/L NaCl (the 10 substances listed are a selection of 28 substances studied).

Timasheff *et al.* [42] explained the stabilizing or destabilizing effect of the additives by the combination of the additive molecule with the protein (destabilizing) or its rejection by the protein (stabilizing). The predominant effect of the additive depends on its chemical qualities and the surface structure of the protein. For example, NaCl bounds predominantly to the LDH and destabilizes it. Urea had the same effect on LDH during freezing.

A different effect stabilized PFK during freeze-drying and subsequent storage. As shown in Table 1.13, only disaccharide can protect PFK. Since only a special group of CPAs is effective, one can assume that these CPAs combine with the protein. If water molecules of the hydrated envelope of the protein are removed during freeze-drying, the molecules of the effective CPA can replace these water molecules, keeping the protein stable. Prestrelski *et al.* [43] demonstrated by infrared spectroscopy that the addition of 10 mM mannitol, lactose, trehalose, or 1% PEG to lactate dehydrogenase and phosphofructokinase attenuated the unfolding, but spectral differences in the dried state were still observed. However, a combination of 1% PEG with 10 mM mannitol, lactose, or trehalose preserved full enzymic activity upon reconstitution of the freeze-dried product.

Carpenter *et al.* [44] found that certain polymers (e.g., PVP) could stabilize multimeric enzymes during freezing and freeze-drying by a different mechanism: they cannot replace water molecules in the dried state, and therefore it is assumed that they inhibited the dissociation of the enzymes molecules induced by freezing and freeze-drying.

Rey [45] developed a theoretical diagram of the low-temperature behavior of a system susceptible to present glass formation (Figure 1.27). The diagram

Table 1.13 Activity of phosphofructokinase after freeze- and air-drying in the presence of different CPAs.

CPA (0.5 M)	Remaining activity freeze-dried	Air-dried
None	0.0	
Trehalose	56.0	68.4
Maltose	69.2	51.4
Sucrose	56.3	67.7
Glucose	3.3	2.1
Glycerin	0.0	
Glycine	0.0	2.8

See also Table IV in Ref. [41].

summarizes (a) the behavior of excipients, which can form a glass phase when they are slowly or quickly frozen, and (b) the events that can take place during warming of the glass.

1.1.4 Freezing of Cells and Bacteria

In 1968, Meryman [46] presented his ideas about the "minimum cell volume" and hypothesized that during freezing, cells are damaged in two steps. Initially water

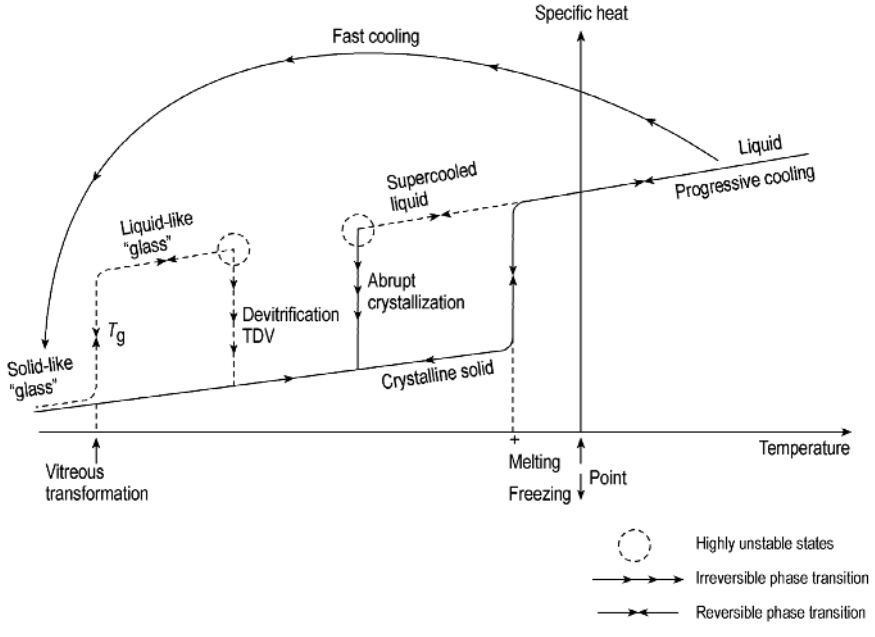

Figure 1.27 Theoretical diagram of the low-temperature behavior of a system susceptible to present glass formation. (See also Figure 9 from Ref. [45].)

diffuses from the cell to the surrounding, the freezing solution concentrating the solution in the cell. However, only a certain amount of water can be withdrawn from the cell until it has shrunk so much (minimum cell volume) that any further withdrawal takes water from the membrane molecules, which are an essential part of the cell's structure. The removal of this water leads to an irreversible change in the membrane structure.

As shown in Section 1.1.3, these structural changes can be avoided if certain sugars or other CPAs replace the water molecules. Pushkar and Itkin [47] showed by cryomicroscopy and X-ray analysis of structures that 15% glycerol in suspensions of marrow cells lowered the beginning of ice nucleation to −15 °C. Down to −10 °C, no nucleation in the cells was observed. With polyethylene oxide (10–15%), a few crystals of 10^{-3}–10^{-4} cm have been detected in an amorphous surrounding. Under these conditions, the function of the cells after thawing remained mostly normal. Nei [48] studied the nucleation of ice crystals during rapid freezing (100–1000 °C/min) using electron microscopy. Ice crystals can be observed in the cells of yeast, whereas in most bacteria (e.g., *coli* forms) almost no ice crystals could be detected. In Nei's opinion, ice crystals were more likely to have been produced in animal cells than in those of microorganisms. Cosman *et al.* [49] showed, using photographs taken with a cryomicroscope, that the volume of mouse islet cells shrank to 40% during cooling from 0 to −10 °C. Figure 1.28 indicates how many cells in rat liver contained ice as a function of cooling rate. The cells were cooled from −1 to −21 °C: Up to 50 °C/min, no ice was formed in the cells, whereas at ∼160 °C/min all cells contained ice crystals.

De Antoni *et al.* [50] demonstrated that the addition of trehalose during freezing and thawing of two strains of *Lactobacillus bulgaricus* improved the survival rate differentially, but in both cases considerably. The samples (1 mL) were frozen at 18 °C/min to −60 °C and thawed to 37 °C at 15 °C/min. The

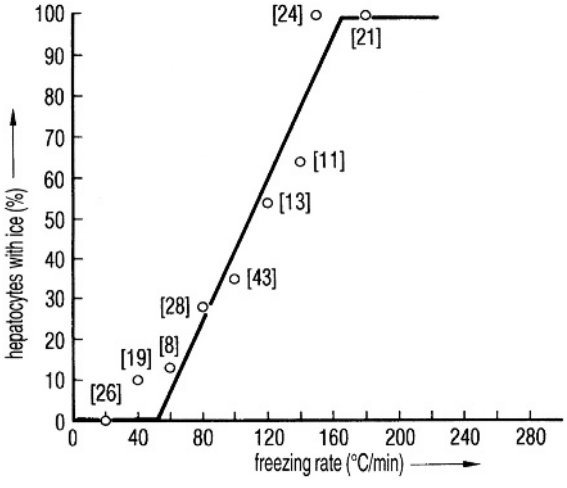

Figure 1.28 Percentage of hepatocytes of rats, which show intracellular ice as a function of freezing rate in the range of −1 to −21 °C. The numbers in brackets indicate the number of hepatocytes participating in each test. (See also Figure 8 from Ref. [49].)

solution consisted of distilled water, culture medium, and 10% milk with or without trehalose. It was shown that after three freeze–thaw cycles, milk alone resulted in a survival rate of 24 or 65%, whereas with trehalose this was could be improved to 32 and 100%, respectively. The efficacy in the case of both strains was clearly different. De Antoni *et al.* suggested that the efficiency of milk was related to its Ca^{2+} content, whereas the trehalose could replace water molecules in the phospholipids of the membranes. However, no mention was made of whether other sugar molecules in milk showed any effect.

1.1.5 Methods of Structure Analysis

The knowledge that successful freeze-drying depends largely on the structure of the frozen product has inspired the development of methods to analyze and understand these structures more quantitatively. Rey [51] has shown that in addition to the electrical resistance (ER) of a freezing substance, the thermodynamic behavior can also be used to study the freezing process and the frozen product.

1.1.5.1 Measurements of Electrical Resistance (ER)

Measurement of ER is done in an apparatus (Figure 1.29) in which the sample is cooled by LN_2 and electrically heated. Two electrodes are immersed in the sample, which is placed in a vial. The resistance between the two electrodes is measured with an alternating current of 50 Hz. For complete information, high

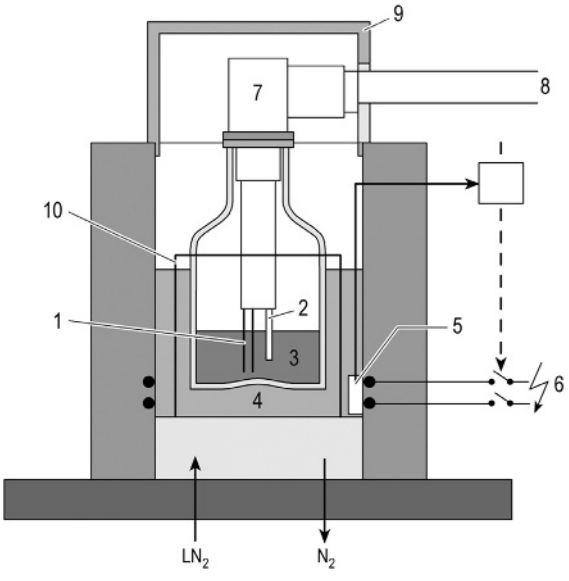

Figure 1.29 Schematic drawing of an instrument to measure the electrical resistance (ER) of a sample during cooling and rewarming. (Figure 1 from Ref. [52].) 1, platinum electrodes; 2, temperature sensor in the product; 3, product sample; 4, heat transfer medium; 5, temperature sensor in the heat transfer medium; 6, resistance heating; 7, highly insulated sensor head; 8, shielded cable; 9, electrical and magnetic shield; 10, vial holder.

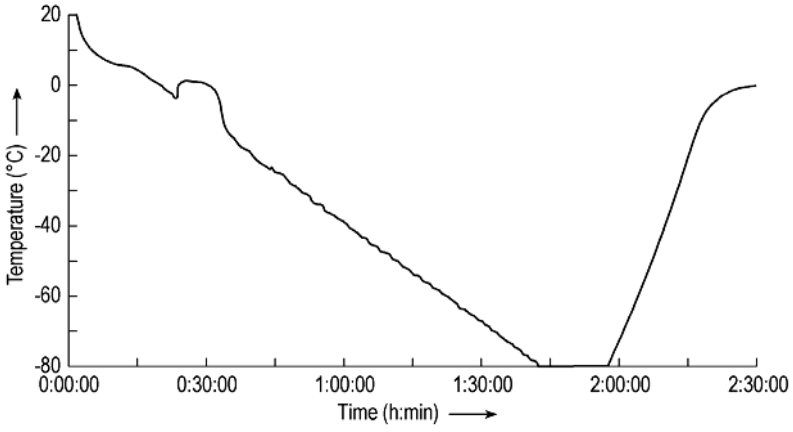

Figure 1.30 Check of cooling and heating rate. Preset data in this example: cooling 1.0 °C/min ±10%, warming 3 °C/min ±10%.

resistance up to 10^{11} Ω should be measurable. This requires high resistance, up to 10^{12} Ω, not only between the electrodes itself but also in the temperature sensor and surroundings. In addition to high insulation between the electrodes, the preset cooling and heating rates should be qualified as shown in Figure 1.30. The cooling rate is 1 °C/min between 0 and −50 °C and the heating rate is 3.3 °C/min between −80 and −10 °C. The measurement and interpretation of ER plots should consider the following:

- ER data reflect the mobility of the ions as a function of temperature.
- The sample size is comparable to a product in vials.
- The cooling rates chosen should be smaller than, the same as, and larger than in the pilot and production plant, for example, if the cooling rate in the production plant is 0.8 °C/min, then a minimum of three measurements at 0.4, 0.8, and 1.6 °C/min are recommended, each repeated three times, if the plots are practically identical.
- The first derivative of the ER plot should also be calculated and printed.
- If the product is frozen on the shelves of the plant, the cylindrical part of the sample vial in the instrument should be isolated from the heat transfer medium.

The use of an ER measuring system and the interpretation of the results require some familiarization with the possibilities and limitations of the method.

Solutions of salts, for example, 0.9% NaCl, will normally show the eutectic temperature, but the event can be at lower temperatures during cooling owing to the degree of supercooling and the cooling rate: For example, the event has been found with 1 °C/min (average of six measurements) at −24.1 °C, standard deviation (SA) 1.2 °C; with 3 °C/min at −30.2 °C, SA 2.3 °C. During rewarming, the event can be close to the expected temperature: −21.5 °C, SA 0.5 °C at 1 °C/min and 21.3 °C at 3 °C/min. Figure 1.31 shows a complete plot down to −120 °C at 3 °C/min. The behavior below −80 °C can be speculated as a reversible change in the crystal structure. Above 1×10^{12} Ω, the measurement is inaccurate, the

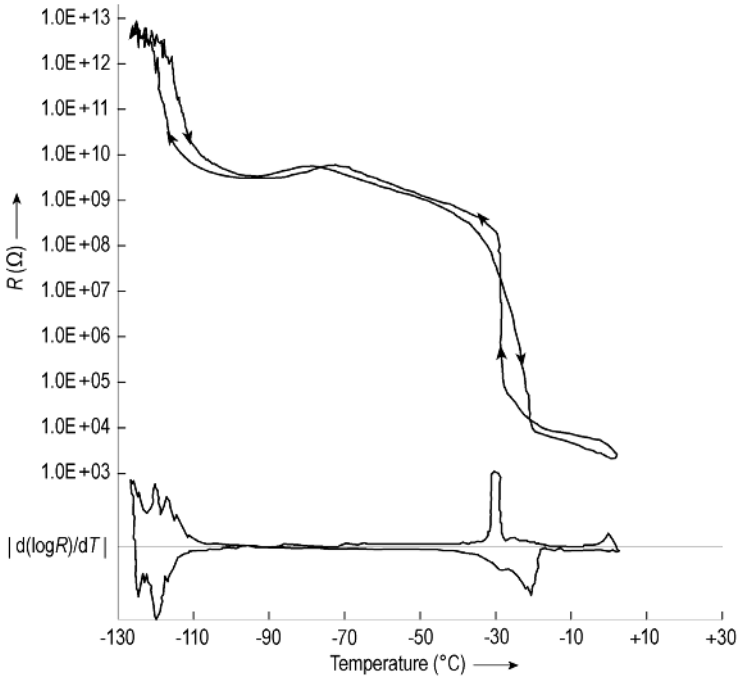

Figure 1.31 Electrical resistance as a function of temperature of 1% NaCl solution. Cooling rate 3 °C/min, warming rate 3 °C/min, and the first derivative d(log*R*)/d*T* measured down to −120 °C.

resistance of the sensor and its cable is $\sim 10^{12}$ Ω. The crystallization delay during cooling to −28/−30 °C is visible (see Figure 1.32), and also some event starting at −28 °C during warming. Figure 1.33 is a typical plot for 0.9% NaCl solution at a cooling rate of 1 °C/min (all rewarming plots are at 3 °C/min) and Figure 1.34 shows the enlarged derivative. Figure 1.35 presents the average of 22 0.9% NaCl measurements at 1 °C/min between −10 and −70 °C and the minimum and maximum data at each temperature. The resistance change covers six decades and the frequency distribution of the resistance data at each temperature (Figure 1.36a–g) reflects the very different or uniform development of the structure during freezing and rewarming: If the freezing of this solution at a rate of 1 °C/min were terminated at −30 °C, the resistance of the product would vary substantially, improving at −40 °C and becoming statistically predictable below −50 °C. The freezing of a product is not a uniform operation, it is influenced by several factors that can only be judged by sufficient statistical data.

One of the advantages of ER compared with other methods discussed later is the dimensions of the sample, especially its thickness of 10–15 mm. This is comparable to frequently used filling heights of vials for pharmaceutical products. If the cake thickness is substantially larger, for example, 40 mm, the freezing rates in a study should be chosen accordingly: 1 °C/min cannot be expected with freezing on the shelves: 0.2 or 0.3 °C/min is more likely. Therefore, tests for these thicknesses may be carried out, for example, at 0.15, 0.25, and 0.35 °C/min.

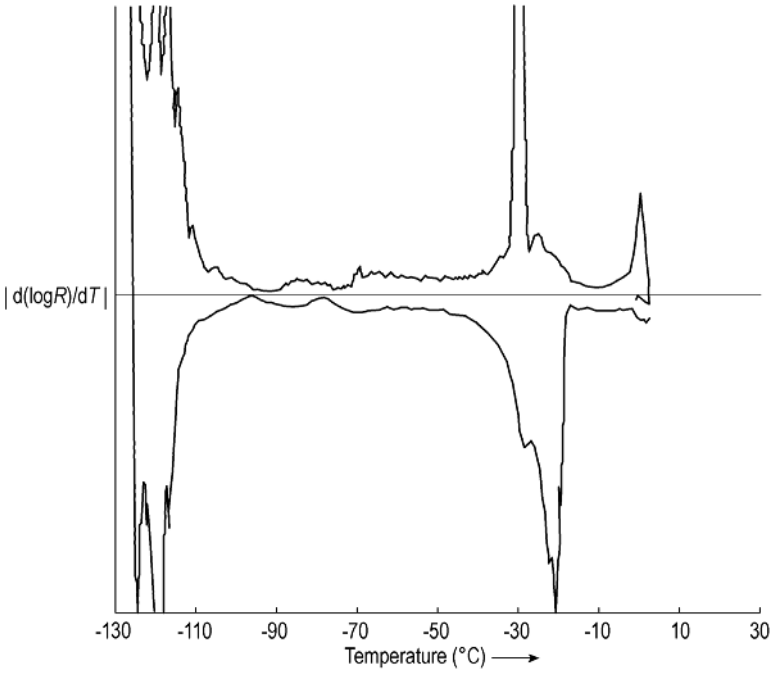

Figure 1.32 The first derivative of Figure 1.31 (approximately five times linearly enlarged).

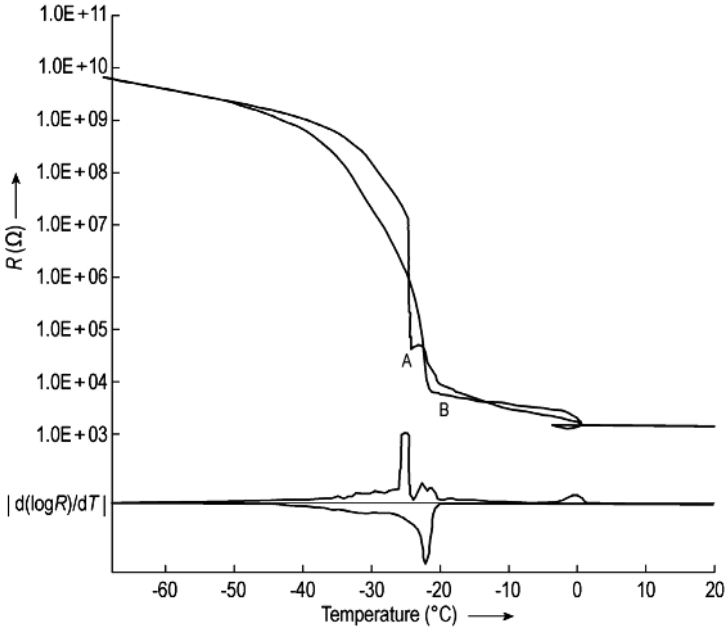

Figure 1.33 Typical electrical resistance plot of 1% NaCl solution with 1 °C/min cooling: event A at −24.5 °C during cooling and event B at 21.8 °C during warming.

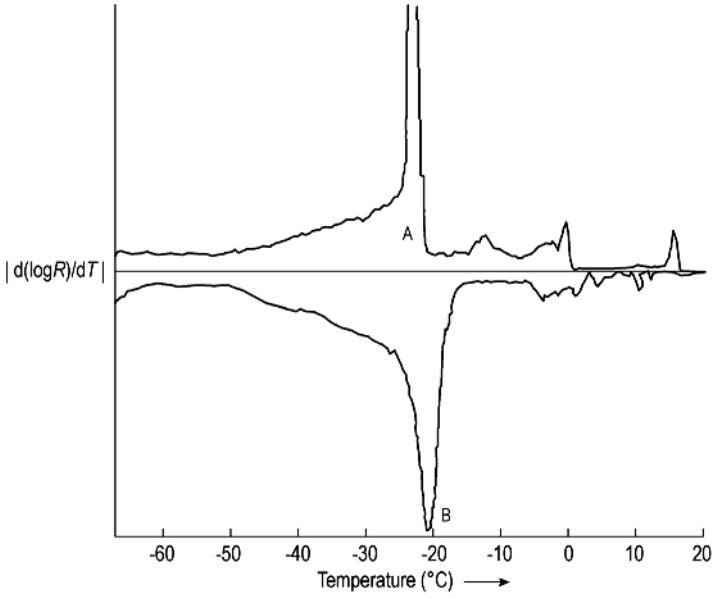

Figure 1.34 Enlarged derivative of Figure 1.33.

As can be seen from Figures 1.31–1.34, the derivative plots are helpful in determining the temperatures of changes in the slopes of log$R$ more accurately. Enlarged derivative plots may show some undulation, which can be disregarded. The main events can still be clearly detected.

If the product in vials is frozen on the shelves, the energy flow is mostly through the bottom of the vial and not through the wall. To simulate this condition, the wall of the sample vial can be isolated from the heat transfer medium by a layer of, for example, glass-fiber material. The difference in the cooling and warming behavior can be seen in Figures 1.37 and 1.38 as an example. In Figure 1.39, the influence of the isolation is typical for this product. The suspension subcools twice at events 1 and 2. Also, event 3 is a mixture of subcooling and crystallization. During rewarming, no event can be detected, since the water has been frozen to the maximum possible content. The product then starts to melt at $\simeq$12 °C.

The resistance plot of a 10% egg albumin solution with a freezing rate of 1 °C/min is completely different, as shown in Figure 1.40. The reproducibility of several measurements is within the drawing accuracy of the plots, except the degree of subcooling, which varies with the freezing rate. In pharmaceutical and food products, one finds mixtures of the two extremes shown above. Examples of ER measurements are given in Figures 1.40 and 1.42. In Figures 1.41 and 1.42, the influence of the freezing rate on two human blood derivatives is shown. The slow freezing in Figure 1.41 (1 °C/min) leads to larger crystals with larger inclusions of high-viscosity concentrates between them. This results in a softening of the structure during rewarming at a lower temperature: d(log$R$)/dT drops from −60 °C to a minimum at −47 °C; in the fast-cooled product, the inclusions

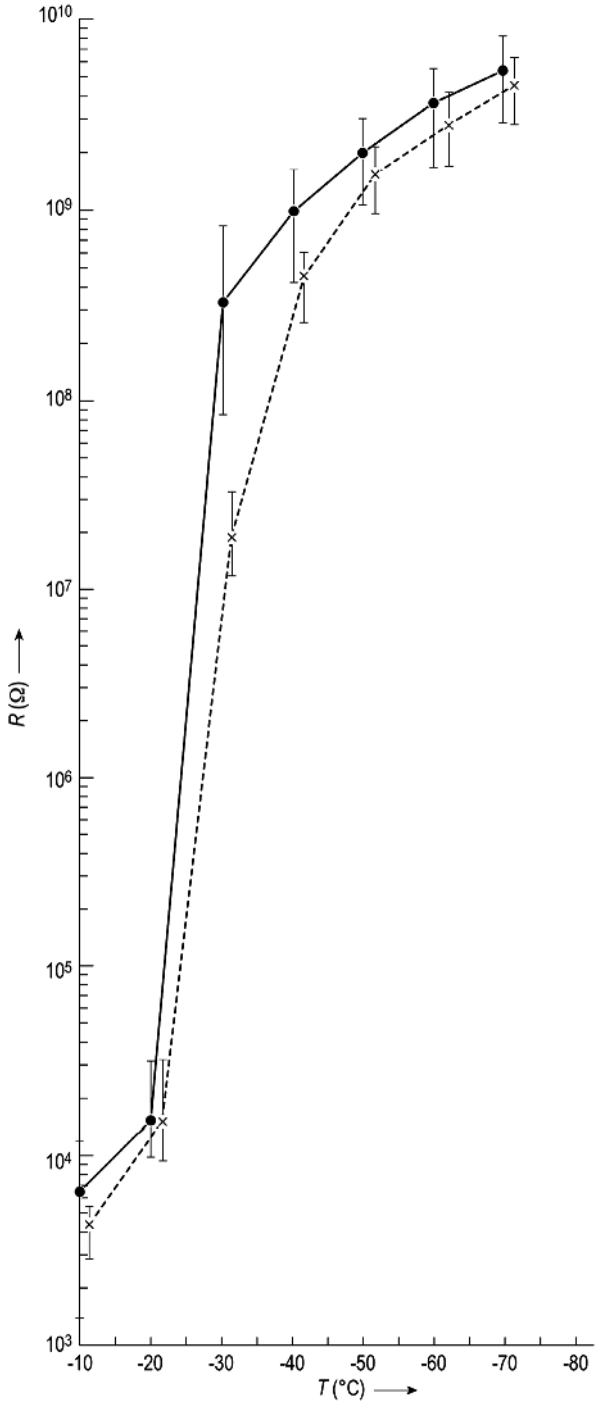

Figure 1.35 Average of 22 electrical resistance plots of 1% NaCl solution (1 °C/min cooling) from −10 to −70 °C. Solid line, cooling; vertical bars, average ± SD. Dashed line, warming; vertical bars, average ± SD.

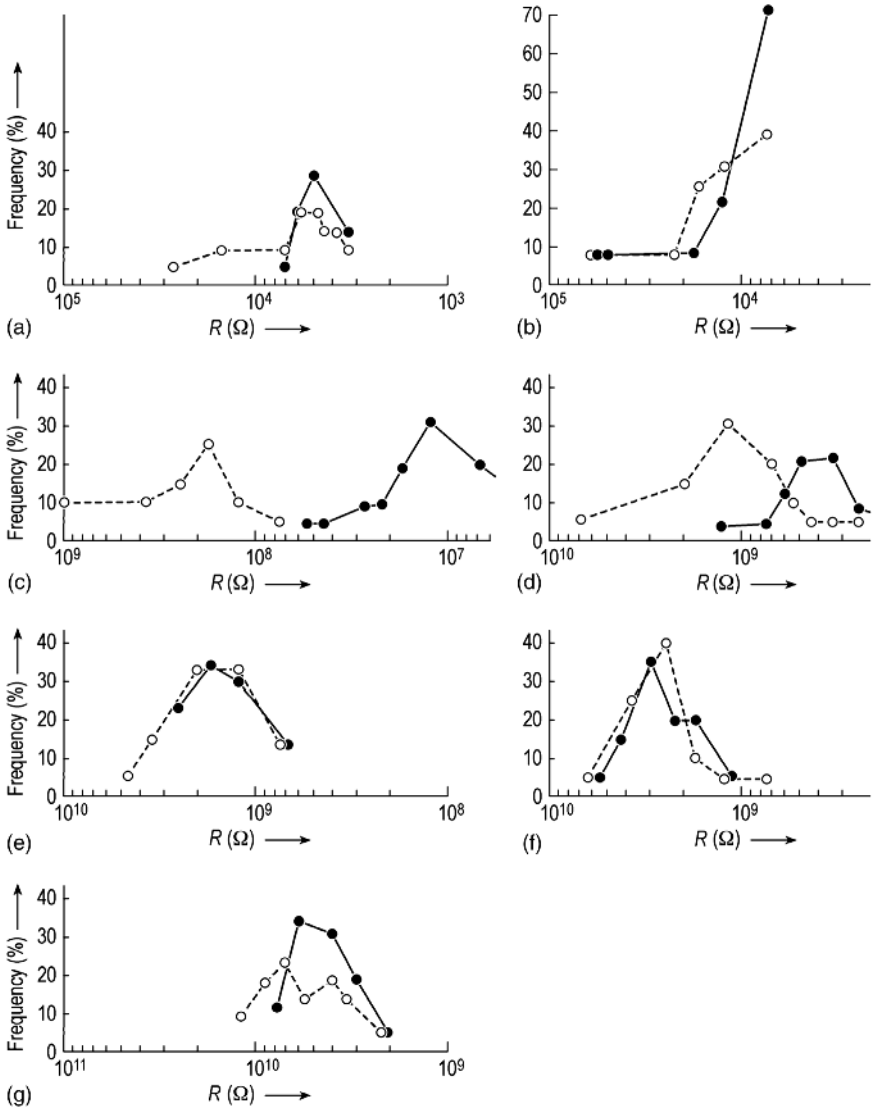

Figure 1.36 Frequency distribution (% of all measurements) of the 22 resistance measurements at (a) −10; (b) −20; (c) −30; (d) −40; (e) −50; (f) −60; (g) −70 °C. Cooling and warming as in Figure 1.35: (•) average resistance of all measurements during cooling and (×) average resistance of all measurements during rewarming.

remain smaller and more evenly distributed, and the minimum of $d(\log R)/dT$ is at −40 °C. A similar result can be seen in Figure 1.42: The difference in the freezing rate seems to be small (1 and 0.4 °C/min), but the consequences for the drying process are substantial. The temperature at the sublimation front for plot 1 should be ≃54 °C and for the product of plot 2 ≃45 °C (see the note below). As shown in Section 1.2.1, the operating pressure (p_c) for plot 1 will be in the region of 1×10^{-2}

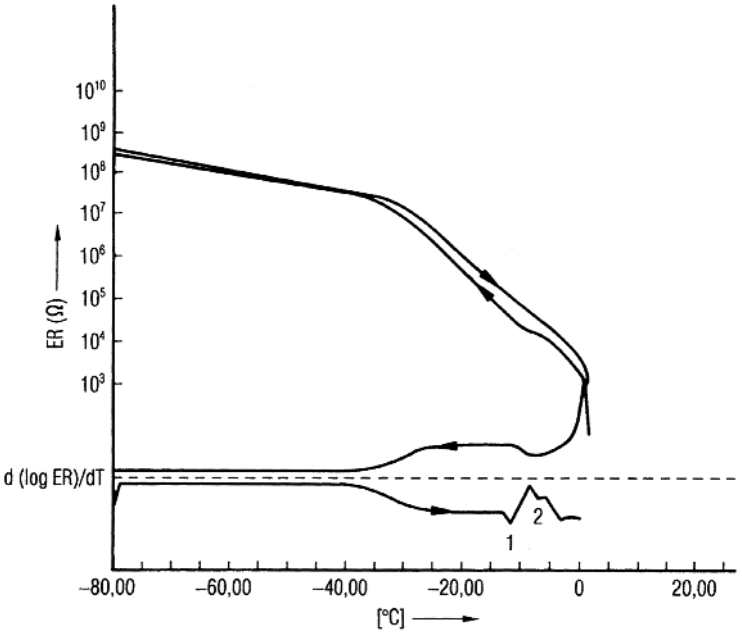

Figure 1.37 Electrical resistance of a pharmaceutical product as a function of temperature during cooling at 1 °C/min and rewarming at 3 °C/min. Heat transfer medium and product are approximately uniformly heated.

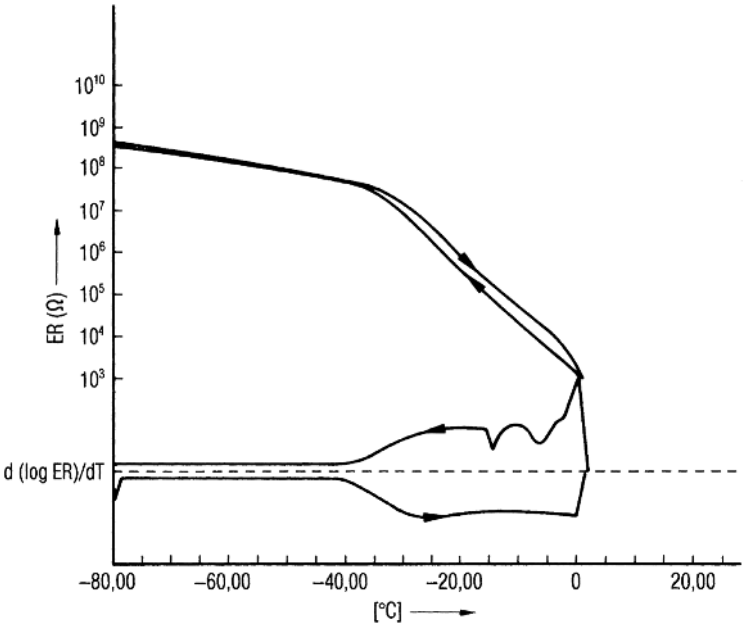

Figure 1.38 Measurement of the electrical resistance as in Figure 1.37 except that the wall of the vial is insulated by a plastic tape up to the filling height of the product. Therefore, the heat is mostly removed through the bottom of the vial (see also (Willemer, H. unpublished results, Köln)).

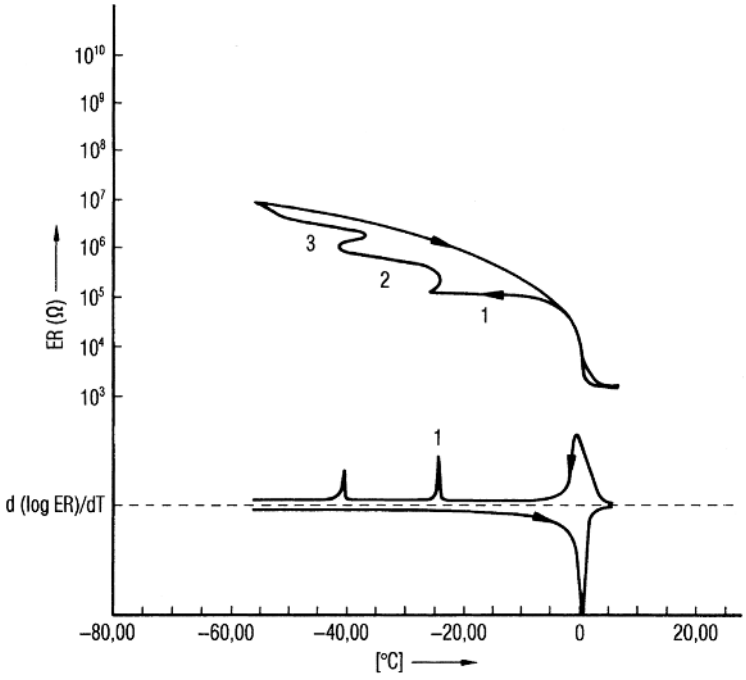

Figure 1.39 Electrical resistance as a function of temperature of a suspension cooled at 0.8 °C/min and heated at 3 °C/min. The vial is insulated as described in Figure 1.38 (see also (Willemer, H. unpublished results, Köln)).

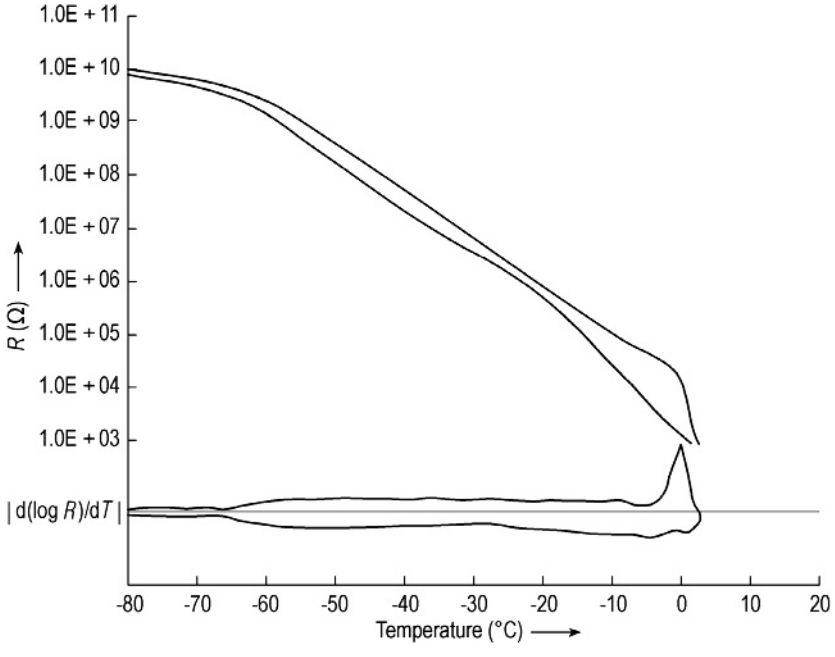

Figure 1.40 Electrical resistance of a 10% egg–albumin solution.

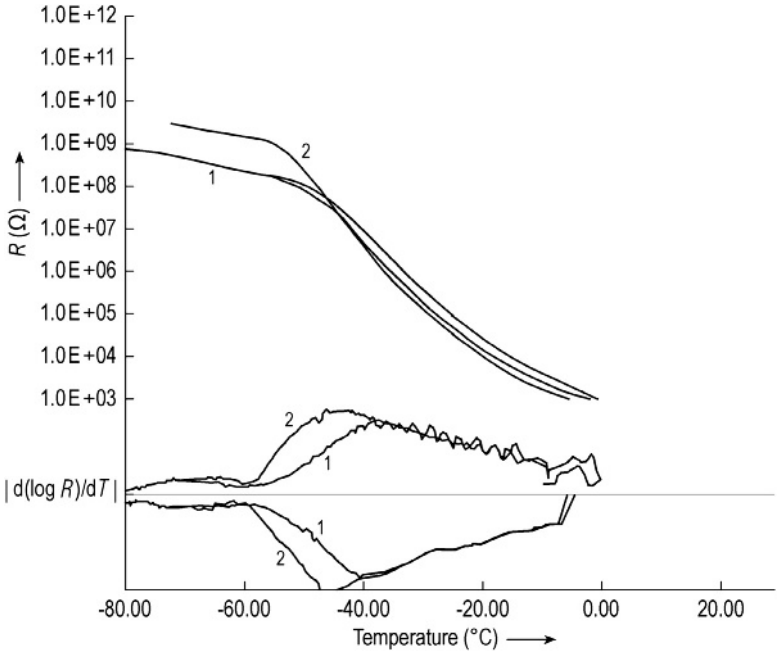

Figure 1.41 Electrical resistance of a human blood derivative. Cooling rate: (1) 14 and (2) 1 °C/min.

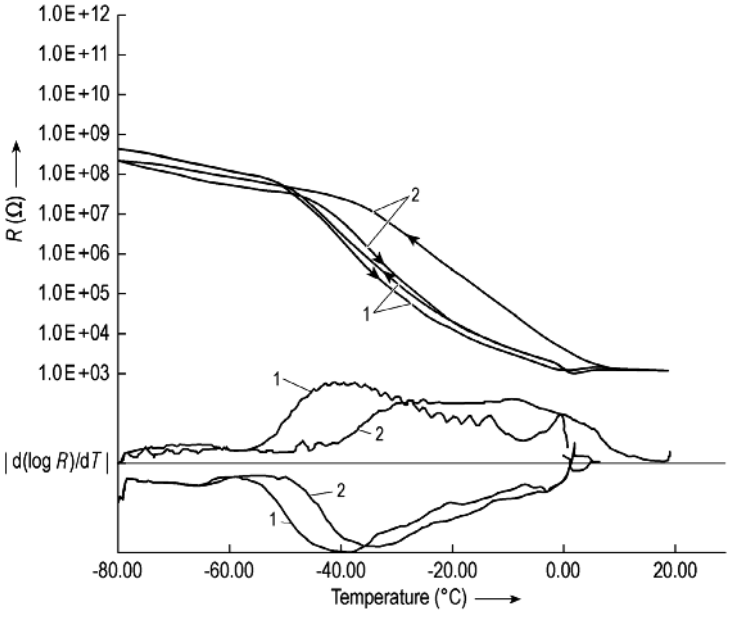

Figure 1.42 Electrical resistance of a different human blood derivative to Figure 1.41. Cooling rate: (1) 0.4 and (2) 1 °C/min.

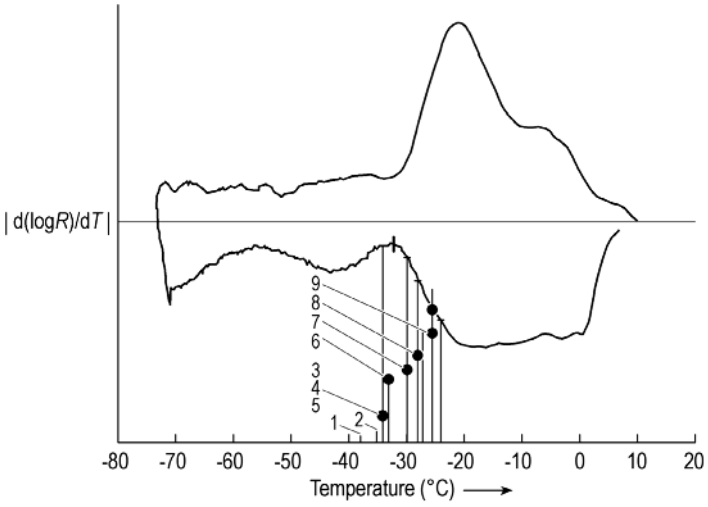

Figure 1.43 Electrical resistance of a human protein solution. The numbers 1–9 refer to photographs taken with a cryomicroscope (see text and note).

mbar and for plot 2 at $\sim 4 \times 10^{-2}$ mbar. For many production, freeze-drying installations $p_c \approx 10^{-2}$ mbar will be difficult or uneconomical to operate on, whereas 4×10^{-2} mbar is usually operable in a modern plant. The limitation will not only be in the shelf and chamber design, but also in the vapor transportation from the chamber to the condenser (Section 1.2.4). Structure analysis of the product during its development phase can help to avoid costly operations or changes later. (*Note:* Comparisons of protein ER measurements with cryomicroscope observations have led to a rule of thumb: In Figure 1.42 the $d(\log R)/dT$ plot 2 starts to change at −50 °C with a minimum at −34 °C, difference 16 °C, 1/3 of 16

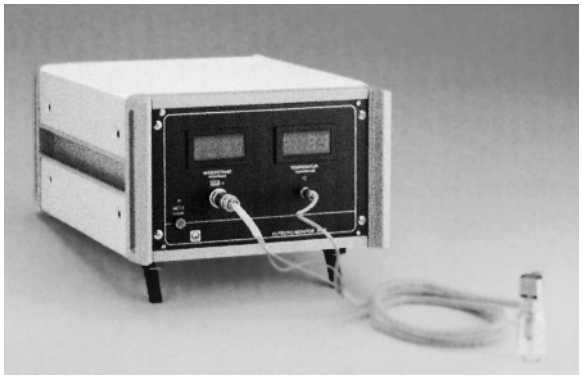

Figure 1.44 Monitor AW 2. In the foreground, right: sample vial with measuring electrodes and resistance thermometer. Behind, to the left: the control and analysis unit. The storage of LN_2 and its control valve are not shown. The resistance in the sensor head has to be large compared with the resistances to be measured, for example, 10^{11} Ω. (Steris GmbH, Hürth, Germany.)

≈ 5, stable freeze-drying should be possible at −50 °C minus 5 °C = −45 °C. With the same rule for plot 1, one arrives at −54 °C. Figure 1.43 shows the enlarged plot of d(log$R$)/dT for a different protein. With the rule, one would arrive at $T_{ice} \approx$ −28 °C. The numbers 1–9 indicate the photographs taken with the cryomicroscope. In photographs 1–7, no structure change is visible. In photographs 9 and later, the structure softens visibly. The temperature in photograph 8 is regarded as acceptable, which is between −28 and −27 °C.)

Figure 1.44 shows an instrument to measure log$R = f(T)$ and calculate d(log$R$)/dT.

1.1.5.2 Differential Thermal Analysis (DTA)

Another method to study structures during cooling and warming is differential thermal analysis (Figure 1.45). It measures the different course of temperature

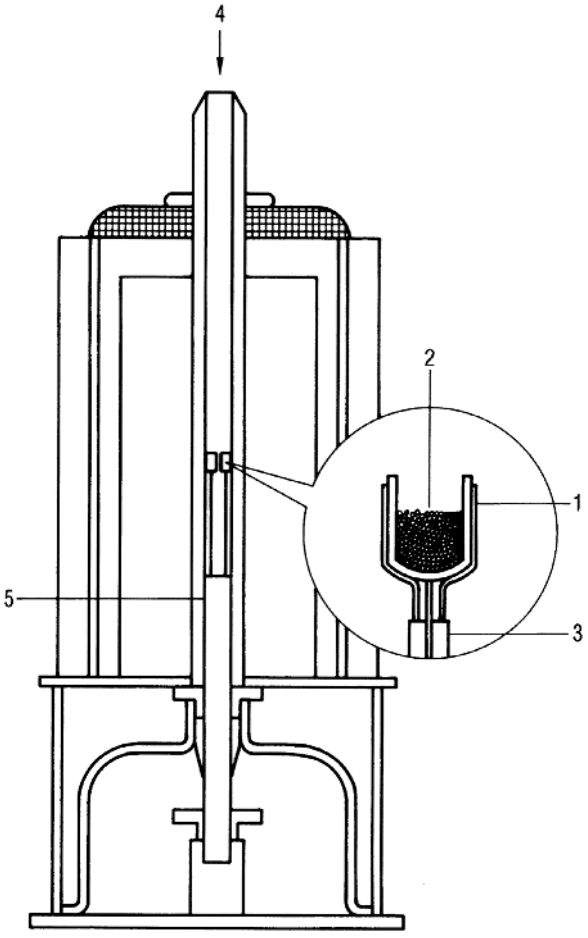

Figure 1.45 Scheme of a DTA measuring cell. 1, crucible with sample; 2, sample; 3, thermocouple (reference crucible not enlarged); 4, gas inlet; 5, ceramic support. (See also TA Instruments, New Castle, DE, USA.)

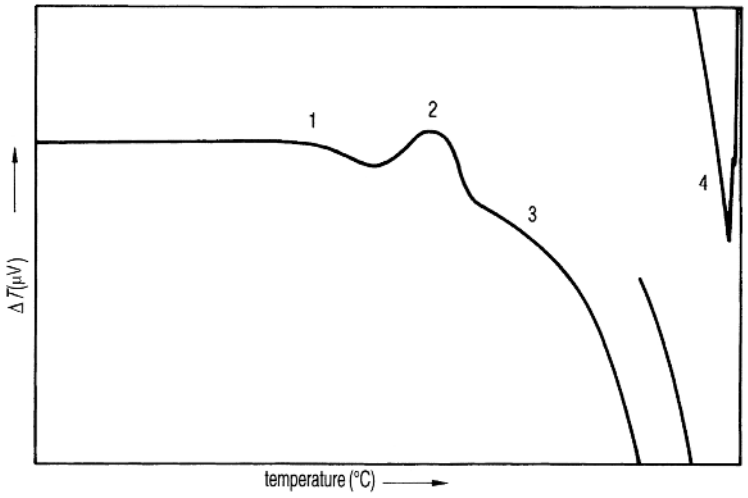

Figure 1.46 DTA measurement of a 24% sucrose–6% NaCl solution during slow rewarming after quick (200 °C/min) freezing. 1, glass transition at ≃78 °C; 2, growth of crystals (exothermic) at ≃52 °C; 3, increase of c_p, water is formed between the crystals; 4, ice melts at ≃7 °C. (See also Figure 1 from Ref. [53].)

between the sample and a probe, which changes its thermal behavior uniformly but does not have a phase transition in the measured temperature range.

Using DTA and ER measurements of quickly frozen (200 °C/min) sucrose–NaCl solutions, MacKenzie presented the different events occurring during slow rewarming [53]. Among others, two sucrose–NaCl solutions were studied: a 24% sucrose solution with 6% NaCl (sucrose:NaCl ratio = 80: 20) (Figure 1.47) and a 10% sucrose solution with 10% NaCl (ratio 1: 1) (Figure 1.48). In Figure 1.46, event

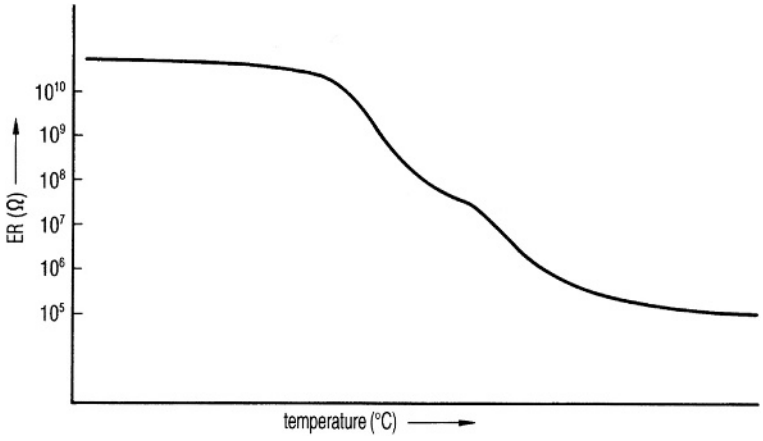

Figure 1.47 Electrical resistance (ER) measurement of the same solution as in Figure 1.46; identical temperature scale. (See also Figure 2 from Ref. [53].)

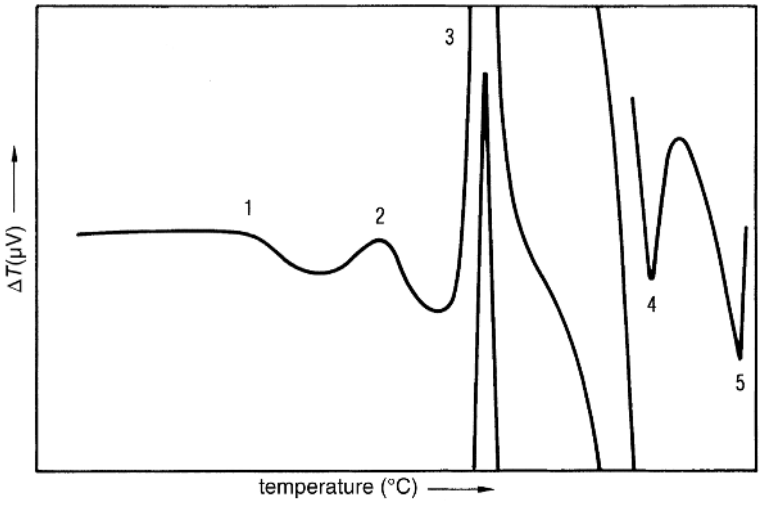

Figure 1.48 DTA measurement of a 10% sucrose–10% NaCl solution during slow rewarming after quick (200 °C/min) freezing. 1, glass transition at ≃93 °C; 2, crystal growth (exothermic) at −65 °C; 3, significant exothermic event, crystallization of NaCl at ≃44 °C; 4, eutectic melting at ≃22 °C; 5, melting of ice at ≃7 °C. (See also Figure 5 from Ref. [53].)

1 at ≃78 °C can be explained as a glass transition. In Figure 1.47, event 1 reduces the ER significantly. In event 2 at ≃50 °C, the mobility of the molecules has increased so much as to allow the growth of crystals (exothermic) and the resistance drops more slowly. At event 3, some water is formed between the crystals and c_p rises. The c_p of water is about twice that of ice. At event 4 (at ≃7 °C) the ice melts.

In Figure 1.48, event 1 is at ≃93 °C, event 2 at ≃66 °C, and the exothermic event 3 at ≃44 °C results from the crystallization of NaCl. Event 4 at ≃22 °C represents the eutectic melting and event 5 corresponds to event 4 in Figure 1.46.

In Figure 1.49, the softening of the glass phase can be seen in the change of the ER, whereas at event 2 the resistance changes more slowly, corresponding to Figure 1.48. The crystallization of NaCl can be seen from the increase in ER at event 3, which does not exist in Figure 1.47. Events 4 and 5 cannot be observed in the ER curves shown. The interpretation of ER measurements is substantially improved by using the derivative of the ER curve, as shown in Figures 1.32 and 1.34.

The results of several measurements by MacKenzie [53] are shown in Figure 1.50. The glass transition line 4 exists over the whole concentration range studied, while lines 2 and 3 are absent in the area of high sucrose and high NaCl concentrations, respectively. Later measurements proved that the mobility in the solid matrix is too reduced to observe the events during the observation time used. Only the rotation of the water molecules is still possible. With an increase in temperature (line 3), the energy increases sufficiently to allow some movements of the molecules, which can also be seen as a decrease in

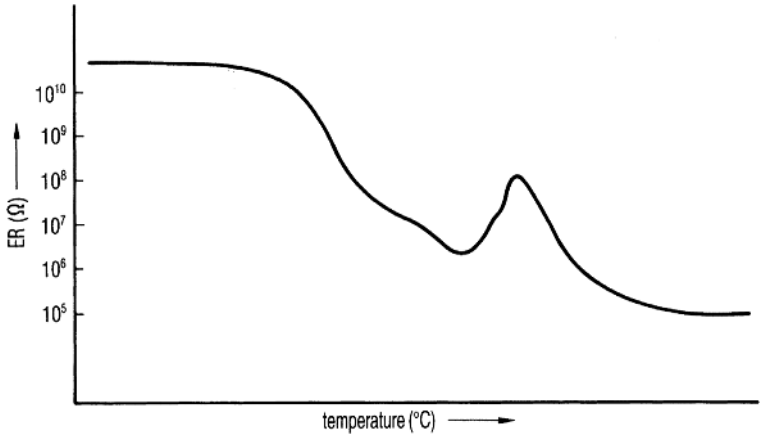

Figure 1.49 ER measurement of the same solution as in Figure 1.48; identical temperature scale. (See also Figure 6 from Ref. [53].)

ER. MacKenzie denoted this temperature "antemelting," although he subsequently suggested (note in Ref. [54] that the term should not be used, but should be replaced by "collapse temperature" (T_c, for alternative opinions on the subject, see Section 1.1.3).

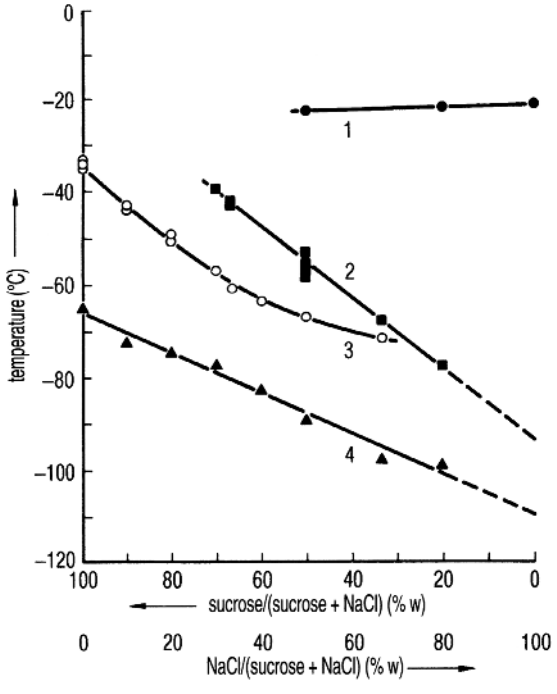

Figure 1.50 Behavior of a sucrose–NaCl solution at different sucrose–NaCl concentrations and temperatures after quick freezing (200 °C/min) during slow rewarming. (Figure 8 from Ref. [53].) 1, eutectic melting temperature of NaCl; 2, crystallization temperature of NaCl; 3, temperature at which the glass phase starts to soften; 4, glass transition temperature.

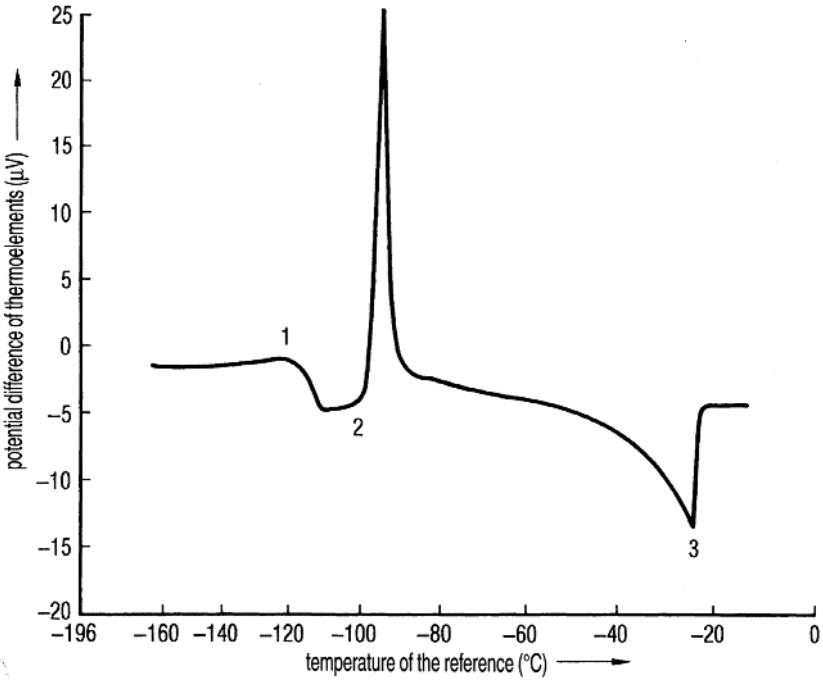

Figure 1.51 Plot of the DTA measurement of a 50% glycerin solution during slow rewarming after quick freezing at 75–200 °C/min. 1, T_g; 2, T_d; 3, T_m. (See also Figure 1 from Ref. [55].)

Another event called "incipient melting" at a temperature T_{im} is the melting of ice crystals between crystallized eutectic mixtures or the dissolution of crystals surrounded by highly concentrated inclusions, known as interstitial melting of ice. Luyet and Rasmussen [55] have studied the phase transitions by DTA of quickly frozen (75 or 200 °C/min) water solutions of glycerol, ethylene glycol, sucrose, and glucose during warming (5 °C/min). Figure 1.51 shows a typical DTA curve, if measurable amounts of amorphous product have been formed during freezing, which starts to crystallize after T'_g is exceeded at a temperature T_d (exothermic event). At the temperature T_d, one can expect a viscosity of $\sim 10^9$ P. At T'_g, the viscosity, in agreement with other authors, is on the order of 10^{13} P. This concept is shown in Figure 1.52: If the solution freezes relatively slowly (3 °C/min), all freezable water is crystallized; if the rewarming is interrupted before the melting starts and the product cooled again to, for example, −150 °C, the rewarming curves resemble that in Figure 1.52. There is no water left that can crystallize at T_d. There are only two events that are denoted (according to MacKenzie) antemelting and incipient melting.

From DTA measurements, phase diagrams can be constructed as shown for ethylene glycol in Figure 1.53. A solution of 40% ethylene glycol is only stable in the glass phase below ≃135 °C; at ≃120 °C, unfrozen water starts to crystallize, at ≃65 °C recrystallization is observed, and at ≃45 °C, melting will start. As recrystallization is the growth of existing crystals and not the nucleation of new ones, this event cannot be detected by DTA, but can be observed under a microscope when a transparent area becomes opaque.

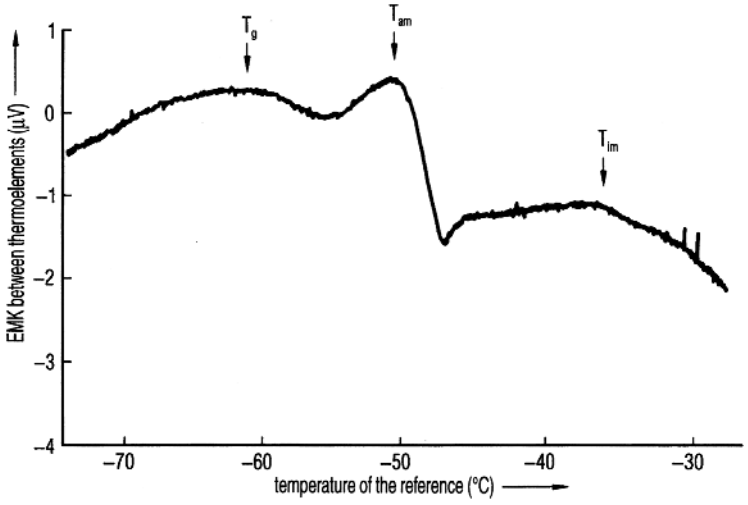

Figure 1.52 DTA plot of a 50% glucose solution, frozen at 3 °C/min during rewarming. T_g, start of devitrification; T_{am}, start of ante-melting; T_{im}, start of incipient melting. (See also Figure 1 from Ref. [56].)

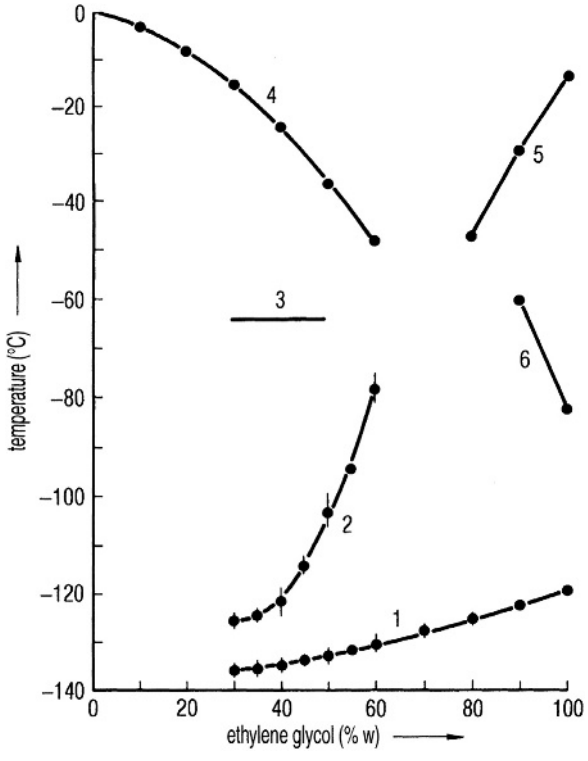

Figure 1.53 Phase diagram of ethylene glycol, in which the following events are shown: 1, glass transition; 2, devitrification; 3, recrystallization; 4, melting; 5 and 6, devitrification and melting of ethylene glycol. (See also Figure 4 from Ref. [55].)

1.1.5.3 Cryomicroscopy

Hsu *et al.* [57] observed recrystallization on the recombinant CD4-IgG with a cryomicroscope cooled to −60 °C by a cascade of four Peltier modules. The observation cell can also be evacuated for freeze-drying studies.

Willemer [52] compared ER measurements with photographs made by a cryomicroscope, a scheme of which is shown in Figure 1.54. ER measurements of complex products are sometimes difficult to interpret. Figure 1.55 shows the ER curve of a cryoprotectant solution for a virus. The solution freezes partially by cooling to −10 °C, subcools thereafter down to ≃46 °C, and crystallizes at ≃65 °C. Upon rewarming, the resistance changes rapidly at ≃32.5 °C. The photographs taken using a cryomicroscope show at −40 °C a uniform structure in both the already dried and the frozen parts. At −30 °C, both parts show a mix of dark and gray zones, indicating that some ice is melted and is also diffused into the dried part. In such cases, ER measurements can be used as a relatively quick method to study the influences of different CPAs, varying their concentrations and selecting an optimal freezing rate. The finally selected combination can be tested in the cryomicroscope. Figures 1.56–1.58 show the structural changes of a pharmaceutical product in a cryomicroscope during freezing, during the thermal treatment, and before drying. Figures 1.56–1.58 are from one experiment showing different details in one sample. Figure 1.56a is during quick cooling at ≃25 °C, Figure 1.56b during first warming from −50 to ≃35 °C, and Figure 1.56c during second cooling at −50 °C. In Figure 1.56a, the crystals (dark) are mostly uniformly distributed between the amorphous concentrated solids (lighter color). In Figure 1.56b, the crystals have grown and some water from the concentrate has crystallized. In Figure 1.56c, the boundaries between crystals and glass inclusions are more clearly visible, especially in the upper right corner. In Figure 1.57, another part of the microscope sample close to the border of the samples is shown at comparable temperatures: (a) at ≃23 °C, (b) during first warming at ≃30 °C, and (c) after second cooling at −60 °C. In Figure 1.57b, the crystals have grown without much change in their general structure, especially in the upper left corner. In Figure 1.57c, the boundaries between crystals and glass have become clearer.

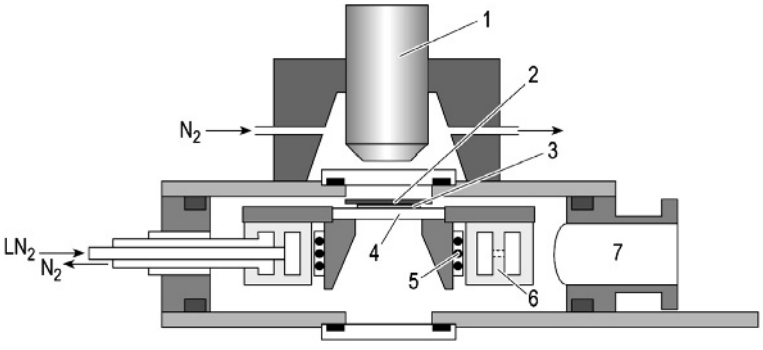

Figure 1.54 Scheme of a cryomicroscope. 1, objective of the microscope; 2, cover-glass; 3, sample; 4, sample support; 5, electrical heating; 6, cooling chamber with LN_2 connection; 7, vacuum connection. (See also Figure 1 from Ref. [52].)

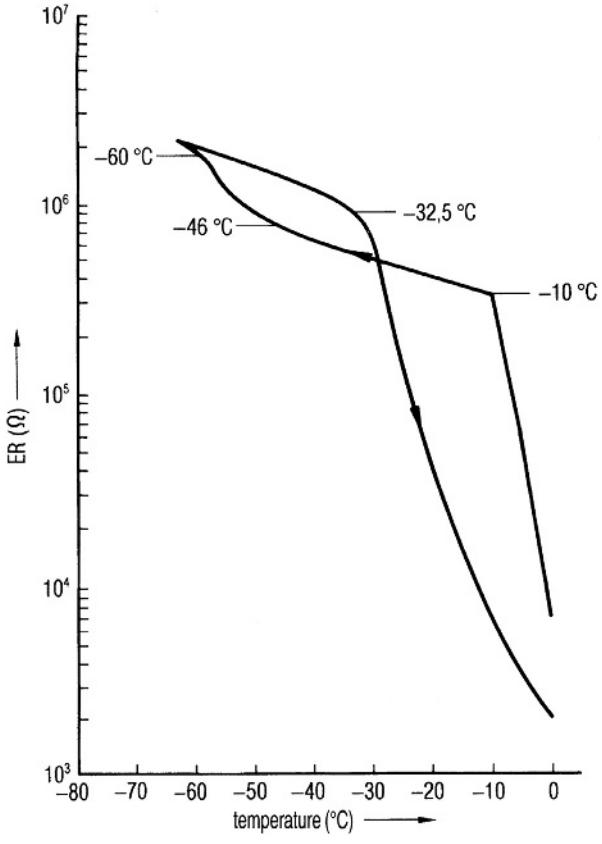

Figure 1.55 Electrical resistance as function of temperature during cooling and rewarming of a virus suspension. The suspension subcools from −10 to ≃46 °C and freezes at −60 to −65 °C. During rewarming, the resistance drops clearly at ≃33 °C. This product should be freeze-dried at $T_{ice} = -40$ °C or slightly higher. (See also Figure 7 from Ref. [52].)

Figure 1.58 represents a third part of the sample: (a) after cooling to −65 °C and (b) after thermal treatment, a second cooling to −60 °C and the beginning of freeze-drying at −40 °C. Again the overall structure has not been changed by the thermal treatment, but the structure of the crystals is clearer, indicating that water molecules between the glass phase and the crystals have migrated to the crystals. The photographs in Figure 1.57 show that the quick freezing does not produce a uniform structure throughout the sample; it is influenced by boundary effects. Nevertheless, the effect of thermal treatment can be seen in all parts of the sample. Figure 1.59 shows the effect of crystal growth without thermal treatment during the temperature rise from the end of freezing (−60 °C) to the beginning of drying at −42 °C. This is of interest during automatic loading on cold shelves. The product in the first vials loaded will have a structure different from those loaded, for example, 2 or 3 h later.

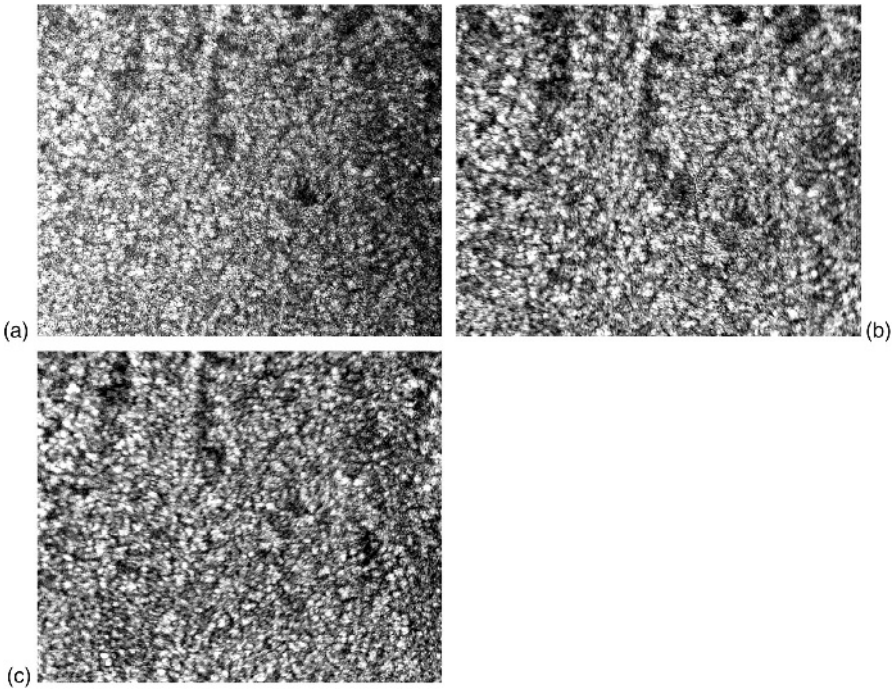

Figure 1.56 Cryomicroscope photograph of a pharmaceutical product frozen at a rate of ~4 °C/min: (a) during cooling at ≃24 °C; (b) after cooling to −54 °C and thermal treatment (TT) at −36 °C; (c) after cooling again to −55 °C. (Steris GmbH, Hürth, Germany).

Cryomicroscope studies have the advantage of showing pictures of the structural changes and the frozen product can be freeze-dried in most instruments. The product layer is very thin and the product is quickly frozen. The behavior of the product during warming and drying therefore corresponds exactly only to a quickly frozen product. To simulate a thermal treatment is difficult because of the thin layer. However, experience shows that critical temperatures taken from such studies are valuable, especially if they are supported by, for example, ER data of a more slowly frozen product.

Nunner [58] photographed with a special cryomicroscope the changes of the planar front of 0.9% NaCl solution during directional freezing in 360 s to a stable dendritic ice structure (Figure 1.60). The concentrated NaCl (dark border) can be seen on the surface of the ice crystals.

A cryomicroscope that permits quantitative evaluation of the pictures was described by Cosman *et al.* [49]. The unit has four distinctive features:

- Temperature generation, measurement, and control are programmable.
- The picture of the microscope is documented for later use.
- The documentation can be partially used for automatic picture recognition.

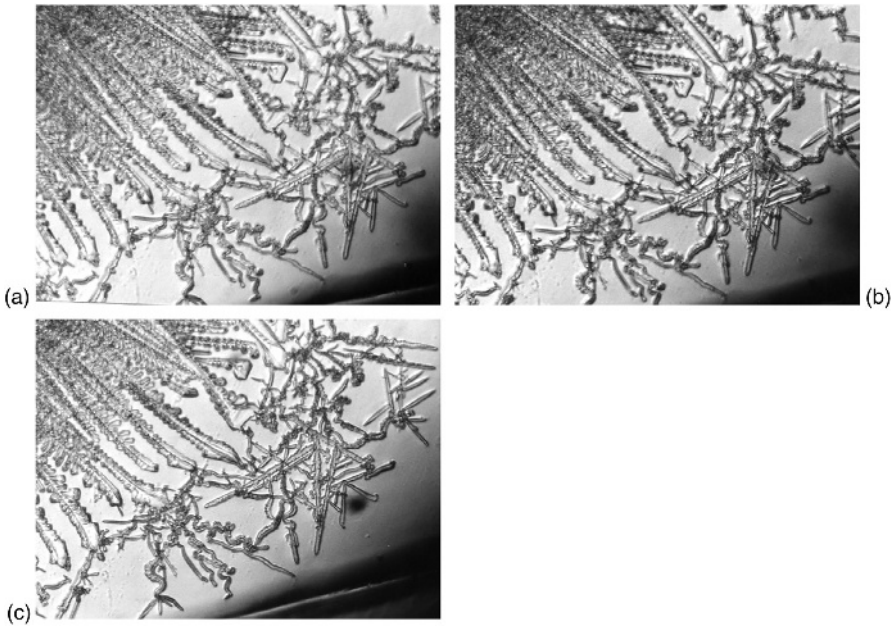

Figure 1.57 As Figure 1.56, showing a different part of the sample, close to the border: (a) during freezing at ≃24 °C; (b) after cooling to −54 °C and TT at −36 °C; (c) after cooling again to −60 °C. (Steris GmbH, Hürth, Germany.)

- The amount of data can be reduced in such a way that a freezing process can be described mathematically and the behavior of cells predicted.

Figure 1.61 shows the layout of the system. By the use of a very good heat-conducting sapphire window and a cooling system with LN_2, the authors achieved cooling rates of several hundred degrees per minute down to −60 °C and temperature gradients in the sample of 0.1 °C at a temperature of ∼0 °C.

Three examples will show how freezing processes can be studied quantitatively and documented using this microscope system. Figure 1.62 shows the change in volume of an isolated islet cell of a mouse as a function of temperature. The

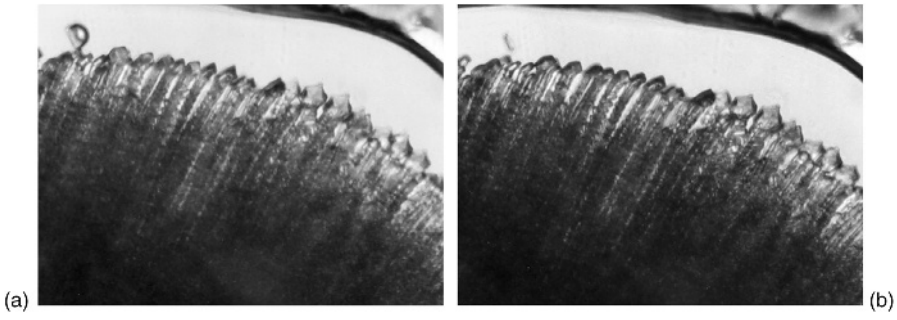

Figure 1.58 As Figure 1.56, showing a third part of the sample: (a) after freezing to −64 °C; (b) after TT at the beginning of drying at ≃45 °C. (Steris GmbH, Hürth, Germany.)

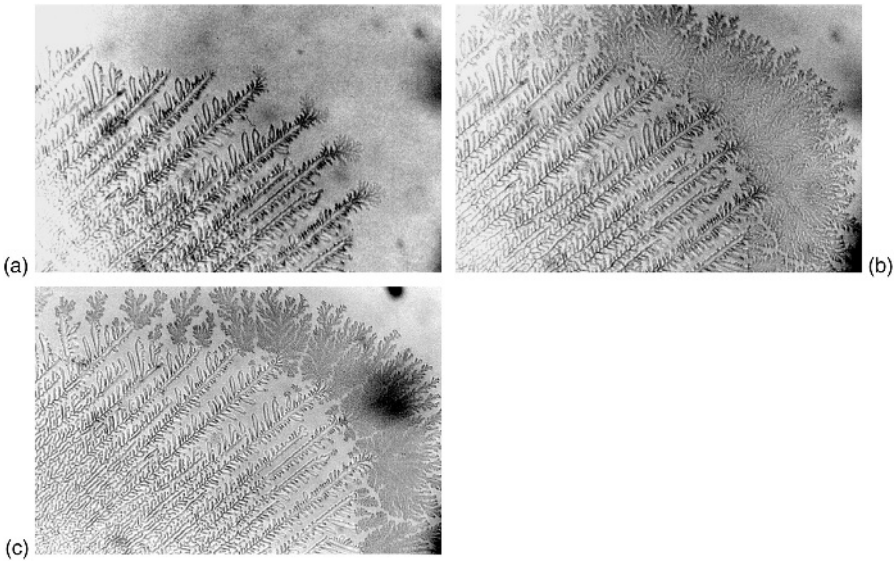

Figure 1.59 Cryomicroscope photograph of a pharmaceutical product (different from Figure 1.56) frozen at a rate of ~4 °C/min without TT: (a) cooled to −60 °C; (b) during warming for drying at −48 °C, the recrystallization of unfrozen water is visible; (b) at −42 °C, the softening of the structure starts, especially in the left lower corner and the newly formed crystals start to disappear. The product frozen at this rate should be thermally treated. (Steris GmbH, Hürth, Germany.)

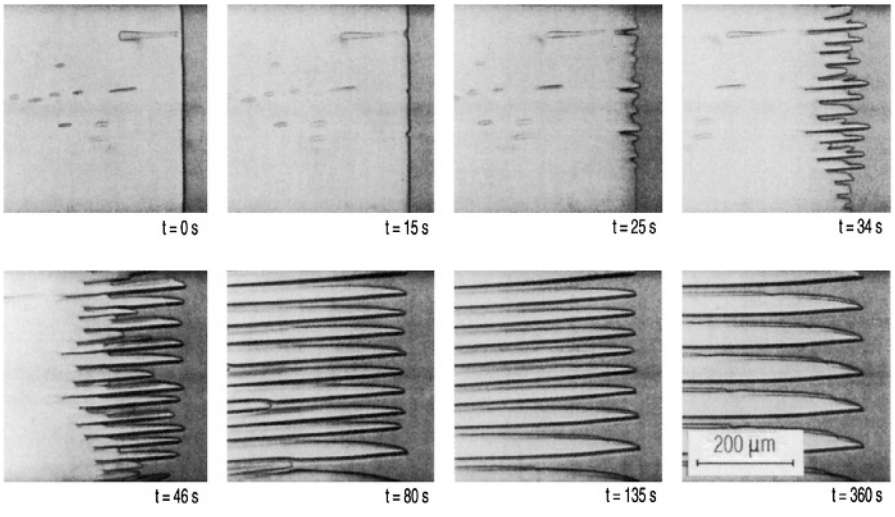

Figure 1.60 Change of the planar front of ice ($t = 0$ s) through an unstable phase ($t = 34$ s) into a dendritic structure. A 0.9% NaCl solution is directionally frozen in a temperature field having a gradient of 67 K/cm. The sample is moved at a rate of 15 µm/s through the temperature field. (From Ref. [58].)

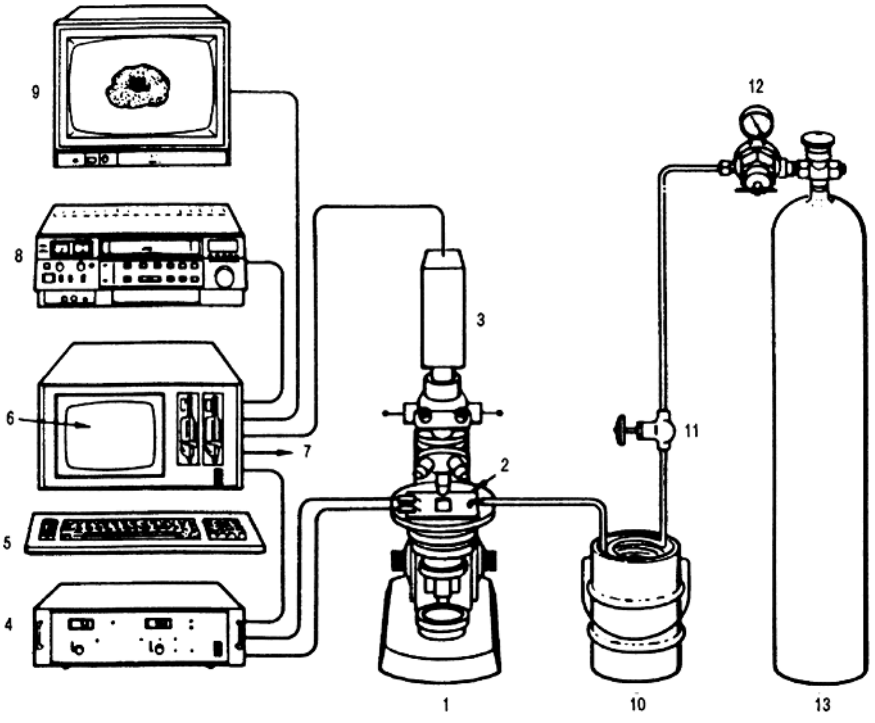

Figure 1.61 Scheme of a cryomicroscope research system. 1, microscope; 2, cryostat; 3, video camera; 4, temperate control; 5, keyboard; 6, menu display; 7, printer connection; 8, video recorder; 9, video monitor; 10, Dewar flask with LN_2; 11, metering valve; 12, pressure reducer; 13, N_2 cylinder. (See also Figure 1 from Ref. [49].)

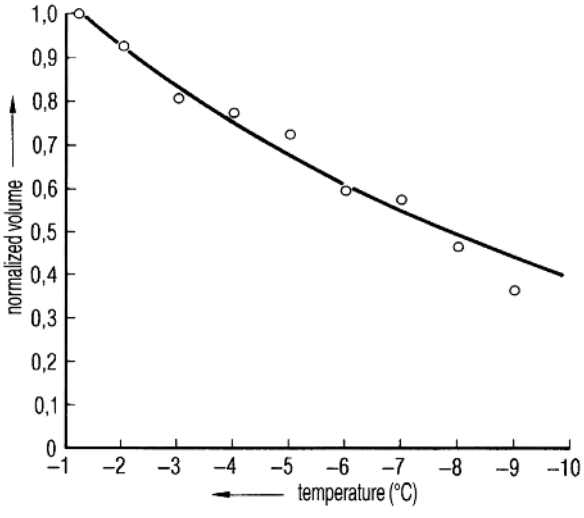

Figure 1.62 Volume change as a function of temperature of an insulated islet cell of a mouse. (See also Figure 4 from Ref. [49].)

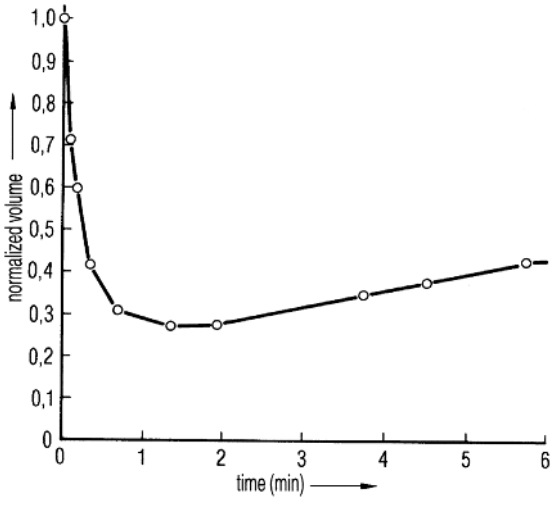

Figure 1.63 Volume changes of oocytes of rhesus monkeys as a function of the time elapsed after their exposure to 10% dimethyl sulfoxide solution. (See also Figure 6 from Ref. [49].)

different permeabilities of cell membranes for H_2O and CPAs are important for freezing of cells, as Figure 1.63 shows.

The volume of oocytes of a rhesus monkey placed in 10% v/v DMSO is reduced to almost one third, since the water can diffuse out of the cell into the surrounding, but the DMSO cannot enter the cell during the same time (measured at 23 °C).

The nucleation of ice in the cell is considered as the cause of cell damage. Figure 1.64 indicates in how many mouse oocytes intracellular ice is found as a

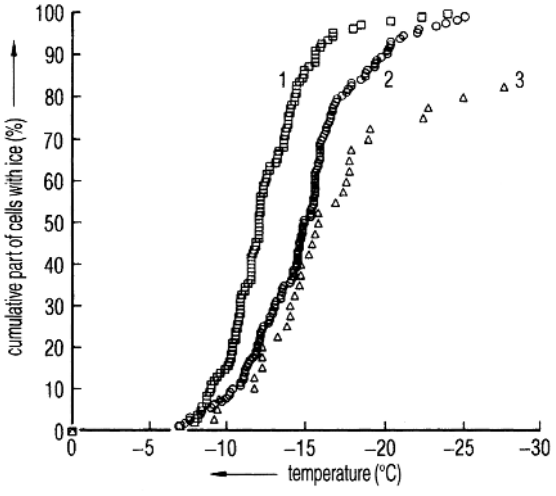

Figure 1.64 Cumulated abundance of intercellular ice forming in mice oocytes as a function of temperature with three different cooling rates: 1, 111 oocytes at 120 °C/min; 2, 132 oocytes at 5 °C/min; 3, 34 oocytes at 3.5 °C/min. (See also Figure 9 from Ref. [49].)

function of temperature at different cooling rates. In hepatocytes of rats, no ice could be detected during cooling to −21 °C up to a cooling rate of ∼40 °C/min, whereas at a rate of 140 °C/min practically all cells contained ice. The water did not have sufficient time to diffuse into the surrounding and froze in the cells. Figure 1.64 also demonstrates how the intracellular nucleation of ice depends on the absolute temperature and cooling rate: At ≃25 °C and a rate of 5 °C/min, practically all cells contain ice, whereas at 3.5 °C/min, ∼20% of the cells were without ice.

Dawson and Hockley [59] used scanning electron microscopy (SEM) to show the morphological differences between quick (150 °C/min) and slow (1 °C/min) freezing of trehalose and mannitol solutions. Figure 1.65 shows the surface of (a) a slowly and (b) a quickly frozen center part of a 1% trehalose solution. On the slowly frozen sample (c), a cracked surface can develop by concentrated solids, whereas the structure in the quickly frozen sample is amorphous and fibrous. Figure 1.66 shows the (a) coarse and (b) fine structure in the center part of

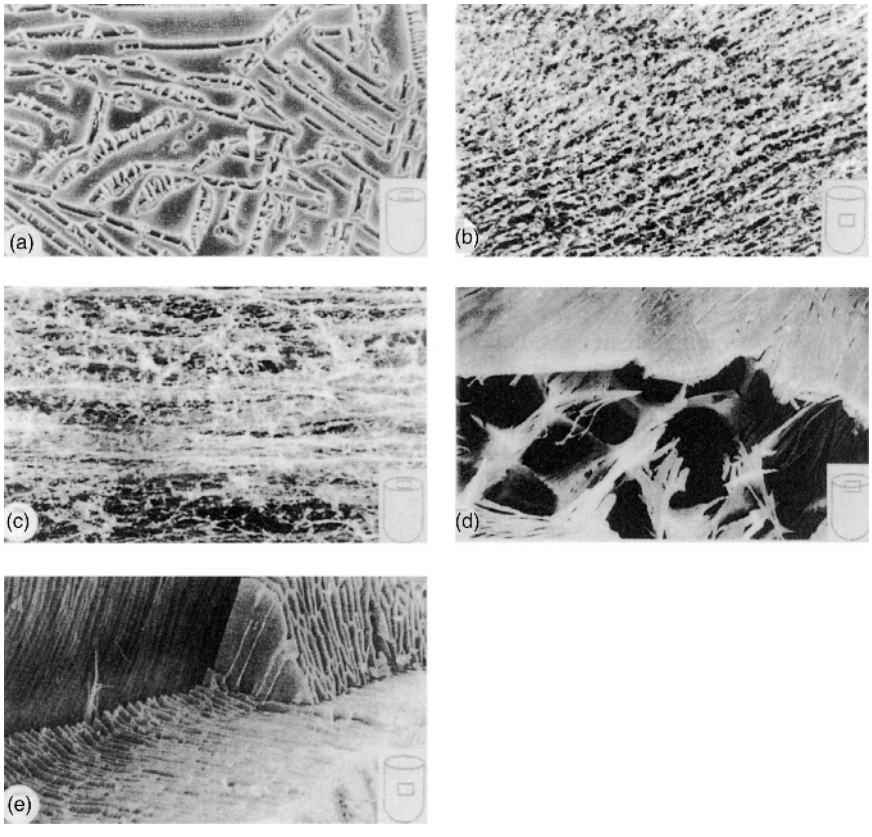

Figure 1.65 Photographs of different freeze-dried products obtained by scanning electron microscopy. (a) 1% trehalose solution, 1 °C/min, cut out of the surface. (b) 1% trehalose solution, 150 °C/min, cut out of the center. (c) 1% trehalose solution, 1 °C/min, cut out of the uppermost surface. (d) 1% mannitol solution, 1 °C/min, shows sugar crystallization. (e) Serum, 150 °C/min, morphology similar to plasma. (See also part of Figure 1 from Ref. [59].)

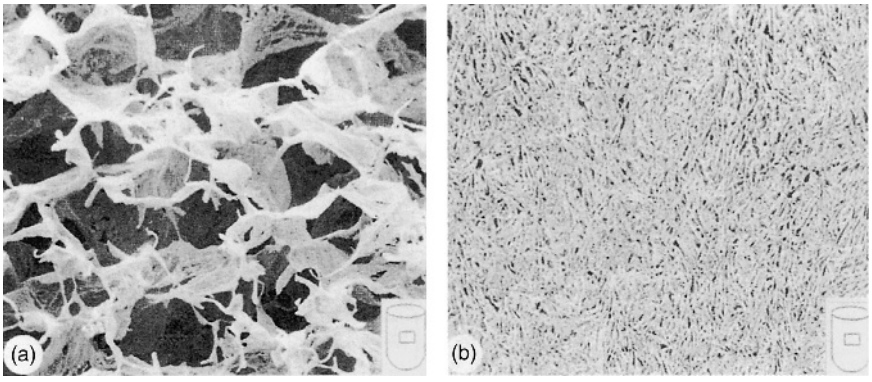

Figure 1.66 Photographs of a 1% lactose solution by scanning electron microscopy: (a) with 1 °C/min and (b) with 150 °C/min frozen. (See also Figure 3 from Ref. [59].)

(a) slowly and (b) quickly frozen 1% lactose. A collapsed part of a trehalose solution can be found in Figure 1.67a, while Figure 1.67b shows the dried product stored with too high a moisture content for 6 months. The pictures prove that different freezing rates will result in different structures and may concentrate solids on the surfaces, which reduces the drying speed or prohibits a low residual moisture content during drying.

1.1.5.4 Freeze-Dry Microscopy

Freeze-drying is still the method of choice to achieve improved stability of biopharmaceuticals when the product is not sufficiently stable in liquid formulation. Meister and Gieseler [60] used a freeze-drying microscope system consisting of a Zeiss Axio Imager.Al (Carl Zeiss MicroImaging, Goettingen, Germany) with a

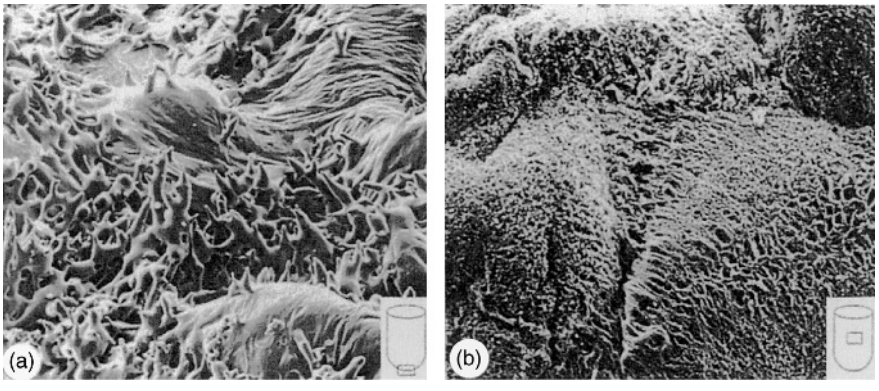

Figure 1.67 Photographs of trehalose solution freeze-dried in a vial, obtained by scanning electron microscopy. (a) Collapsed product from the bottom of the product. (b) Shrunk product after 6 months of storage at +20 °C with a too high RH and stored at too high a temperature. (See also Figure 6 from Ref. [59].)

lambda plate plus spectrum analyzer and an FDCS freeze-drying stage (Linkam Scientific Instrument, Surrey, UK) with a liquid nitrogen cooling system and a programmable temperature controller.

Abstract: The purpose of this study is to investigate the change of collapse appearance and temperature of protein/sugar mixtures as a function of nucleation temperature (T_a), sublimation velocity (V_{sub}), and the sugar/protein mole ratio when performing freeze-drying microscopy experiments.

HSA (human serum albumin) and BSA (bovine serum albumin) were used as samples, proteins were mixed with either sucrose or trehalose. Sucrose and trehalose are the most commonly used stabilizers for protein pharmaceuticals.

Differential scanning calorimetry (DSC) was used to determine the corresponding glass transition temperature (T'_g). To allow a more representative comparison between these analytical methods, a collapse midpoint temperature (T_c-50) was introduced. While there was no distinct correlation between T_a and the onset of collapse (T_{oc}) for either mixture, V_{sub} was found to correlate with the measured collapse temperature that is important for comparability of experiments. Application of the Gordon–Taylor equation failed to predict the critical temperature for any of the protein/sugar mixtures studied. (© 2008 Wiley-Liss, Inc. and the American Pharmacists Association, *J. Pharm. Sci. 98*, 3072–3087, 2009).

Applications: A well-designed freeze-drying cycle forms a glassy solid that can minimize degradation reactions of complex structures such as proteins or peptides and may provide acceptable shelf life for worldwide shipping and storage. It was estimated that more than 200 new antibody products are currently in development, many of them in a lyophilized form. However, formulation and cycle development become challenging if protein therapeutics require a large amount (>50 mg/mL) of active ingredients in the formulation to achieve the desired therapeutic effect.

Recent emphasis within the FDA on manufacturing sciences and practical analytical technology (PAT) encourages the pharmaceutical industry to further optimize and improve current freeze-drying processes and to design new cyc1es that are robust and economical.

1.1.5.5 Differential Scanning Calorimetry (DSC)

Differential scanning calorimetry measures the energy absorbed (endotherm) or produced (exotherm) as a function of time or temperature. It is used to characterize melting, crystallization, resin curing, loss of solvents, and other processes involving an energy change. Differential scanning calorimetry may also be applied to processes involving a change in heat capacity such as the glass transition, for example, glassmaking.

Meister and Gieseler [60] used DSC (Figures 1.68–1.70) to evaluate the critical temperature to characterize thermal transitions such as glass transitions (T_g), eutectic melting points (T_{eut}), and the glass transition temperature of the maximally freeze-concentrated product (T'_g). FDM is a better measure of collapse in a product that has been widely used in more recent years; here a user visually measures via microscopy the collapse temperature (T_c) of a given product during primary drying.

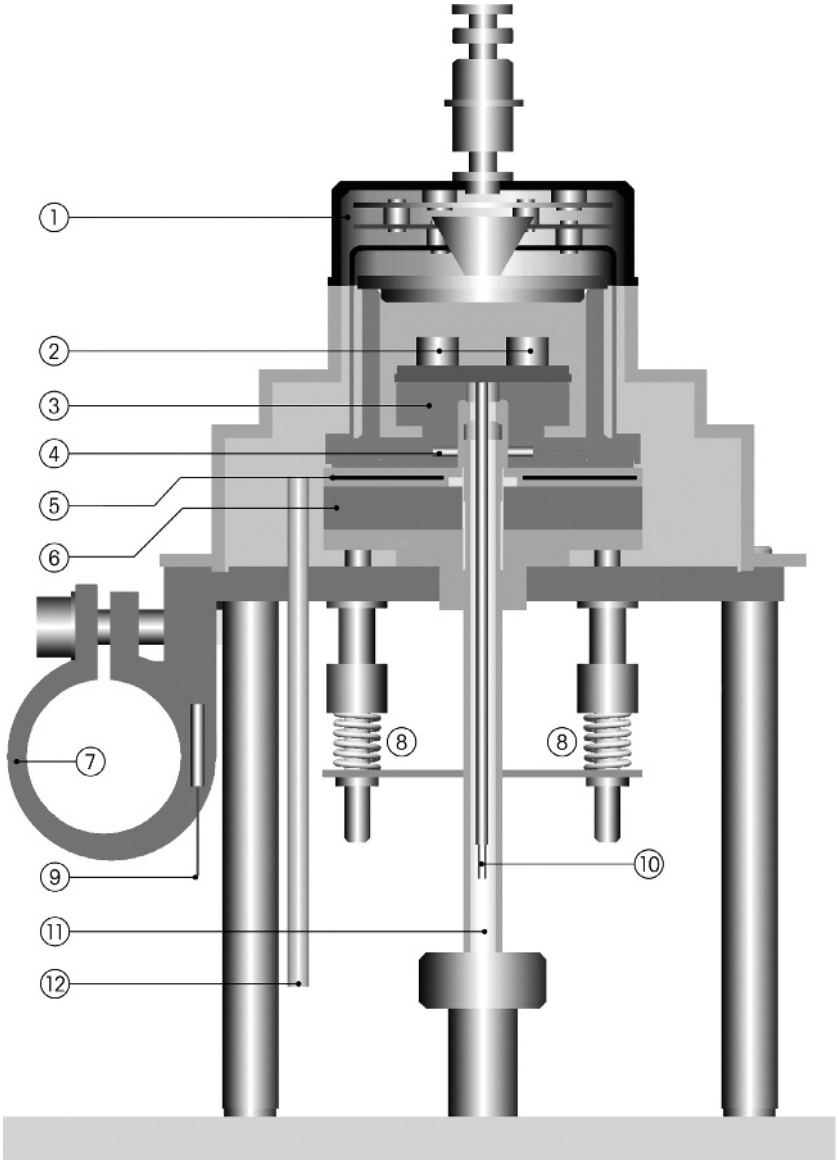

Figure 1.68 Schematic drawing of a DSC 3+ instrument: 1, furnace lid; 2, crucibles on the DSC sensor; 3, silver furnace; 4, PT100 of furnace; 5, flat heater between two insulating disks; 6, thermal resistance for cooler; 7, cooling flange; 8, compression spring construction; 9, cooling flange PT100; 10, DSC raw signal for amplifier; 11, purge gas inlet; 12, dry gas inlet. (Mettler-Toledo GmbH, Gießen, Germany.)

It is important to emphasize that the two technologies do not use the same experimental conditions to describe the physical property parameters, that is, the maximum allowable product temperature for primary drying. With DSC, it is an apparent glass transition temperature (T'_g) that is measured, which is commonly

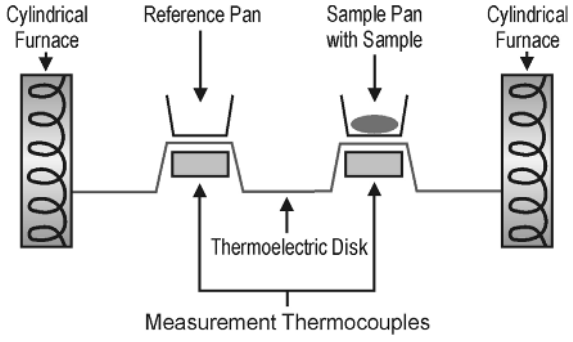

Figure 1.69 Scheme of a commercial apparatus for DSC measurements. The sample is placed in an aluminum pan. The sample pan and an empty reference pan are placed on small platforms within the DSC chamber. (See also Q100 DSC, TA Instruments, New Castle, DE, USA).

Figure 1.70 The DSC 3+ replaces the modulated DSC® apparatus, Model Q 1000, using the details of Figure 1.68. (Mettler-Toledo GmbH, Gießen, Germany.)

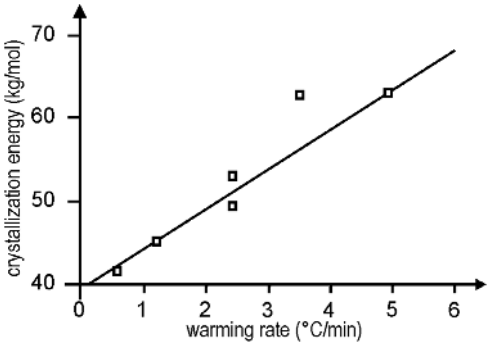

Figure 1.71 Crystallization energy of Na-cefazolin as function of the warming rate, measured by DSC.

described as the glass transition of a maximally freeze-concentrated solution. This transition appears as an endothermic shift in heat capacity that arises from a decrease of the viscosity of the glassy structure in a small temperature range, which in turn allows the system to access additional degrees.

Gatlin [61] measured not only T'_g for mannitol and Na-cefazolin by DSC, but also the dependence of the exothermic crystallization energy on the rewarming rate (Figure 1.71). The crystallization energy, extrapolated to a warming rate of zero, was calculated for mannitol (13.5 kJ/mol) and for Na-cefazolin (39.1 kJ/mol). These values agree with measurements by other methods. The activation energies were calculated with certain assumptions to be 335 kJ/mol for mannitol and 260 kJ/mol for Na–cefazolin. DeLuca [62] derived slightly different data: at a warming rate of 0.625 °C/min, he found 16.3 kJ/mol for mannitol and 41.8 kJ/mol for Na-cefazolin.

Na-cefazolin is unstable in its amorphous state. Takeda [63] described a method to ensure complete crystallization in which microcrystalline Na-cefazolin was added to supersaturated Na-cefazolin solution at 0 °C, frozen, and freeze-dried. The product did not contain amorphous or quasi-crystalline components.

Roos [64] measured T'_g of fructose and glucose by DSC and showed the influence of annealing/heat treatment. In Figure 1.72, DSC curves are shown for 60% solutions, cooled at 30 °C/min to −100 °C and rewarmed at a rate of 10 °C/min to −48 °C and cooled again to −100 °C at a rate of 10 °C/min. T_g of the nonannealed products were −85 and ≃88 °C, respectively. In the region of −50 °C, the crystallization of unfrozen water was seen as an exothermic event in both solutions (curves A). If rewarming was interrupted at ≃48 °C, the product remained at that temperature for ∼15 min (thermal treatment) and cooled again to −100 °C; the curves B were measured during warming: T'_g was increased to ≃57 °C, the exothermic of crystallization had disappeared, and all freezable water was frozen to ice. The temperature T_m is the onset temperature of the softening process in the product.

Talsma *et al.* [65] described the freezing behavior of certain liposomes by DSC measurements. Besides the expected influences of freezing and rewarming rates, and of the CPAs (mannitol and mannitol in tris buffer solutions), it was shown that heterogeneous and homogeneous crystallization in mannitol solutions exist and the nucleation of ice depends also on the liposome size: In small liposomes

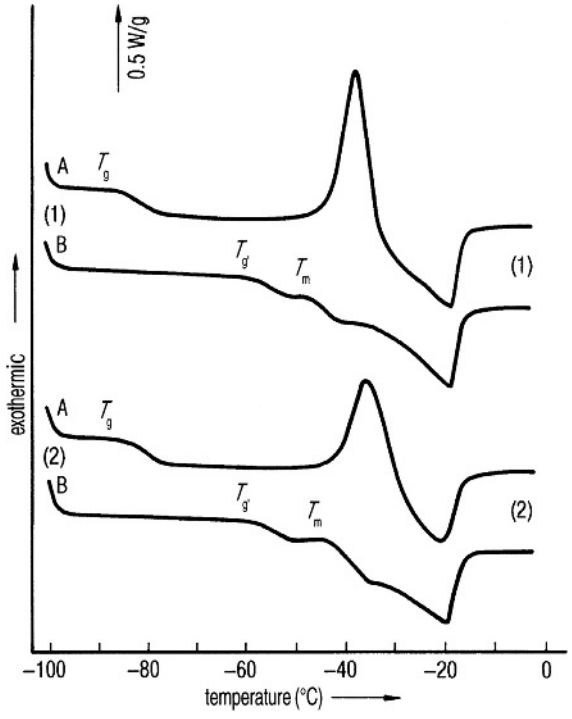

Figure 1.72 Results of annealing (thermal treatment) on the formation of ice in (1) 60% fructose and (2) 60% glucose solution. A: After cooling at 30 °C/min to −100 °C, the DSC plots were recorded during rewarming at 5 °C/min. $T_g \sim -85$ and −88 °C, respectively. At ≃48 and −44 °C, respectively, ice crystallization clearly starts, followed by the beginning of melting of ice (during freezing only part of the water has been crystallized). B: After cooling to −100 °C, the product was warmed at 10 °C/min to −48 °C, kept for 15 min at this temperature (thermal treatment), again cooled at 10 °C/min to −100 °C, and the DSC plot (B) was measured during rewarming. During the thermal treatment, all freezable water is crystallized, T'_g is increased to −58 and −57 °C, respectively. During rewarming, no crystallization can be detected. (See also Figure 2 from Ref. [64].)

(e.g., 0.14 μm), mannitol suppressed the heterogeneous crystallization more effectively than in large (0.87 μm) liposomes.

If in certain substances no crystallization or eutectic mixtures can be found by DSC (cephalosporin [66] with the experimental conditions used, one has to seek different conditions [63].

The development of DSC equipment with a low heat capacity and quick response times has made it possible to modulate the normal temperature ramp by a sinusoidal temperature oscillation, called modulated DSC (MDSC)®. By using Fourier transformation, the total heat flow can be separated into a reversing and a nonreversing »kinetic« component. The reversing heat flow will especially show glass transition events, which may be difficult to find in the total heat flow signal, or overlap with other nonreversing events. The reversing flow signal can be used to calculate heat capacity and its changes. The nonreversing component represents the kinetic events such as crystallization and enthalpic relaxation. Knopp

et al. [67] used temperature-modulated DSC (TMDSC) to define the collapse temperatures of sucrose solutions and compared the results with cryomicroscopy photographs. After substantial efforts at temperature calibration and reduction in temperature gradients in the sample, the collapse temperatures T_c of a 5 and 10% sucrose solution were determined: onset −37.7 °C. Earlier data for 10% sucrose solution (−32, −34 °C) were discussed as being too low for experimental reasons. Measurements of total heat flow, heat capacity, and kinetic heat flow for 5–80% sucrose solutions showed that below 20% w/w sucrose concentration, only one transition is observed, and for 40 and 60% a second transition is observed at a lower temperature. The kinetic heat flow signal for 60% sucrose shows a crystallization exotherm overlapping with the lower transition temperature range.

The authors considered that the higher transition temperature, as frequently accepted, does not indicate the collapse temperature T_c. They claimed T_c to be the midpoint between the end of the lower and the beginning of the higher transition, a reasonable average of −37 °C. They concluded that the structural relaxation time for water–sucrose glasses is short (<30 min) compared with the kinetics of ice crystallization. Kett and Craig [68] studied the glass transition region of 20, 30, and 40% sucrose solutions by modulated-temperature DSC (MTDSC). The heating rate was 2 °C/min with modulation of ±0.3 °C over 60 s. Before scanning, all samples were ›jump‹ cooled to −55 °C and then either annealed for 20–960 min at this temperature (isothermal) or annealed for 20 min at temperatures from −30 to −55 °C (isochronal). All transition temperatures were determined by the reversing and all enthalpies by the nonreversing signal. The glass transition region shows two transitions and one endotherm close to each transition.

Isothermal annealing shows an increase in the relaxation enthalpy with increasing annealing time and increasing sucrose concentration with a maximum at 400 min independent of the concentration. Figure 1.73 shows the effect of annealing temperature on the T_g onset. The authors recommended an optimum annealing temperature for 20–40% sucrose solutions between −38 and −42 °C and summarized that the onset temperature of glass transition and the accompanying endotherm relaxation signal increase with increasing annealing time up to ~7.5 h and then plateau. Chang *et al.* [69] performed modulated DSC (MDSC)

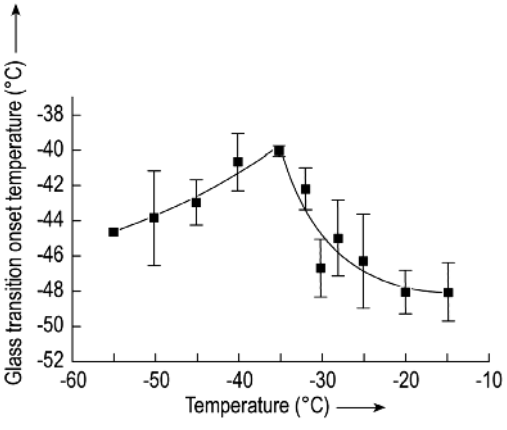

Figure 1.73 T_g onset of 40% sucrose solution as a function of annealing temperature. (See also Figure 4 from Ref. [68].)

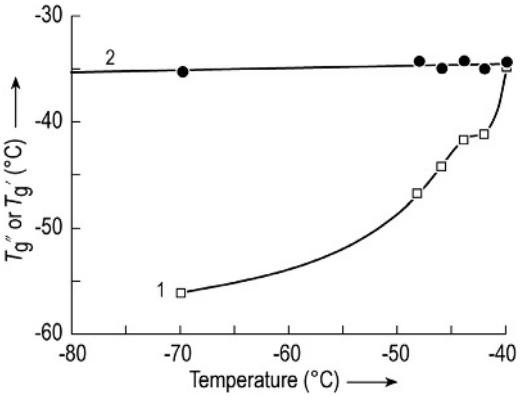

Figure 1.74 (1) T_g'' and (2) T_g' as function of annealing temperature for a 10% sucrose solution. (See also Figure 3 from Ref. [69].)

studies on 10% sucrose solutions that had been annealed between the two glass transition temperatures, T_g'' and T_g' (range −48.5 to −40.5 °C). The samples were treated in two ways: (1) quench cooled in LN_2, warmed to the selected annealing temperature and kept there for the annealing time (usually 1 h), modulated with an amplitude of 0.5 °C and a period of 100 s for 10 min to start from the steady state, beginning the linear scan at 1 °C/min; or (2) cooled at 1 °C/min to −68 °C, heated at 1 °C/min to the annealing temperature, and MDSC scan started after annealing as in (1). It was found that annealing shifts the reversing heat flow data for T_g'' to higher temperatures, close to the annealing temperature, and decreases the change in c_p. The authors concluded that T_g'' originates from a metastable condition, that is, excess water trapped in the sucrose phase, which crystallizes when $T > T_g''$, thereby raising T_g''. When the temperature reaches T_g', the product goes through a glass transition nearly coincident with reversible melting, both transitions being true glass transitions. Figure 1.74 shows T_g'' and T_g' as a function of the annealing temperature.

Craig *et al.* [70] assessed the behavior of amorphous lactose by MTDSC. The relaxation time of 10% freeze-dried amorphous lactose as a function of the difference between annealing (storage) temperature and T_g is given in Figure 1.75:

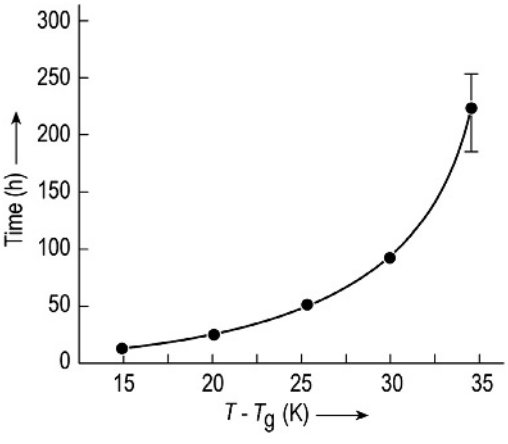

Figure 1.75 Relaxation time as a function of the difference between annealing temperature and T_g for a 10% amorphous freeze-dried lactose. (From Craig, 2000 [70]. Reproduced with permission of Springer.)

The relaxation time 15 K below T_g is ~10 h and 35 K below T_g is ~250 h. The authors discussed the difference between T_g measured with MTDSC and a ›fictive‹ T_g that would be measured by a linear heating signal. T_g is between 2.0 and 0.2 °C higher than the fictive value, decreasing with increased annealing time from 10 min to 16 h.

Another method to differentiate between reversible and the irreversible heat flow is StepScan® DSC [71]. The precondition for its use is a DSC system with ›power compensation‹: Sample and reference material are held in two separate calorimeters, each with its own heating elements. Both systems are maintained in equilibrium conditions. The amount of energy to keep the equilibrium is directly proportional to the energy change in the sample. The power compensation system measures heat flows, normal DSC systems measure temperatures. The StepScan method applies the heating (e.g., 10 °C/min) over a small temperature increment (e.g., 1.5–2 min), holds this temperature for a short time (e.g., 30 s), and calculates the heat capacity at that temperature. The irreversible or kinetic part of the total heat flow represents the ›slow‹ processes that take place during the scan: enthalpic relaxation, crystallization, and melting. With this method, a 5% sucrose solution was analyzed, as shown in Figure 1.76.

Van Winden *et al.* [72] used MTDSC in lyoprotected liposomes to detect the glass transition in samples in which it overlaps with the bilayer melting endotherm.

Kett *et al.* [73] studied T_g in freeze-dried formulations containing sucrose as a function of relative humidity and temperature during storage by TMDSC and thermogravimetric analysis. Craig *et al.* [74] found it helpful to assess the relaxation behavior of freeze-dried amorphous lactose by MTDSC. Relaxation times were calculated from measurements of T_g, c_p, and the magnitude of the relaxation endotherm. Scanning was performed at 2 °C/min with a modulation amplitude of ±0.3 °C and a period of 60 s.

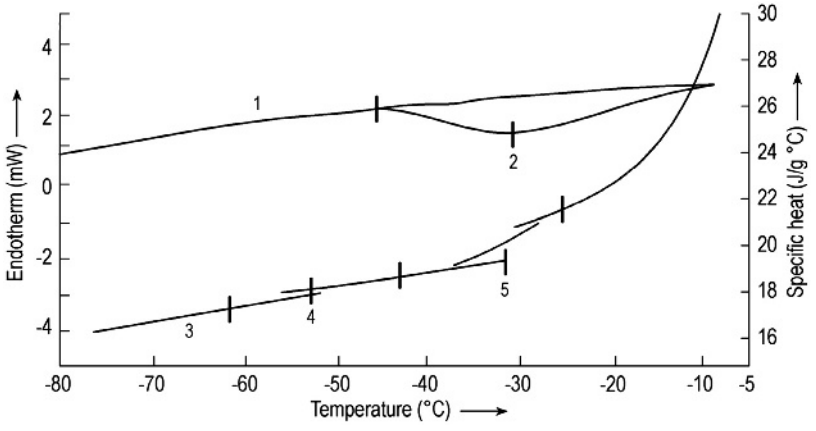

Figure 1.76 c_p and IsoK baseline data for 5% sucrose solution. 1, IsoK baseline; 2, recrystallization, −30.35 °C; 3, c_p; 4, T_g'' extrapolated to −52.38 °C, $dc_p = 4.08 \times 10^{-2}$ J/g °C; 5, T_g' extrapolated to −32.06 °C, $dc_p = 0.12$ J/g °C. (See also Figure 5 from Ref. [71].)

Figure 1.77 NMR analyzer, the ›Minispec‹ mq series, measurement range −100 to +200 °C. (See also Bruker Optik, Rheinstetten, Germany.)

1.1.5.6 Nuclear Magnetic Resonance

Nuclear magnetic resonance (NMR) is a highly sensitive analytical method. It can be used to study the way in which water behaves during freezing in aqueous saccharide and protein solutions and also in coffee extracts. Using NMR, it is possible to determine whether water is bound to other molecules (e.g., proteins) and cannot crystallize, how the collapse temperature T_c is influenced by unfrozen water and the changes in a glass of highly concentrated solutions during warming from low temperatures below and above T_g.

NMR spectroscopy (a commercial unit is shown in Figure 1.77) uses the fact that some atomic nuclei have a magnetic moment, for example, very distinct in a proton, the nucleus of hydrogen, but also in ^{13}C, ^{31}P, ^{14}N, and ^{33}S. In an external magnetic field, the energy levels split, as described in quantum mechanics. The size and extent of the split are given by Eq. (1.9):

$$\Delta E = \mu B g H_{\text{eff}} \tag{1.9}$$

where μB is the nuclear magneton, g is a constant (characteristic for the magnetic quality of a given nucleus), and H_{eff} is the effective strength of the magnetic field at the location of the nucleus.

The transition energy can also be described as a frequency of electromagnetic radiation:

$$\Delta E = hf \tag{1.10}$$

where h is Planck's constant and f is the frequency of radiation, or

$$\Delta E = h\, c/\Lambda$$

where c is the speed of light and Λ is the wavelength.

The energy difference between the levels depends on the field strength of the external magnetic field. To use 60, 100, or 270 MHz for NMR measurements with protons, the magnetic field strengths must be 14.1×10^3, 23.5×10^3, or 63.4×10^3 gauss (G). The last value is only possible with superconducting magnets. Since all other nuclei have a magnetic momentum that is small compared with that of the

proton, still higher magnetic field strengths are necessary. The magnetic momentum of a nucleus is, according to electrodynamic laws, the consequence of a rotating electric charge. This rotation is described in quantum mechanics as the spin (S) of the nucleus. Spin can only have discrete, defined energy levels parallel or vertical to the direction of the magnetic field ($S = \pm 1/2$). Transitions, for example, to higher levels (absorption) are only possible (they happen with a certain degree of probability) if S is not changed with the transition ($\Delta S = 0$) and the projection of the spin in the direction of the magnetic field changes by ± 1 ($\Delta S_z = \pm 1$). If a sample with a magnetic momentum is irradiated by ultrashort waves in an external magnetic field, only radiation of a defined wavelength and defined energy can be absorbed. This wavelength at a given external magnetic field is characteristic for the isolated nucleus.

In the nuclear (e.g., proton) part of a molecule, the external field is changed by factors that are characteristic for that molecule. The resonance frequency of isolated protons is shifted in a way typical of the chemical compound in which the proton is located. This shift is called the chemical shift of the resonance frequency (at a given external magnetic field).

The chemical shifts are small, for example, at a proton up to 30 ppm of the used frequency; if 100 MHz (10^8 Hz) is used, 10 ppm corresponds to 10^3 Hz. The shift is normally not measured absolutely, but compared with the known frequency of a reference substance, for example, for protons tetramethylsilane (TMS). The area of the resonance is proportional to the number of nuclei that give rise to it.

Besides the chemical shift of the resonance line, under certain conditions the lines split into two or more lines. This reflects the influence of the spin orientation of two or more neighboring nuclei on the magnetic field in the surrounding nuclei. The size of the splitting is called the coupling constant, *J*. *J* represents the quantity of influences between the nuclei, while the number of split lines and their intensity represent the number of influencing nuclei. The lines in an NMR spectrum are not infinitely small, but show certain linewidths, since the magnetic field at the location of a nucleus changes slightly, albeit constantly. After the high-frequency impulse is terminated, the earlier equilibrium is reinstated by magnetic noise and the system relaxes. Bloch connected the two possible relaxation processes with two characteristic times: t_{SGR}, the spin–lattice relaxation time, and t_{SSR}, the spin–spin relaxation time. The half-width of the resonance line measured at the half-height of the peak equals $1/t_{SSR}$. As shown in Figure 1.78, for very small molecular correlation times t_c, t_{SGR} and t_{SSR} are identical. The correlation time is the time that one molecule requires to travel the distance of its own diameter; it is a measure of the mobility of the molecules.

In aqueous solutions with small molecules, the relaxation is slow (0.1–0.5 s), while t_{SSR} of ice is very small (some 10^{-3} s) [76]. Close to the glass temperature of a substance, the relaxation time does not decrease exponentially and thus a different means of description must be used (Ref. [9] of Chapter 3).

Hanafusa [76] showed with this method how the amount of unfrozen water in a 0.57% solution of ovalbumin reaches practically zero at −20 °C, if 0.01 M sucrose is added (Figure 1.79). For globular proteins, Hanafusa described the freezing process as follows: between 0 and −20 °C, water molecules from the multilayer hydrate shell are decomposed. Below −45 °C, molecules from the monohydrate

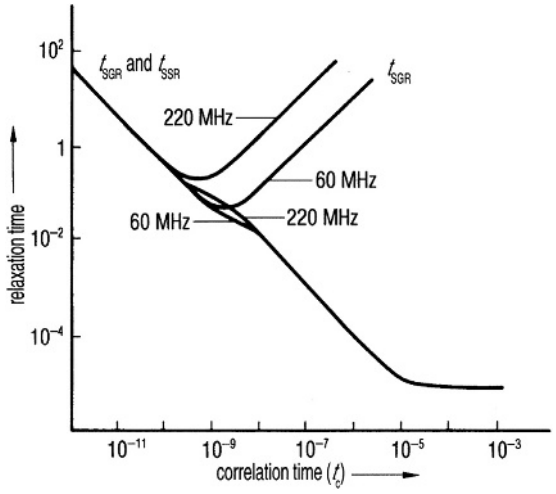

Figure 1.78 Relaxation time as a function of the molecular correlation time for two spectrometer frequencies, 60 and 220 MHz. t_{SGR}, spin–lattice-relaxation time; t_{SSR}, spin–spin relaxation time. (From Knowles, 1977 [75]. Reproduced with permission of John Wiley & Sons.)

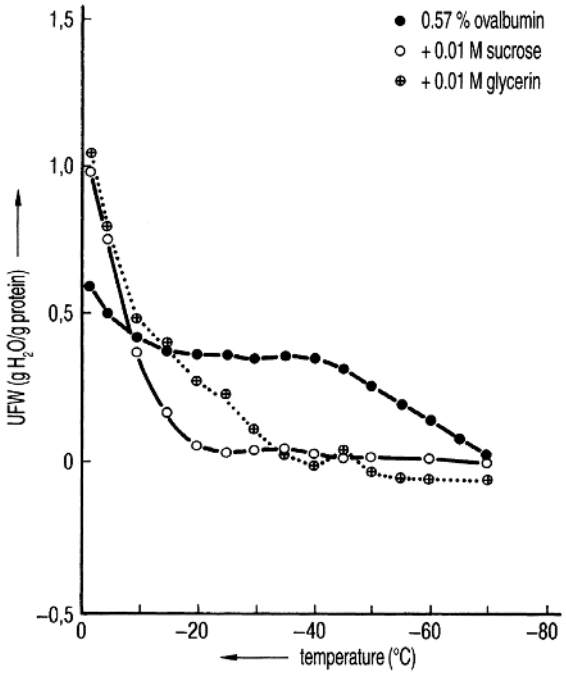

Figure 1.79 Unfreezable water (UFW) in a 0.57% ovalbumin solution as a function of the freezing temperature with different CPAs. (See also Figure 4 from Ref. [76].)

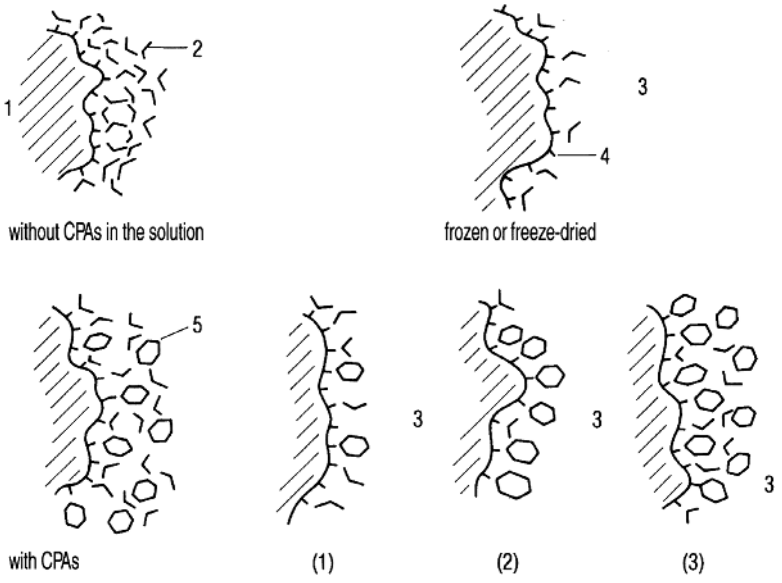

Figure 1.80 Schematic model of the action of CPAs in protein solutions during freezing and freeze-drying. (See also Figure 10 from Ref. [76].) *Top row:* Without CPA; the hydrate water of the ovalbumin has migrated into the ice and the freed valences are exposed to the influence of the environment. *Bottom row:* With CPA; part of the hydrate water of the proteins becomes replaced by CPA molecules. The molecules of the CPA, the remaining water molecules, and the protein molecule form a ›quasi‹ (replacement) hydrate layer. 1, protein; 2, water molecule; 3, ice or air; 4, exposed valence; 5, CPA molecule.

shell are removed, thereby destroying the shell; between −20 and −45 °C, an equilibrium exists between the hydrate bond to the protein molecule and the forces to insert additional water molecules into the ice crystals. By adding CPAs, the amount of bound water is much reduced. Water molecules are replaced by CPA molecules and form a ›quasi-hydrate‹ shell, which protects the protein during freezing and freeze-drying against denaturation. Hanafusa showed (Figure 1.80) a simplified, graphic picture of how, with rising concentration (1) to (3), the CPA molecules form a new shell for the protein. Some water molecules are so strongly incorporated that they can no longer diffuse to the ice crystals.

Nagashima and Suzuki [77] used NMR to show the interdependence of UFW, T_c, the cooling rate, and the concentration before freezing. The amount of UFW in g H_2O/g dry substance is measured, for example, of coffee extract with 25% solids (Figure 1.81), which at −20 °C has ~30% UFW (0.3 g/g) but is reduced at −50 °C to 0.1 g/g. Above −20 °C, the UFW rises rapidly. During freeze-drying above −20 °C, the structure will collapse. The authors demonstrated that after quick freezing (3–5 °C/min) of mannitol solution, crystallization of mannitol can be seen during rewarming. The UFW rose to ~50%, water then crystallized, and UFW was reduced to a few percent. The crystallization temperature measured agreed well with other reports (e.g., Ref. [54] using DSC. During slow freezing, mannitol crystallizes and there is no hysteresis (Figure 1.82). Figure 1.83 shows the strong dependence of UFW for Japanese miso sauce. At −50 °C and a

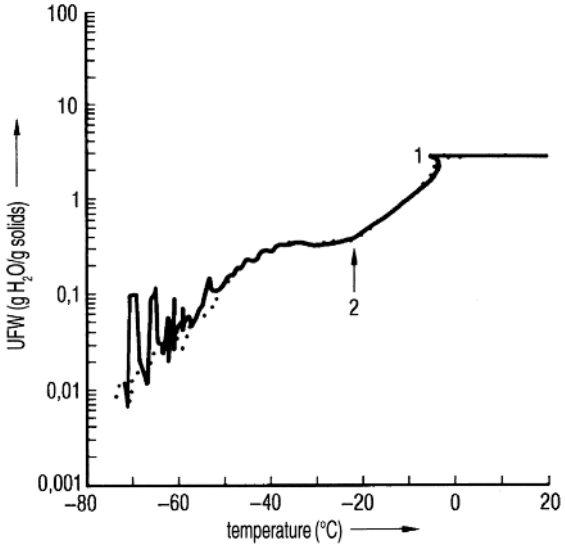

Figure 1.81 Freezing and thawing plot of coffee extract with 25% solids. UFW (g H_2O/g solids) as a function of temperature. 1, subcooling; 2, collapse temperature. (Figure 2 from Ref. [77].)

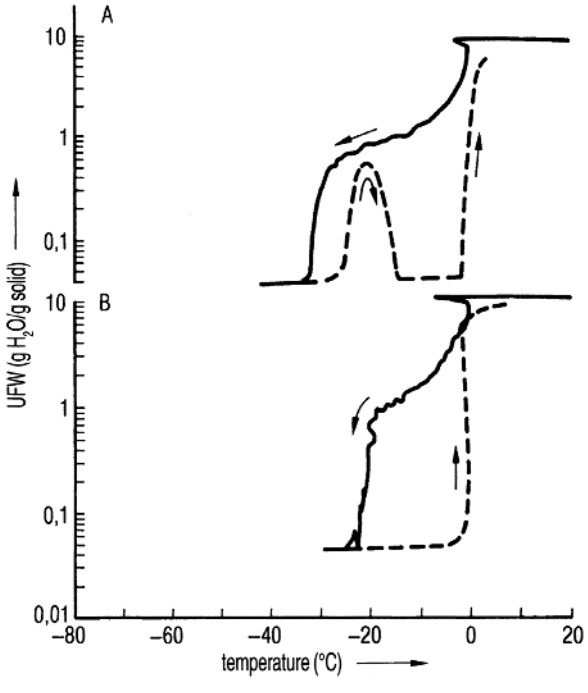

Figure 1.82 Freezing -and thawing plot of 9.1% D-mannitol solution. Freezing rate: (A) 5 and (B) 0.5 °C/min. (See also Figure 4 from Ref. [77].)

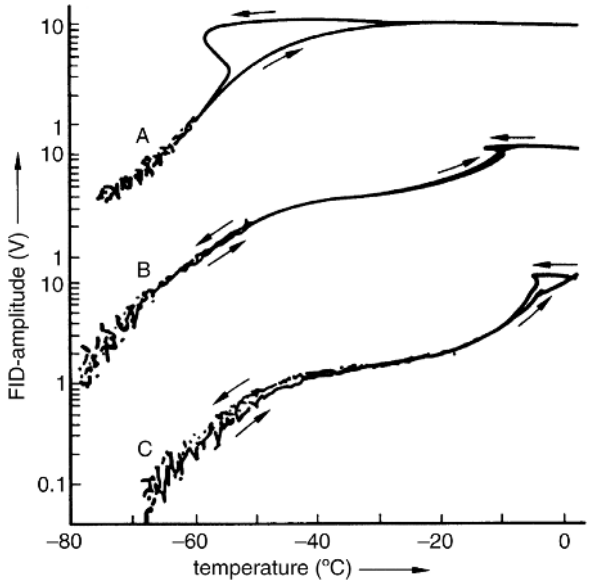

Figure 1.83 UFW content of miso sauce (A) and two dilutions (B and C) as a function of temperature. The solid content is (A) 52.7, (B) 26.4, and (C) 13.2%. (See also Figure 5 from Ref. [77].)

concentration of 52.7%, UFW is ~5 units, whereas at 26.4% solids in the original product, UFW remains at ~2 units and only at 13.2% solids ≈ 0.6 units UFW does not freeze.

Harz *et al.* [78] demonstrated by NMR spectroscopy that freezing of food (e.g., grapefruit juice) almost never followed the ideal expectation. The crystallization of carbohydrates is much hindered and further reduced by the high viscosity of the solutions. Water crystallizes much below the eutectic temperature, producing further increases in viscosity and leading to a glass phase during further cooling. Depending on the carbohydrates, this metastable phase at −18 °C can last for weeks or, on occasions up to 1 year.

Girlich [79] studied by NMR the molecular dynamics of aqueous saccharin solutions. At concentrations down to 30% solids, the saccharin molecules do not influence each other, while with decreasing temperature the existing H-bond bridges prevent a reorientation of the H_2O molecules. Dissolved saccharin molecules can destroy the H bonds, such that subcooling becomes possible. At >40% solids, associations of saccharin molecules are formed. H_2O is increasingly bound by H bridges and loses translational and rotational mobility. With increasing concentration of the solution, the saccharin molecules cross-link, and hydrate water becomes freed and can lead locally to low concentrations. T'_g of water becomes different from that of saccharin hydrates. Below 70% solids, the cross-linked system of saccharin molecules develops into a gel. During the observation time, no crystallization takes place and a metastable glass exists with a viscosity $>10^{12}$ Poise. The mechanical behavior is like that of solids.

Kanaori *et al.* [80] studied the mechanism of formation and association of human calcitonin (hCT) fibrils using NMR. hCT associates and precipitates during storage in aqueous solution. The freeze-dried hCT and its behavior were described.

Yoshioka *et al.* [81] studied the mobility of protons by NMR in freeze-dried bovine serum albumin (BSA) and γ-globulin (BGG) and its relation with aggregation susceptibility. The spin–spin relaxation time t_{SR} of protons in BSA and BGG was measured as a function of the water content in the range of 0.2–0.5 g/g (g water/g protein) in both products. The increase in t_{SR} and the increase in the aggregation susceptibility were strongly related.

1.1.5.7 Thermomechanical Analysis (TMA)

Carrington *et al.* [82] used thermomechanical analysis (TMA) to study the ice-crystallization temperature of 30% w/w fructose, sucrose, and glucose with and without sodium carboxymethylcellulose (CMC). TMA has been used to measure the expansion of the sample during freezing and rewarming. Parallel studies have been done using DSC. A typical result of TMA measurements during freezing is shown in Figure 1.84 for fructose with and without CMC during freezing with a rate of 5 °C/min. Figure 1.85 shows the plot of the warming profile of slowly frozen and annealed 30% sucrose solution, as determined by TMA. Figure 1.86 shows the warming DSC curve of 30% sucrose solution slowly frozen and annealed. On comparing the two temperatures T_{r1} and T_{r2} (as shown in Figures 1.85 and 1.86) by both methods for sucrose, $T_{r1} \approx -60$ °C (TMA) and −41.2 °C (DSC), $T_{r2} \approx -35$ °C (TMA) and −32.6 °C (DSC), it is obvious that several factors influence the resulting data, as discussed by the authors (onset data for DSC from a table in the publication, TMA estimated from the plot).

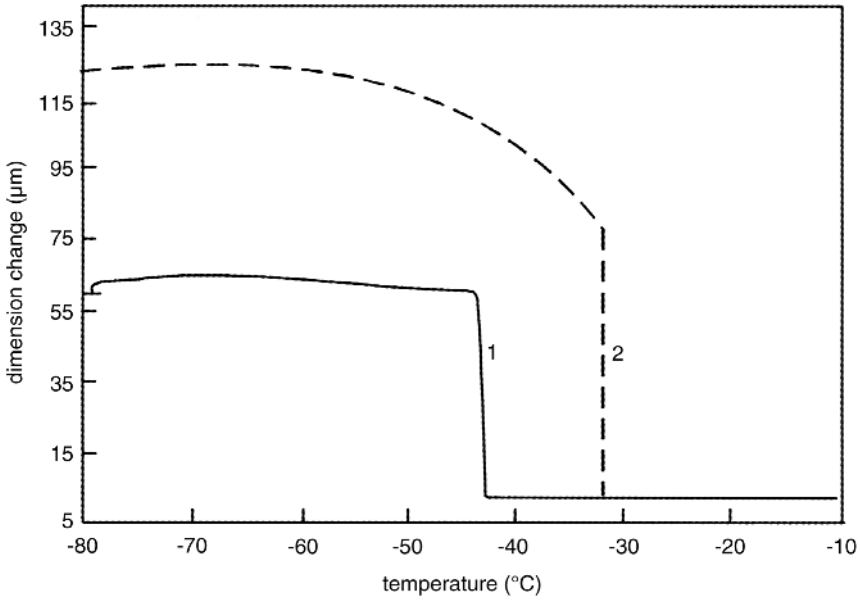

Figure 1.84 Dimension change as a function of temperature for 30% sucrose solution during freezing at 5 °C/min down to −80 °C. 1, fructose alone; 2, fructose plus 0.25% sodium carboxymethylcellulose (CMC) . (See also Ref. [82].)

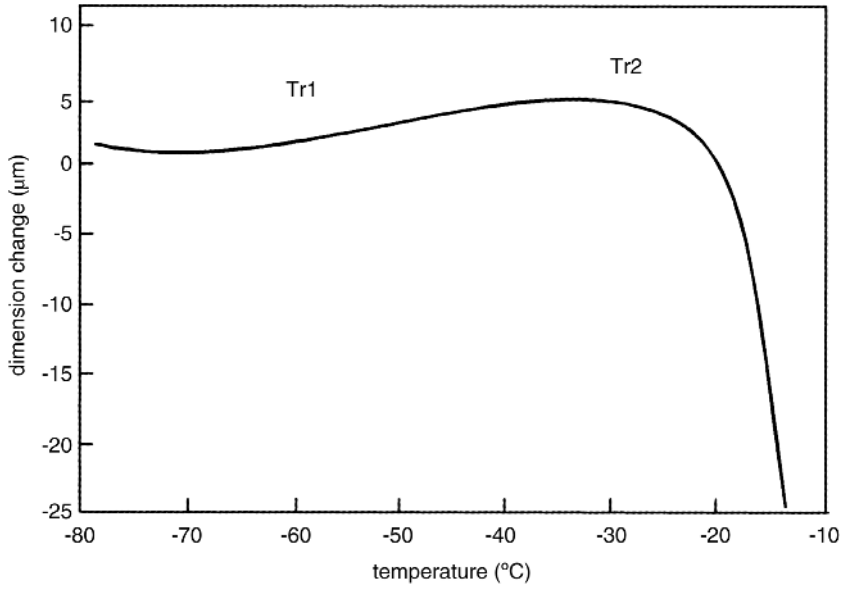

Figure 1.85 Dimension change as a function of temperature for 30% sucrose solution during warming at 2 °C/min after slow freezing to −80 °C and annealing up to −35 °C. (See also Ref. [82].)

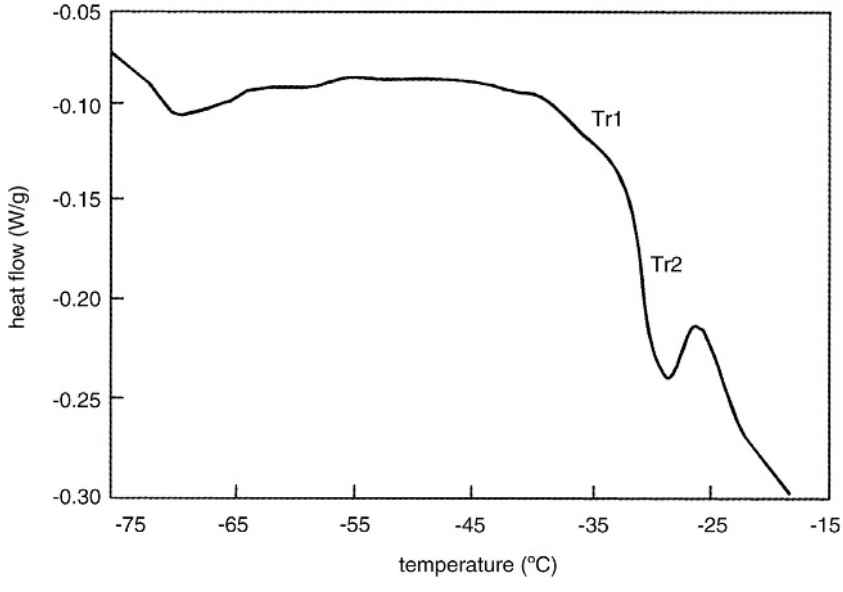

Figure 1.86 Heat flow as a function of temperature in the DSC thermogram of 30% sucrose solution frozen at 5 °C/min to −80 °C during warming (5 °C/min) after annealing up to −35 °C. (See also Ref. [82].)

TMA measurements have been helpful in explaining the breakage of vials during the warming of frozen solutions of mannitol and other stereoisomers [83]. For example, above −25 °C, mannitol expands 30 times more than standard type 1 flint glass. Depending on the filling volume and the concentration, 10–40% of the vials break when filled with 3% mannitol solution.

1.1.5.8 Dielectric Analysis (DEA)

Pearson and Smith [84] explained the advantages that DEA can provide to optimize freeze-drying processes by three examples. (i) The different relaxation behavior of bound water (two hydrogen bonds) and sorbed water (one hydrogen bond) can be used to determine the end of freeze-drying when the sorbed water is desorbed and the bond water still in place. (ii) The dielectric response of a material can be related to its crystal size and the level of hydration. (iii) The glass-forming property of excipients and their molecular mobility (viscosity) are strongly influenced by temperature and hydration. Dielectric studies have shown a non-Arrhenius behavior of glass-forming sugar solutions, resulting in a viscosity change of several orders of magnitude within small temperature or hydration changes.

Morris *et al.* [85] proposed the use of dielectric analysis to predict the collapse temperature of two-component systems. The background of DEA is explained and the ›take-off frequency‹ (TOF) is chosen as the best analytical method to identify the collapse temperature. Figure 1.87 shows the dielectric loss factor as a function of the frequency. The frequency at the minimum of this curve is called TOF by the authors. TOF varies with the temperature as shown in Figure 1.88. The extrapolated intersection of the two linear portions identifies the collapse temperature. The predicted T_c by TOF for 10% sucrose, 10% trehalose, 10% sorbitol, and 11% Azactam™ solution deviates from observations with a freeze-drying microscope (Table 1 in Ref. [85]) to slightly lower temperatures, the differences being −3, −1.4, 2.2, and 0.7 °C.

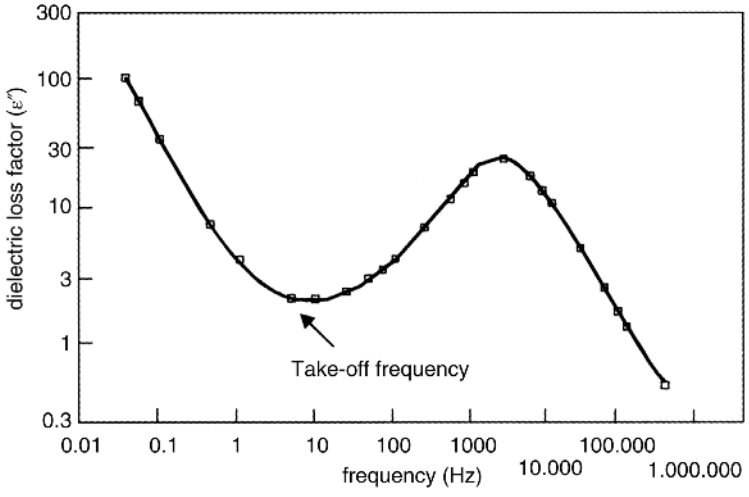

Figure 1.87 The take-off frequency, at a given temperature, occurs at the first minimum in the dielectric loss factor (ε'') versus frequency curve as frequency increases. (See also Figure 9 from Ref. [85].)

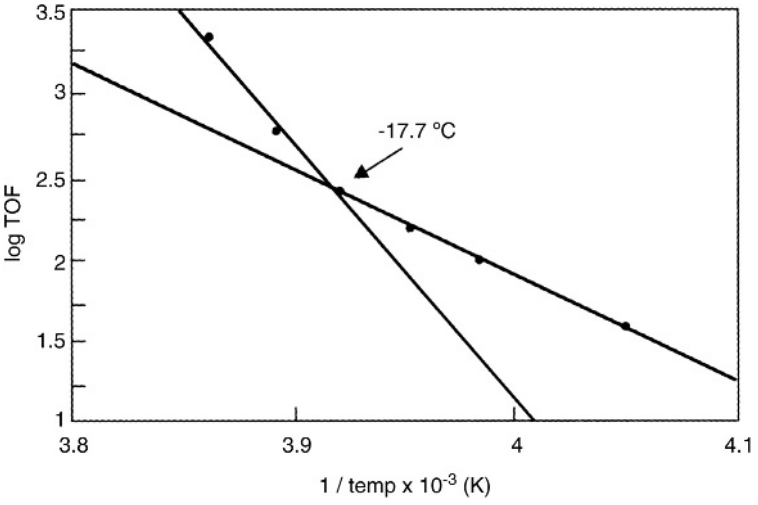

Figure 1.88 Collapse plot of log(TOF) versus 1/K. The extrapolated intersection of the two linear portions identifies the collapse temperature of the system. (See also Figure 10 from Ref. [85].)

Smith *et al.* [86] reviewed dielectric relaxation spectroscopy (DRS) as a method for the structural characterization of polymers and proteins providing, among others, information about the water content and states of water.

1.1.5.9 XRPD Diffractometer–Raman Spectroscopy

X-ray diffractometry on lyophilized products provide the following information:

- Crystalline samples can easily be distinguished from amorphous samples.
- Crystallinity (CI) can be determined in crystalline samples.
- Polymorphism (different modifications) of a substance can easily be identified.
- Hydrates (mannitolhydrate) are easily recognized.

The X-ray powder diffractometer (XRD) measurement is based on the diffraction of X-rays at the higher level structure of a crystalline substance. The wavelength of the X-ray is in the range of the lattice spacing in the crystal[1]. It is based on the Bragg law:

$n\lambda = 2d \times \sin\theta$
n = hole number
λ = wave length
d = distance
θ = angle

Cavatur and Suryanarayanan [87] have developed a low-temperature XRD technique to study the solid states of solutes in frozen aqueous solutions. In

1 Dr. Stefan Seyferth, Institute for Pharmaceutical Technology, University Nuerberg- Erlangen, Germany (2009).

frozen nafcillin sodium solution (22% w/w), no eutectic crystallization was observed. Annealing at −4 °C caused solute crystallization, which increased with annealing time. Two other products studied showed that XRD provides information about the degree of crystallinity without the interference of other events.

Raman spectroscopy was used by Sane *et al.* [88] to quantitate structural changes in proteins freeze-dried or spray dried. Monoclonal antibodies (e.g., RhuMAbVEGF) underwent secondary structural changes in the absence of a lyoprotectant. Increasing molar ratios of cryoprotectant could lead to complete structural preservation. The long-term stability of the dried proteins correlates with structural changes observed by Raman spectroscopy.

1.1.6 Changes of Structure in Freezing or Frozen Products

Independent of the growth of ice crystals (Section 1.1.2), which can be observed down to ≃100 °C, and possible recrystallization (Section 1.1.3), this section describes only such developments or changes of structures that can be influenced by additives. The addition of CPAs to albumins, cells, or bacteria influences the nucleation of ice – or at least its growth – in such a way that their natural structures are retained as much as possible. On the other hand, additives are introduced to crystallize dissolve substances. If this method does not help, for example, with antibiotics, the solution increasingly concentrates until a highly viscous, amorphous substance is included between ice crystals. This condition has disadvantages:

- The water is not crystallized to its maximum and can be removed during freeze-drying only with difficulty or not at all. The residual moisture content remains undesirably high.
- Drugs are often less stable in the amorphous state than as crystals [89–92].

The phase transition from amorphous to crystalline can sometimes be promoted by thermal treatment (annealing) (TT) [93]. It is recommended first to search for CPAs and process conditions that would lead to crystallization. The evaluation can be carried out using methods such as described in Section 1.1.5 (see also Yarwood and Phillips [94]. If this is not successful, the time and temperature for TT should be chosen in such a way that the tolerances for time and temperature are not too narrow, for example, -24.0 ± 0.5 °C and 18 ± 1 min are difficult to operate, while -30 ± 1.5 °C and 40 ± 2 min might be easier to control.

A suitable freezing rate, start-up concentration, and an amount of product per vial (e.g., for Na-ethacrynate) can be selected that result in a stable, crystalline phase. However, the addition of CPAs may provide another means of achieving crystallization, as seen for several pharmaceutical products [95].

De Luca *et al.* [96] showed that the addition of 5% *tert*-butyl alcohol (*t*BA) to aqueous sucrose and lactose solutions (up to 40%) resulted in a frozen matrix, which could be easily freeze-dried. They demonstrated by DSC that the melting point rose distinctly (with 60% solution to −10 °C), but the endotherm of melting returned to 25%, indicating that not much water had frozen. In solutions with 5%

*t*BA, the exotherm of crystallization became more visible and the melting of *t*BA could be recognized.

Kasraian and De Luca [97] developed a phase diagram by DSC for *t*BA. Two eutectics were observed at 20 and 90% *t*BA concentrations. Using a freeze-drying microscope, the change of ice crystals by *t*BA became visible, although 3% *t*BA was required to form large needle-shaped ice crystals. A solution with 10% *t*BA grew finer, needle-shaped ice crystals, and a 70% *t*BA solution formed very large hydrate crystals. The rate of sublimation of water and *t*BA depended on the concentration. The crystallization behavior of the water–*t*BA mixtures could explain the influence of *t*BA on the freeze-drying of sucrose and lactose, when used in certain concentrations. Oesterle *et al.*[98] showed that not only can *t*BA speed up the sublimation of ice from amorphous freeze-concentrated mixtures, but also similar effects can be achieved with volatile ammonium salts such as ammonium acetate, bicarbonate, and formate. In an 8.5% excipient solution, 0.1 M ammonium salt solutions and 5% *t*BA were studied. The onset temperatures of T'_g were determined by DSC as sucrose −33.6, PVP −21.1, and lactose −29.7 °C. The onset temperatures for *t*BA–ammonium mixtures were between 3 and 14 °C lower than without additives. Main drying (MD) was carried out 5 °C lower than the respective T'_g. The percentage weight losses during the first ~7 h of drying were the largest with 5% *t*BA in PVP and lactose solutions. In the sucrose solution, *t*BA and ammonium salts show approximately equal effects. The authors concluded that the sublimation rates can be enhanced by *t*BA and other additives, but the influence of these additives on the stability and activity of proteins is not clear.

Wittaya-areekul and Nail [99] studied the effect of formulation and process data on residual *t*BA. Sucrose and glycine were used as models for noncrystallizing and crystallizing solutes. The variables examined were initial *t*BA concentrations, cake thickness, freezing rates, temperature, and duration of SD. Freeze-dried glycine (crystallized) contained 0.01–0.03% *t*BA, regardless of freezing rate and initial *t*BA concentration. The level of *t*BA in freeze-dried sucrose was two orders of magnitude higher and effected by freezing rate (rapidly frozen contained twice as much *t*BA as slowly frozen) and initial *t*BA concentration (*t*BA concentrations above the threshold concentration for eutectic crystallization resulted in relatively low residual *t*BA, concentrations below contained significantly higher levels of *t*BA). Time and temperature of SD had a minimal influence on residual *t*BA in the dried product.

1.2 Drying

Drying is basically well understood and is governed by two transport mechanisms: (i) the energy transport to transform ice into water vapor (between −21 and −30 °C approximately 2805 kJ/kg) and (ii) the transport of the water vapor from the sublimation surface through the already dried product into the drying chamber to the condensation or absorbing system for the vapor. Figure 1.89 shows the process of the main drying (MD) observed with a cryomicroscope. A 10% aqueous solution of hydroxyethyl starch (HES) has been directionally frozen

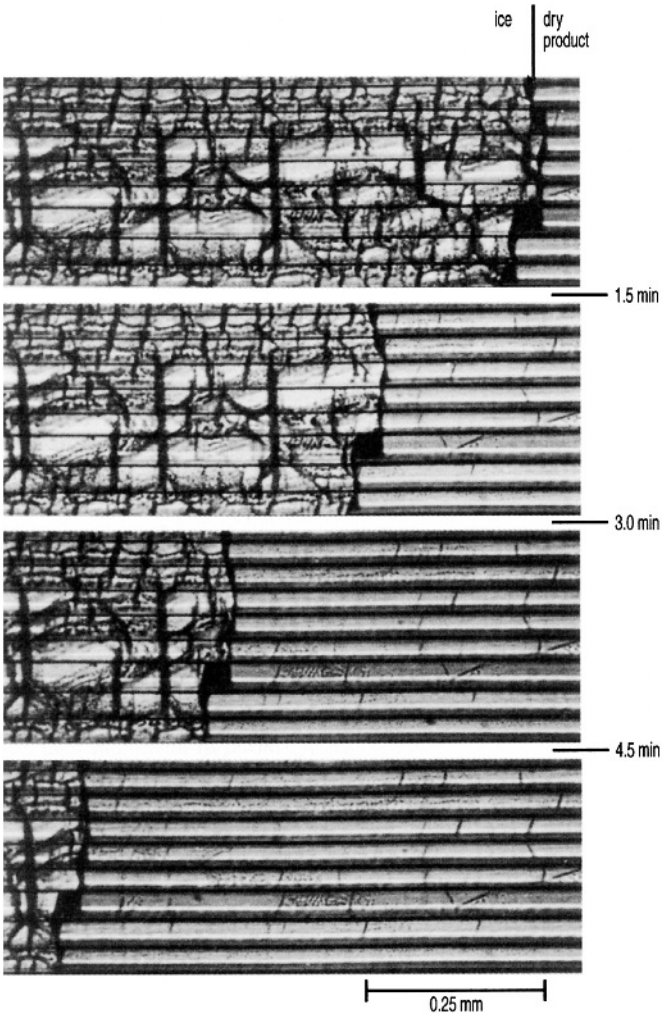

Figure 1.89 Main drying observed with a cryomicroscope. The HES solution was frozen under optimum conditions (see Figure 1.60). The solid, dark lines show the form of the sublimed ice crystals. (From Kochs, 1991[100]. Reproduced with permission of Elsevier.)

(see Figure 1.60). The ice dendrites are surrounded by the concentrated solid, which can be seen as a dark line after the ice is sublimed. In spite of optimal freezing, the sublimation speed is not uniform for all dendrites.

After the ice has been sublimed, the adsorbed water is desorbed from the solid. This process is governed by laws different from those of the main drying. This step is called secondary or desorption drying. During the secondary drying (SD), the energy transport does not play an important role, since the amount of water is normally less than 10% of the solids. Nevertheless, SD time-wise can be an important part of the total process and consume half or the same time as MD.

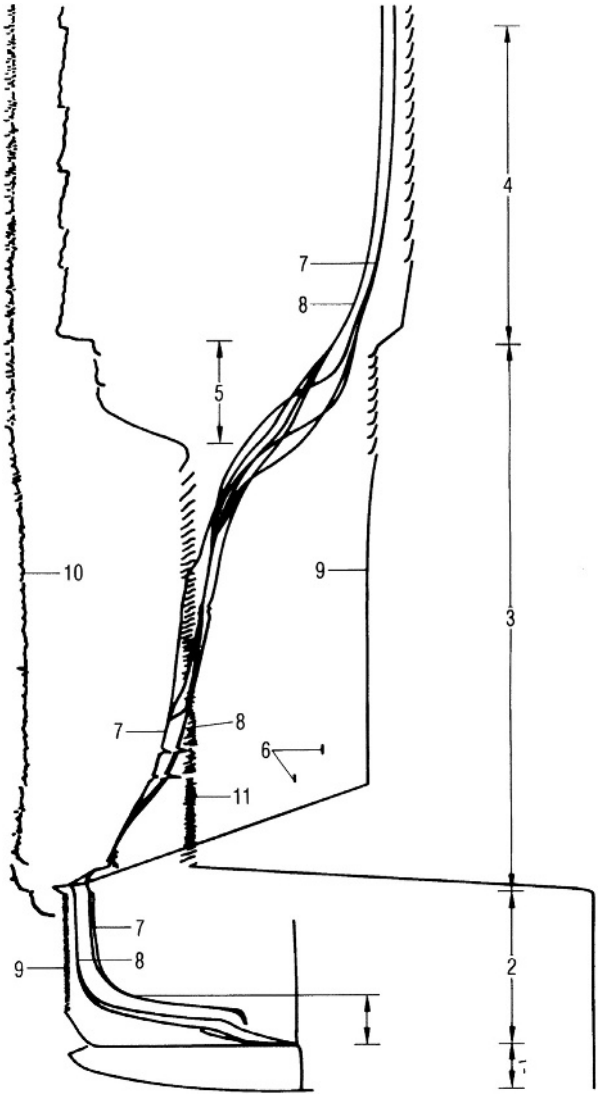

Figure 1.90 Course of a freeze-drying process. 1, precooling of the shelves; 2, freezing of the product; 3, evacuation and main drying (MD); 4, secondary drying (SD); 5, changeover from MD to SD; T_{sh} raised to maximum tolerable product temperature; 6, T_{ice} measurements by BTM; 7, temperature sensors RTD in the product; 8, temperature sensors Th in the product; 9, temperature of the shelves (T_{sh}); 10, ice condenser temperature; 11, pressure in the drying chamber (p_{ch}).

Figure 1.90 shows a typical run of a freeze-drying process, which can be divided into two parts: In MD, large amounts of water vapor (for example, 900% (w/w) of the solids) are sublimed and transported at an almost constant temperature at the sublimation front, (T_{ice}); in SD, the product temperature rises to the maximum tolerable temperature of the product and the water content is lowered, for example, by 9% (w/w) of the solids.

1.2.1 Main Drying (Sublimation Drying)

The amount of energy necessary for the sublimation depends on the sublimation temperature, but between −10 and −40 °C the energy varies by less than 2%. Furthermore, energy is consumed to heat the vapor during the transport through the already dried product or in contact with the warmer shelves. The specific heat of water vapor is 1.67 kJ/kg and the maximum increase in temperature is up to +20 or +40 °C. The energy consumption in this process can almost be neglected compared with the sublimation energy; heating the vapor from −30 to +30 °C results in ∼100 kJ/kg or ∼3.5% of the sublimation energy.

The necessary energy can be transduced to the ice in four different forms:

1) by radiation of heated surfaces;
2) by conduction from heated plates or gases;
3) by gas convection; or
4) by dielectric losses in the ice in a high-frequency field. The method is not discussed, since high-frequency fields with the necessary field strength in the pressure range of MD freeze-drying (1–0.01 mbar) start gas discharges.

(1) An infinite plate with a temperature K_{str1} and radiant efficiency ε_1 will transmit, independent of the distance, to a similar plate of frozen product with a temperature K_{str2} and a radiant efficiency ε_2 an amount of radiation energy. The surface heat flux q is

$$q = \delta(K_{Str1}^4 - K_{Str2}^4) \times 1/[(1/\epsilon_1) + (1/\epsilon_2) - 1) \tag{1.11}$$

where $\delta = 2.05 \times 10^{-7}$ kJ/m^2 h K^4.

This presentation is simplified. In practice, part of the energy, depending on the distance of the plates, will hit the walls of the chamber. This effect is small as long as the dimensions of the plates are large compared with their distance. For two plates of 1 × 1 m and a distance of 0.1 m, the effective radiation is ∼0.8q and with two plates of 0.5 × 0.5 m it is ∼0.7q [101].

The values of ε for products will normally be close to 1, which is also true for anodized aluminum and varnished steel. For polished steel, $\varepsilon = 0.12$. Figure 1.91 shows the energy transmission by radiation if both ε are 1.

At a shelf temperature of 100 °C, ∼2000–4000 kJ/h m^2 are transmitted, depending on the product temperature. At lower shelf temperatures, as is usual in freeze-drying plants for pharmaceutical products, q values between 500 and 1500 kJ/m^2 can be expected. However, for $\varepsilon = 0.12$, these data are reduced by a factor of 0.12.

At a shelf temperature of 100 °C and both $\varepsilon = 1$, at the beginning of a freeze-drying cycle (surface temperature −20 °C) ∼1.4 kg ice/h m^2 can be evaporated; at +30 and −30 °C, ∼0.4 kg/h m^2 remain. If $\varepsilon_1 = 0.12$, the sublimation rate is reduced to ∼200 and 50 g/h m^2, respectively.

In freeze-drying of pharmaceuticals in vials at 0.1 mbar, the contribution of radiation can be 20–30%, of gas conductivity 50–60% and of contact conductivity 10–30% of total energy transfer.

(2 and 3) An important part of the energy transfer is by conductivity, as well by direct contact of the product container with the shelf, as by the gas. Furthermore,

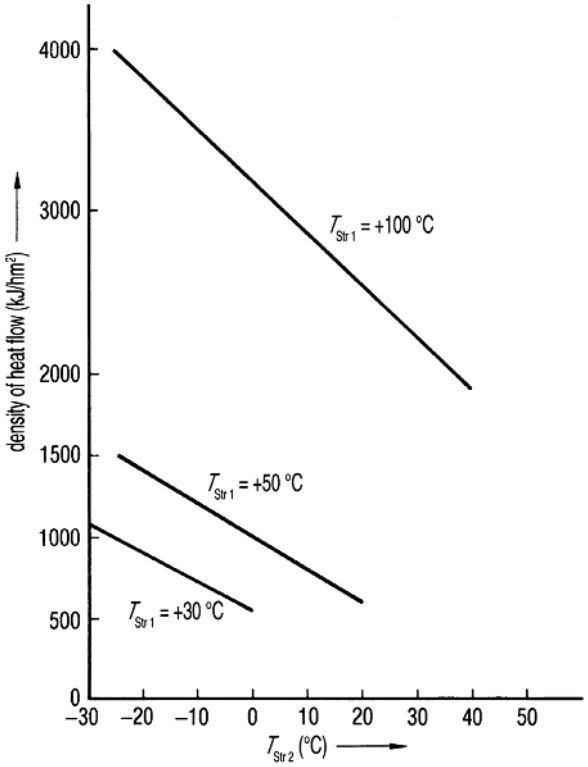

Figure 1.91 Heat transfer by radiation only. The figure shows only the order of magnitude. Density of heat flow (q) as a function of T_{Str2} (ice or product surface temperature) at three temperatures T_{Str1} of the radiation surface (+100, +50, +30 °C) as parameter.

the gas transports energy by convection, which becomes an essential factor, if the distance between the shelf and tray or vial becomes small. Figure 1.92 [5] shows that for distances larger than 10 mm, the energy transfer is independent of the pressure and becomes very small. However, for small distances, for example, 0.5 mm, the heat transfer coefficient rises between 0.13 and 1 mbar by a factor of 4.

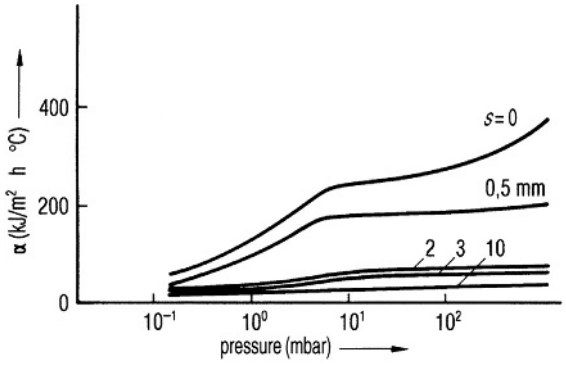

Figure 1.92 Heat transfer coefficient α as a function of pressure. Parameter s = distance between shelf and bottom of the product container (mm). Data measured in air. (Figure 4a from Ref. [5].)

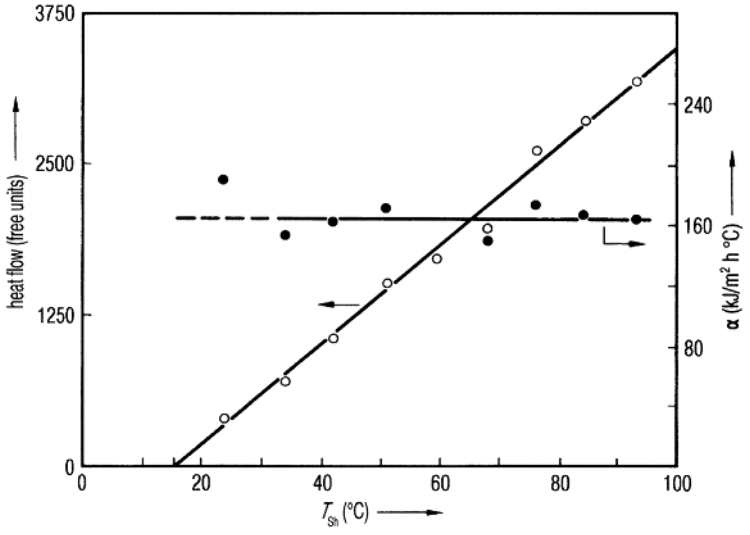

Figure 1.93 Heat transfer from a shelf with temperature T_{St} to the bottom of the product container with temperature T_{Bo} at pressure $p_{H_2O,ch} = 0.9$ mbar. (Adapted from Figure 4b in Ref. [5].)

If the shelf and the tray are as planar as technically possible, the plot marked $s = 0$ applies. At 0.2 mbar, a heat transfer coefficient of ~85 kJ/m^2 h °C can be achieved, rising by a factor of 2 at 1 mbar. In a well-designed freeze-drying plant with planar trays or vials, a heat transfer coefficient of 160 kJ/h m^2 °C at 0.9 mbar is possible (Figure 1.93), while at a pressure of 0.45 mbar, ~120 kJ/h m^2 °C (Table 1.14) is measured for the heat transfer coefficient K_{tot}. To sublime 1 kg of ice per hour and per m^2 with a coefficient of 120 kJ/h m^2 °C, the temperature difference between T_{ice} and T_{sh} (temperature of the shelf) must be an average of 23 °C.

Until now, only the heat transfer from the shelf to the tray or vial has been considered. The heat transfer to the sublimation front and the transport of the water vapor from the sublimation front into the chamber will now be included. Wolff *et al.* [102] described a model for a uniformly retreating ice front and experiments with milk and water to confirm the usefulness of the model. Three parameters were studied: the water diffusion in the dried layer, the external mass transfer, and the heat transfer from the shelf to the product. The last parameter was found to control the dehydration kinetics. Ybeme *et al.* [103] used a conductive paste on the shelves to reduce the heat transfer resistance between the shelf and the vials. The resistance toward mass transport was varied by using different restrictive capillaries. The conclusion of the experiments confirmed that the heat transfer to the vials limits the rate of sublimation. Chang and Fuscher [104] showed how and under which circumstances it was possible to use the T_{sh}, applied during secondary drying, already during the main drying. Recombinant human interleukin-1 receptor antagonist (rhIL-1ra) in various concentrations was studied in a solution of 2% (w/v) neutral glycine, 1% (w/v)

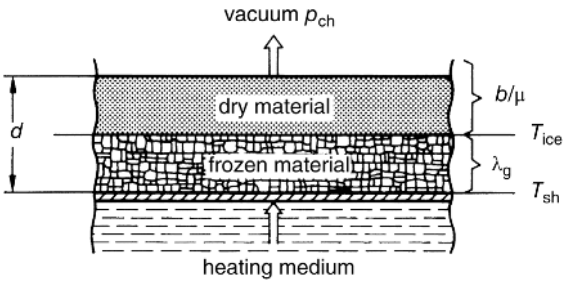

Figure 1.94 Scheme for the calculation of the drying time t_{MD} for the main drying. The product is frozen in plates. (see also Figure 6 from Ref. [105].)

sucrose, and 10 mM sodium citrate buffer at pH 6.5 (25 °C). At a 100 mg/mL rhIL-1ra concentration, no devitrification was seen to start at −37 °C and no recrystallization began at −27 °C as measured at lower concentrations (10–50 mg/mL). For this product, a temperature of −22 °C was considered low enough to avoid collapse. This temperature was controlled by pressure control as described in Table 1.15, its related text and Figures 2.115 and 2.116. The shortest drying time, keeping the temperature below −22 °C, was found to be at a shelf temperature of +40 °C, which was also used during SD. As the authors noted, this method cannot be applied to all formulations and is also dependent on the whole system, on the type of vial, heat transfer from the shelf to the sublimation front of the ice, water vapor transport, and so on. In Figure 2.116, an example is given in which the ice temperature range can be adjusted by pressure, valid for one product in one type of vial in one plant and with one shelf temperature.

The author has used a model and an equation developed by Steinbach [105] for many years and for many experiments in a wide field of applications. The model, shown in Figure 1.94, uses an infinitely expanded plate of the product with thickness d. Equation (1.12) describes the time of the main drying part of the freeze-drying cycle:

$$t_{md} = (\rho_g \xi_w LS \Delta m d)/T_{tot}[(1/K_{tot}) + (d/2\lambda_g) + (d/2LSb/\mu)] \qquad (1.12)$$

where

ρ_g = density of the frozen product (kg/m^2);
ξ_w = part of water (kg/kg);
LS = sublimation energy (2.805 kJ/kg);
T_{tot} = temperature difference ($T_{sh} - T_{ice}$);
K_{tot} = total heat transmission coefficient from the shelf to the sublimation front of the ice;
λ_g = thermal conductivity of the frozen product;
d = thickness of the layer (m);
Δm = content of frozen water = 0.9
b/μ = permeability (kg/m h mbar) for water vapor through the dried product.

In this equation the following simplifications are made:

- The layer is endless, energy is only transmitted from the shelf to one side of the layer.
- The vapor is only transported from the ice front through the porous dried layer.
- The frozen layer is not porous.
- The heat transport in the already dried layer is neglected.

The error resulting from the last assumption at $T_{tot} = 100\,°C$ is ~4% and at $T_{tot} = 50\,°C$ ~2% [105].

For the evaluation of the equation, four data are necessary in addition to those already known:

$$T_{tot} = T_{sh} - T_{ice}$$

K_{tot} heat transfer coefficient by conduction and by convection from the shelf to the sublimation front.
λ_g heat conductivity of the frozen product (ice), and
b/μ mass transport coefficient.

The equilibrium vapor pressure (p_s) can be measured by barometric temperature measurement (BTM) and be converted into temperature by the water vapor pressure diagram (see Section 1.2.3).

To develop an idea of how the various terms of Eq. (1.12) influence the drying time, some experimental date are used, described in this section.

m_{ice}	= mass of the frozen water	1.243 kg
F	= used surface area of the shelves	0.2193 m^2
d	= thickness of the product layer	7×10^{-3} m
T_{sh}	= temperature of the shelf during MD, maximum	+29 °C
T_{ice}	= temperature of the ice at the sublimation front	−22 °C
T_{tot}	= $T_{sh} - T_{ice}$, average temperature difference during main drying	43.88 °C
$p_{H2O,ch}$	= partial vapor pressure in the chamber during MD	0.245 mbar
p_s	= equilibrium vapor pressure at T_{ice}	0.85 mbar
Δp	= $p_s - p_{H20,ch}$	0.605 mbar
t_{MD}	= time of MD (frozen water is sublimed) (see Figure 1.116)	2.5 h
LS	= sublimation energy of ice	2.805 kJ/kg
ξ_w	= part of water in the initial product	0.931
ρ	= density of the frozen product, assumed as	900 kg/m^2
Δm	= part of freezable water, assumed as	0.9
λ_g	= heat conductivity in the frozen product	6.28 kJ/m h °C

With these data,

$$K_{tot} = (m_{ice} LS)/(t_{MD} F) \times 1/(T_{tot}) = 144.9\ \text{kJ/m}^2\ \text{h}\ °\text{C} \quad (1.12a)$$

$$b/\mu = (m_{ice}/(t_{MD} F)(d/2/\Delta p) = 1.3 \times 10^{-2}\ \text{kg/h m mbar} \quad (1.12b)$$

Using Eq. (1.12), t_{MD} is calculated::

$$\begin{aligned} t_{MD} &= \rho(\xi_w \Delta m L S d)/T_{tot}[(1/K_{tot}) + (d/2\lambda_g) + (d/2LSb/\mu)] \\ &\quad \underset{374.5}{\text{term A}} \quad \underset{6.9\times10^{-3}}{\text{term B}} \quad \underset{0.56\times10^{-3}}{\text{term C}} \quad \underset{0.096\times10^{-3}}{\text{term D}} \\ t_{HT} &= 3744.5(6.9\times10^{-3} + 0.56\times10^{-3} + 0.096\times10^{-3}) \\ t_{HT} &= 2.8\ \text{h(calculated)} \end{aligned} \tag{1.12c}$$

Equation (1.12) describes the main drying reasonably well if some experimental data are used.

The influence of different parameters on the MD is now discussed.

Term A: A variation of d changes this term proportionally; the T_{tot} influence is the inverse ratio. *Term B:* This is approximately 12 times larger than term C, and 70 times larger than term D. In both terms, d enters a second time, but as the absolute numbers are much smaller than term A, the influence of d in these terms is reduced.

If term A is constant, term B, the influence of the heat transfer term on t_{MD}, is in the example 91%. Term C, the influence of the heat conductivity, is 10 orders of magnitude smaller than term B. The heat conductivity depends on the characteristics of the product. In Ref. [5], an average value of 6.28 kJ/m h °C is used at −30 °C; in Ref. [3], a value of 5.9 kJ/m h °C is reported. However, even if λ_g varies by ±50%, term C would vary approximately between 0.37×10^{-3} and 1.1×10^{-3} and the influence on drying time is hardly noticeable (±5%).

Term D, also linear with d, shows the influence of the water vapor transport from the sublimation surface through the dried product into the vial or tray on t_{MD}. b/μ (kg/m h mbar) has often been measured: Steinbach [106] measured 1.3×10^{-2}, Gehrke and Deckwer [107] found for different groups of bacteria an order of magnitude of 4×10^{-2}, Sharon and Berk [6] demonstrated how b/μ decreases for tomato pulp from 3×10^{-2} to 0.8×10^{-2} when the solid concentration rose by a factor of 4, while Oetjen and Eilenberg [5] used 1.3×10^{-2} as an average value. Kasraian and DeLuca [108] measured the resistance of the vapor transport through the dried cake of a 5% (w/w) sucrose solution with and without 3–5% *tert*-butyl alcohol (*t*BA) and obtained the following results: In the absence of *t*BA, and with a skin on the surface, $b/\mu = 0.13\times10^{-2}$ kg/m h mbar. After the skin had cracked, $b/\mu = 0.77\times10^{-2}$ and with BTA, b/μ is in the range of 15.4×10^{-2}–2.5×10^{-2} kg/m h mbar. By using the two extreme data for b/μ 0.13×10^{-2} and 15.4×10^{-2} kg/m h mbar, t_{MD} rises to ~2.8 h or remains at ~2.5 h. The influence of b/μ becomes measurable in the example given only at very small values of b/μ resulting from a skin on the surface. With the normal variation of b/μ, its influence remains in the region of a few percent.

As long as the sublimation energy is not to be transported through the already dried layer of product (see Figure 1.94), the heat transfer (term B) is the decisive factor. For a layer thickness of 25 mm (for freeze-drying a large thickness), term $A = 1.205\times10^{3}$, term B remains (heat transfer is not modified) at 6.9×10^{-3}, term $C = 1.99\times10^{-3}$, and term $D = 0.34\times10^{-3}$. t_{MD} then becomes 11.1 h. The drying

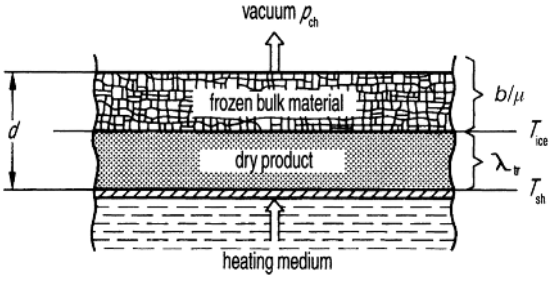

Figure 1.95 Scheme for the calculation of the drying time t_{MD} for the main drying of granulated product. (See also Figure 4 from Ref. [105].)

time is not extended by a factor of 25/7 = 3.6, but by a factor of 4.4, owing to the increase mainly in term C and slightly in term D.

If the material is granulated, for example, frozen and granulated coffee extract, having a solid content perhaps of 40% and a density of 0.6 g/cm^3 (Figure 1.95), Eq. (1.12) is still applicable, but the product data are different. The heat transfer through the dried product is $\lambda_{tr} = 8.37 \times 10^{-2}$ kJ/m h °C. To make the results more comparable, $d = 0.7$ cm and T_{tot} have been retained from the earlier example, even though T_{tot} were normally higher, for example, 100 °C:

$$t_{MD} = (\rho \xi_w LSd)/T_{tot}(1/K_{tot} + d/2\lambda_{tr} + d/2LSb/\mu)$$

$$t_{MD} = (0.6\times10^3\times0.6\times 2805\times7\times10^{-3}\ )/51\times(6.9\times10^{-3}+41.8\times10^{-3}+0.096\times10^{-3})$$

term A	term B	term C	term D
138.6	6.9×10^{-3}	41.8×10^{-3}	0.096×10^{-3}

$$t_{MD} \approx 6.8\ \text{h} \qquad (1.13)$$

In this example of the granulate, the main drying time (term A is assumed constant) depends largely on term C, while the vapor transport has virtually no influence.

λ_{tr} is given in Ref. [5] as 8.4×10^{-2}–16.8×10^{-2} kJ/m h °C, while Magnussen [7] uses for freeze-dried beef at 0.4 mbar a value of 15.5×10^{-2} and at 1.1 mbar a value of 17.2×10^{-2}. Sharon and Berk [6] found for concentrated tomato pulp with 28% solids $\lambda_{tr} = 28.5\times10^{-2}$ kJ/m h °C at 0.5 mbar and 31.8×10^{-2} at 1 mbar. If the concentration of solids is only 6%, the values were 12.6×10^{-2} and 15.9×10^{-2} kJ/m h °C, respectively. Steinbach used 16.7×10^{-2} and Gunn *et al.* [8] found 5.9 and 9.2×10^{-2} kJ/m h °C for turkey meat at 0.5 and 1 mbar, respectively.

With the two extreme values 5.9×10^{-2} and 31.8×10^{-2} kJ/m h °C, term C becomes 59.3×10^{-3} or 11×10^{-3} and $t_{MD\ (5.9)} \approx 9.1$ h and $t_{MD(31.8)} \approx 2.5$ h. The heat conductivity in the product becomes the decisive value. It is a function of the chamber pressure, but changes in the interesting pressure range 0.5–1 mbar by only 15%. However, it varies with the solid content by a factor of 2 and is dependent on the structure. The λ_{tr} of turkey meat parallel to the fiber structure is three times larger than given above.

In Figures 1.96–1.98, three runs of freeze-drying in two different plants are shown. Figure 1.99 gives the scheme of the plant for the run in Figure 1.96 and Figure 1.100 gives the scheme of the runs plotted in Figures 1.97 and 1.98.

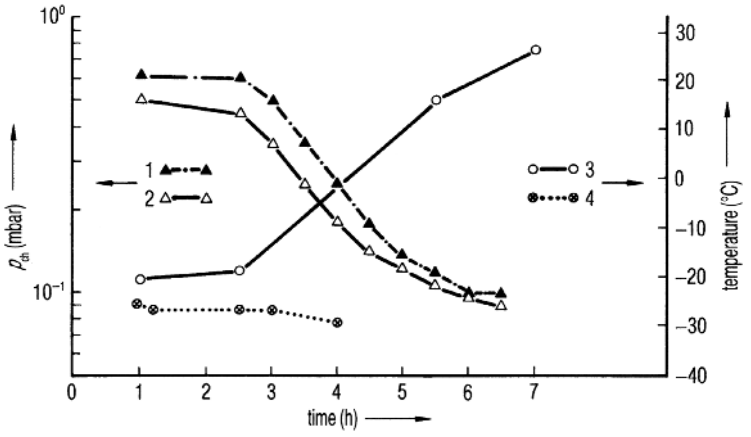

Figure 1.96 Course of a freeze-drying process in a plant as shown in Figure 1.99. Pressure control during MD not activated. 1.0 kg of product in four aluminum trays with machined bottom, T_{St} after evacuation controlled at +29 °C, $d = 0.6$ cm. 1, p_{ch} heat conductivity gauge (TM); 2, p_{ch} capacitive gauge (CA); 3, T_{Pr} resistance thermometer (RTD); 4, T_{ice} by barometric temperature measurement (BTM); end of MD: 3.5 h.

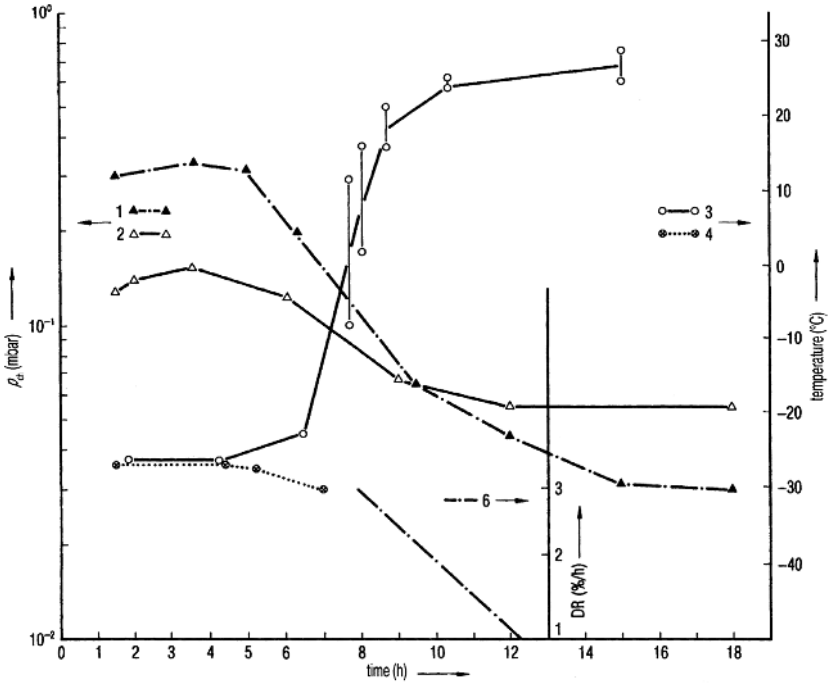

Figure 1.97 Course of a freeze-drying process in a plant as shown in Figure 1.100. Pressure control not activated. 2.4 kg of product in three welded stainless steel trays with flattened bottom. T_{sh} after evacuation controlled at +29 °C, $d = 0.6$ cm. 1–4, as in Figure 1.96; 6, desorption rate (DR), desorbable water in % of solids (see Section 1.2.2); end of MD: 5 h.

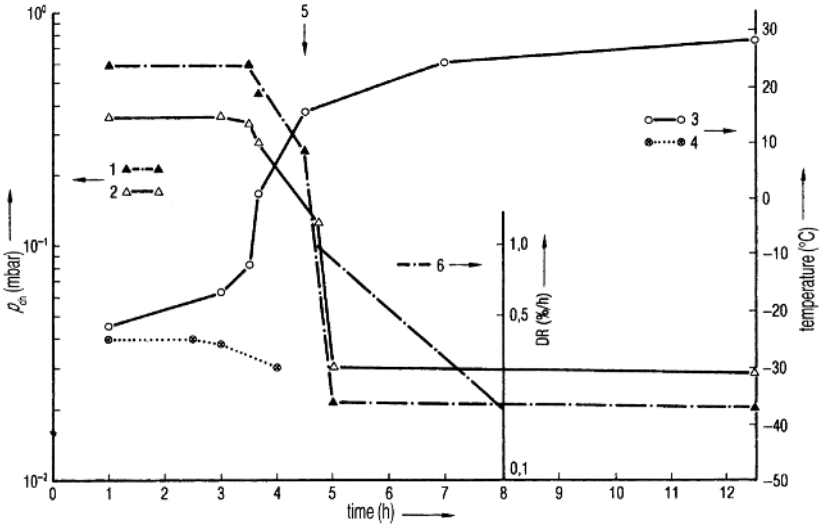

Figure 1.98 Course of a freeze-drying process in a plant as shown in Figure 1.100. Pressure control during MD 0.36 mbar (CA). 0.678 kg of product in 404 vials. T_{sh} controlled up to +29 °C in such a way that $p_{ch} = 0.36$ mbar was not exceeded during MD. $d = 0.64$ cm. 1–4, as in Figure 1.96; 5, end of pressure control; 6, DR (see Section 1.2.2); end of MD: 3.0 h.

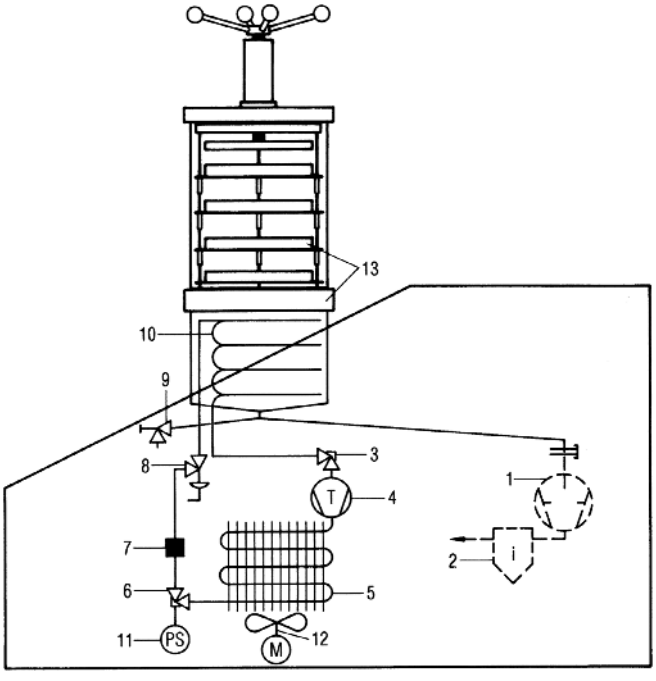

Figure 1.99 Scheme of the freeze-drying plant in which the tests shown in Figure 1.96 were carried out. 1, vacuum pump; 2, exhaust filter; 3, valve; 4, refrigeration machine; 5, liquefier; 6, valve; 7, filter; 8, expansion valve; 9, drain valve; 10, ice condenser; 11, pressure switch; 12, ventilator; 13, drying chamber with heated shelves. (Lyovac® GT 2, Steris GmbH, Hürth, Germany.)

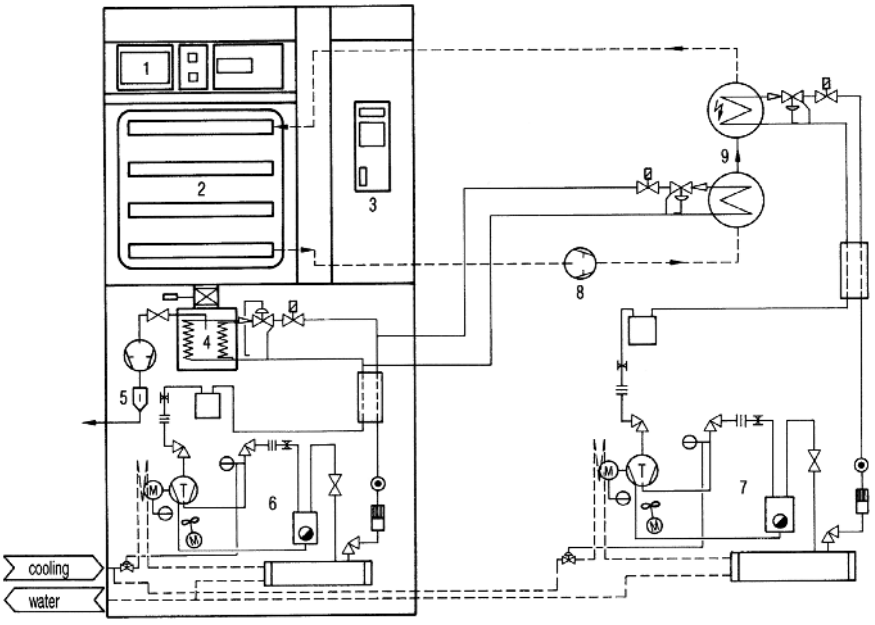

Figure 1.100 Scheme of the freeze-drying plant in which the runs in Figures 1.97 and 1.98 were carried out. 1, process documentation; 2, drying chamber with shelves; 3, operation control; 4, ice condenser; 5, vacuum pump with exhaust filter; 6, refrigeration machine for the ice condenser; 7, refrigeration machine for the shelves; 8, circulation pump for the brine; 9, heat exchanger (Lyovac® GT 6, Steris GmbH, Hürth, Germany.)

Table 1.14 summarizes the plant, the experimental data, and the relevant results. From these data, the values to calculate t_{MD} in Eq. (1.12) can be deduced when they are unknown.

Data for the three test runs:

ρ	density	0.9×10^3 kg/m^3
ζ_w	part of water	0.931 kg/kg
Δm	part of frozen water	0.9 kg/kg
LS	sublimation energy	2805 kJ/kg
λ_g	heat conductivity in the frozen product	6.3 kJ/m h °C

Data for test run in Figure 1.96:

d	thickness	6×10^{-3} m
T_{tot}		38.6 °C
t_{MD}	time of main drying	3.5 h

Data for test run in Figure 1.97:

d	7×10^{-3} m
T_{tot}	56 °C
t_{MD}	5.0 h

Data for test run Figure 1.98:

d 7×10^{-3} m

T_{tot} 51 °C

t_{MD} 3.0 h

With the help of these data, K_{tot} and b/μ can be calculated, if the water pressure at the sublimation front (p_s) and the partial vapor pressure in the chamber, measured by a hygrometer, are taken from the respective curves.

The results are summarized in Table 1.14: The K_{tot} values show the dependence on pressure (see results in Table 1.15), rising from ~62.4 kJ/m h °C at 0.15 mbar to ~119.3 kJ/m h °C at 0.45 mbar. The accuracy of the measurements to determine K_{tot} can be estimated in the two runs 1.62 and 1.62/W (Table 1.15) as ~±5%. Jennings [109, p. 612] claims that means of increasing K_{tot} to vials by a factor of 5–10 have been obtained. Nowhere in the literature studied were such data found. In Section 2.5.3, a continuous freeze-drying plant for granulated food

Table 1.14 Summary of the conditions during test runs and their results derived from Figures 1.96–1.98; $P_{H_2O,ch}$ was measured with a hygrometer during MD.

Parameter	Test run, Figure 1.96	Test run, Figure 1.97	Test run, Figure 1.98
Shelf area used (m^2)	0.166	0.343	0.172
Heating of shelf	Electrical resistance	Circulated brine	Circulated brine
T_{co} (°C)	Down to −45	Down to −53	Down to −53
Product	Skimmed milk, 9.67% solids		
Freezing method	Freezer down to −30 °C	Precooled shelves	−45 °C
T_{ice} (°C)	−22.3	−27	−21
p_s of T_{ice} (mbar)	0.83	0.51	0.94
Average p_{ch} during MD (mbar)	0.45	0.15	0.36
K_{ges} (kJ/m^2 h °C)	119.3	65.7	90.4
b/m (kg/h m^2 mbar)	0.010	0.011	0.011
t_{MD} taken from run, approx. (h)[a)]	3.5	5.0	3.0
t_{MD} calculated Eq. (1.14) (h)	3.0	4.3	3.4
Pressure control (mbar)	No	No	0.36

a) MD assumed terminated if T_{ice} is approximately 1–1.5 °C smaller than the average of all T_{ice} measured during MD. The amount of sublimed ice during MD is assumed to be 90% of the freezable water.

Table 1.15 Comparison of four test runs in the same plant (type as in Figure 1.99) with the same product and the same product thickness as in the run of Figure 1.96 in Table 1.14.

Parameter	Test run, Figure 1.96	Test run, Figure 1.96/W	Test run, Figure 1.96/ 0.36 mbar	Test run, Figure 1.69/ 0.20 mbar
T_{ice} (°C)	−22.3	−22.5	−26.8	−30.5
p_s (mbar)	0.83	0.81	0.53	0.36
p_{ch} (mbar)	0.45	0.50	0.36	0.21
p_{H2O} (mbar)	0.31	0.31	0.23	0.19
K_{tot} (kJ/m^2 h °C)	119.3	114.5	79.1	62.4
b/μ (kg/m^2 h mbar)	0.01	0.009	0.011	0.014
$t_{MD,}$ taken from run (h)	3.5	3.5	4.5	6.0
t_{MD} calculated (Eq (1.14)	3.0	3.1	4.4	5.8
$T_{Sh} - T_{ice}$ (°C)	38.6	39.1	38.1	36.3

Test run Figure 1.96/W: best possible repeat of test run Figure 1.96, both runs not pressure controlled. Test run Figure 1.96/0.36 mbar and 1.62/0.21 mbar differ from 1.62 and 1.62/W by pressure control 0.36 and 0.21 mbar, respectively. The results show:

1) The deviation between the two repeated runs is smaller than 5%, (the higher p_{ch} could indicate a larger content of permanent gases in the product).
2) T_{ice} can be controlled by pressure in a temperature range of 8–10 °C (with otherwise equal conditions).
3) K_{ges} decreases with decreasing p_{ch} (from 0.5 to 0.21 mbar) by approximately 50%.
4) t_{MD} decreases with increasing pressure to approximately 50%, since the decisive data in Eq. (14) is K_{tot}. T_{sh}–T_{ice} changes only slightly, the control avoids exceeding the controlled pressure. T_{sh} increased more slowly, which means that MD T_{sh}–T_{ice} is smaller than without pressure control.
5) Pressure control does not always shorten the MD, as can be read frequently. The pressure control adjusts a desired T_{ice}. If T_{ice} without pressure control is larger than with pressure control (as in this example), MD would only decrease when the run would have been operated at 0.7 mbar (if the product tolerates the increased T_{ice}.

is described (Ref. [17] of Chapter 2) in which the sublimation rate (kg/m^2 h) is 5–10 times higher than in standard plants. In the described plants, the granulated product is in direct contact with the heated shelf, which vibrates at 50 Hz for product transportation. By this vibration, the granulates are constantly and thoroughly mixed; each particle comes in contact with the heated shelf between 5 and 10 times per second (see Figure 2.108).

The permeability (kg/m h mbar) for water vapor through the dried product fluctuates by a larger margin, which can be estimated from all six test runs (Tables 1.14 and 1.15) as $1.1 \times 10^{-2} \pm 25\%$. However, the measurement of these data is of interest to judge whether the b/μ will influence the process time, as can be the case with products that have a high solid content and are dried with a large thickness. Small b/μ can also result from a skin on the surface of the

product (see Ref. [108]). Overcashier *et al.* [110] investigated the relationship between resistance to water vapor flow through the dried layer and the microstructure of the dried cake. Recombinant humanized antibody HER2 (rhuMAb HER2) formulated in trehalose and protein-free formulations containing trehalose and sucrose were studied. The mass transfer resistance decreased with increase in temperature for all materials, and the resistance also decreased from rhuMAb Her2 to trehalose to sucrose. The dry cake was porous with a denser layer at the top. The formulated trehalose and sucrose possessed 2–20 μm holes in a plate-like structure. Material dried at higher temperatures or with lower T_c showed more holes and a lower resistance to water vapor flow. The authors concluded that a lower resistance to water vapor flow may be due to small-scale product collapse.

Schellenz *et al.* [111] confirmed that the assumption of an infinite plate in Eq. (1.12) is a reasonable approximation, even for drying of products in vials. They show by the measurement of temperature profiles and by X-ray photographs during drying of a 5% mannitol solution, 23 mm filling height that the sublimation front retreats mostly from the top parallel to the bottom. The heat transfer from glass vials deforms the flat surface only to some extent close to the wall.

Drummond and Day [112] studied the influence of different vials, molded glass, glass tubing, and molded resin on the freeze-drying of 5% solutions of maltose and mannitol with arginine added. The freeze-drying performances, the inter- and intravial uniformity, and the morphology were compared. The lyophilization performance was best for glass tubing vials, with molded vials only marginally lower but better than resin vials. Intravial uniformity was found to be best for the resin vials. However, during drying this depends on the cycle parameters used. Intervial uniformity differences were measured both by the time at which nucleation of ice occurred and by temperatures during the drying process, but the differences for the three types of vial were in the same range. The morphology of mannitol in resin vials was found to be similar to the morphology in both types of glass vials. The authors concluded that the temperature distribution in a vial indicates a greater degree of uniformity in the cake, the temperatures from vial to vial are more consistent with resin vials, and the morphology in resin, molded, and tubing vials was not significantly different.

Pikal [113] compared the heat transfer mechanisms for three types of vials at a pressure of 0.13 mbar (T_{sh}, T_{ice} not specified):

Gas conduction	50–60% of total heat transfer
Radiation	20–30% of total heat transfer
Contact conduction	10–30% of total heat transfer

He gave for seven types of vials the part for the contact heat transfer coefficient between 0.2×10^{-4} and 1.7×10^{-4} cal/s cm^2 $K = 3$–25.7 kJ/h m^2 °C. At an average of 20%, K_{tot} can vary between 15 and ~130 kJ/h m^2 °C.

In Table 1.14, $K_{tot} = 65.7$ kJ/h m^2 °C was measured at 0.15 mbar and in Table 1.15, $K_{tot} = 62.4$ kJ/h m^2 °C was found at 0.21 mbar. In Eq. (1.12a), 144.9 kJ/h m^2 °C at ~0.3 mbar is calculated.

Table 1.16 Freezing and subcooling.

	5% mannitol (6R design)		10% sucrose (10 R design)	
	Freezing rate (+10 °C/ – 30 °C) (°C/min)	Subcooling (°C)	Freezing rate (+10 °C/ – 30 °C) (°C/min)	Subcooling (°C)
s-vial	0.92	−10	1.06	−7
qc-vial	1.07	−7	1.11	−8
p-vial	0.79	−10	0.67	−12

s-vial, tubing glass vial; qc-vial, quartz-coated tubing glass vial; p-vial, resin vials, 6R-design.
Source: Data from Ref. [114].

Summarizing, the selection of vials could influence the main drying time theoretically by a factor of 10 (see Eq. (1.12)), but the difference can easily be a factor of 2, and sometimes a factor of 4.

Willemer *et al.* [114] studied the influence of tubing glass, coated tubing glass, and resin as vial materials on the freezing and freeze-drying of 1 and 5% mannitol and 10% sucrose solution. During freezing, the different forces between the walls and liquid influence the structure of the freezing product and its subcooling, as shown in Table 1.16. The freezing speed in the coated vials was up to 16% greater than in standard vials, but in the resin vials the freezing speed was 14% lower. As shown in Table 1.17, the main drying is ∼20% longer in resin vials than in glass vials. The weight loss in the quartz-coated vials during sublimation is faster than in the other vials; also, the standard deviation of weight loss in the quartz-coated vials is by far the lowest, indicating high intercontainer homogeneity of the product. The secondary drying time is almost the same for glass and polymer vials and partially reduces the difference in the total drying time.

The discussions so far about main drying have assumed that trays or vials are exposed to uniform temperatures on the shelves.

Table 1.17 Weight loss during main drying of a 5% mannitol solution in R6 vials.

Drying time (h)	3.5	4.5	6.0	6.5	3.5	4.5	6.0	6.5
	Weight loss (% of initial weight)				Standard deviation of 12 vials			
s-vial	91.85	94.40	94.81		2.89	0.8	0.7	
qc-vial	90.24	95.05	94.47		1.59	0.35	0.63	
p-vial	71.87	87.68		95.22	2.53	3.0		0.41

Source: Data from Ref. [114].

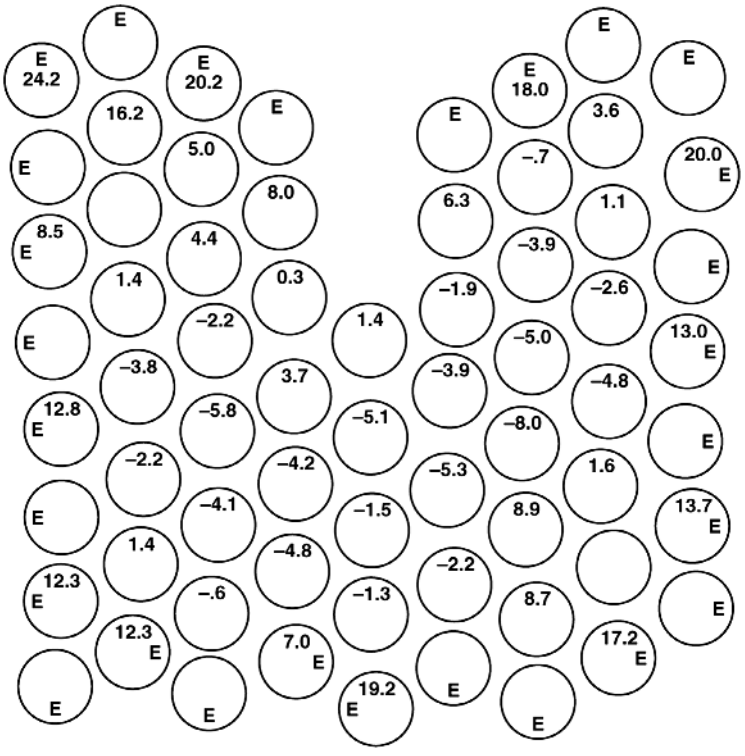

Figure 1.101 Vials on the shelf of a freeze-drying plant. Vials on the edge marked E, figures indicate the % deviation of the sublimed water in the vial from the average amount of water sublimed from all nonedge vials. The average deviation of all E vials is 15% and the average deviation of all non-E vials is 0.11%. (See also Figure 35 from Ref. [113].)

Pikal *et al.* [115] freeze-dried pure water in vials at 0.25 mbar and $T_{sh} = 5\,°C$ until ~25% of the water had sublimed. Then the vials were weighed and the loss of water was determined for each vial. The results are shown in Figure 1.101. All edge vials are marked E. The figure in the circle is the percentage deviation from the average sublimation rate for all nonedge (nE) vials. The average deviation for all nE vials is 0.83%, SD 5.13%. The average deviation of all E vials is 15.0%, SA 5.3%. The E vials receive additional energy from the walls (~15 °C) and ~15% more ice sublimes in the same time.

Kobayashi [116] has shown that this condition exists in some freeze-drying plants, as the walls and doors of chambers can have temperatures different from those of the shelves. During freezing, this could lead to slower freezing at the edges of the shelves.

During main drying, the influence of the wall temperatures can be small, as long as the shelves are only heated to +15 or +25 °C. If the shelf temperature during main drying is, for example, −10 °C, the vials at the edge will receive more energy than planned, which could lead to collapse or melting of the product in these vials. In contrast, during secondary drying, the vials at the edge will be warmed up more slowly than those in the center if the shelf temperature is, for example, +35 °C.

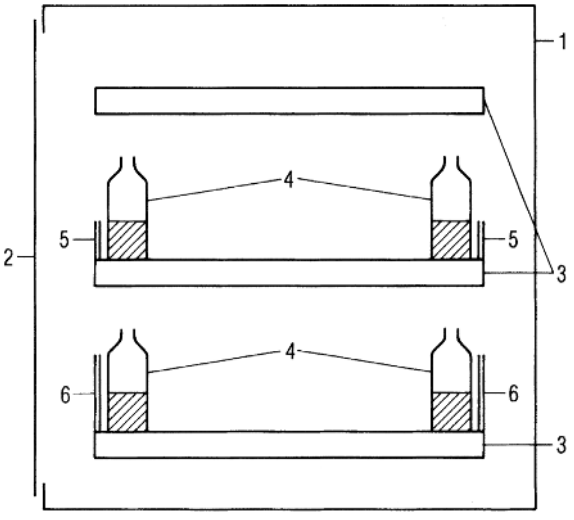

Figure 1.102 Scheme related to the plots in Figure 1.103. 1, chamber wall; 2, chamber door; 3, shelves; 4, vials with product; 5, radiation shield, height ≥ filling level of the vials; 6, radiation shield, height ≈ cylinder length of the vials.

Kobayashi proposed that all walls and the door are operated at the same temperatures as the shelves, although this is not always necessary if the shelves are shielded from the walls and the door, as shown schematically in Figure 1.102. The curves in Figure 1.103 indicate that this shielding is sufficient in some cases: During freezing, the vials at the edges of the shelves are exposed practically to the shelf temperature, whereas during secondary drying, the influences of the walls and the door are reduced.

Wall and door influences exist mainly by radiation or by the small heat conductivity of the gas. It can be seen from Figure 1.103 that the shielding in the temperature range between −40 and 0 °C is effective. However, the shielding becomes more important with an increasing temperature difference between the shelves and surrounding and it is especially necessary if the vials contain only a small amount of product.

In Figure 1.104 the influence of shielding the product in vials from the walls and doors is summarized. For each run (a), (b) and (c), six groups of vials (168 vials each) filled with 2.8 cm^3 (9 mm thickness) of human albumin product, containing 6% solids, were used. Rows 4, 5, and 6 were close to the door and 1, 2, and 3 close to the back wall; the condenser connection was at the bottom of the chamber. The RM were determined by the Karl Fischer method. Figure 1.105 shows the program of the tests.

In run (a) no shield was used, in run (b) a shield as sketched in Figure 1.102 was used, and in run (c) a temperature-controlled shielding as shown in Figure 2.66. The results are summarized in Table 1.18. The results should be considered as an example; they are influenced by the following factors: the product temperature at the end of freezing, T_{ice} during MD, the amount of product per vial, the cake thickness, and the geometric design of the chamber and the room temperature. As

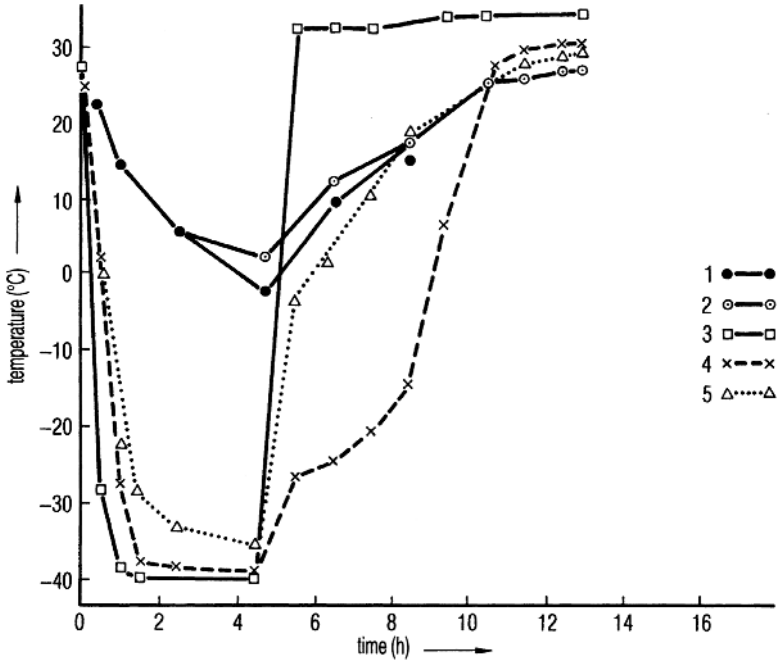

Figure 1.103 Temperature distribution during freezing (4.5 h) and freeze-drying (8 h). Each shelf carries a frame for radiation shielding. The design can be different depending on the kind of vials and the loading and unloading system. 1, internal temperature of wall of the chamber; 2, internal temperature of the door; 3, T_{sh}; 4, T_{pr}; 5, temperature on the inner side of the radiation shield.

can be seen from Figures 1.103 and 1.105, the main influence is a low shelf temperature during freezing and MD. If the amount of product is small, the influence of wall temperatures is relatively large (radiation and gas conductivity depend on the wall and vial surfaces and on the temperatures; if the amount of product is small, their relative importance increases).

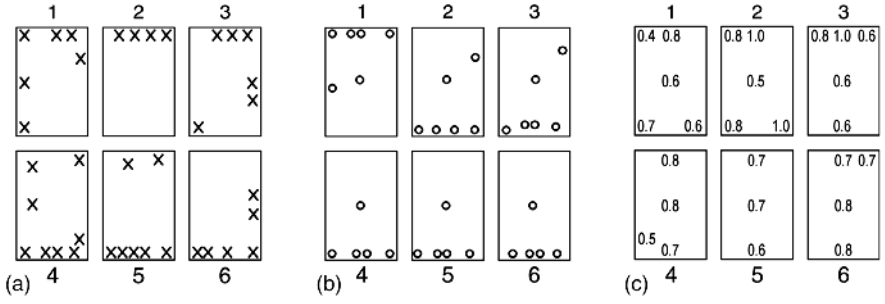

Figure 1.104 Residual moisture content in three identical runs with different shielding between vials and walls and door(s). In each run, six groups of vials were formed (168 vials each). Rows 4–6 were close to the door and rows 1–3 to the back wall. (a) No shielding. (b) Shielding as shown in Figure 1.102. (c) Shielding as described in Section 2.3.2, Figures 2.66–2.68.

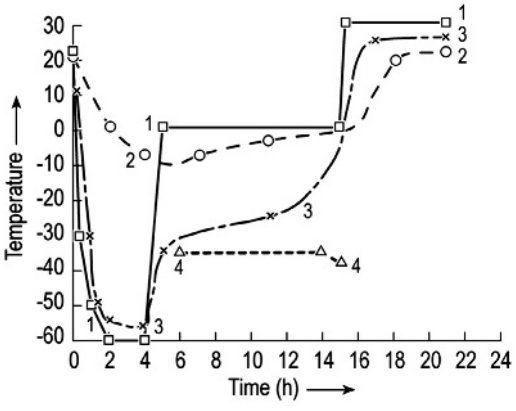

Figure 1.105 Temperature as a function of time in a pilot plant of ~170 L chamber volume, loaded with 1008 vials, containing ~2.8 kg of product with 169 g of solids, $d = 9$ mm. 1, T_{sh}; 2, wall temperature; 3, T_{pr}; 4, T_{ice}.

In Table 1.14 two different plants and three different types of container were used; in Table 1.15 it was always the same plant. During main drying, different pressures were applied.

The control of a desired constant total pressure is called pressure control (p_c) and can be operated by two methods:

- A dry inert gas, for example, nitrogen, is fed into the chamber by a needle-valve in such a way that the desired total pressure is built up.
- The valve between the condenser and vacuum pump set (Figures 1.99 and 1.100) is closed until the desired total pressure is built up. If the controlled pressure is exceeded, the valve opens.

Table 1.18 Residual moisture content distribution in three runs with and without shielding between walls and product.

	Run a	Run b	Run c
Shrunk product			
Row 1–3	10	0	0
Row 4–6	13	0	0
RM			
In shrunk product	7/21%	–	–
	av. 15%, SD 6.2%		
Product in center vials	0.9/1.1%	0.6%/1.0%	–
	av. 1%, SD 1%	av. 0.85, SD 0.15	
Product row 1–6	–	0.9%/4.5%	–
		av. 1.9%, SD 1.6%	
All vials	–	–	0.4%/1.0%
			av. 0.72%, SD 0.15%

Run a, no shielding. Run b, shielding as sketched in Figure 1.102. Run c, shielding as shown 2.3.2 Figure 2.58.

In the second case, the gas included in the product is released during sublimation of the ice and used for pressure control. In every liquid product, some gas is dissolved. Indeed, liquids [117] may contain gas contents from 5×10^{-5} up to 1×10^{-3} kg/kg, often very close to the upper value, although the actual content depends very much on the history of the product.

The test run in Figure 1.98 contained 1.535 kg of product having a water content of 1.39 kg and containing 0.7 g of air. The total pressure of 0.37 mbar, including 0.25 mbar water vapor pressure, was to be controlled. The air had to be pumped off at a partial pressure of air of 0.12 mbar; 0.7 g of air at 0 °C and 0.12 mbar represents a volume of ~7.3 m^3. During the main drying time of 3.0 h, 2.4 m^3/h must be removed. If the vacuum pump has an effective pumping speed for air of, for example, 4.8 m^3/h, the pump would operate on average for 50% of MD. If the dissolved amount of gas is 10-fold larger, this must to be considered in the layout of the vacuum pump.

The second method has two advantages:

- Only gas of the product is used and no additional inert gas supply is needed.
- At the end of MD, when less and less dissolved gas is freed, the chamber pressure drops automatically, as is necessary for secondary drying.

The advantage of pressure control is the improved heat transfer leading to shorter drying times or possibly lower shelf temperatures. On the other hand, which is equally important, the ice temperature can be accurately controlled by the controlled pressure: In Table 1.15, the ice temperature at the sublimation front is −26.8 °C at a pressure of 0.36 mbar and −30.5 °C at 0.21 mbar (see column 3 or 4). In the test run in Figure 1.98, 0.36 mbar results in $T_{ice} = -21$ °C, since K_{tot} is larger between vials and shelves at the same shelf temperature of +29 °C. Should the total pressure exceed the desired value, the shelf temperature must be reduced accordingly. Figure 1.106 illustrates how T_{ice} is reduced in 4 h from −26.8 to −28 °C. The shelf temperature should have been raised slightly or the controlled pressure of 0.36 mbar increased. The change in shelf temperature is usually much too slow for such small changes; however, the change in pressure is quick and can easily be performed in small steps. The method of pressure control can only be applied as long as the partial vapor pressure is large compared with the pressure of permanent gases. If the pressure of permanent gases is of the same magnitude as or larger than the vapor pressure, the water vapor transport is hindered and the ice temperature is no longer a well-defined function of the control pressure.

To summarize, main drying is controlled by only two variables:

- the controlled operation pressure p_c;
- the selected shelf temperature T_{sh}.

These two data result in a temperature of the ice at the sublimation front T_{ice} in a given plant and a given product.

The uniformity of the drying rate for all vials in a charge depends on

- the shielding of the vials at the border of each shelf from influences of the walls and door(s);
- the uniformity of freezing and thermal treatment (annealing) in all vials.

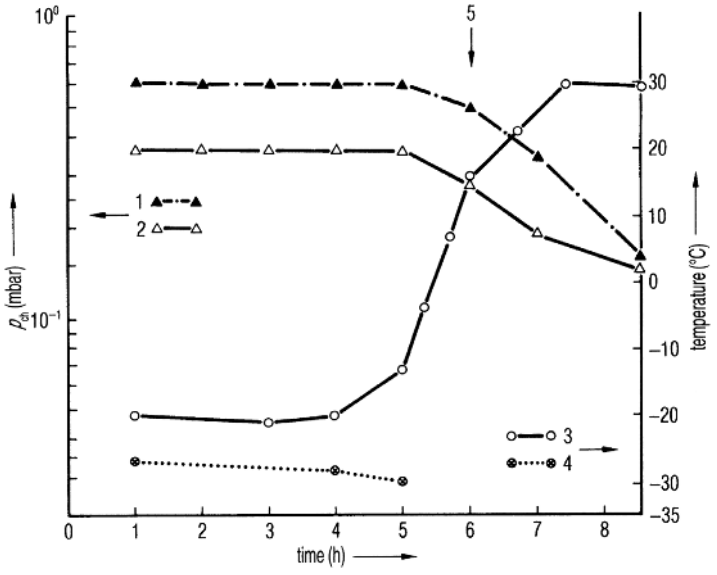

Figure 1.106 Course of a freeze-drying process during which T_{ice} was not kept constant at −26.8 °C. To avoid a decline in temperature, either T_{sh} could have been increased after 2 h (difficult to control as the inertia of the heating system is substantial) or p_c increased until T_{ice} is constant at −26.8 °C. 1, p_{ch} (TM); 2, p_{ch} (CA; 3, T_{pr} (RTD; 4, T_{ice} (BTM; 5, end of pressure control.

Two notes can be raised regarding the last point: Searles *et al.* [118] stress the influence of the ice nucleation temperature T_n on the primary drying rate and its uniformity. T_n (see Section 1.1.2) is stochastic, cannot be directly controlled, and depends on, among others, the particulate content, vial surface, and the time and temperature history of the product before freezing. The same authors [119] underline the importance of annealing up to T'_g to reduce the heterogeneity of sublimation rates. They found an increase in the drying rates of hydroxyethyl starch after annealing of up to 3.5-fold.

1.2.2 Secondary Drying (Desorption Drying)

During secondary drying (SD), the water will be removed that interacts with the solids such that the water cannot crystallize. The water can be bound to the surface of crystals in a crystallized product or can be included in amorphous product.

Fakes *et al.* [27] described the moisture sorption behavior of mannitol, anhydrolactase, sucrose, D-(+)-trehalose, dextran 40, and providone (PVP K24) before and after freeze-drying in a 10% solution. All products were frozen at 0.50 °C/min to −40 °C and freeze-dried at 0.13 mbar and $T_{sh} = -15$ °C for 28 h. SD lasted for 14 h at $T_{sh} = 25$ °C. Table 1.19 shows the moisture contents before and after freeze-drying. Figure 1.107 present the weight change in % of sucrose, trehalose, mannitol, and lactose in an atmosphere with increasing relative

Table 1.19 Moisture contents of bulking agents.

Bulking agent	Before lyophilization (% w/w)	After lyophilization (% w/w)
Mannitol	0.12	0.15
Lactose, anhydrous	0.86	1.63
Sucrose	0.15	2.51
Trehalose	9.2	1.17
Dextran 40	5.8	0.24
Povidone K24	8.6	0.37

Table 1 from Ref. [27].

humidity (RH) with time, before (top) and after (bottom) freeze-drying. In Figure 1.108, the same data are shown for providone and dextran. The results can be summarized with simplifications: Lyophilized mannitol is practically nonhygroscopic. Lactose gains ~10% up to 55% RH, followed by rapid desorption thereafter. DSC and X-ray diffraction (not shown) confirmed that the amorphous freeze-dried lactose was converted to the crystalline state at 55% RH and 25 °C. Sucrose behaves in a similar manner, but the uptake at RH 55% is ~4%, followed by desorption with increasing RH, being converted into the crystalline state, which is also possible by heat only. Lyophilized trehalose adsorbs an additional 10% up to 45% RH and is converted to the crystalline state at more than 50% RH. Dextran and providone absorbed up to 18 and 30% moisture, respectively, at 70% RH and remained amorphous. Under the experimental conditions of this study, all products were freeze-dried under the same freezing and drying conditions, and all moisture sorption measurements were at 25 °C and for a relatively short time. The authors considered this study as a useful guideline for the selection of optimal bulking agents.

In addition to substantial differences in the sorption behavior of products, the moisture distribution in each vial of one charge must be considered when the SD process is developed. Pikal and Shaw [120] studied this distribution in dextran 40, human serum albumin (HSA), bovin somatotropin (BST), and glycine. Thirty vials where filled with 10 or 20 mm cake thickness, loaded on shelves at 5 °C, cooled to −40 °C, and frozen in 30–45 min. T_c was determined for all products as >−12 °C. In Table 1.20, the water content of four products is shown in four different positions in the vials after 6 and 8 h of SD. With one exception, the water content in the core is twice as high as in the total vial, which is close to the content near the wall. Figure 1.109 shows the mean water content and the ratio of the content near the wall/mean content of a 1 cm BST cake. The error of the mean content decreases with time and the error of the ratio increases.

Pikal [121] described three possibilities for defining the change from main to secondary drying:

- an increase in product temperature;
- a decrease in the partial water vapor pressure;
- a pressure rise dp/dt (dt time) measurement.

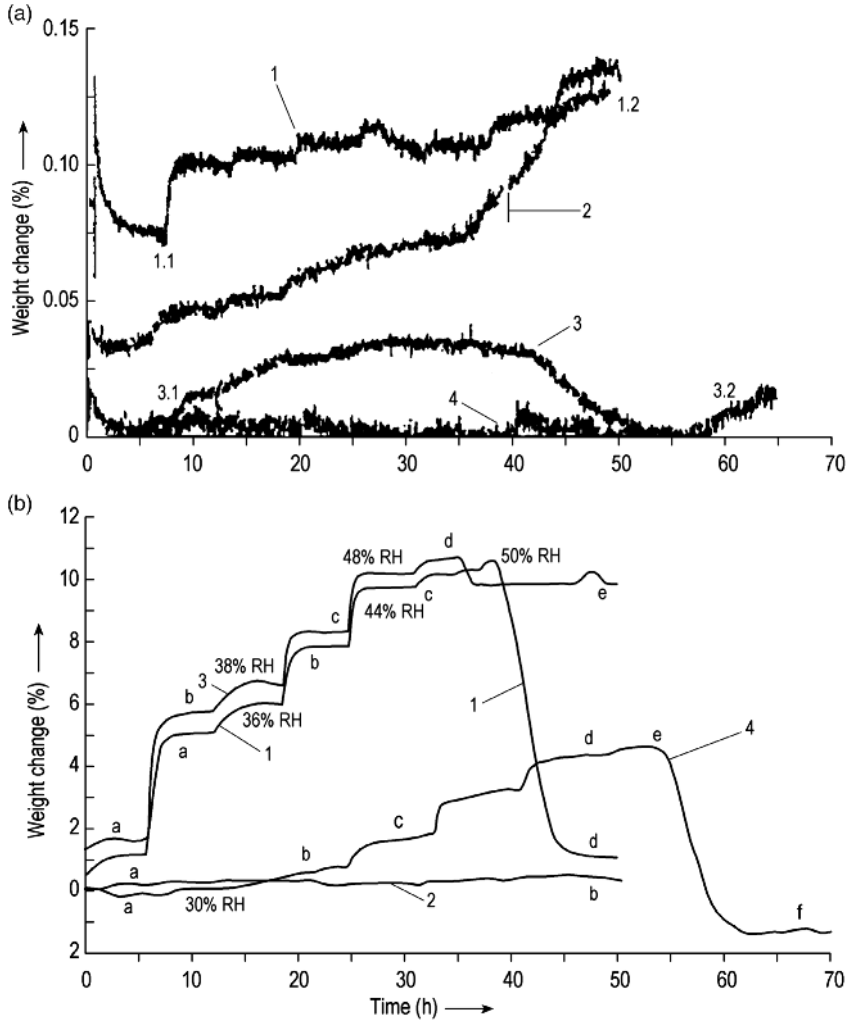

Figure 1.107 Moisture sorption profiles of anhydrous lactose (1), mannitol (2), trehalose (3), and sucrose (4). Before (a) and after (b) lyophilization (% weight change from the data in Table 1.18) at different relative humidity (RH) changes over 50–60 h. Before lyophilization: 1, lactose – 1.1 RH 10%, 1.2 RH 60%; 2, mannitol; 3, trehalose – 3.1 RH 10%, 3.2 RH 60%; 4, sucrose. After lyophilization: 1, lactose – 1a RH 30%, 1b RH 40%, 1c RH 50%, 1d RH 80%; 2, mannitol – 2a RH 10%, 2b RH 80%; 3, trehalose – 3a RH 10%, 3b RH 30%, 3c RH 40%, 3d RH 50%, 3e RH 80%; 4, sucrose – 4a RH 10%, 4b RH 30%, 4c RH 40%, 4d RH 50%, 4e RH 60%, 4f RH 80%. (see also Figure 1 from Ref. [27].)

As shown in Figures 1.96 and 1.97, the product temperature increases at the end of main drying; the measurements made by temperature sensors vary widely and are therefore a relatively uncertain indicator for the end of the main drying. The partial water vapor pressure changes during the transition from main drying to secondary drying over a period of several hours depend on the process

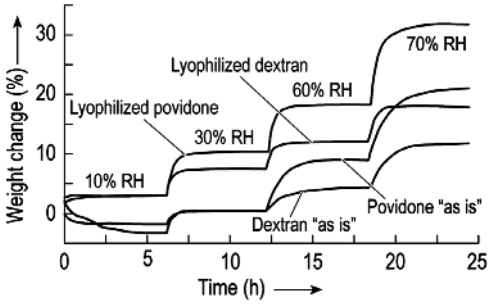

Figure 1.108 Moisture sorption profiles of dextran and povidone: % weight change from the data in Table 1.18. (Figure 2 from Ref. [27].)

Table 1.20 Water distribution given in % (w/w) (standard error) after 6 or 8 h of secondary drying in a 2 cm cake.

	Dextran	has	BST (6 h)	BST (8 h)
Whole vial	2.4 (0.2)	2.4 (0.8)	3.0 (1.0)	2.0 (0.4)
Position				
Core top	5.0 (0.3)	3.5 (0.3)	5.0 (0.2)	4.5 (0.3)
Core middle	5.0 (0.3)	4.5 (1.0)	5.2 (0.3)	4.2 (0.2)
Core bottom	4.9 (0.3)	3.8 (0.6)	15.0 (3.0)	4.5 (0.3)
Near vial wall	2.0 (0.1)	2.6 (0.6)	3.2 (1.0)	2.0 (0.4)

From Figure 4 in Ref. [120].

conditions (e.g., 2–3 h in Figures 1.96 and 1.97). In practice, one may have to wait several hours before the higher temperature for the secondary drying can be applied in order to avoid partial collapse. It is well known that the third possibility, pressure rise measurements for a given time, can be used to determine the changeover. The method can be applied more generally if the amount of water desorbed per unit time is measured and related to the solid content. This can be

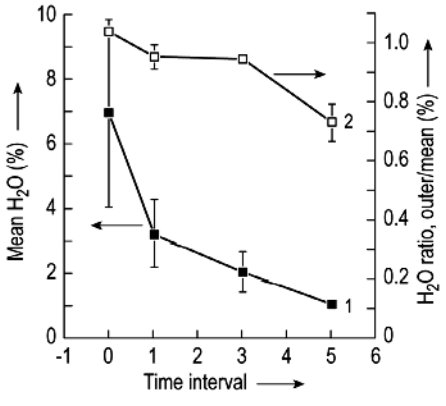

Figure 1.109 Mean water content (1) and ratio of water content (2) near the wall/mean water content in 1 cm cake of BST as a function of drying time. 0 h, start of SD. (Figure 5 from Ref. [120].)

defined as desorption rate (DR):

$$\mathrm{DR} = \frac{\text{amount of water desorbed} \times 100}{\text{time} \times \text{mass of solid}} (\%/\mathrm{h}) \tag{1.14}$$

The amount of water desorbed can be calculated by the pressure rise after the valve between the chamber and condenser has been closed, divided by the time of closure and the chamber volume (see Section 1.2.3, Eq. (1.16a)).

Calculation of the desorption rate:

$$\mathrm{DR} = 2.89 \times 100 \times \frac{V_{\mathrm{ch}}}{mf} \times \frac{\mathrm{d}p}{\mathrm{d}t} \tag{1.14a}$$

V_{ch} = chamber volume in liter (L)
m_{f} = mass of product solids (kg)
$d_{\mathrm{p}}/d_{\mathrm{t}}$ = pressure rise in time (mbar/s)
G = weight
V_{N} = nominal volume of water (= 22.4 L/mol). This corresponds to 22 400 L at 1 mbar and neglects the temperature change. From this, a linear dependence formulated as follows:
1 mol water (H_2O) has a volume of 22 400 L at a pressure of 1 mbar.
Converted to g (with $M_{H2O} = 18$ g/mol) results to
1 mol × 18 g/mol = 18 g

With these assumptions, the molar volume at 1 bar (1000 mbar) can be calculated as follows:

$$V1_{\text{mol } H_2O} = 22.400 \text{ L mbar}/1000 \text{ mbar} = 22.4 \text{ L/mol(nominal volume)}$$

What happens during the pressure rise?

There is an increase of H_2O molecules. To calculate the increase of mass, a comparison between state 1 and state 2 must be determined. For this purpose, the fixed chamber volume is taken as a reference and $p1 = 0.02$ mbar and $p2 = 0.1$ mbar selected. Thus, one can define the number of moles in the chamber as follows:

state 1: $V1_{\mathrm{H2O}}$ (L/mol) = 22 400 L mbar/0.02 mbar mol = 1 120 000 L/mol
state 2: $V2_{\mathrm{H2O}}$ (L/mol) = 22 400 L mbar/0.10 mbar mol = 224 000 L/mol.

$V1$ and $V2$ are the volumes that take up 1 mol under the given pressure.

With these values, the number of moles (with reference to the chamber volume) and thus the mass of water vapor (which is inside chamber) can be determined:

$$V_{\mathrm{N1}} = \frac{160\,l}{1,120,000 \text{ L/mol}} 1.429 \times 10^{-4} \text{ mol} \Rightarrow V_{\mathrm{N1}} \times 18 \text{ g/mol} = 0.0025722 \text{ g} = \mathbf{m1}$$

$$\mathrm{V_{N2}} = \frac{160\,l}{224,000 \text{ L/mol}} = 7.143 \times 10^{-4} \text{ mol} \Rightarrow V_{\mathrm{N2}} \times 18 \text{ g/mol} = 0.0128574 \text{ g} = \mathbf{m2}$$

The increase of mass is therefore $m2 - m1 = 0.102\,858$. This increase on mass refers to 30 s measuring time, converted to 1 h:

$$\Delta m = \frac{0.102852 \times 3600}{30} = 1.234224\ \mathrm{g/h}\left(\frac{\mathrm{g} \times \mathrm{s}}{\mathrm{s} \times \mathrm{h}}\right)$$

Thus, the desorption rate is

$$100 \times \frac{1.234224}{500} = 0.025\ \mathrm{g/h} \quad \left(\frac{\mathrm{g} \times \mathrm{s}}{\mathrm{s} \times \mathrm{h}}\right) = \left(\frac{\mathrm{g}}{\mathrm{h}}\right)$$

For confirmation: The same results calculated using the equation:

$$2.89 \times 100 \times \frac{160\ \mathrm{l}}{500\ \mathrm{g}} \times \frac{0.08\ \mathrm{mbar}}{30\ \mathrm{s}} = 0.025\ \mathrm{g/h}$$

Both calculation methods yield the same result. Herewith the constant 2.89×10^2 in the above equation is nothing but a constant that includes the following conversion:

- conversion to standard nominal volume;
- conversion to gram (mass);
- conversion to hour.

To understand the calculation steps here,

$$\left\{ \left[\frac{22400 \frac{1}{\mathrm{mol}}}{p_2 - p_1} \right]^{-1} \cdot V_k \right\} \cdot 18 \frac{\mathrm{g}}{\mathrm{mol}} \left(\frac{3600 \frac{s}{h}}{\mathrm{d}t} \right) \cdot \frac{100}{m_\mathrm{f}}$$

$$p_2 - p_1 = \mathrm{d}p$$

This makes

$$\frac{V_\mathrm{k}}{m_\mathrm{f}} \cdot \frac{\mathrm{d}p}{\mathrm{d}t} \cdot \left[\frac{3600 \frac{s}{h}}{22400 \frac{1}{\mathrm{mol}}} \times 100 \times 18 \frac{\mathrm{g}}{\mathrm{mol}} \right] = \underline{\underline{2.89 \times 10}}$$

This confirms the previous equation:

$$\mathrm{DR} = 2.89 \times 100 \times \frac{V_\mathrm{ch}}{m_\mathrm{f}} \times \frac{\mathrm{d}p}{\mathrm{d}t}$$

Figure 1.110 shows the three times repeated measurement of desorption rates, without pressure control, to demonstrate the reproducibility and two measurements where the main drying was pressure controlled at 0.36 and 0.21 mbar. The process conditions for these five measurements correspond to those in Table 1.15.

By barometric temperature measurements (BTM) and the measurements of the desorption rate (DR), the influence of varied drying conditions can be seen and analyzed. Figure 1.111 compares four different test runs:

1) *Test run (see Figure 1.97 and Table 1.14):* Without pressure control, in this installation – with the given shelf area, condenser temperature, the dimensions of the connection between chamber and condenser – a total pressure of

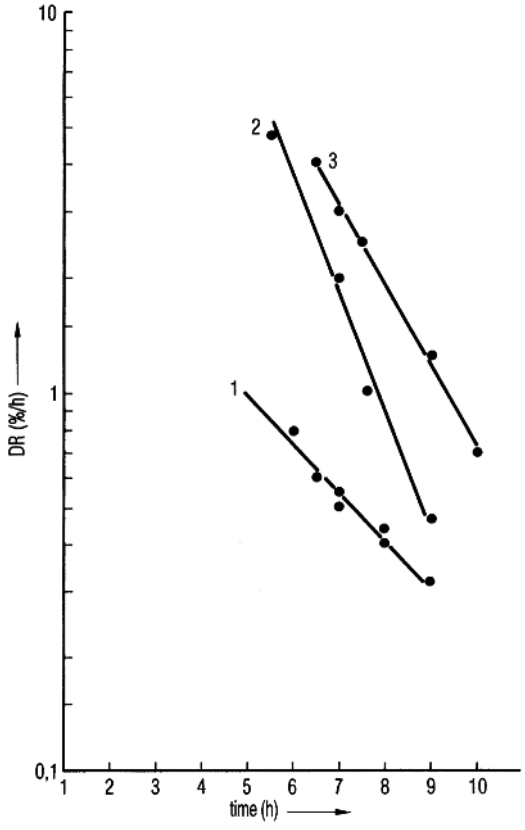

Figure 1.110 Desorption rate (DR) data as a function of drying time. 1, three repeated tests, pressure control not activated, process data as in the two left columns in Table 1.15; 2, process data as in Table 1.15, pressure control activated at 0.36 mbar; 3, process data as in Table 1.15, pressure control activated at 0.20 mbar.

0.15 mbar exists for ~5 h. The gas in the chamber is always pure water vapor. The ice temperature during this time is almost constant at ≃27 °C. The heat transfer coefficient at this pressure is small at ~65.7 kJ/m^2 h °C. The product temperature (resistance thermometer) increases only after these 5 h above the ice temperature. After 11.5 h, the desorption rate (DR) is ~0.8%/h. The total drying time, depending on the desired residual moisture content, is between 13 and 15 h.

2) *Test run:* Curves 2 in Figure 1.111 are taken from the test run, as shown in Figure 1.97, but with pressure control 0.36 mbar (total pressure measured with Capacitron). The ice temperature was −22 °C (constant) for 3 h and DR reached 0.5%/h after 10 h. Secondary drying could have been started much earlier, thus shortening the drying process.
3) *Test run:* The results of this run are only shown in Figure 1.111 in curves 3. In this run the shelf with the tray was inclined in such a way that a uniform thickness of 7 mm was varied from 5 to 9 mm. Otherwise, the conditions were the same as those in the second test (Figure 1.98). The ice temperature during main drying was similar but the DR value of 5.5%/h at ~9 h shows the variation of thickness of the layer. A DR of 0.5%/h was reached not in 10 h, but in 13 h. The test also showed (not in the figure) that the product temperature (T_{pr}) varied at 9 h from 0 to +22 °C.

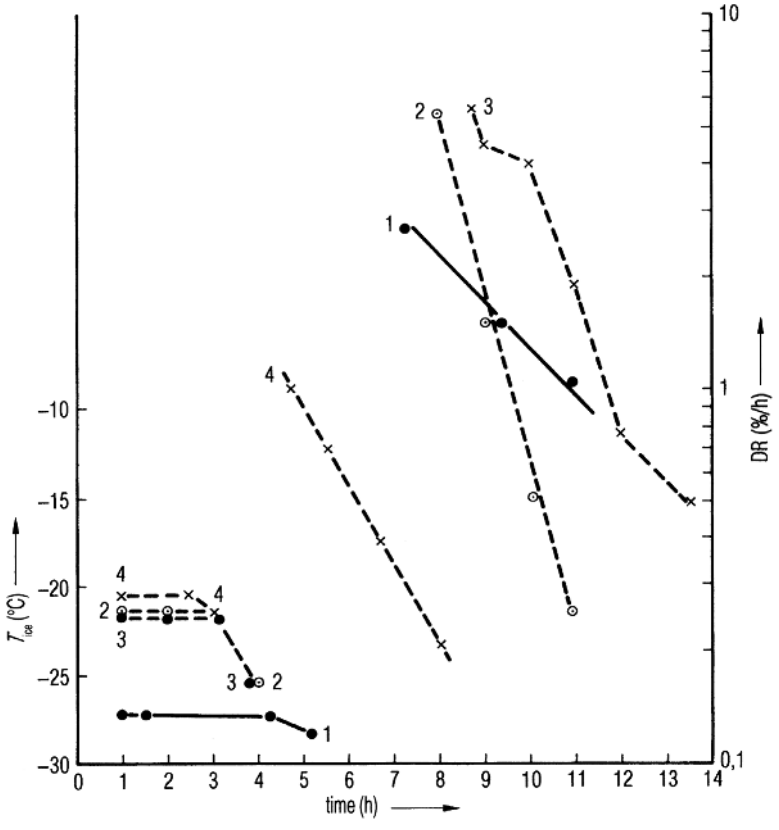

Figure 1.111 Synopsis of T_{ice} and desorption rate of the two tests in Figure 1.97 (1) and Figure 1.98 (4) and comparison with two other tests: (2) carried out as (1) but with activated pressure control at 0.36 mbar and (3) only one tray used (instead of three trays in Figure 1.97), which was placed at such a slope that the thickness of the product was 0.5 cm on one side and 0.9 cm on the other. The DR data measures, in spite of the chosen process data, the amount of desorbed water per hour in % of solid content. It can be seen that a DR value of 0.5%/h in test 4 is reached in 6.2 h, in test 2 in 10.2 h, and in test 1 in 13.5 h, but in test 3 the time cannot be estimated. Because of the unequal product thickness, the DR values can change (9.5 h), and the desorption process is not uniform for such a product.

4) *Test run (see Figure 1.98 and Table 1.14):* The analysis of the run shows that the relatively high heat transfer coefficient of 90.4 kJ/m^2 h °C at a controlled pressure of 0.36 mbar resulted in a constant ice temperature of −22 °C for 2.5 h. Secondary drying was started after 3.5 h and a DR of 0.5%/h was reached at ∼6 h.

The measuring of desorption rates can be used, as the above examples show, to determine the amount of desorbable water if the following prerequisites are fulfilled:

- The product shows a reproducible desorption isotherm, meaning that it is not measurably changed at the applied temperature.

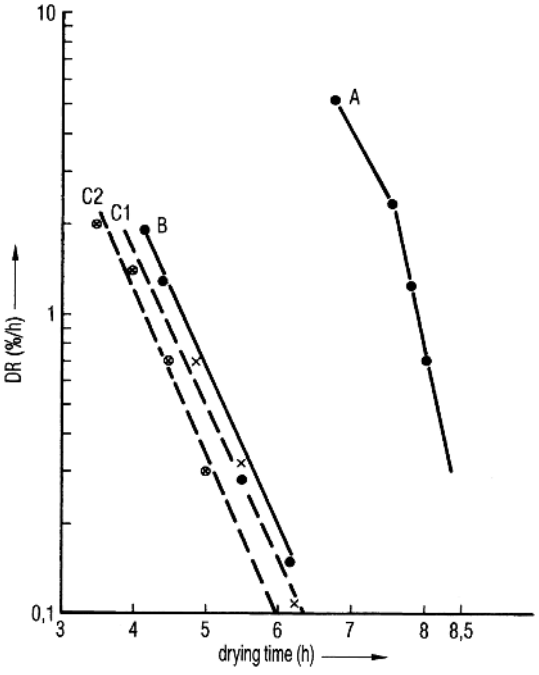

Figure 1.112 Desorption rate (DR) as a function of time for three different foodstuffs: A, B, and C. C1 and C2 differ in the product temperature, +42 and +47 °C, respectively. Product A contains ~85% water, whereas B and C contain only ~60% water. The slope change in A at 7.5 h indicates that the final product temperature was reached at around that time. (The plots are based on measurements by Dr. Otto Suwelack, Billerbeck, Germany.)

- The final temperature must be applied for some time, depending on the layer thickness, in order to reduce the temperature gradient in the product.

The DR values on a semilogarithmic scale plotted as a function of time (Figure 1.112) can be straight lines as long as the temperature of the product is approximately constant and the DR values are not less than 0.1%/h (sometimes 0.05%/h). In Figure 1.112, the change in inclination in plot A at 7.5 h indicates that the final temperature was only reached at ~7.5 h. After a drying time of ~8 h at a temperature of ~50 °C, product A showed a DR of 0.7%/h and after 8.5 h a DR of ~0.3%/h. Product B has, at 42.5 °C shortly before 6 h, a DR of 0.25%/h and at 6.3 h a DR of 0.14%/h. The desorption rate of product C1 at 42 °C was reached at 6.3 h, whereas at 47 °C (C2) already after 5.8 h only 0.1%/h are desorbed.

By integrating the DR values over time, it is possible to calculate the residual moisture content (RM) . The integral is calculated from the last measurement of DR over time up to any other measured DR. The integral is the RM at the time up to which the integral was calculated. The RM calculated in this way is too small by the amount of water that would have been desorbed after the measured DR. Thus, a method of calculation can be deduced: The straight line of the DR values is extrapolated until the still desorbable RM is small compared with the RM to be measured.

Example: By integrating the DR value for product C1 from 0.1 up to 2%/h, the line C1 in Figure 1.113 is obtained; at 3.6 h, the RM was 2.5%. The RM at 3.6 h is too small by the amount of water that would have been desorbed after 6.2 h. Between 6.2 and 7 h, 0.08%/h would have been desorbed. The RM at 3.6 h would not have been 2.5% but 2.56%. This example shows that it is always possible to extrapolate the desorption rates, as long as the error introduced by the integration can be made small compared with the RM to be calculated.

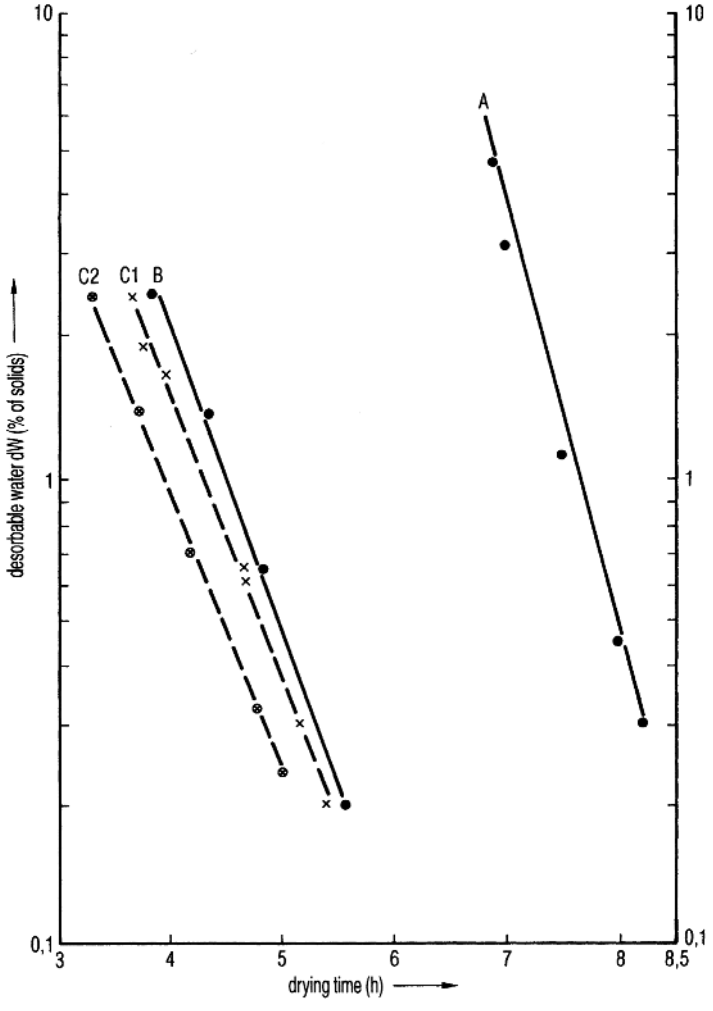

Figure 1.113 Desorbable water in % of solids (dW) as function of the drying time. The dW values were calculated from the data in Figure 1.112. In plot A, after 7.5 h only, 1% (of solids) water can be removed by further drying at this temperature. If, for example, 0.3% is required, the drying can be terminated at 8.3 h.

It should be clear that the RM calculated in this way, for example, 0.1%, must not be identical with residual moisture contents measured using other methods (see Section 1.3.1) because there will always be some water that cannot be desorbed at the end temperature of the drying. This content of bound water for one product and one temperature is a stable value that can be taken from the measurements of absorption isotherms.

The residual moisture content measured by desorption is therefore called desorbable water (dW) and it indicates how much water can still be desorbed at that temperature – or put other way – how much water could be desorbed by further drying, for example, a product having dW = 0.5% can only be further dried by a maximum of 0.5% at the chosen $T_{sh,SD}$. This is of interest for products in which the water content should not be lower than a predetermined value. Pikal [121] missed the exact proof that overdrying (removal of a certain amount of bound water) is detrimental to the product. Hsu *et al.* [122] have shown that freeze-drying of tissue-type plasminogen activator (tPA) below 7.6% RM denatures the product, as 7.6% RM corresponds to a monolayer of water molecules on the tPA molecule. However, the dried product having 7.6% RM at a temperature of 50 °C during storage for 50 days loses more of its activity than a product with a lower water content. Hsu *et al.* recommended examining the optimum water content that cannot be reached on the basis "the lowest residual moisture is the best."

Secondary drying is dominated by the sorption behavior and the structure of the product. Therefore, the DR plots are not always as straightforward as shown so far. Figure 1.114 gives the DR plots of a 10% mannitol solution frozen in 300

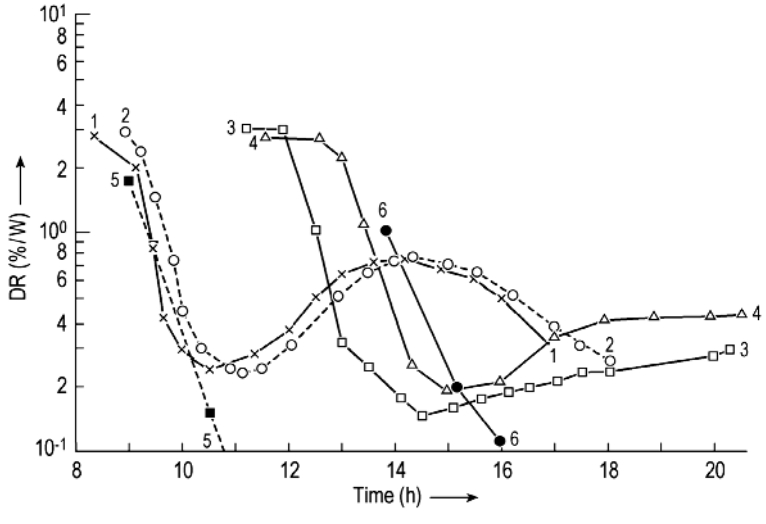

Figure 1.114 DR as a function of drying time of 10% mannitol solution frozen in 300 vials on a shelf with a freezing rate of 0.3–0.6 °C/min, $d = 10$ mm. Process data during MD: In plots 1 and 2, $T_{sh} = 20$ °C, $p_c = 0.3$ mbar, and $T_{ice} = -22.50$ and -22.53 °C, respectively; in plots 3 and 4, $T_{sh} = 5$ °C, $p_c = 0.3$ mbar, and $T_{ice} = -24.92$ and -25.26 °C, respectively. For comparison, plot 5, 10% egg albumin, 400 vials, 10 mm, 0 °C, 0.3 mbar; plot 6, 10% saccharose, 400 vials, 10 mm, 0 °C, 0.15 mbar. (From Ref. [123].)

vials on a shelf with a freezing rate of 0.3–0.6 °C/min, $d = 10$ mm. The process data during MD were as follows:

Plots 1 and 2: $T_{sh} = 20$ °C, $p_c = 0.3$ mbar, $T_{ice} = -22.50$ and -22.53 °C
Plots 3 and 4: $T_{sh} = 5$ °C, $p_c = 0.3$ mbar, $T_{ice} = -24.92$ and -25.26 °C

and for comparison:

Plot 5: 10% egg albumin, 400 vials, 10 mm, 0 °C, 0.3 mbar
Plot 6: 10% saccharose, 400 vials, 10 mm, 0 °C, 0.15 mbar

The drying at a lower T_{sh} did not change the desorption behavior. In the product there exists a combination of two or more structures. Slow freezing produces in a 10% mannitol solution a mixture of α- and β-polymorphs, and fast freezing the δ form (Ref. [124], see also Ref. [23]). If the mannitol solution is frozen in LN_2 at a rate of ~30–60 °C/min, Figure 1.115, a single structure exists. The product in plot 1 is collapsed. The DR plot 3 turns flatter at 0.3%/h. After annealing (plot 2) or MD at a lower p_c (0.08 mbar) and a lower T_{ice} (5 °C) (plot 4), the flatter part disappears into a straight line (see caption of Figure 1.115).

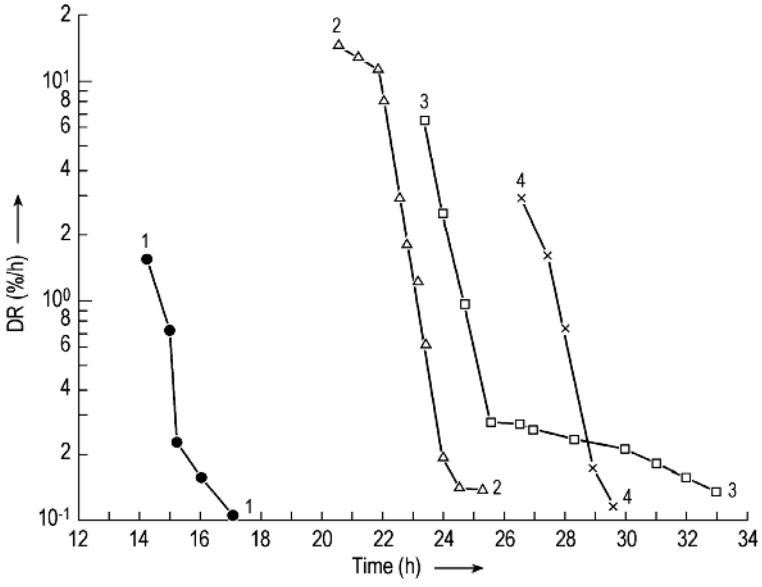

Figure 1.115 DR as a function of drying time of 10% mannitol solution frozen in LN_2 in 130 vials. Plot 1: Product is collapsed because 380 vials have been loaded (also confirmed by visual inspection of the dry product); after a short time of SD, the water evaporates with difficulty from the highly viscous concentrates. Plot 3: In liquid, nitrogen frozen at a rate of 30–60 °C/min, below DR = 0.3%/h the unfrozen water in viscous inclusions is difficult to remove. Plot 2: As plot 3, but the product is annealed after freezing before drying, the unfrozen water is crystallized. Plot 4: As plot 3, but dried at T_{ice} 5 °C lower than in plot 3 (−41 °C); at this temperature, the viscosity is about two decades higher. The product can be successfully dried, but the drying time is ~5 h longer. E: indicates the error in the range of 0.2%/h (From Meister, 2009 [60]. Reproduced with permission of Elsevier.)

Desorption rates not only document the progress of SD and permit the calculation of dW, they also reflect the history of the product during freezing and main drying. For technical details, see Section 1.2.3.

1.2.3 Temperature and Pressure Measurement

Temperature and pressure measurements during freeze-drying are difficult tasks. Thermal elements (Th) and temperature-depended electrical resistance (RTD) systems measure only their own temperature and that of their surroundings only if they are in very close contact with them. Furthermore, they heat themselves and their surroundings by the current flow through the sensors. Also, they influence the crystallization of the product in their surroundings:

- by the energy they produce;
- by inducing heterogeneous crystallization, which can be different in the product without sensors [125]; and
- by different subcooling, which can be smaller around the sensor and result in a coarser structure.

These structure changes and the heat input by the sensors also influence the main drying of vials with sensors. In addition to these problems of principle, there are also practical ones: Ths and RTDs have to be inserted into the product and connected with vacuum-tight lead-throughs to the measuring system. During freezing, the type of sensors used can have the influence shown in Figure 1.116 [126]. The position of the sensors during freezing has a limited influence [127], as shown in Figure 1.117. During freezing, temperature sensors provide a reasonably accurate temperature picture, even if the product with sensors reacts differently to the way it does without sensors.

During main drying, the situation is very different: The condition of a close contact with the product is only true at the beginning of MD; thereafter, the measured temperature depends on circumstances that are difficult to analyze.

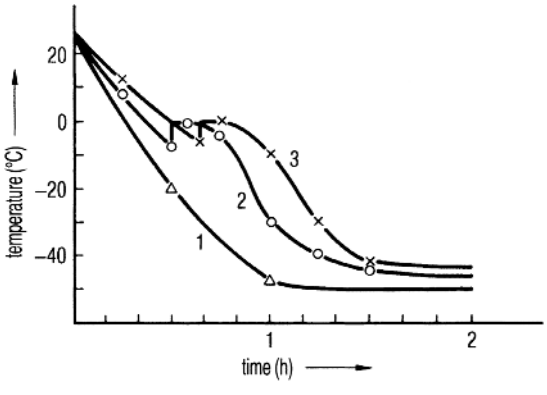

Figure 1.116 Temperature in the product as a function of freezing time, measured by one RTD and one Th each in three vials. The vials had been distributed diagonally on one shelf (the differences between the three vials are within the accuracy of the drawing). 1, T_{sh}; 2, T_{pr} measured by RTD; 3, T_{pr} measured by Th. (See also Figure 3 from Ref. [126].)

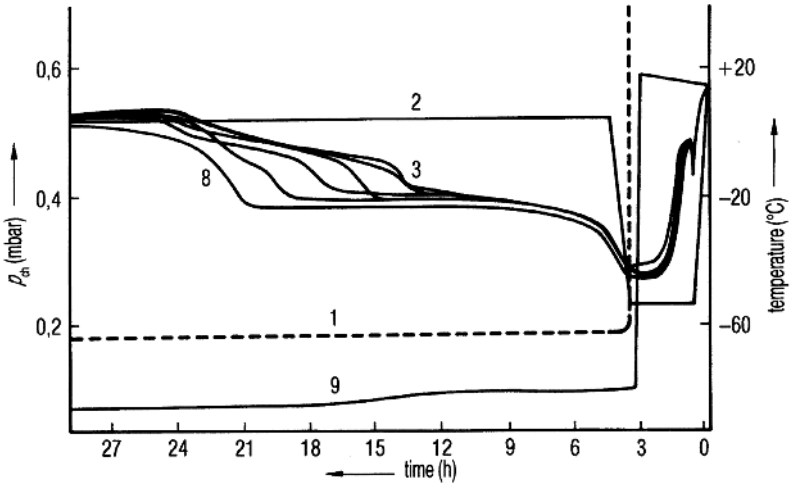

Figure 1.117 Temperature and pressure as a function of the process time. During freezing, the data measured by six temperature sensors are reasonably close together. The split-up after 12 h shows that the progress of MD has reached a level at which the different locations of the sensors become relevant. 1, p_{ch}; 2, T_{sh}; 3–8 temperature sensors; 9, T_{co}. (See also Figure 3 from Ref. [127].)

The position of the sensor, on top, in the center, or near the bottom contact with the vial wall, decides the measured data, as shown in Figure 1.118. If the filling volume of vials is small (a few millimeters layer thickness) or if the product is granular, it is especially difficult to obtain useful data. Also, in homogeneous layers with a thickness of 6–10 mm, temperature differences during main drying can be 10–20 °C when measured with three RTDs, as shown in Figure 1.97. Such differences can also be found between two vials in the same charge during main drying.

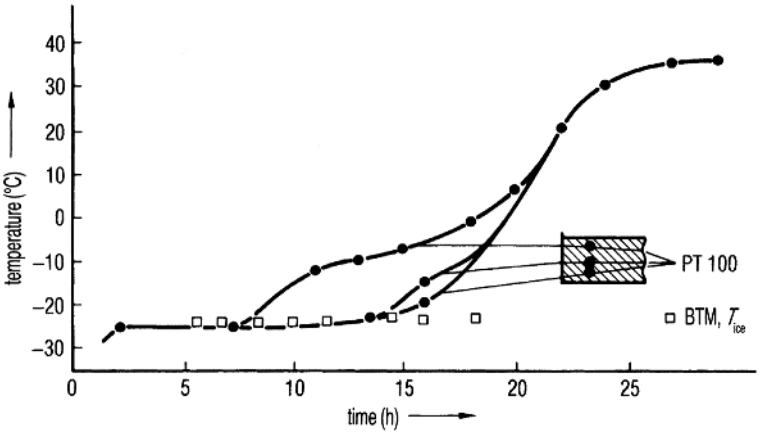

Figure 1.118 Product temperature measured in three different locations in the product as function of the drying time. T_{ice} is measured simultaneously by BTM. (See also Figure 3 from Ref. [128].)

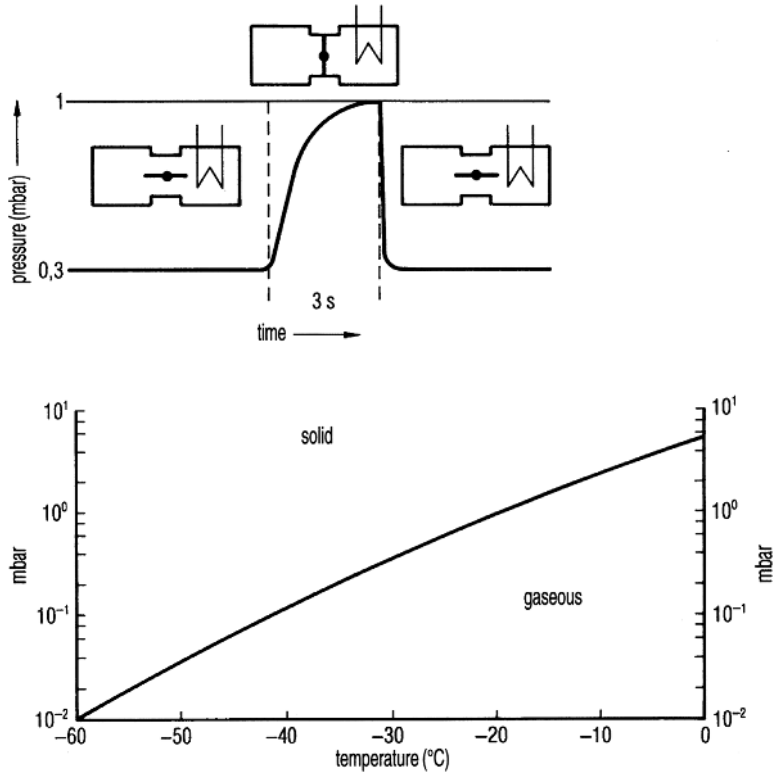

Figure 1.119 Scheme of the "barometric temperature measurement" (BTM) and plot of the water vapor pressure of ice. (Figure 4 from Ref. [130].)

The most important parameter during main drying is the temperature at the moving sublimation front, which cannot be measured by Ths or RTDs. In 1958, Neumann and Oetjen [129] showed that the barometric temperature measurement (BTM) measures exactly this value. This is shown schematically in Figure 1.119: If the drying chamber is separated from the condenser by a valve for a short time, the pressure in the chamber rises to the saturation vapor pressure (p_s) corresponding to the temperature of the sublimation front. p_s can be converted into the ice temperature by the water vapor–temperature diagram (e.g., 0.3 mbar = −30 °C). Data for accurate conversion are given in Table 1.21 for temperatures between −100 and −1 °C.

Milton *et al.* [131] used this method and referred to it as manometric temperature measurement. They used times of pressure rise of up to 30 s. During this time, the ice temperature will increase, mainly owing to continued heat flow. Therefore, an equation has been developed to transform the experimental pressure data, including three other corrections, into the true vapor pressure of the ice. If the valve is closed for only a very short time, <5 s, and the pressure is measured and recorded 60–100 times/s, these data can be recorded as shown in Figure 1.120. The automatic pressure rise measurements (1) can then be plotted and the computer calculates the first derivative (2). The peak time represents the

Table 1.21 Equilibrium water vapor pressure of ice and the related specific density of the vapor.

t °C	p_s mbar	ρ_D g/m^3	t °C	p_s mbar	ρ_D g/m^3
−100	$1.403 \cdot 10^{-5}$	$1.756 \cdot 10^{-5}$	−50	39.35	38.21
−99	1.719	2.139	−49	44.49	43.01
−98	2.101	2.599	−48	50.26	48.37
−97	2.561	3.150	−47	56.71	54.33
−96	3.117	3.812	−46	63.93	60.98
−95	3.784	4.602	−45	71.98	68.36
−94	4.584	5.544	−44	80.97	76.56
−93	5.542	6.665	−43	90.98	85.65
−92	6.685	7.996	−42	102.1	95.70
−91	8.049	9.574	−41	$114.5 \cdot 10^{-3}$	106.9
−90	9.672	11.44	−40	0.1283	0.1192
−89	11.60	13.65	−39	0.1436	0.1329
−88	13.88	16.24	−38	0.1606	0.1480
−87	16.58	19.30	−37	0.1794	0.1646
−86	19.77	22.89	−36	0.2002	0.1829
−85	23.53	27.10	−35	0.2233	0.2032
−84	27.96	32.03	−34	0.2488	0.2254
−83	33.16	37.78	−33	0.2769	0.2498
−82	39.25	44.49	−32	0.3079	0.2767
−81	46.38	52.30	−31	0.3421	0.3061
−80	$0.5473 \cdot 10^{-3}$	$0.6138 \cdot 10^{-3}$	−30	0.3798	0.3385
−79	0.6444	0.7191	−29	0.4213	0.3739
−78	0.7577	0.8413	−28	0.4669	0.4127
−77	0.8894	0.9824	−27	0.5170	0.4551
−76	1.042	1.145	−26	0.5720	0.5015
−75	1.220	1.334	−25	0.6323	0.5521
−74	1.425	1.550	−24	0.6985	0.6075
−73	1.662	1.799	−23	0.7709	0.6678
−72	1.936	2.085	−22	0.8502	0.7336
−71	2.252	2.414	−21	0.9370	0.8053
−70	$2.615 \cdot 10^{-3}$	$2.789 \cdot 10^{-3}$	−20	1.032	0.8835
−69	3.032	3.218	−19	1.135	0.9678
−68	3.511	3.708	−18	1.248	1.060
−67	4.060	4.267	−17	1.371	1.160
−66	4.688	4.903	−16	1.506	1.269
−65	5.406	5.627	−15	1.652	1.387

Table 1.21 (*Continued*)

t °C	p_s mbar	ρ_D g/m^3	t °C	p_s mbar	ρ_D g/m^3
−64	6.225	6.449	−14	1.811	1.515
−63	7.159	7.381	−13	1.984	1.653
−62	8.223	8.438	−12	2.172	1.803
−61	9.432	9.633	−11	2.376	1.964
−60	$10.80 \cdot 10^{-3}$	10.98	−10	2.597	2.139
−59	12.36	12.51	−9	2.837	2.328
−58	14.13	14.23	−8	3.097	2.532
−57	16.12	16.16	−7	3.379	2.752
−56	18.38	18.34	−6	3.685	2.990
−55	20.92	20.78	−5	4.015	3.246
−54	23.80	23.53	−4	4.372	3.521
−53	27.03	26.60	−3	4.757	3.817
−52	30.67	30.05	−2	5.173	4.136
−51	34.76	33.90	−1	5.623	4.479

Source: From Smithsonian Metrological Tables, 6th edn, 1971 and VDI-Wasserdampftafeln, 6. Ausgabe (1963).

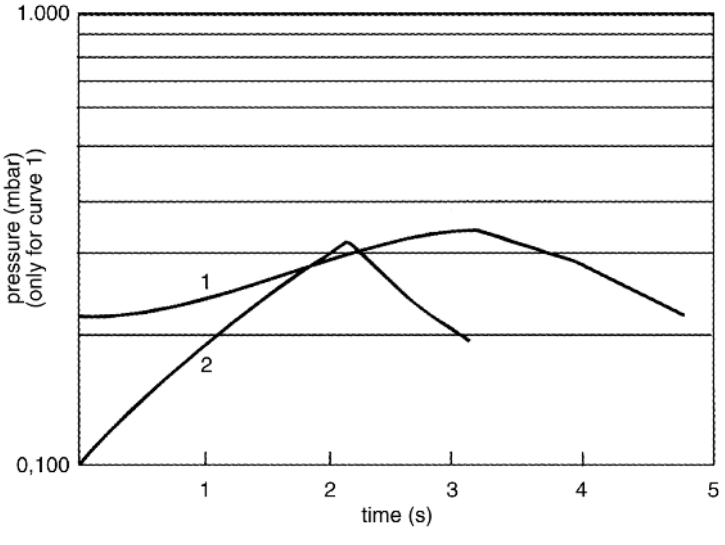

Figure 1.120 Pressure rise as a function of time. 1, pressure rise in the chamber after the valve is closed; 2, first derivative of 1. A maximum of 2 is reached at 2.14 s, the related equilibrium vapor pressure is $p_s = 0.286$ mbar corresponding to $T_{ice} = -32.7$ °C. (Figure 2 from Ref. [132].)

Table 1.22 Protocol of T_{ice} during main drying.

t_{MD} (h)	T_{ice} (°C)	$T_{ice/n}$ (°C)	t_{MD} (h)	T_{ice} (°C)	$T_{ice/n}$ (°C)
02.0	−23.5	−23.5	02.3	−23.3	−23.4
02.5	−23.5	−23.5	02.8	−23.6	−23.5
03.0	−23.3	−23.4	03.3	−23.4	−23.4
03.5	−23.4	−23.4	03.8	−23.4	−23.4
04.0	−23.7	−23.5	04.3	−24.1	−23.5
04.5	−24.4	−23.6	04.8	−24.3	−23.7
05.0	−25.1	−23.8	05.3	−25.9	−23.9

$T_{ice/n}$: sum of all n T_{ice} measurements divided by n, after thermal equilibrium has been reached (in this run after 2 h). The main drying in this run could have been terminated after 5 h, but it is useful to wait for the next data, so that the decision is not dependent on one measurement.

time when p_s has been reached. In the example this time was 2.14 s after the valve had been closed. The related equilibrium pressure is $p_s = 0.286$ mbar corresponding to $T_{ice} = -32.7$ °C. Table 1.22 shows the results of such measurements. The average temperature from 2.0 to 4.8 h is −23.66 °C, the standard deviation being 0.39 °C.

In a production plant, the valve between the chamber and condenser could have a diameter of 1 m or more, and it cannot be closed in 5 s or less, 6–7 s may also work. However, the method can be applied with some changes in the software: The movement of the valve is controlled for its reproducibility and accuracy and the pressure rise is used for the calculation of T_{ice} after the valve has reached a certain position. Table 1.23 shows such measurements for a valve with a diameter of 1.1 m.

T_{ice} data depend on the number of vials in the chamber. T_{ice} is the temperature at the sublimation front of the ice at which the heat transfer from the shelf to the

Table 1.23 Extracts of T_{ice} data measured in a plant with a valve of 1.1 m diameter between the chamber and condenser (Measurement Steris GmbH).

t_{MD} (h)	T_{ice} (°C)	t_{MD} (h)	T_{ice} (°C)
01.65	−42.0	05.17	−41.7
02.10	−41.9	05.23	−41.8
02.80	−41.8	05.38	−42.0
AV	−41.9 SA 0.1 °C	AV	−41.8 SA 0.15 °C
04.45	−42.0		
04.70	−41.9		
04.95	−41.6		
AV	−41.8 SA 0.21 °C		

AV= average value of all measurements −41.85 °C SA 0.14 °C.
SA = Standard deviation.

Table 1.24 Comparison of runs with different numbers of vials.

No. of vials	Average T_{ice} (°C)	Saturation vapor pressure p_s (mbar)	Standard deviation of T_{ice} (°C)	Main drying time t_{MD} (h)
50	−35.75	0.206	0.192	9.9
100	−34.33	0.230	0.162	10.7
400	−32.38	0.296	0.228	11.4

T_{ice} data are the average of four runs with each number of vials. All vials with the same product and filling height.

ice front is in equilibrium with the energy consumption at this front by the sublimation of ice. The heat transfer coefficient is constant; with more or fewer vials the heat transfer surface increases or decreases, producing more or less vapor. The vapor passes the same geometric dimensions of the plant. For more vapor transport a higher and for less vapor transport a smaller pressure difference is needed. T_{ice} increases with more vials, as shown in Table 1.24. $p_{co} \ll p_c$, therefore dp for 400 vials is ~50% larger than for 50 vials. If, for example, −35 °C is not to be exceeded, p_c for 400 vials has to be lowered (see Figure 2.116 and text).

T_{ice} data not only show the ice temperature of the sublimation but also provide some information about the composition of the cake. In Figure 1.121, the

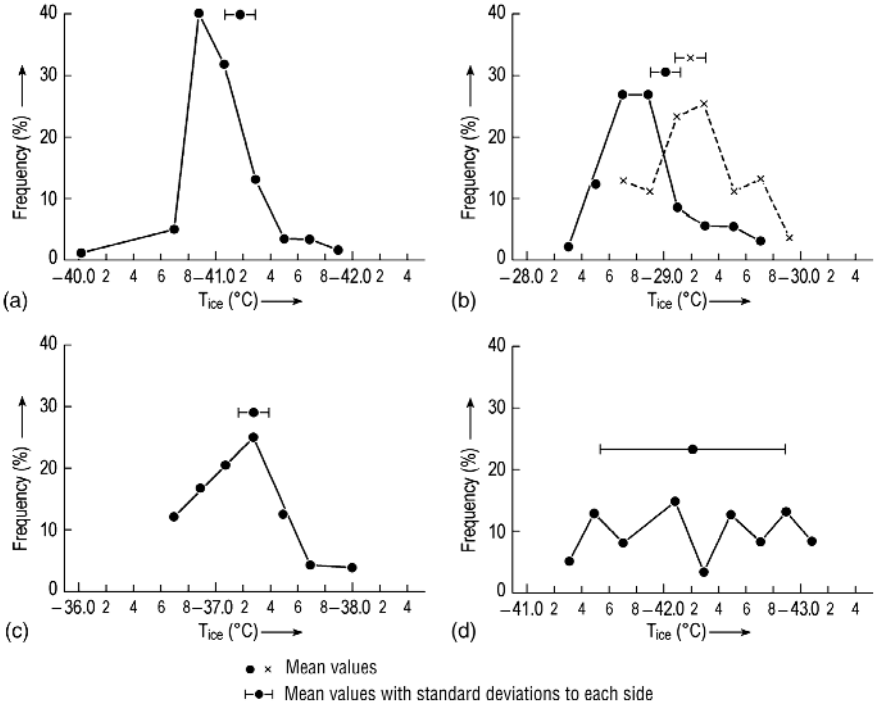

Figure 1.121 Frequency distribution of T_{ice} in five runs (two runs together shown in part (b)). Data in Table 1.25.

Table 1.25 Data for the four runs in Figure 1.122.

	Product egg albumin (ea)	ea	ea + 0.9% NaCl	Pharmaceutical
Code in Figure 1.121	(a)	(b)	(c)	(d)
Cake thickness (mm)	20	20	20	20
Freezing method	Shelf (sh)	LN_2	LN_2	sh
T_{sh} (°C)	−5	20	20	0
p_c (mbar)	0.1	0.3	0.1	0.07
Mean T_{ice} (°C)	−41.1	−29.2	−37.3	−42.2
SA (°C)	0.18	0.3	0.3	0.6

frequency of T_{ice} data for runs a–d is shown. Table 1.25 provides the process conditions for these runs.

a) The albumin is freeze-dried at low p_c and T_{sh}, resulting in a very stable, uniform cake; 70% of all T_{ice} data are between −40.9 and 41.1 °C with SA <0.2 °C.
b) The albumin in two runs is frozen in LN_2, not annealed; the two mean T_{ice} are within the SDs, but the frequency analysis shows that freezing without annealing produces slightly different cakes.
c) The addition of 0.9% NaCl made the frequency analysis broader than in (a); the SA is as in (b).
d) In spite of the low p_c (0.07 mbar) and the low T_{ice} (−42.2 °C), the frequency distribution of T_{ice} indicates an incompletely frozen product with high concentrated inclusions, which pass through the sublimation front at irregular intervals. ER measurements (not shown) confirm that the product should theoretically be frozen down to −65 °C and dried at $T_{ice} \leq 50$ °C. The product manufactured with the data shown was not unacceptable. This example shows that a compromise is sometimes necessary, if it can be carefully monitored. A process operated at T_{ice} −40 °C resulted in an unacceptable shrinkage.

Table 1.22 shows also T_{ice}/n, which is the sum of all measurements divided by the number of measurements. After 4.3 h, T_{ice} drops in 1 h by 2.5 °C below the highest T_{ice}/n (−23.4 °C). As shown in Figure 1.122, this decrease in ice temperature marks the end of main drying and can be used to switch over manually or automatically to secondary drying.

As a disadvantage of the BTM method, Bardat *et al.* [127] described the danger of collapse or melting of the product during the pressure rise measurement. This can only happen if T_{ice} and thereby p_s are larger than the maximum tolerable T_{ice}. The measurement is not the reason for the collapse, it is the too high T_{ice} shown by the measurement. Bouldoires [133] pointed out that the BTM method can only be used for discontinuous installations having a valve between the drying chamber and condenser.

For the use of BTM, two conditions have to be fulfilled.

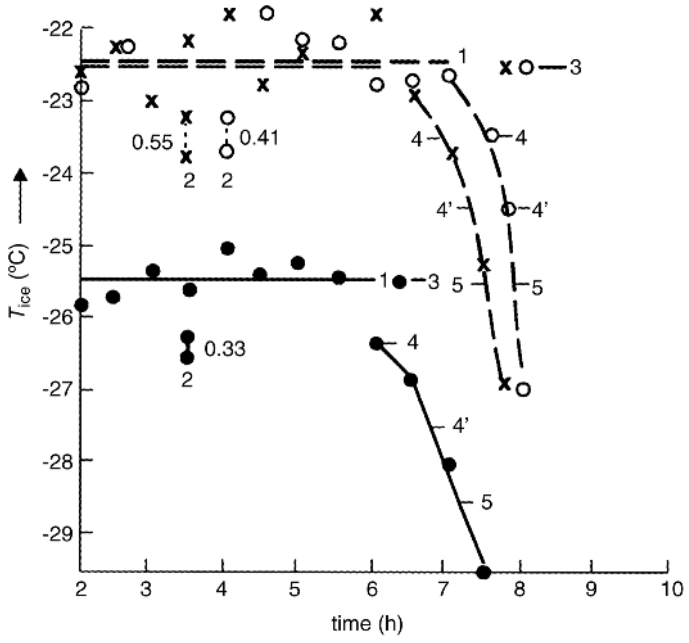

Figure 1.122 T_{ice} as a function of drying time. (○), (×): measurements and repetition with the same product and the same process data; (●) another product with other process data. 1, average T_{ice}; 2, standard deviation of T_{ice}; 3, maximum $T_{ice/n}$ for (○) and (×) identical −22.53 °C; 4, maximum $T_{ice/n}$ −1 °C; 4′, maximum $T_{ice/n}$ −2 °C; 5, maximum $T_{ice/n}$ −3 °C. (Figure 6 from Ref. [132].)

The first condition is that the leak rate of the chamber has to be so small that the pressure rise in the chamber during the time of valve closure due to leak rate is small compared with the pressure rise due to the water vapor.

Example: The pressure in the chamber rises in 3 s from 0.28 to 0.41 mbar. With a chamber volume of 200 L, this is 8.7 mbar L/s of water vapor. This vacuum chamber should have a leak rate not larger than 0.08–0.09 mbar L/s (1% of 8.7 mbar L/s). Such a leak rate has no measurable consequences. Even if it were 10 times larger (0.8–0.9 mbar L/s), the pressure in the chamber would rise in 3 s to 0.42 mbar. Converted into temperature, this would be an error of 0.1 °C. A leak rate of 0.8–0.9 mbar L/s is already larger than could be pumped off by a reasonable pumpset in this size of freeze-drying plant. The partial pressure of air, p_{air}, must be small compared with the water vapor pressure. At 0.28 mbar, total pressure p_{air} should be 0.03–0.04 mbar. A vacuum pump that can pump 0.8–0.9 mbar L/s at 0.03–0.04 mbar must have a pumping speed of ∼100 m^3/h, which is unusually large for a 200 L chamber. A vacuum pump with a 40 m^3/h pumping speed will theoretically evacuate a chamber and condenser (total 500 L) in ∼6 min down to 0.1 mbar. Even if it takes 10 min with the loaded chamber, the pumping speed of the pump is sufficient. With this pump, the leak rate of the plant should not exceed 0.4 mbar L/s, which would be pumped at ∼0.04 mbar.

The necessary leak tightness of a plant can be summarized as follows.

To ensure an undisturbed water vapor transport (see Section 1.2.4), the leak rate of a freeze-drying plant must allow BTM with sufficient accuracy. This applies for vapor pressures with ice temperatures ranging between −50 and −10 °C corresponding to 0.04–2.5 mbar. The pressure range for DR measurements is normally one decade below the above data and this has to be considered in the specification of the plant. All measurements discussed above have to be carried out with a capacitance vacuum gauge, because these instruments measure pressure independently of the type of gas. All vacuum gauges based on the change of heat conductivity as a function of pressure show a result that depends not only on the pressure of the gas mixture but also on the type of gas. Leybold AG [134], a company based in Cologne, Germany, indicates that for instruments based on heat conductivity such as the Thermovac in the pressure range from 10^{-3} to 1 mbar, with measurements in pure water vapor (carried out with an instrument calibrated in air), the reading value must be multiplied by 0.5 to give the correct water vapor pressure. If the mixture of water vapor and air changes, the reading value of, for example, 0.28 mbar water vapor pressure in pure water vapor corresponds to 0.14 mbar. At 80% water vapor, the reading value must be corrected to 0.17 mbar. In freeze-drying plants during main drying, the water vapor content can vary between 60 and 95%. An average correction factor of 0.65 can be used, as can be seen in Figure 1.97: Here 0.34 mbar with a Thermovac corresponds to 0.16 mbar, showing a correction factor of ∼0.5, with the progress of drying after 8 h, 0.11 mbar with the Thermovac corresponding to 0.08 mbar measured with a Capacitron with a correction factor of 0.73. Given that the reproducibility of the heat conductivity manometer in the pressure range of 10^{-2}–1 mbar is ∼10% of the reading [134] while capacitance gauges are rated at 0.5% of the reading [135], the advantages of the capacitance method are clear. The difference in price for the two types of instruments is small compared with the investment cost, even for a pilot freeze-drier. BTM should therefore always be carried out with a capacitance instrument.

The second condition for a reliable BTM is that, in the tolerable measuring time, so much ice can sublime as to fill the chamber with saturated water vapor. The measuring must be chosen in such a way that the temperature of the ice during closing of the valve between the chamber and condenser does not rise to a disturbing degree. Assuming extreme conditions, one can estimate that the temperature of the ice increases by ∼0.25 °C/s under the following stipulations:

- K_{tot} is high, for example, 84 kJ/m^2 h °C;
- ΔT is large, for example, 50 °C;
- the product with 10% solids has been dried so that only 15% of the water is ice and the layer thickness is 0.7 cm.

The measuring time should be <3 s; this is possible, as can be seen from Tables 1.22 and 1.23 and Figure 1.120.

The chamber volume and the amount of ice to be sublimed during MD must satisfy the following conditions:

$$V_{ch} dp/dt \ll m_{H2O}/t_{MD} \tag{1.15}$$

where

V_{ch}	=	chamber volume (L);
dp	=	$p_s - p_{H2O,ch}$ (mbar), pressure rise during measuring time;
dt	=	time (s) until p_s is reached;
m_{H_2O}	=	mass of water to be sublimed during the time of MD;
t_{MD}	=	time of MD (s), secondary drying not included.

An example of Figure 1.98:

V_{ch}	=	160 L
dp	=	0.51 − 0.13 mbar = 0.38 mbar
dt	=	3 s
M	=	2.24 kg water, 85% to be sublimed = 1.90 kg
t_{MD}	=	5 h = 18 × 10 × s
		(1 g H_2O is converted into 1.24×10^3 mbar L)

results in

$$\frac{160 \times 0.38}{3} \ll \frac{1.9 \times 10^3}{18} \times \frac{1.24 \times 10^3}{10^3} \qquad (1.15a)$$

$$20.27 \ll 131$$

With the data of the example condition (1.15) is satisfied, BTM can be applied.

If in this example a chamber of 1000 L were used, the left side of the equation would become 126.7; in this case, the chamber is too large or the amount of water to be sublimed too small. Thus, 2–4 kg of product in a 160 L chamber or 30–80 kg in a 1000 L chamber will satisfy Eq. (1.15).

If these conditions are met, the curves as shown in Figure 1.120 are measured.

Figure 1.122 shows one measurement and one repetition of this measurement and a third measurement with another product and other process data. Toward the end of main drying, the data on T_{ice} will systematically decrease; this effect can be used for an automatic change from main to secondary drying (see Section 2.6.2.2).

The temperature measurement during secondary drying with Th or RTD is possible, as shown in Figure 1.97, with an accuracy of ~±3 °C.

The change from main drying to secondary drying is difficult to determine by the product temperature, as shown in Figure 1.123. This can also be seen in Figures 1.124 and 1.125 [126]. Nail and Johnson [125] compared (see Figure 1.126) the pressure measured by a heat conductivity vacuum gauge (TM) with pressure rise measurements during secondary drying and indicated the related RM. In Figure 1.127, the pressure measured by TM is compared with the p_{H2O} measured by a mass spectrometer. The signal of the mass spectrometer is reduced during the first two time units, but changes very little between the third and seventh time units. Connelly and Welch [136] also used a mass

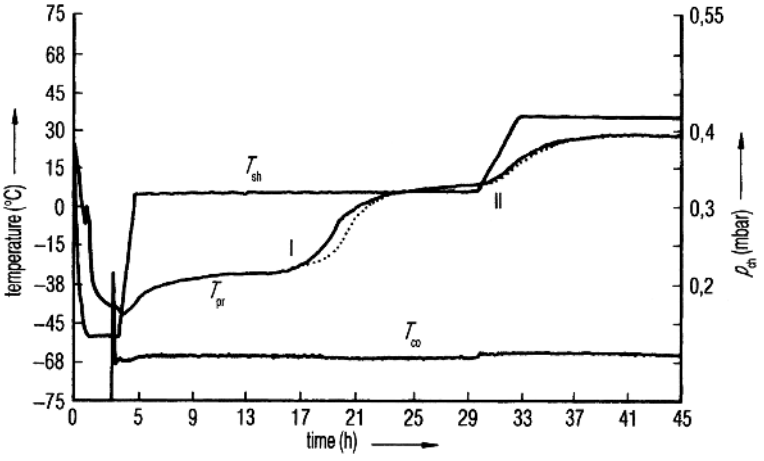

Figure 1.123 Increase in the product temperature T_{pr} as a function of process time. The increase (I) starts at ~16 h and reaches T_{sh} at ~22 h. Secondary drying (SD) started (II) at ~30 h. Between 16 and 22 h, there is no measurable indicator of when to start SD. Also, the safety margin between 22 and 30 h cannot be connected with the measured product temperature. (See also Figure 2 from Ref. [127].)

spectrometer to determine the end of main drying and of secondary drying. They also found that the change in output signal changed by 10: 1 between main drying and the end of secondary drying. It is suggested that one should not use the water vapor pressure measured by the mass spectrometer directly, but divide this data by the total pressure measured by the mass spectrometer. As shown in Figure 1.128, these normalized values show a plateau during the first ~7 h of main drying for 5% bovine serum albumin and afterward a decay between 7 and 23 h. A further suggestion is not to plot these normalized values, but their natural logarithms. By this method, the shape of the plot is meaningful, whereas the absolute value of the *y*-axis is more difficult to interpret. The authors concluded that the main drying is terminated at about 7 h of the cycle. However, there was no measurable indicator of whether to use the exact end of the plateau or 1–2 h later. For example, the decline of the curve in Figure 1.129 changes again at ~12 h (this can also be found in the curve in Figure 1.128). The end of secondary drying is suggested to be established by the following procedure:

1) Taking a baseline measurement of the partial pressure of the ice on the condenser in the empty plant.
2) Measuring the partial pressure during the run and terminating the secondary drying if the two values are close together. In certain cases, this might be too insensitive; in this case, it is suggested to close the valve between the chamber and condenser and measure the increase in water vapor pressure in a certain time. (*Note:* It is surprising that the water vapor pressure at the beginning of main drying is only 40% of the total pressure during the sublimation of distilled water and 30% during the sublimation of bovine serum albumin.)

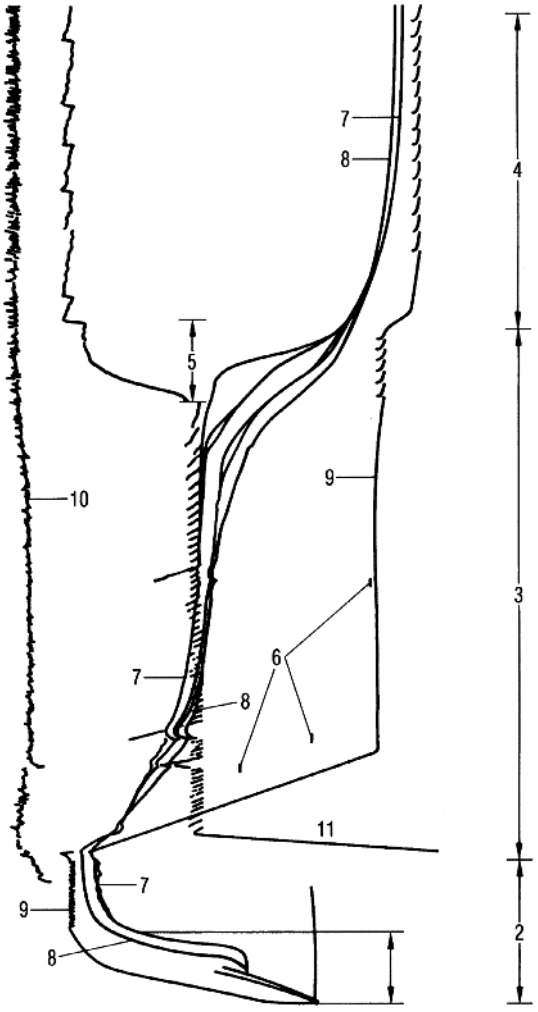

Figure 1.124 Course of the freeze-drying after the product has been frozen at 0.6 °C/min to −50 °C. 2, Freezing; 3, MD; 4, SD; 5, DR measurements to define the end of MD; 6, some BTM; 7–9, as in Figure 1.124; 10, T_{co}; 11, p_{ch}. At the beginning of DR measurements, the pressure control in this example is deactivated. When the DR value has reached a predetermined number, T_{sh} (in this case) is increased to the maximum tolerable temperature. The optimum time frame for the change from MD to SD cannot be estimated from the T_{pr} plot. (See also Figure 6 from Ref. [126].)

The pressure rise measurements in Figure 1.126 change during the final hours from 0.26 to 0.05 mbar, showing that this method is more sensitive than p_{H2O} measurements with the mass spectrometer alone.

Figure 1.130 shows a comparison between measurements made with TM, CA, and a hygrometer and demonstrates that the hygrometer data are not much more sensitive to the change in vapor pressure than the data with the other two instruments. The end of main drying can be between 2.5 and 5 h, depending on

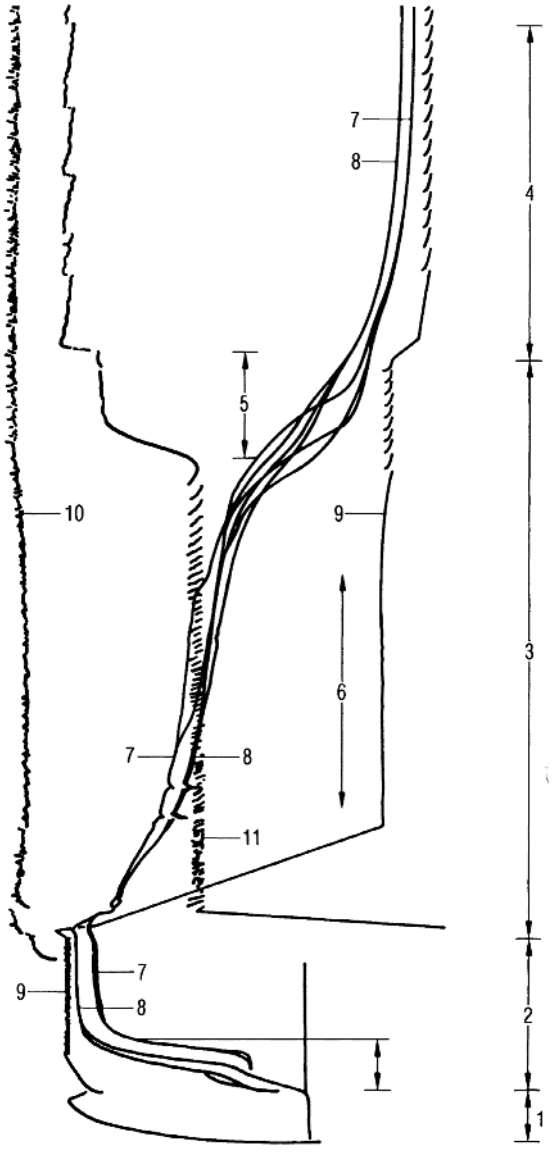

Figure 1.125 Course of the freeze-drying after the product has been frozen on precooled shelves at ~−50 °C at ~1 °C/min. Nomenclature as in Figures. 1.124 and 1.125. The rise of T_{pr} is different. The optimum time frame for the change from MD to SD cannot be estimated from the T_{pr} plot. (See also Figure 7 from Ref. [126].)

which change of inclination is chosen. From the BTM measurements, one can conclude (see Figure 1.122) that the main drying is terminated at ~3.5 h.

Figure 1.131 [138] summarizes the measurements of three runs of the product temperatures with RTD, T_{ice} with BTM, and of the pressures by CA. The plots show that the difference in pressures during main and secondary drying is largest

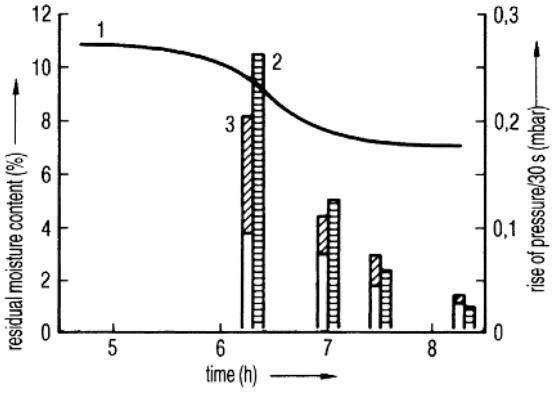

Figure 1.126 Plot of the pressure measured by heat conductivity vacuum gauge (TM) during SD. In addition pressure rises in 30 s and related RM data are shown. 1, p_{ch} measured by TM; 2, pressure rise in 30 s; 3, RM in % of solids. (See also Figure 5 from Ref. [125].)

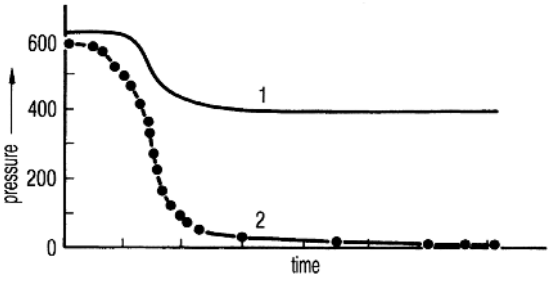

Figure 1.127 Comparison of p_{ch} data: TM measurements and signals of mass spectrometer for mass 18 during freeze-drying. 1, p_{ch} by MT; 2, mass spectrometer signal at mass 18. (See also Figure 10 from Ref. [125].)

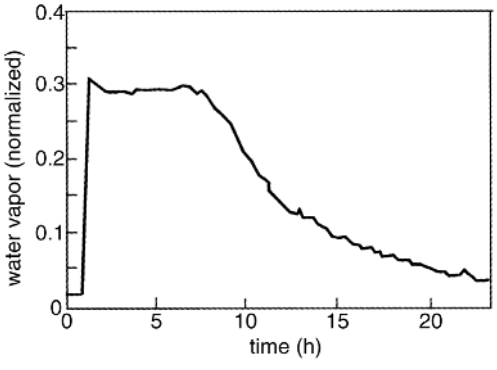

Figure 1.128 Water vapor partial pressure divided by total pressure as a function of time of 5% bovine serum albumin solution. (See also Figure 3 from Ref. [136].)

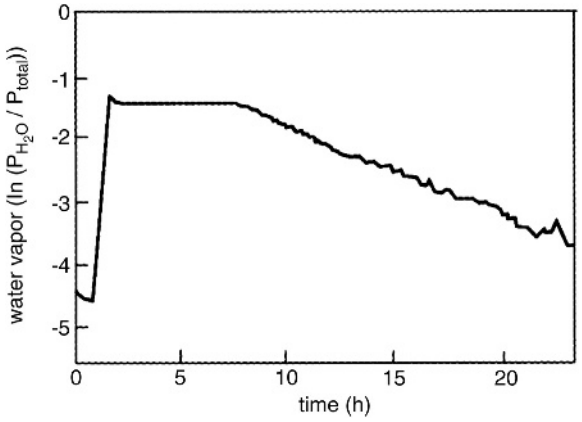

Figure 1.129 Natural logarithm of water vapor partial pressure divided by total pressure as a function of time for 5% bovine serum albumin solution. (See also Figure 5 from Ref. [136].)

with no pressure control and still clearly recognized with p_c at 0.2 mbar in relation to an ice temperature of ≃30 °C.

The water vapor desorption can be measured as shown in the scheme in Figure 1.132 and be calculated by

$$D = \frac{\mathrm{d}pV_{\mathrm{ch}}}{\mathrm{d}t}(\mathrm{mbar\,L/s}) \tag{1.16}$$

where

V_{ch}	=	chamber volume (L);
$\mathrm{d}p$	=	pressure increase (mbar);
$\mathrm{d}t$	=	measuring time for pressure increase (s).

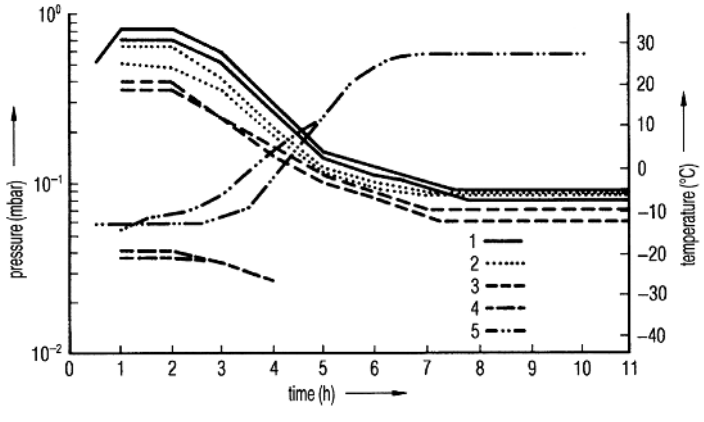

Figure 1.130 Course of two tests with identical products and identical process conditions, also using a hygrometer. The pressure drop at the end of MD, measured by the hygrometer, is not more informative than the data provided by CA. Below a certain pressure (in this case, below ~0.09 mbar), the hygrometer had to be recalibrated for the lower pressures. 1, p_{ch} (mbar) TM; 2, p_{ch} (mbar) CA; 3, hygrometer (System 3A, Panametrics, Hofheim, Germany); 4, T_{ice} (BTM) (°C); 5, T_{pr} (°C) RTD. (See also Figure 7 from Ref. [137].)

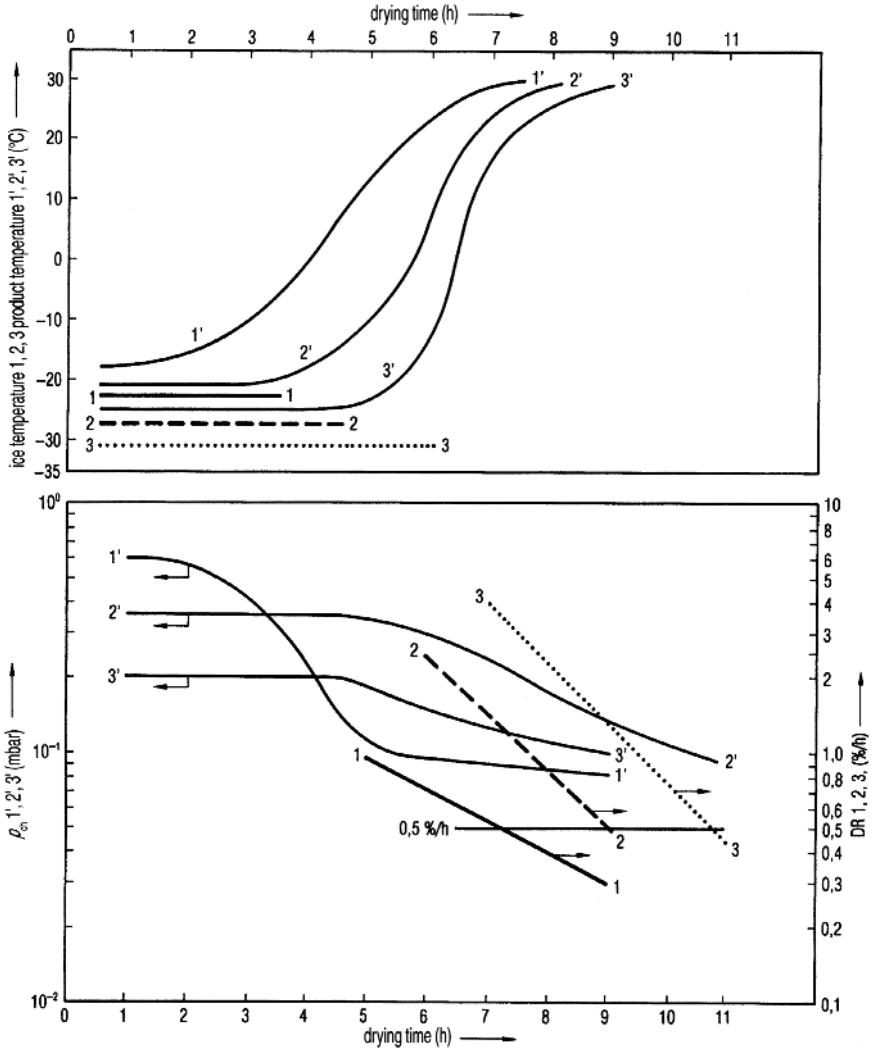

Figure 1.131 Summary of the results of three runs, which are differentiated by the control pressure: 1, no pressure control; 2, pressure controlled at 0.36 mbar; 3, pressure controlled at 0.20 mbar. The graphs show T_{Ice} marked as 1, 2, 3 and T_{pr} marked as 1′, 2′, 3′ in the upper drawing. In the lower drawing, the DR are marked as 1, 2, 3 and the p_{ch} as 1′, 2′, 3′. The increase in the product temperature (T_{pr}) and decrease of chamber pressure (p_{ch}) depend on the chamber pressure, because K_{tot} is pressure-dependent and T_{sh} has been programmed up to +30 °C in such a way that the control pressure has never been exceeded. In the test 1, T_{sh} has been raised to +30 °C as quickly as technically possible. The end of MD and SD are difficult to define by T_{pr} and/or by p_{ch}. The DR values measure the amount of water desorped from the product per hour in % of solids. The end of drying has been determined by DR: 1, after 7 h, DR = 0.55%/h; 2, after 8.5 h, DR = 0.65%/h; 3, after 11 h, DR = 0.45%/h. As shown in Figure 1.113, dW (RM) can be calculated from DR data and the end of drying can be expressed as residual moisture content in % of solids. (Based on Figure 1 from Ref. [138].)

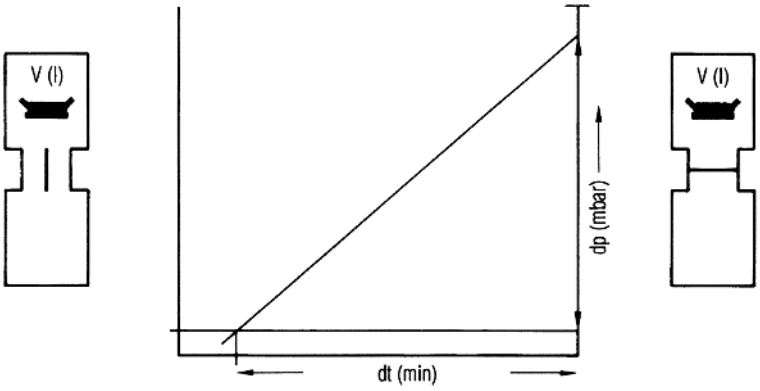

Figure 1.132 Scheme of the measurement of the desorption rate (DR).

By using $22.4 \times 10 \times$ L mbar, corresponding to 18 g H_2O, the units mbar L can be converted into g. This relationship is accurate enough as the temperature of the water vapor depends on several factors and will also be modified by a change of T_{sh}. The desorption process can be best illustrated by using the desorption rate (DR), which measures the desorbed amount of water in % of solids of the product per hour:

$$DR = 2.89 \times 10^2 (V_{ch}/m_{solid})(dp/dt) \tag{1.16a}$$

(desorption of water vapor in % of solids per h), where V_{ch}, dp, and dt are as in Eq. (1.16) and

$$m_{solid} = \text{mass of solids (g)}.$$

Measurements of the desorption rate (DR) require three conditions:

- For a product, a reproducible desorption isotherm exists and the product does not change at the end temperature during secondary drying.
- The end temperature has to be applied for some time depending on the cake thickness in order to minimize the temperature gradients in the product.
- The leak rate of the plant must be so small that a pressure rise due to the leak rate is also small compared with the pressure rise resulting from the desorbed water.

To measure DR values, one has to use measuring times of ~30 s. A prolonged time (compared with BTM) can be used, since the product temperature during this time is almost constant. On the other hand, the absolute pressures are approximately one decade smaller than during BTM (Figure 1.98, $p_{MD} =$ 0.36 mbar, $p_{SD} = 0.03$ mbar). To measure, for example, 1%/h in the run in Figure 1.98, one must calculate 65.5 g solids in a chamber volume of 160 L by Eq. (1.16b):

$$dp/dt = DR/V_{ch} = 1.4 \times 10^{-3} \text{ mbar/s} \tag{1.16b}$$

This pressure range can be measured by a CA if $dt > 15$ s. Manufacturers of CAs give the reproducibility of such instruments as ±0.005 mbar. With a few years of

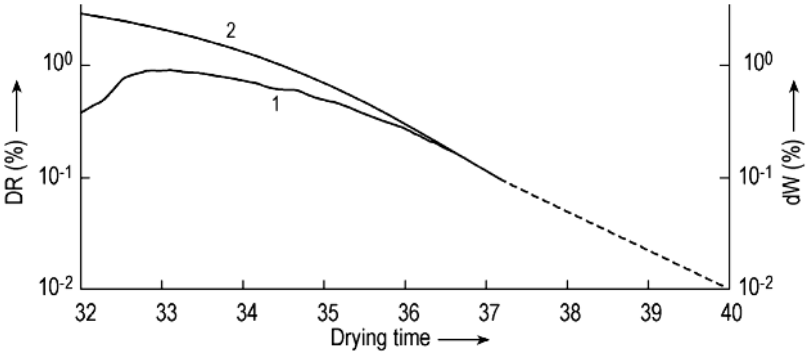

Figure 1.133 DR as a function of drying time. Plot 1, DR; plot 2, integration of plot 1 over time to calculate dW.

experience, the authors found a reproducibility of better than ±0.003 mbar between the calibration intervals of 3–4 months. If a long time, 120 s, is taken and the error should be smaller than ±10%, dp has to be a minimum of 0.034 (±0.003) mbar in 120 s. If the chamber volume is 160 L and $m_{solid} = 65.5$ g (or 160 g), DR = 0.2%/h (or 0.08%/h) can be measured within ±10%. The necessary accuracy of the DR measurement depends on the order of magnitude of dW to be achieved and its desired accuracy. If, for example, 1% RM ± 10% is required, DR measurements down to 0.1%/h are sufficient as shown in Figure 1.133: Plot 1 extrapolated to 0.01%/h is reached in 40 h; the integration of DR over time from 37.2 h until the change from MD to SD results in dW = 2.60% at 32 h. DW 1% is reached in 34.0 h. If the DR data from 37.2 to 40 h were to be included in the extrapolation, the time would have been 34.2 h as shown in the graph. For the two plots in Figure 1.134, the ratio of solids to the chamber volume was too small for plot 1 for data <0.05%/h and for plot 2 for data <0.3%/h. Plot 1 could be used to calculate ~1% dW; the ratio in plot 2 is too small.

Figure 1.135 shows the influence of the filling height on DR data: plot 1, two runs with 300 vials and identical process data; plot 2, 10% of 300 vials were overfilled by 10%; plot 3, 50% of 300 vials were overfilled by 10%. These data demonstrate that it is not possible to freeze-dry vials with the same product, but different filling heights in one charge. The plots indicate that in plot 1 the final $T_{sh,SD}$ is reached at ~8.1 h, in plot 2 at ~8.2 h, and in plot 3 the change from MD to SD was not finished at 7 h and it took 8.5 h before $T_{sh,SD}$ was reached. The desorption behavior of the product in all four runs is identical; when the temperature is reached, all plots are parallel.

As a rule of thumb, the following can be used: 1 g of solid in a chamber volume of 1 L is sufficient to measure dW at 1% with an error of ±10%. If the ratio m_{solid}/V_{ch} becomes smaller than 1, the error in dW increases. It is possible to prolong dt, for example, to 180 or 320 s, and improve the accuracy, but 90–120 s has been shown to be a practical range.

The leak rate (qL, mbar L/s) has to be small compared with the pressure rise to be measured in the chamber volume. For the example [Eq. (1.16b)] above, $qL \ll 1.4 \times 10^{-3} \times 160 \ll 0.22$ mbar L/s or the maximum qL, $qL_{max} = 2.2. \times 10^{-2}$ mbar L/

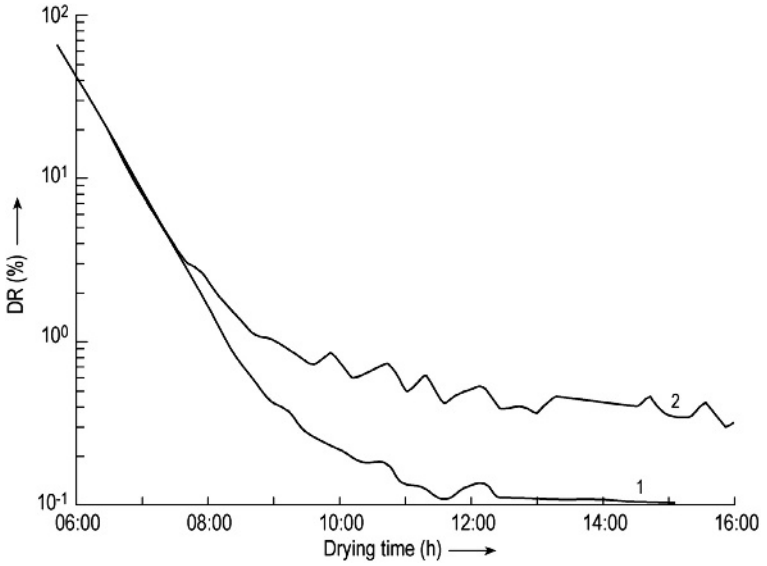

Figure 1.134 DR as a function of drying time. The ratio m_{solid}:V_{ch} is too small in plot 1 for DR data <0.05%/h and for plot 2 for data <0.3%/h. The ratio in plot 2 is too small for reproducible measurements.

s. With this qL_{max}, the "true" DR is measured as 0.24 mbar L/s or ~10% too large, DR = 1%/h is calculated as 1.1%/h or a DR 0.1%/h is calculated as 0.2%/h. For many freeze-drying plants, one can expect that the leak rate will be in the region of 10^{-3} mbar L/s. If the leak rate of a plant is stable and known, it can be accounted for in the DR value. In normal operation, one would expect that a 100 L chamber

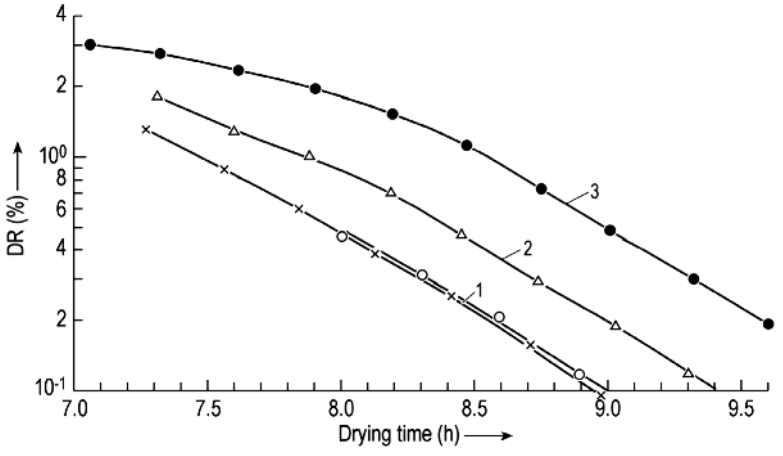

Figure 1.135 Four DR plots as function of drying time in the same plant, with the same product and process conditions, 300 vials per run. Plot 1, two runs on two different days; plot 2, one run, 270 vials normally filled, 30 vials 10% overfilled; plot 3, 1 run, 150 vials normally filled, 150 vials 10% overfilled.

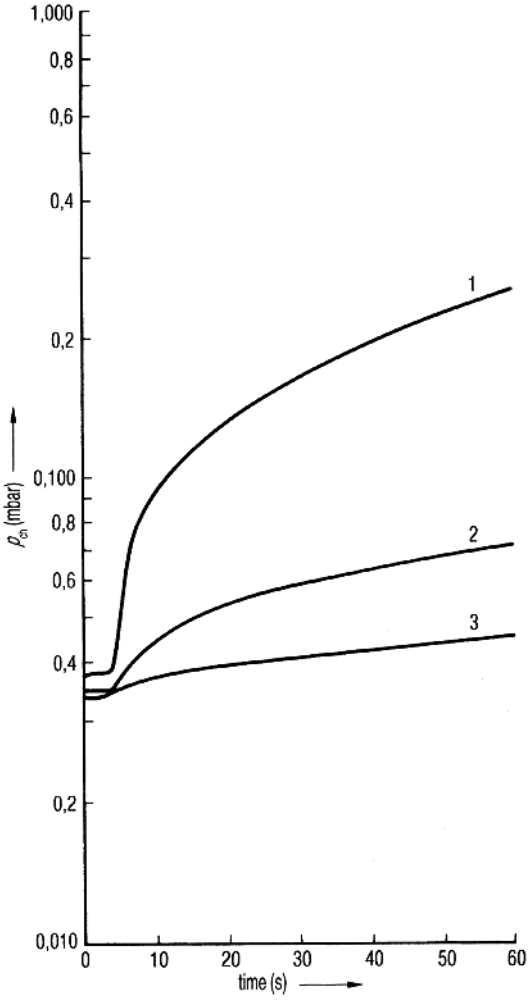

Figure 1.136 Automatically measured and recorded pressure rise as a function of time after the valve between the chamber and the condenser has been closed. Three measurements were selected: 1, shortly after the valve has been closed; 2, 2.5 h later; 3, 5.75 h later. A computer can calculate d*p*/s from the measured $p_t - p_0/t$; p_0, pressure after closing the valve; p_t, pressure after the measuring time *t*. (Based on measurements of Steris GmbH, Hürth, Germany.)

is loaded with 2.5 kg of liquid product, containing 250 g of solids, and the leak rate could then be fourfold larger, as mentioned above.

The pressure rise measurement can be made automatically, as shown in Figure 1.136.

The leak rate becomes critical if the solid content is small, for example, 1%, then qL_{max} has to be $\sim 2 \times 10^{-3}$ mbar L/s, all other conditions being equal. In such cases, the leak rate of the chamber should be measured before charging the product.

The secondary drying step depends on only one factor: the sorption behavior of the product and its temperature dependence that is shown for one product in Figure 1.137. Table 1.26 illustrates the consequences. RM data can only be achieved as quickly as possible if the water vapor pressure in the chamber is small compared with p_{eq} (e.g., 10% of p_{eq}); this parameter is called $p_{eq,0.1}$ in the table and the pressure of the permanent gases p_p is small compared with $p_{eq,0.1}$, as also

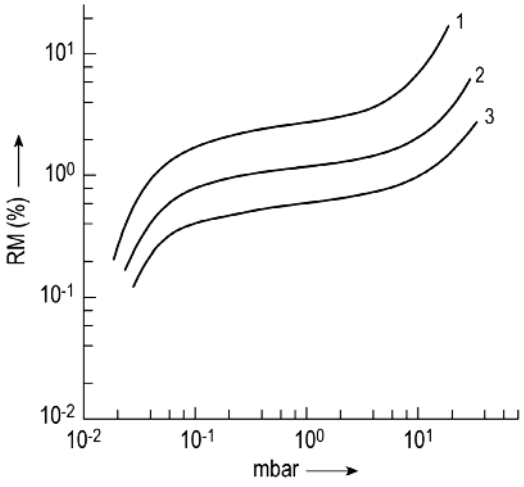

Figure 1.137 Desorption isotherms of the residual moisture content (% w/w) as a function of water vapor pressure: (1) 20; (2) 40; (3) 60 °C.

shown in Table 1.26. One may argue that the chosen factor of 10 is too large and a factor of 8 might have a similar effect. The answer can only be given for a given geometry of the plant and the absolute pressure in question. Therefore, a factor of 10 has been chosen for simplicity. To operate SD at $p_{eq,0.1}$, the condenser temperature T_{co} has to be smaller than given in the table as $T_{co}<$ (how much smaller depends on the condenser configuration, that is, to condense the vapor on the surface with a minimum of flow resistance and interference with permanent gas and water molecules). For $T_{co}<$ in the table, it is assumed that the equilibrium pressure of the ice on the condenser surface needs to be only 10% below $p_{eq,0.1}$.

The main consequences of Table 1.26 are as follows:

At a product temperature of 20 °C, it is difficult to achieve an RM of <0.5%; ~2% can be realized if the pumpset consists of, for example, one roots pump and a two-stage gas ballast main pump.

At 40 °C 1% RM is possible with a more standard pumpset: a large two-stage gas ballast pump or for production plants better 1 roots pump plus a small gas ballast pump.

Table 1.26 RM (%) in a matrix of product temperature T_{pr} and water vapor equilibrium pressure p_{eq}, together with data for $p_{eq,0.1} = 0.1 p_{eq}$ and p_p = pressure of permanent gas.

$p_{eq}/p_{eq,0.1}/p_p$	$T_{co}<$	T_{pr} (°C)		
(mbar)	(°C)	20	40	60
0.02/0.002/2 10^{-4}	≃73	0.2	0.1	0.06
0.04/0.004/4 10^{-4}	≃68	0.9	0.4	0.2
0.1/0.01/0.001	≃61	1.9	0.8	0.4
1.0/0.1/0.01	≃43	3.0	1.4	0.6
10/1.0/0.1	≃20	6.0	2.0	1.0

If the product can be brought to, for example, 50 °C during SD, 0.6–1% can be achieved and the product could be cooled before unloading to, for example, 25 °C. This type of program shortens the SD and the RM can be reached more easily.

If RM, for example, <3% is the goal, two possibilities can be used: 20 °C and $p_p \approx 0.01$ mbar or roughly estimated ~30 °C and $p_p \approx 0.03$ mbar.

1.2.3.1 Wireless Temperature Measurement

In Section 1.2.3 is described how difficult and questionable it is to measure a temperature in the product. It is irrelevant whether thin wire thermocouples (Tc) or electrical resistance (RTD, PT-100) are used [129]. Apart from the described negative effects at the measuring points, it is practically impossible to position the sensor (PT-100) in the center of the vial. The wire (cable) always exerts a leverage effect on the sensor, thereby preventing a precise positioning. A new wireless and battery-free temperature measurement system (TEMPRIS – Temperature Remote Interrogation System) makes it possible. The temperature is an important physical parameter to measure the product temperature during a freeze-drying process. In particular, to measure and record temperature as accurate as possible, as genuine as possible, as reproducible, in real-time as possible, in a wide measurement range as possible and over an adequate period of time.

The advantage of this technology is that process parameters can be acquired in real-time, wireless, and battery-free sensor technology.

Principle: The TEMPRIS wireless temperature system (iQ mobil solution GmbH, Wolfratshausen, Germany) [139,140] uses 8–16 sensors, the interrogation unit (IRU), including transmitter and a computer system with associated software installed to record the data to file. The battery-free sensors receive their power by excitation of the passive transponder by means of an amplitude-modulated electromagnetic signal in the internationally available 2.4 GHz ISM band, with evaluation of the backscatter response. The signal is demodulated in the transponder by means of a diode detector and used to stimulate a quartz-based circuit. This way the resonator itself is used as an energy storage device. The maximum possible storage time is defined by the quality factor Q of the resonator. In the second step, the amplitude modulation is deactivated and only the continuous-wave (CW) carrier is radiated. The stimulated resonance circuit continues to oscillate at its characteristic frequency that depends on its temperature. This free oscillation is mixed with the CW carrier and then retransmitted to the IRU. The IRU measures the modulation frequency of the response and the exponential drop in amplitude. In combination with the statistical parameters of several consecutive responses, the key variable is derived. In order to avoid interferences, the system changes automatically to a new carrier frequency within the ISM band after each interrogation cycle. As a result, the duration of the usable oscillations depends directly on the resonant frequency and the quality factor of the resonant circuit used.

One of the most important features of TEMPRIS is that literally the same sensors can be used during laboratory-scale development and subsequent routine manufacturing [141]. The use of TEMPRIS therefore eliminates the obstacle of interpreting temperature profiles obtained from different temperature sensors

Figure 1.138 TEMPRIS Wireless temperature system for precise measurement of product temperature in lyophilization. (IQ-mobil solutions GmbH, Holzkirchen, Germany.)

during scale-up, thermocouples in the laboratory, and RTDs that are typically used in production (Figure 1.138).

An integral benefit of the wireless sensors is their application as a complementary PAT (practical analytical technology) tool to monitor product temperature profiles during cycle development and optimization [142,143].

1.2.4 Water Vapor Transport during Drying

The water vapor transport in a freeze-drying plant can be described schematically with the aid of Figure 1.139. The ice (1) is transformed into vapor and has to flow out of the container (2) into the chamber (4). Between the chamber wall or any

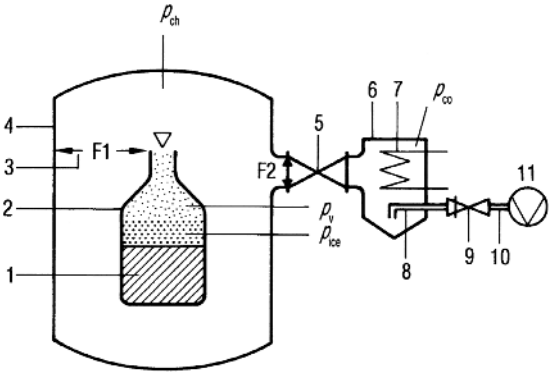

Figure 1.139 Scheme for the estimation of the water vapor transport in a freeze-drying plant. 1, Frozen product; 2, vial or the end of a shelf; 3, open surface (F1) for the water vapor flow between 2 and 4; 4, chamber wall; 5, valve with an open area F2; 6, condenser chamber; 7, cooling and condensing surface in the condenser chamber having a surface F3; 8, vacuum pipe with diameter *d*; 9, stop valve; 10, vacuum pipe with length *l* (from 8 to 11); 11, vacuum pump; p_{ice}, water vapor pressure at the sublimation front of the ice; p_v, pressure in the vial; p_{co}, pressure in the condenser.

other limitation, an area (3, F1) is necessary. The vapor then flows through the area F2 into the condenser (7), having a surface of F3 on which the water vapor will mostly condense. A mixture of remaining water vapor and permanent gas is pumped through (8)–(10) by a vacuum pump (11).

Example: p_{ice} at the sublimation front is 0.937 mbar (−21 °C) (see example in Table 1.14), in the chamber a $p_{H_2O} = 0.36$ mbar has been measured, resulting in a pressure difference of ~0.6 mbar. With these data, the water vapor permeability $b/\mu = 1.1 \times 10^{-2}$ kg/h m mbar is calculated. With these data known, it is possible to calculate dp for different conditions, if the mass of frozen water m_{ice}, the time t_{MD}, the thickness (d), and the surface (F) are known. This dp depends on the amount of vapor transported (Tables 1.14 and 1.15). In the examples given, it changes between 0.15 mbar in a slow drying process (6 h) to 0.6 mbar for a shorter drying time ~3 h.

Transport out of the container (2) into the drying chamber produces no measurable pressure drop if the product surface is equal to the opening of the container (e.g., with trays). Vials without stoppers in the vial neck do not produce a measurable pressure drop if, for example, 1 g/h water at a T_{ice} of −20 °C and a pressure difference of 0.6 mbar are transported. In this example, the velocity of water vapor is a few m/s.

If stoppers are in the vials, in the freeze-drying position, the situation is different: Depending on the type of stopper (Figure 1.140), the drying

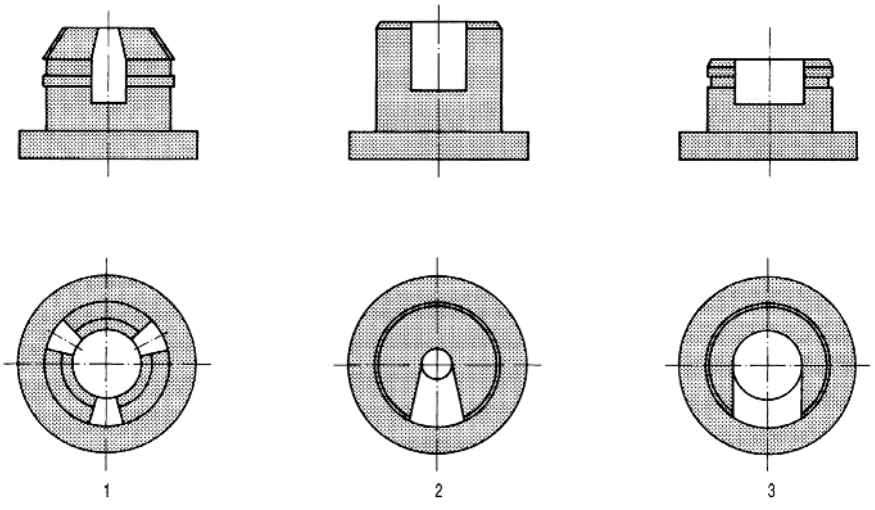

Figure 1.140 Influence of different forms of stoppers on the water vapor transport out of the vials into the chamber. At a pressure of 1 mbar in the vial the following relative amounts of water vapor are transported into the chamber in 3 h:

Stopper:	None	1	2	3
	100%	77%	75%	66%

performance can be reduced to 66 or 77%, or generally 60–80%. To achieve the same performance, the temperature would have to be increased from −20 to −17 °C, resulting in a 30% higher pressure. If the temperature increase is not tolerable, the pressure in the drying chamber must be reduced and a slower drying process could result.

If the main drying time is long (e.g., 33 h), the vapor flow through the stopper openings is small, t_{MD} can be identical within measuring limits, but t_{SD} can be prolonged by the increased flow resistance at low pressures (e.g., 4×10^{-3} mbar). During SD[2] without stoppers, dW = 0.4% was reached in ~1.5 h, with a type 1 stopper in ~2.5 h, and with type 2 in ~3.5 h. An optimum stopper form for a given product cannot be calculated; its influence should be measured when the process data are finalized.

Vapor transport into the condenser depends strongly on the geometric design of the plant. Under favorable conditions and including a valve between the chamber and condenser, a vapor speed of 60–90 m/s can be expected, resulting in a pressure drop between the chamber and condenser of a factor of 2, as an order of magnitude.

With these estimated conditions and a condenser at, for example, −45 °C = 0.07 mbar, the following pressures can be assumed:

- p_{co} times 2 = 0.144 mbar (p_{ch})
- p_{ch} times 1.5 = 0.216 mbar (p_{F1})
- p_{Fl} + 0.2–0.6 mbar = 0.4 to 0.8 mbar

This results in $p_s \approx -29.5$ to ≈ -22.5 °C.

At this condenser temperature and in this plant, products could be dried at ice temperatures between −29 and −23 °C. As shown in Table 1.14, an ice temperature of −22.3 °C (test run in Figure 1.96) has been successfully operated at a condenser temperature of −45 °C and a pressure difference $p_{ch} - p_{co}$ ~0.4 mbar.

If the freeze-drying conditions are extreme, namely, small solid content and low sublimation temperature, for example,

- solid content 1.7%,
- T_{ice} during MD −40 °C,
- layer thickness 3.8 mm, and
- vials with stoppers,

one has to consider that the water vapor permeability b/μ will be larger as in the earlier example. If $b/\mu = 6.9 \times 10^{-2}$ kg/m h mbar and ice temperature −41 °C = 0.115 mbar are measured, the water vapor pressure in the chamber will be 0.065 mbar. The condenser temperature should therefore represent a pressure of ~0.035 mbar, which would require a condenser temperature of ≃51 °C.

If stoppers with more favorable channels are used, the vapor pressure in the vials could have been 0.09 mbar, leaving a $\Delta p = p_{ice} - p_{F1} = 0.025$ mbar, which is in agreement with $b/\mu = 6.9 \times 10^{-2}$ kg/h m mbar in this test.

2 Measurements by Steris GmbH, 50354 Hürth, Germany.

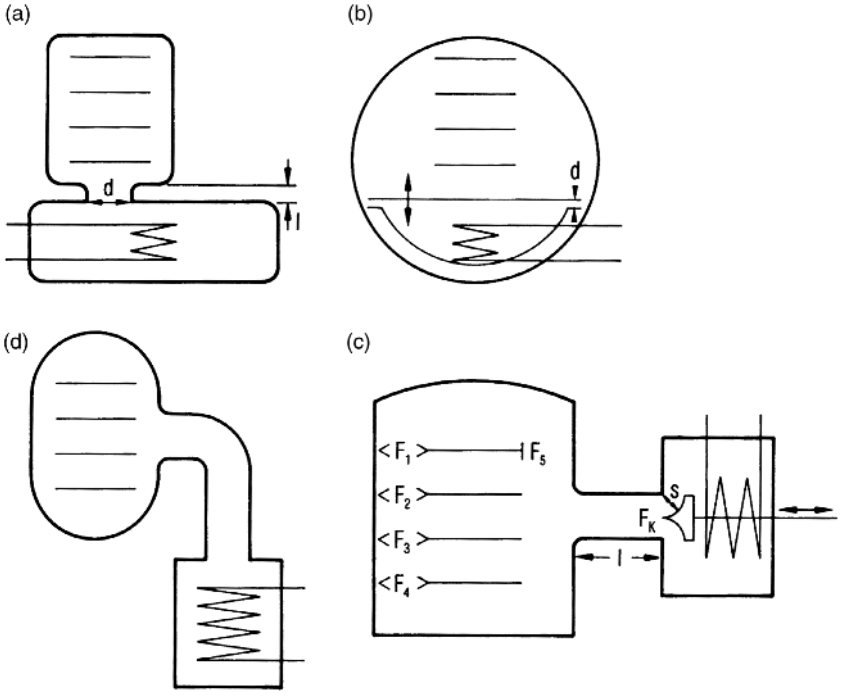

Figure 1.141 Four different geometric layouts of condenser and drying chamber. (a) Chamber and condenser in a housing not divided by a valve, water vapor transport into the condenser through an opening d with the length l (d, maximum approximate condenser or chamber diameter). (b) Chamber and condenser located in the same housing; the condenser compartment can be separated from the drying chamber by a lid. In the open position, the water vapor flows through a clearance with height d. (c) Drying chamber with four shelves, a connecting pipe to the condenser with the cross section d (area F_K) and a length l. In the open position of the valve, a circular clearance s can be an additional bottleneck after F_K. (d) Layout similar to part (c), but the chamber and condenser are connected by a 90° bend.

The water vapor transport from the chamber to the condenser depends largely on the geometric design of the installation. Assuming that only one bottleneck exists between the chamber and condenser having a diameter (d), which is large compared with the length (l) of the connection (Figure 1.141a), one could expect a jet flow that follows Eq. (1.3.9) in Ref. [144], For this case, the connection must have the shape of a jet with no obstacle in it (e.g., a valve lid). Technically, this case is not possible. Even in a plant as shown in Figure 2.93, the water vapor has to pass through a ring-type jet and is then deflected toward the condenser surface. To estimate the influence of p_{ch}, d, and l, the Günther–Jaeckel–Oetjen equation, Eq. (1.3.11) in Ref. [144], or its graphical plots, Figures 1.3.4 or 1.3.6 in Ref. [144], can be used. Figure 1.142 is an evaluation of the quoted equation and plot for the area of interest for freeze-drying. It shows the specific flow of water vapor through tubes with a ratio of $l/d = 1$, 1.6, 2.5, and 5 as a function of pressure at the inlet of the tube.

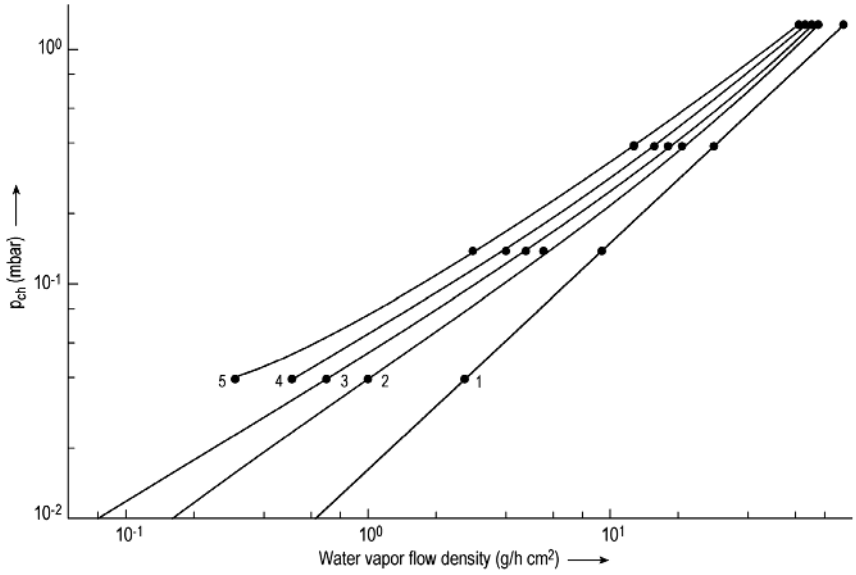

Figure 1.142 Density of water vapor flow (g/cm^2 h) as function of p_{ch} with jet flow (1) and $l/d = 1$ (2), 1.6 (3), 2.5 (4), and 5 (5) as parameter; (4) and (5) are not plotted below 4×10^{-2} mbar, these data depend very much on the design details of the plant. They should be measured if needed.

In the pressure region of 1 mbar, the expected specific flow of water vapor is reduced for the mentioned ratio to ~60% of that passing through an ideal jet. At 0.04 mbar pressure in the chamber, the specific throughput is reduced to 25 or 10%. This becomes even more drastic if the velocity of the water vapor is plotted as a function of p_{ch} (Figure 1.143). In an ideal jet, the velocity of the vapor flow under the conditions chosen is approximately the velocity of sound. However, even with $l/d = 1$, the velocity is strongly reduced as a function of pressure and reaches 0.04 mbar at only approximately one-third of this maximum speed for $l/d = 1$ and 10% for $l/d = 5$.

To summarize, one can say that in the pressure range 0.1–0.3 mbar and $l/d = 5$, a vapor velocity between 50 and 100 m/s can be expected. The graphs and figures are given to underline the influence of the pressure in the chamber and the geometry of the plant. General guidelines for the design of a plant can be as follows:

- All cross sections, through which the vapor has to flow, ahead of the smallest one must be large compared with the smallest, for example, F_k in Figure 1.141c $> F_1$ to F_5.
- If a valve is installed in F_k, its cap should influence the vapor flow as little as possible (see, for example, Figures 2.20 and 2.88).
- The path of the vapor should be deflected as little as possible; a deflection of 90° (Figure 1.141d) not only prolongs l, but it also transpires that l has been increased by a multiple of l.

To predict the vapor flow in a plant from Figure 1.142 is difficult since not only is the flow influenced by the design of the valve, the method of connecting the

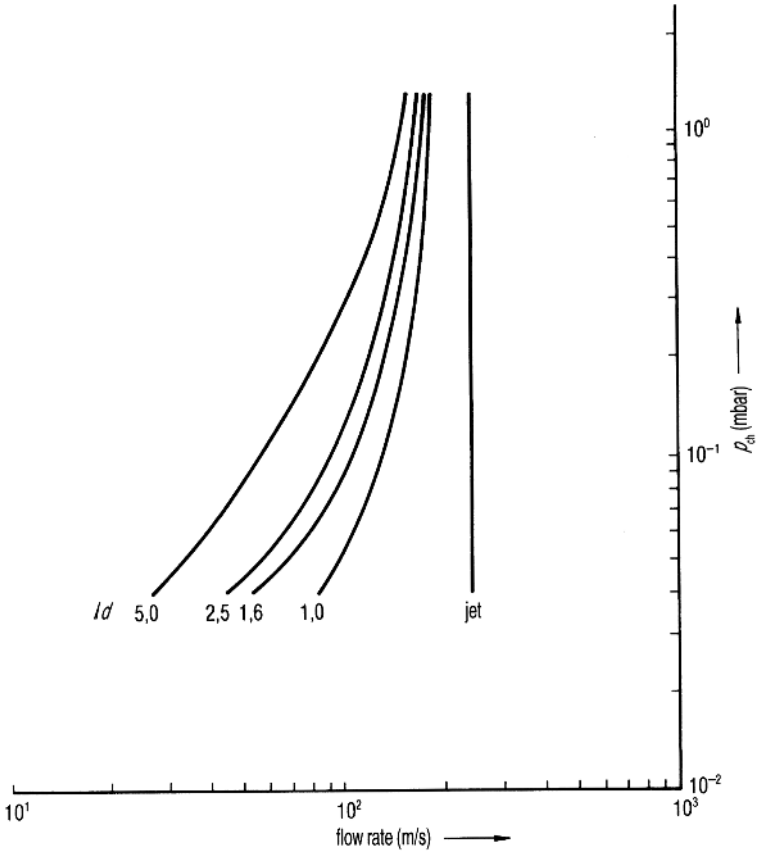

Figure 1.143 Rate of water vapor flow (m/s) as a function of p_{ch} through a jet and different *l*/*d* pipe dimensions as parameter.

chamber wall and condenser, and the location of the condenser surfaces, but also each factor depends differently on the chamber pressure. Since the vapor flow in a plant is a very important characteristic quality of a plant, it should be measured and taken into account for processes at different pressures in one plant or if a given process is to be transferred to another plant. The recommended 2–3 flow measurements can be carried out with distilled water filled into the maximum possible number of vials in the plant to be studied. The vials are filled to a uniform level, for example, 15 mm. The amount of water in all vials and the total weight of all bottles and stoppers are determined. The vials are loaded on the shelves, cooled to $\leq$45 °C, and freeze-dried until 50–60% of the water has sublimed. Depending on the pressure range for which the plant is designed, 2–3 runs should be carried out with approximately the following data for pharmaceutical freeze-drying:

Run 1: $T_{sh} = 20$ °C, controlled operation pressure $p_c = 0.2$ mbar, T_{ice} measured, for example, −32 °C. In this test three things can happen: (1) the test runs as planned; (2) a p_c of 0.2 mbar cannot be maintained and the pressure rises to, for

example, 0.4 mbar; the amount of water vapor produced under these conditions cannot be transported to the condenser, as 0.4 mbar is needed (the reason could also be the condenser capacity, which can be identified by a rising condenser temperature); (3) $p_c = 0.2$ mbar cannot be reached; the surface of the shelves or the heat transfer from the brine to the sublimation front is not large enough to produce the amount of water vapor that could be transported from the sublimation front to the condenser. At the equilibrium pressure (after 1–2 h from start), for example, 0.1 mbar, the plant is capable of transporting XX kg/h. With the vials used and $T_{tot} = 52\,°C$, only XX kg/h of water can be sublimed. With this information, K_{tot} can be calculated. By a few additional tests (not discussed here), one can decide whether the heat transfer from the brine to the shelf surface or the heat transfer from the shelf to the vial is the reason (or both). Run 1 gives either the kg/h transported at 0.2 mbar or the maximum kg/h evaporated under these conditions and transported at, for example, 0.1 mbar.

Run 2: $T_{sh} = 0\,°C$, controlled operation pressure $p_c = 0.08$ mbar, T_{ice} measured, for example, −40 °C. In this test, three things can happen: (1) the test runs as planned; (2) a p_c of 0.08 mbar cannot be maintained and the pressure rises to, for example, 0.1 mbar. The amount of water vapor produced under these conditions cannot be transported to the condenser as 0.1 mbar is needed (the reason could also be the condenser capacity, which can be identified by a rising condenser temperature); (3) $p_c = 0.08$ mbar cannot be reached; this case cannot be imagined with the data given in run 2. $T_{tot} = 40\,°C$ must transfer enough energy for a sublimation at 0.08 mbar, which may exceed the possible flow (point 2 above).

Run 3: This run is only necessary if the plant has to freeze-dry products at very low p_c, for example, 0.03 mbar corresponding to $T_{ice} \approx -48\,°C$. At 0.03 mbar, the mean free path is ∼15 mm and the calculation of the flow depends on design details of the plant, which cannot be expressed in an equation, but the flow can be measured as in runs 1 and 2. *Data for run 3:* $T_{sh} = -10\,°C$, $p_c = 0.03$ mbar, T_{ice} measured = −50.2 °C. Before the test one can guess what might happen: Assuming that the plant is expected to sublime 1 kg/h of ice at $T_{ice} = -50\,°C$, from Figure 1.142 the extrapolated flow in a well-designed plant is ∼0.3 g/cm^2 h, and the valve between the chamber and condenser has to have a diameter of 65 cm or more. These figures limit the size of a plant for these low pressures: a valve diameter of 1.1 m may be technically the maximum. At 0.03 mbar and 0.3 g/h cm^2, a flow of 2850 g/h is possible. If the main drying time is, for example, 30 h, the maximum amount of water in the plant can be 85 kg if each vial is filled with 4 cm^3 of water, and ∼20.000 vials per charge are the technical limit for this pressure range. The consequence of these estimates is the limitation of T_{ice} in production plants to ≃50 °C with the techniques used today. The data on size and temperature limitations are examples and not absolute values: If one accepts a longer t_{MD} than optimally possible, for example, 90 h instead of 30 h used above, the 20.000 vials can theoretically be increased to 60.000 if T_{tot} is reduced from ∼40 to ∼13 °C. T_{sh} will not be 0 °C but has to be −27 °C. This will raise some problems during the last part of MD mainly depending on the cake thickness. They have to be evaluated and will likely lead to a compromise between an acceptable t_{MD} and a useful T_{tot}.

Table 1.27 Water vapor flows in two production plants (Pr 1 and Pr 2) and two pilot plants (Pl 1 and Pl 2).

	Pr 1[a)]	Pr 2[b)]	Pl 1[c)]	Pl 2[d)]
Shelf area (m^2)	30	40	0.04	0.04
p_c (mbar)	0.3/0.4	0.06	0.3/0.16/0.07	0.06
g/h cm^2	4.7	1.4	12.0/4.2/1.1	1.5
Valve diameter (cm)	80	110	12.5	10
Ratio l/d	>>5	1.6	~3	~1.5

a) Pr 1 Connection between chamber and condenser approximately 500 cm with a 90° bend.
b) Pr 2 Designed as shown in Figure 1.141, chamber and condenser directly connected.
c) Pl 1 Designed as shown in Figure 1.144.
d) Pl 2 Designed as in Figure 1.145.

In Table 1.27 measured l/d data are presented for two production and two pilot plants. With a valve and a chamber/condenser design as shown in Figure 2.20, the effective l/d can be 1.6 or slightly smaller. Figure 1.144 is a sketch of the chamber/condenser design in Pl 1, characterized by $l/d = 3$. After the chamber/condenser configuration has been changed to the principle in Figure 1.145, the data for Pl 2 were measured.

In an expediently designed plant, one can expect to reach in the pressure range above 8×10^{-2} mbar a vapor velocity in the cross section F_k of between 50 and 80 m/s ($l/d = 2.5$–5). However, 90 m/s will be reached only if the design uses special features, for example, a funnel-like connection between the chamber wall and the location of the valve, slow changes in the outline, and smooth surfaces

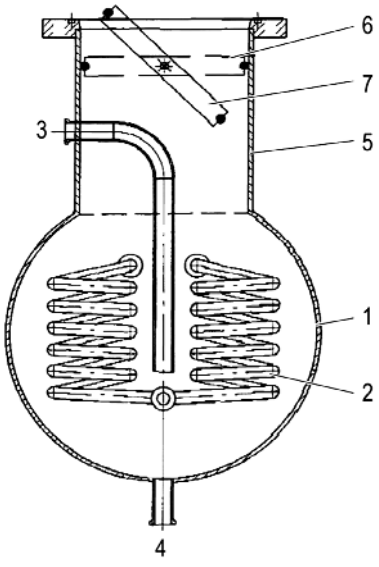

Figure 1.144 Scheme of the condenser design in plant Pl 1 in Table 1.27. 1, condenser wall; 2, condenser coil; 3, suction tube of vacuum pump; 4, water drain; 5, connection to drying chamber; 6, valve with seal in closed position; 7 valve in open position.

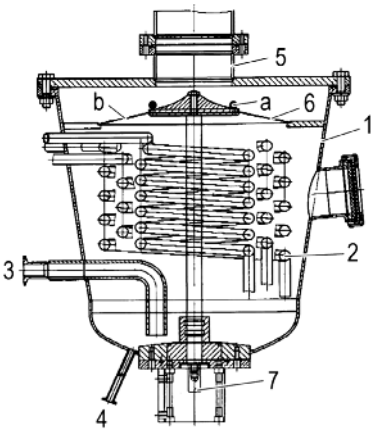

Figure 1.145 Scheme of the condenser design in plant Pl 2 in Table 1.27. 1, condenser wall; 2, condenser coils; 3, suction tube of vacuum pump; 4, water drain; 5, connection to drying chamber; 6, valve with seal (a) in open position and temperature shield (b); 7, hydraulic for valve operation.

without sharp edges or holes. It is also recommendable to clarify the maximum amount of vapor transportable at several pressures in a plant specification; examples and data are given above and in Figure 2.20 and the related text.

1.2.4.1 Endpoint Determination of Main and Secondary Drying

The known methods are described in Section 1.2.3. Neumann and Oetjen [129] have made BTM and PRM familiar and developed to reliable and valuable measuring methods (see Figure 1.119).

The change from main drying to secondary drying is difficult to be determined by product temperature sensors (see Figures 1.123 and 1.124). Nail and Johnson [125] used mass spectrometry to determine the end point of MD and SD. Also, Connelly and Welch [136] report about this method. The vacuum gauges (common TM) were compared with the p_{H2O} measured by a mass spectrometer. Deviations were visible.

TDLAS (tunable diode laser absorption spectroscopy) is a technique for measuring the concentration of certain species such as water vapor and many other gases, in a gaseous mixture using TDLAS. The advantage of TDLAS compared to other techniques for concentration measurement is the ability to achieve very low detection limits. Apart from concentration, it is also possible to determine the temperature, pressure, velocity, and mass flux of the gas under observation. TDLAS is one of the common laser-based absorption technique[3]. The principles are gas molecules absorb energy at specific wavelengths in the electromagnetic spectrum. By transmitting a beam of light through a gas mixture sample containing a quantity of the target gas (water vapor), and tuning the beams wavelength to the target gas – water vapor – absorption lines, and accurately measuring the absorption of that beam, one can deduce the concentration of the target gas molecules integrated over the beams pathway length. This measurement is usually expressed in units of ppm-m. Dealing with TDLAS requires some experience with this technique. The detection limit for water vapor is 1 ppm-m.

3 TDLAS, Add. No. 38 RD; Huanghe, Dongying; Shandong-China.

Another method is the use of a mass spectrometer. Mass spectrometers are highly sensitive measuring instruments that determine the composition (mixture) of gases. The device operates with a turbo-molecular pump in a high vacuum range[4,5]. A mass spectrometer decomposes the molecules of a gas in atoms and ionizes them. In a mass filter, the mass/charge ratio of the atoms is measured. The deflection depends on the field strength and the molecule mass/weight. The measuring limit is 10 ppm.

With TDLAS and mass spectrometry, the drying progress is primarily measured via the gas humidity. Both methods are partly suitable to determine the switchover point from MD to SD. However, the residual moisture in the product cannot be measured.

The freeze-drying process cannot be controlled by this technique.

1.2.5 Collapse and Recrystallization

A possible collapse of the product during main drying and recrystallization during the drying can have a significant influence on the quality of the final product. Therefore, these two events will be discussed again with regard to the drying process.

If, during freezing, not all freezable water has been frozen, the collapse temperature depends strongly on the amount of unfrozen water present. The highly concentrated, highly viscous, amorphous substance does not show at a temperature of, for example, −85 °C any measurable mobility. The water molecules can no longer migrate to the existing crystals and the unfrozen water is solidified. If the temperature is increased, the viscosity of, for example, 10^{14} P does not decrease with temperature, but with the difference in the temperatures $T - T'_g$. T'_g represents the highest possible T_g if all freezable water is frozen. Incompletely frozen products have an unnecessarily low T_g, for example, −85 °C, while T'_g for this product is only −58 °C. If such an incompletely frozen product is freeze-dried above −85 °C, the structure will soften and at T_c will collapse.

T'_g, T_c, and T_r can be close together or are approximately in a 10% range, as shown in Table 1.28. For sorbitol, T'_g is shown at a higher temperature (−43 °C) than T_c (−57 °C), a fact that cannot be explained.

All temperatures mentioned are influenced by the methods of their measurement [146], for example, very thin samples in a cryomicroscope, very small amounts of product (mg range) in an installation for differential scanning calorimetry, and some temperature gradients in the sample during the measurement of the electrical resistance (ER). T'_g, T_c, and T_r measured with pure substances can supply helpful information about the temperature range to be expected. For products containing two or more ingredients, the data must be measured for the specific mix since traces of additives or residues can change the data substantially; see, for example, Figures 3.9 and 3.10.

The question of aroma retention was of special interest between 1968 and 1975 for the freeze-drying of food. Thijssen and Rulkens [147,148] are of the opinion that slow freezing and quick freeze-drying provide good retention of the test

4 Oerlicon Leybold Vacuum GmbH, Cologne; Bonner Str. 498/Germany.
5 Pfeiffer Vacuum GmbH, Berliner Str. 43: 35614 Asslar/Germany.

Table 1.28 T'_g data, related UFW (unfreezable water), and T_r and T_c data.

Substance	T'_g (°C)	UFW (%)	T_r (°C)	T_c (°C)
Dextran	−9		−10	−9
Fructose	−42	49.0	−48	−48
Glucose	−43	29.1	−41	−40
Glycerin	−65	45.9	−60/−65	
Lactose	−28	40.8		−31
Trehalose	−30	16.7		
Maltose	−30	20.0		−30/−35
Ovalbumin	−10		−10	−10
Polyethyleneglycol	−13		−65	−13
Polyvinylpyrrolidone	−19.5		−24	−23
Sorbitol	−43	18.7		−57
Sucrose	−32	35.9	−32	−32

T'_g and UFW data from Ref. [6] of Chapter 3; T_r and T_c data from Ref. [145].

substance, 0.1% acetone in a dextrin solution, because the slow freezing produces large ice crystals, which include highly concentrated solutions between them. The pore size in a solution of 20% dextrin frozen at 0.5 °C/min is ∼3 μm, whereas at a freezing speed of 20 °C/min, it is only 1.8 μm. The freeze-drying speed with 3 and 1.8 μm pores has a ratio of 0.17:0.07. Furthermore, the retention increases with increasing solid content: In a 10% solution, retention is practically nil, but between 20 and 30% solids, it increases to 45–60%. Flink and Karel [149] showed (Table 1.29) that the loss of volatile substance, 1-butanol in a maltose solution, occurred in the first 6 h of the MD; during SD from 6 to 24 h, the volatile content remains practically unchanged.

Voilley *et al.* [150] confirmed the increasing retention with decreasing freezing speed and with the increasing number of carbon molecules of the alcohol (Figure 1.146).

Table 1.29 Loss of 1-butanol during the freeze-drying of a maltose solution.

Drying time (h)	Average water content (g/100 g solid)	Average content of 1-butanol (g/100 g solid)
0	430	4
3	178	3.30
6	36	2.20
12	11	2.45
24	0.7	2.50

Table IV in Ref. [149].

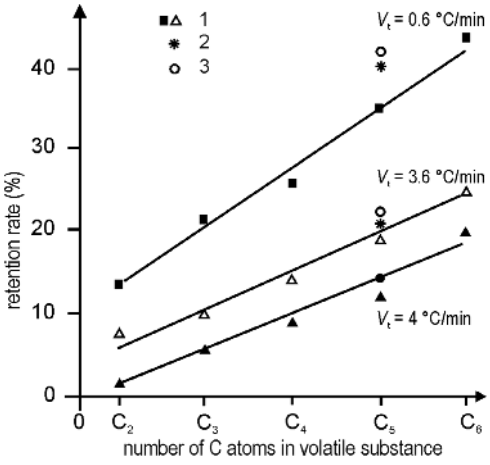

Figure 1.146 Percentage of alcohol retained as a function of the number of carbon molecules in the alcohol molecule with three freezing speeds as parameter. The solution consists of 30 g of saccharose, 15 g of glucose, 15 g of fructose, 15 g of citric acid, 5 g of $CaCl_2$, 15 g of pectin, 5 g of freeze-dried albumin, 900 g of water, and 100 ppm of volatile substance. 1, Homologous series; 2, 3-methyl-1-butanol; 3, cyclopentanol.

During MD, the retention is unchanged with time, but decreases with increasing temperature during SD. Flink [151] proved, by additional tests, his model about the retention of volatiles, called "microregion entrapment." A product frozen and ground up does not lose more volatiles than when frozen in a block. The microregions are smaller, as can be achieved by grinding, and there is no concentration of volatiles in the surfaces. If the microstructure is destroyed, for example, by collapse, the retention decreases. Maltose, sucrose, and lactose each have a better retention for volatiles than either glucose or dextran (Table 1 in Ref. [151]).

Gero and Smyrl [152] showed the retention from formic acid to butyric acid as a function of the dextran concentration and a special behavior of the acid (Figure 1.147), while Seger *et al.* [153] demonstrated that organic solvents

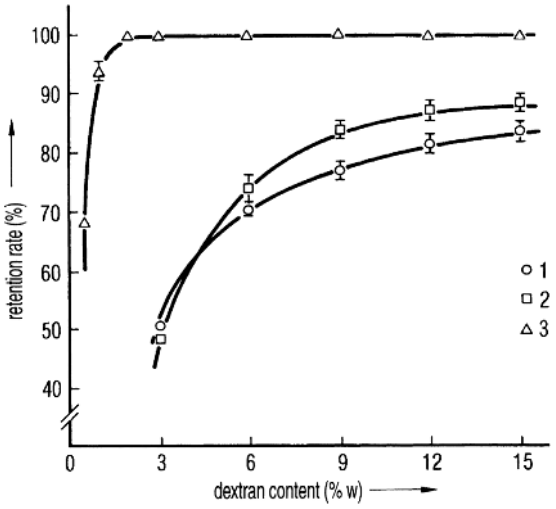

Figure 1.147 Retention of acid as a percentage of the initial concentration (0.05 M) as a function of dextran concentration. Three retained acids: 1, *n*-butyric acid; 2, isobutyric acid; 3, lactic acid. (From Gero, 1982 [152]. Reproduced with permission of John Wiley & Sons.)

used during the production of a formulation, for example, methanol, ethanol and *n*-butanol, cannot be completely removed by freeze-drying as they influence the freezing structure and freeze-drying process. During freezing, methanol and ethanol often form films on the surface, which makes drying difficult or impossible. The residues are pushed to the surface by the crystallizing ice and dry by evaporation from the liquid phase, thus forming skins. (*Note*: It is also possible that the mixture under the chosen conditions does not freeze completely and cannot be dried at all.)

1.2.6 Drying Processes without Vacuum

From time to time, drying at low temperatures at atmospheric pressure has been discussed and tried experimentally, because vacuum installations are high-cost investments and expensive to operate. There are three basic problems that must be solved in such a low-temperature drying process:

1) 1 kg of ice, when sublimed at 0.6 mbar, has a volume of ~2000 m^3. Since the atmospheric pressure is ~1700 times larger, ~3.4×10^6 m^3 of air must be transported to carry the water vapor (the vapor content is <1/1000).
2) If only the diffusion of vapor in resting air is used to transport the vapor from the sublimation front to the condenser (or vapor absorber), only 4×10^{-2} g/m^2 h can be transported over a distance of 100 cm. Even if the condenser could be positioned at a distance of 1 cm, the result is only 4 g/m^2 h. Transport of vapor by diffusion cannot be used practically.
3) By mixing an absorbing granulate or powder with the product to be dried, the distance of the diffusion can become very small or the water molecules may move by surface diffusion. In both cases, the problem is the same: first to find an acceptable drying agent (absorber) and then to separate it quantitatively from the dried product.

In recent years, several publications have tackled these problems. Kahn-Wyler [154] lists four reasons that prove that fluidized-bed drying (solving problem 2 above) is not suitable:

- The structure of the frozen product is difficult to control.
- The abrasion of the already-dried product is too large.
- The separation of the carrier-substrate (glass spheres) from the dried product is not complete enough.
- Abrasion of the installation results in product contamination.

Labrude and Rasolomana [155] reported an atomizer–spray-drying system for oxyhemoglobin in a 0.25 M sucrose solution at temperatures between +80 and +100 °C, which resulted in an unchanged dry product if the relative humidity was kept below 3%. When this dry product was compared with a freeze-dried product, in both cases a met-oxyhemoglobin (met-HBO) content of ~3% was found. By ESM (electron scanning microscopy) and spectrometric measurement, it was shown that the structure of the dried molecules had not changed measurably.

However, with this process described, two problems remain: at +80 °C, water has a vapor pressure of ~470 mbar; 3% of this value is ~14 mbar. Depending on the efficiency of the heat exchanger and water condenser, ~100 times more transport gas must be cooled than water vapor can be condensed. If the partial pressure of the vapor in the transport gas were to be, for example, 3–4 mbar (to allow an increase to 14 mbar during drying), condensation of the vapor must occur at ≃5 °C. The transport gas must be cooled to that temperature and reheated to +80 °C. Absorption systems to remove water vapor are technically feasible, but the temperature of +80 °C would still very likely have to be lowered and the dust produced by abrasion becomes a problem (see problems 1 and 3).

Wolff and Gibert [156] described the freeze-drying of small pieces (maximum 5 mm) in a fluidized bed process at −5 to −15 °C. The absorber was granulated corn starch added to the product in an amount 10 times the amount of water to be absorbed. The operating pressure was 0.5 mbar. Whether the enumerated advantages, including low investments, 35% saving of energy, and shorter drying time, outweigh the disadvantages of the above-mentioned point 3 was not discussed by the authors.

Mumenthaler [157] discovered similar problems, as already mentioned: freezing in a fluidized bed with CO_2 clogs the filters, reducing the yield to only 80–90%, with an additional loss of 10% fines.

1.2.7 Microwave Freeze-Drying

The limitations on heat transfer rates in conventionally conducted freeze-drying operations have led to attempts to provide internal heat generation by the use of microwave power. Basically, a faster drying can be achieved with microwaves because they generate the heat directly inside the product.

Principle: A microwave freeze-drier in simple terms is a conventional freeze-drier, with the added capability of allowing microwaves to be applied in the drying chamber. The whole drying process proceeds under vacuum environment of 0.5–2.5 mbar by sublimation. The quality of microwave freeze-dried products differs from conventional freeze-dried products substantially and not only in the texture. Compared to conventional freeze-drying where drying starts from the outside to the inside of the product, the microwave system generates heat within the product itself so that sublimation takes place within the complete product volume. And here is the uncertainty of this technology. There is too much and too fast water vapor generated that cannot be removed, leading to partial melting.

However, this drying technique was never successful in the conversation of food or pharmaceutical products. The damages to the product are too big. A microwave freeze-drying in the pharmaceutical industry is almost impossible, because products in vials are not suitable for microwaves.

Definition and regularities: Microwaves are electromagnetic waves within a frequency band of 300 MHz to 300 GHz. Within the electromagnetic spectrum, they are embedded between the radio frequency range at lower frequencies and infrared and visible light at higher frequencies.

Due to international regulations for industrial microwaves applications, mainly the frequencies 2450 and 915 MHz are being used.

1.2.8 Spray Freeze-Drying

The method consists of two steps: spray-freezing into a cryogenic gas or spray-freezing into vapor over liquid. Freeze-drying mostly is a fluidized bed process. Malecki (1970) dried an egg–albumin solution (10% solids) and apple juice (14% solids) after spraying in liquid nitrogen frozen droplets in a fluid-bed process. The droplet sizes ranged between 250 and 600 μm. The droplets were dried at −20 and −34 °C, respectively. It is mentioned that spray drying of products is possible that do not tend to agglomerate. However, longer drying times were found, compared to conventional freeze-drying.

Wolff (1990) talks about his work in the field of food technology, the drying of potato cubes in a fluidized-bed process at different temperatures, with minimum success, the mechanical stress on the product due to the turbulences is high.

Kahn (1987) dried pharmaceutical granulates for the first time. Freeze-drying is recommended for temperature-sensitive API (active pharmaceutical ingredients). However, this technology (spray freeze-drying) was not followed.

Only in early 2002, Webb [158] reports an application for recombinant interferon-γ-lyophilized and spray-lyophilized formulations. Other authors report on the use of spray drying, but the use in the pharmaceutical industry is limited, because of elaborate time and batch process, complicated handling of cryogenic liquids, possible protein instability during spraying, complicated scale-up[6], and sterile work (production) almost impossible.

1.3 Storage

The storage of a freeze-dried product starts with the end of the secondary drying and its transfer into a suitable packing. In the drying plant, a certain residual moisture content (RM) is achieved as a function of the product temperature and the drying time (Section 1.2.2).

The desorption isotherm describes, under equilibrium conditions, the amount of water absorbed on the product at a given temperature as a function of water vapor pressure, as shown in Figure 1.148. To approximate the equilibrium at a given temperature in a short time, the pressure during SD should be small compared with the equilibrium vapor pressure, for example, at +40 °C and a desired RM <1%, p_{ch} should be several times 10^{-2} mbar. If the product (blood plasma) is to be exposed only to +20 °C, the pressure has to be small compared with 10^{-2} mbar. As shown in Section 1.2.2, a prolonged drying time does not result in a lower RM – only a higher temperature will achieve this. To maintain a low RM, a hygroscopic product has to be protected against the reintroduction of moisture already in the drying chamber. If vials are used, they can be sealed in the chamber, as shown in Section 2.3.3. If bulk material or food has been dried, the chamber has to be vented with dry air or inert gas. At +20 °C and 70% relative humidity, air contains $\sim 1.3 \times 10^{-2}$ g H_2O/L. During the venting of a 200 L chamber with this air, 2.6 g of water vapor are introduced. If the chamber is

6 Schiffter, Heiko A.-Institute of Biomedical Engineering; University of Oxford, UK, 2002.

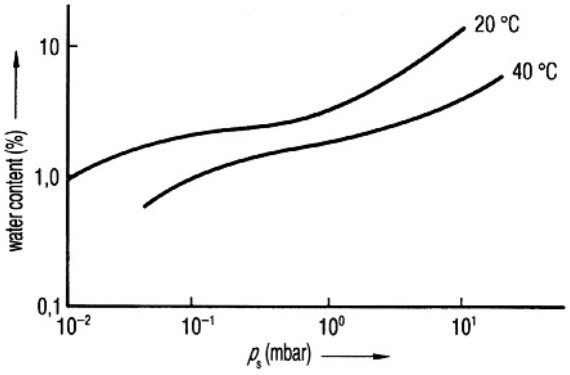

Figure 1.148 Desorption isotherm of blood plasma. (See also Figure 9 from Ref. [126].)

filled with 300 vials each containing 1 cm^3 with a solid content of 10%, the RM will be increased by ~9%. If the solid content is only 1%, the RM rises to ~90%. The dew point of the venting gas should correspond to the end pressure of SD in the chamber, for example, if the end pressure is 2×10^{-2} mbar, the dew point of the gas should be −55 °C, minimum −50 °C.

1.3.1 Measurement of the Residual Moisture Content (RM)

For all measurements of RM, the product must be handled in such a way as to exclude water absorption from the surroundings. Filling a freeze-dried product into another container and/or weighing it should only be done in boxes or isolators filled with dry gas (see above).

The boxes can contain, for example, P_2O_5 or be rinsed with dry gas. Handling in the isolator should be done wearing rubber gloves fixed to the isolator. Balances used in such a dry gas need some modifications to avoid electrostatic charges, which could lead to substantial errors.

1.3.1.1 Gravimetric Method

Until a few years ago, this method had been obligatory, as shown in Title 21 of the *Code of Federal Regulations for Food and Drugs*, Section 610.13 [159]. The weighed sample is stored at temperatures between +20 and +30 °C in a chamber, together with P_2O_5 and repeatedly weighed until the weight becomes constant. The smallest sample should be larger than 100 mg, if necessary taken from several vials. Higher temperatures lead to shorter times before the weight is constant, but they may desorb more strongly any bound water or even change the product. With this method, at 20–30 °C, water can be detected that is weakly bound to the solid.

1.3.1.2 Karl Fischer (KF) Method

By this method, the weighed dry product is dissolved in methanol and titrated with Karl Fischer solution until the color changes from brown to yellow. The visual observation can be replaced by an ammeter, which shows a steep increase in

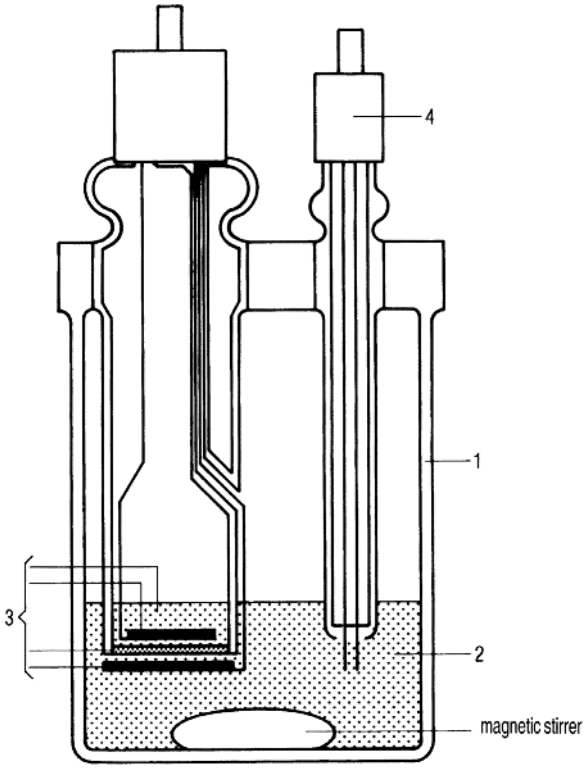

Figure 1.149 Scheme of the Messzelle DL 36 coulometer for measurement of residual moisture content (RM) after Karl Fischer. In the titration cell (1), iodine is electrolytically produced (3) from an iodine-containing analyte (2). Water in the titration cell reacts with the iodine. When the water is used up, a small excess of iodine is produced, which is detected by special electrodes, which leads to iodine production being stopped. The amount of water in the cell can be calculated from the reading of the coulometer and the amount of electrical charge needed. The solids are either introduced into the cell by a lock or the water is desorbed in an oven and carried by a gas stream into the cell. In a sample 10 μg can be detected with an accuracy of reading of 0.1 μg. (KF Coulometer DL36, Mettler-Toledo, Schwerzenbach, Switzerland.)

current when the end point of the titration is reached (dead-stop titration). The samples can be two to four times smaller than for the gravimetric method. To avoid the visual observation completely, iodine can be produced by electrolysis and the water content is calculated using Coulomb's law. Such an apparatus (e.g., Figure 1.149) is available commercially. The smallest amount of water to be detected by such instruments is 10 μg. Wekx and De Kleijn [160] showed how the Karl Fischer method can be used directly in the vial with the dried product. The Karl Fischer titration cannot be used if the product reacts with iodine in the Karl Fischer reagent or does not dissolve in methanol or the moisture cannot be extracted by the methanol. A Karl Fischer apparatus in a glove-box is shown in Figure 1.150.

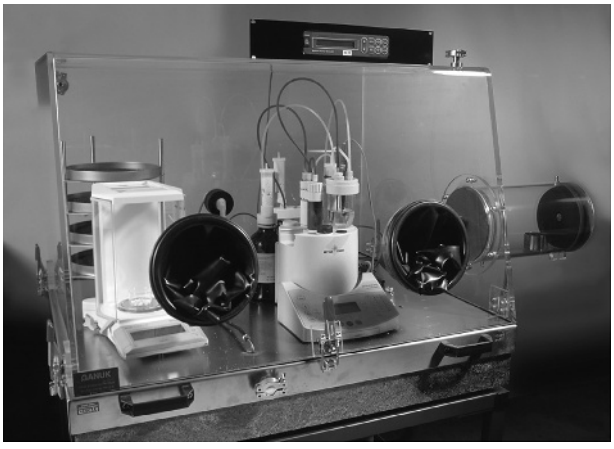

Figure 1.150 Mettler-Toledo DL 38 Karl Fischer apparatus in a glove-box with Mettler-Toledo AG 135 balance (left), drying agent (left, behind), and air lock on the right (Steris, Hürth, Germany).

1.3.1.3 Thermogravimetry (TG, TG/MS)

The weight loss of the product is measured by an electrical balance at constant temperature or at a given temperature–time profile. For the balance and handling of the product, the rules given in Section 1.3.1 should be carefully observed, as the sample with such a balance can be as small as 2 mg. A thermogravimetric analyzer in a glove-box is shown in Figure 1.151. May *et al.* of the Center for Biologic

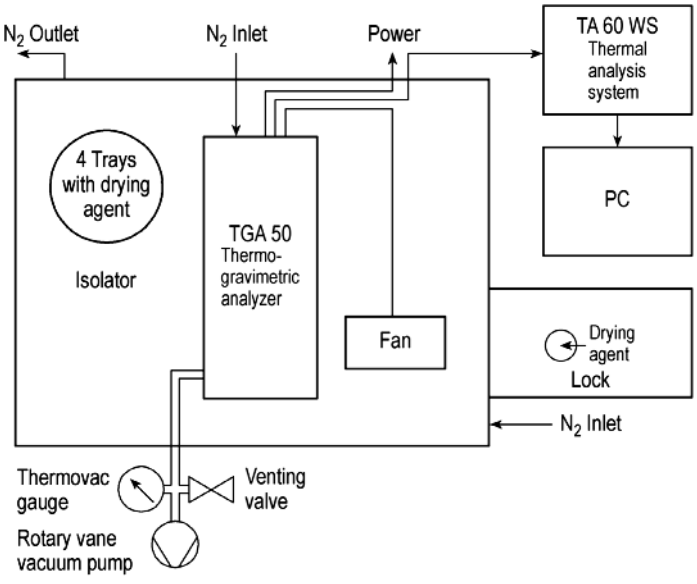

Figure 1.151 Scheme of a thermogravimetric analyzer (Shimadzu TGA 50). (Steris, Hürth, Germany.)

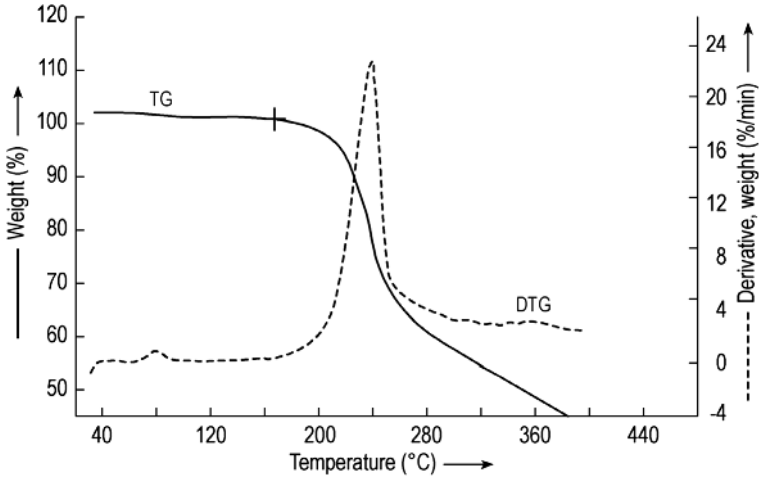

Figure 1.152 Weight (%) as a function of temperature of freeze-dried ×-interferon measured by the thermogravimetric (TG) method and the derivative of weight over time (DTG) (%/min). The assumed end point of water desorption is marked (+). RM by TG, 0.98–1.28%; RM by Karl Fischer, 1.28%. (See also Figure 1 from Ref. [161].)

Evaluation and Research, Food and Drug Administration [159] described the reading of a mass spectrometer (MS) during weighing to differentiate between desorbed water and volatile products, which might come from residual solvents or decomposed parts of the product.

May *et al.* [161] studied the residual moisture (RM) of ×-interferon and US Standard Pertussis Vaccine (Lot 8 and 9) by TG, TG/MS, the KF method, and a new method called "vapor pressure moisture methodology" (VPM). VPM measures the vapor pressure of water in the space above the cake in the closed vial. Light from an infrared diode passes through the vial to a photodetector. The vial temperature is lowered from room temperature to −55 °C at a constant rate. When the water vapor condenses, the light beam is obscured by the condensate, changing the signal to the photodetector. The temperature at the condensation is converted into pressure and the micrograms of water in the headspace volume are calculated. Figure 1.152 shows the TG data for ×-interferon. the mean RM in three different lots was found to be $1.15 \pm 0.15\%$. The RM by the KF method was found in one lot to be 1.28%. Figure 1.153 shows the corresponding data for Pertussis Vaccine Lot 9. The end temperature of water desorption and the beginning of decomposition was decided with the plot of the derivative of weight over time (%/min); the end of water desorption is assumed when the derivative leaves the horizontal line. Table 1.30 summarizes the results obtained by different methods. VMP does not supply information about the RM of the product. It permits repeated measurements over a period of time on the same vial to quantify changes of the water content in the space above the product.

1.3.1.4 Infrared Spectroscopy

Lin and Hsu [162] described the determination of residual moisture in protein pharmaceuticals in sealed glass vials by near-infrared (NIR) spectroscopy. Five

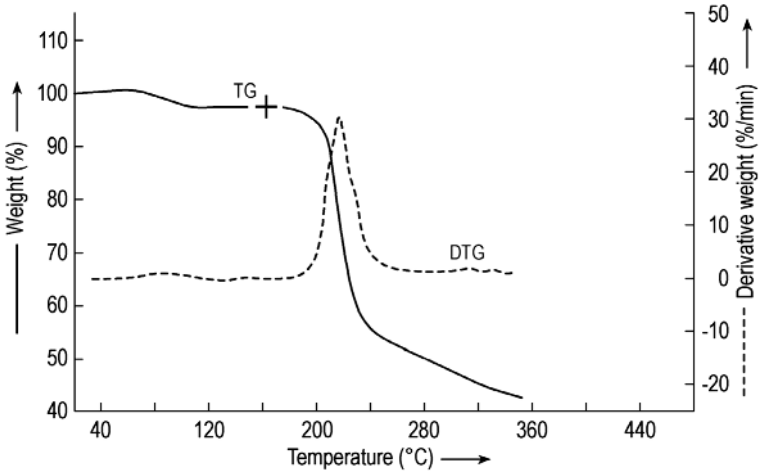

Figure 1.153 Weight (%) as a function of temperature of freeze-dried US Standard Pertussis Vaccine Lot 9 measured by the thermogravimetric (TG) method and the derivative of weight over time (DTG) (%/min). The end point of water desorption is marked (+). RM by TG, 4.75%. (See also Figure 3 from Ref. [161].)

proteins were studied: recombinant humanized monoclonal antibody (rhuMAb) E25, rhuMAb HER2, rhuMAb CD11a, TNKase, and rt-PA. Higher moisture contents (RM) were obtained by adding appropriate amounts of MilliQ water to the wall of the vial in a horizontal position and letting the water vapor diffuse to the dried product. Generally, in 1–2 days an equilibrium state was reached. Three common mathematical tools were used to quantify complex spectra (overlapping peaks from different components or their chemical interaction). The effects of the following influences on the IR calibration were studied: concentration of each

Table 1.30 Comparison of RM data measured by KF, TG, and VPM methods for α-interferon and US Standard Pertussis Vaccines.

Product	RM by KF (%)	RM by TG (%)	Content of water in vial space (mg/vial)
α-Interferon			
Lot A		1.19	2.05
Lot B		0.98	6.67
Lot C	1.28	1.28	4.76
Pertussi vaccine			
Lot 8		2.44	9.50
Lot 9		4.75	26.00

Table 2 from Ref. [161].

excipient, product cake porosity, cake height and diameter, and excipient-to-protein ratio. Karl Fischer titration data (called RF) were used as standards for comparison with the NIR data.

Figure 1.154a–e shows the relationship between RF and RNIF for the five products. The Karl Fischer titration results can fluctuate up to ±0.5% with day-to-day and operator variations. Therefore, a difference between RF and RNIR of ≤0.5% is accepted as good. The porosity change from 30 to 100 mg/mL was ≤0.5%. The cake dimensions must exceed the NIR penetration depth, otherwise the RNIR measured will be too small.

Small changes in the formulation compositions can be accommodated, whereas substantial changes, for example, sucrose from 42.5 to 170 mM, show an increase in absorbance with increasing concentration (Figure 1.155). The RNIR calibration for 85 mM therefore cannot be used for a product with lower (42.5 mM) or higher (>120 mM) concentrations of sucrose; the water signal at 5200 cm^{-1} is changed by the changing product signal at 5200 cm^{-1}. Generally, RNIR calibration is specific for a given formulation and product dimensions. Changes are only tolerated as long as the NIR measurement has an optical path long enough for sufficient reflected radiation and the spectrum of the calibrated product is not changed by modified concentrations of the ingredients.

Summary of Section 1.3.1

Water in the dried product can be bound in many different forms: as surface water, as water bound more or less to the dry substance, or as water of crystallization. Therefore, each method can lead to different results for different substances. There are products for which the RM values by gravimetry and by Karl Fischer titration show very little difference. May *et al.* [159] presented four examples of such substances but, as shown in Table 1.31, the RM obtained by gravimetry can be 0.3–0.6% smaller than by Karl Fischer titration, whereas the thermogravimetric data, within the given errors, are close to the Karl Fischer data. In Figure 1.156, the RM data measured by the KF method are compared with the dW data calculated from DR data during the secondary drying. The vials for KF measurements were closed at the time indicated in the upper graph by the mean points and the error beams. Three runs were carried out with the same pharmaceutical product, the same process data (given in Figure 1.156), and the same load in the same plant. The RM data by the KF method vary after the change from MD to SD by ±1%, which is reduced after ~21 h to ±0.5%. The dW data for all three runs vary after the start of SD by ±0.5% and by less than 0.05% after 21 h. The top and lower plots show that at the end temperature the RM of 0.5% will not be lowered significantly by further drying. The same information is given by dW: After 21 h, the possible desorption of water can be neglected, as it will be less than 0.02%/h. In this product and under the process conditions chosen, the moisture content of 1.5% as found by the KF method cannot be removed by desorption at this temperature in an acceptable time.

1.3.2 Influence of Vial Stoppers on the Residual Moisture Content

The stoppers for vials contain a certain amount of water, which depends on the composition of the stoppers. De Grazio and Flynn [163] showed that the selection

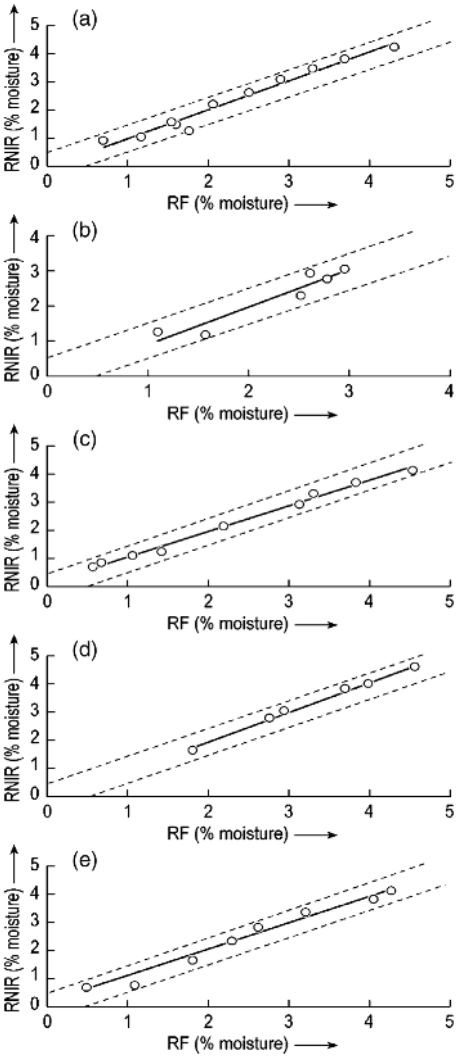

Figure 1.154 Relation between RNIR and RF for (a) rhuMAb E25, (b) rhuMAb HER2, (c) rhuMAb CD11a, (d) TNKase, and (e) rt-PA. Dotted lines represent ±0.5% moisture of solid lines. (See also Figure 1 from Ref. [162].) Data for the plots:

Plot	Equation	R^2 a)	RMSEC b)
(a)	$y = 1.05x - 0.08$	0.97	0.210
(b)	$y = 0.97x + 0.07$	0.97	0.243
(c)	$y = 0.93x + 0.14$	0.99	0.154
(d)	$y = 1.09x - 0.20$	0.99	0.135
(e)	$y = 0.99x + 0.12$	0.98	0.212

a) Coefficient of determination (linearity of calibration).
b) Root mean square error (uncertainty of calibration).

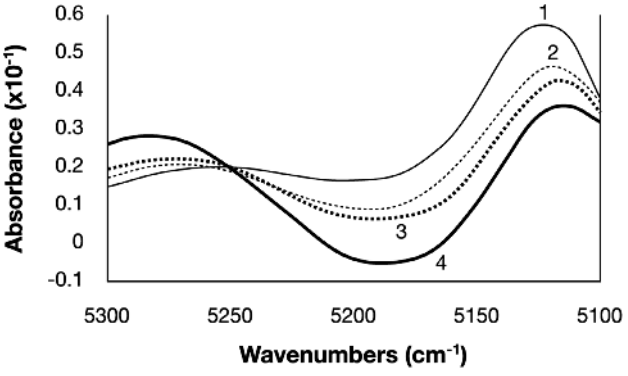

Figure 1.155 Second-derivative spectra of lyophilized rhuMAb containing RF 0.8%. All formulations contained 40 mg/mL rhuMAb E25, 5 mM histidine and 0.01% polysorbate 20. Sucrose concentration: (1) 42.5; (2) 85; (3) 120; (4) 170 mM. (See also Figure 6 from Ref. [162].)

of the polymer, the additives for the vulcanization, and the filler influence the adsorption and desorption of water. However, even the best possible mixture increases the RM in 215 mg of sucrose from 1.95 to 2.65% during 3 months of storage at room temperature. Other stopper mixtures show an increase of up to 1.7%. Pikal and Shah [164] demonstrated that the desorption of water from the stopper and the absorption of water by the product depend, in the equilibrium state, on the mass and water content of the stopper and the water content and sorption behavior of the dry product.

If the stopper is as small as technically possible and its material optimized, the water content of the stopper depends on its prehistory: Steam-sterilized stoppers take up water (e.g., 1.1% of their weight), which can only be removed by 8 h of

Table 1.31 Residual moisture content (RM) of different vaccines measured by four different measurement methods.

Test method	% RM ± standard deviation of the vaccines			
	Rubella virus	Mumps virus	Rubella and mumps virus	Measles, mumps, and rubella virus
Gravimetric[a)]	0.42 ± 0.18	1.10 ± 0.40	0.41 ± 0.26	0.18 ± 0.14
Karl Fischer[b)]	1.03 ± 0.14	1.54 ± 0.20	0.72 +/− 0.16	0.80 ± 0.14
TG-profile[b)]	1.26 ± 0.16	1.54 +/− 0.15	0.76 ± 0.12	0.76 ± 0.11
TG–60 °C hold[b)]	1.17 ± 0.20	1.53 ± 0.17	0.74 ± 0.13	0.70 ± 0.08

a) Average of 5–12 determinations.
b) Average.
TG-profile: thermogravimetric profile by a given course of temperatures.
TG–60 °C hold: by a constant temperature of +60 °C.
Part of Table 1 from Ref. [159].

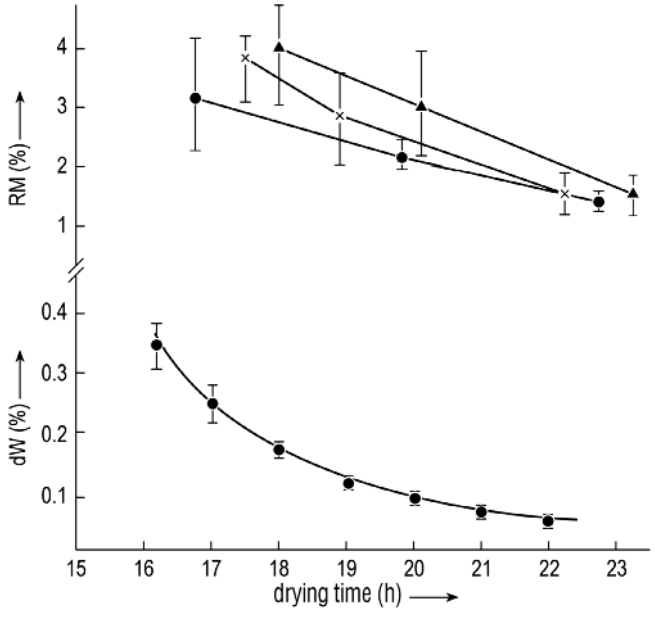

Figure 1.156 *Top:* RM measured by KF as a function of drying time. Ten vials were each closed at the time indicated by mean RM data. The cake from 5–7 vials out of each 10 vials closed was analyzed with 3–5 samples from each vial. The average data shown in the top graph are the mean values of 15 or more measurements. The bars are not standard deviations; they mark the minimum and the maximum of all measured data. (●) Run 1, mean $T_{ice} = -38.56\,°C$, SA = 0.38 °C. (+) Run 2, mean $T_{ice} = -38.59\,°C$, SA = 0.36 °C. [Mean T_{ice} of all runs −38.58 °C, SA = 0.02 °C] (▲) Run 3, mean $T_{ice} = -38.52\,°C$, SA = 0.39 °C. Process data for all three runs: freezing rate ~0.9 °C/min, final temperature −50 °C, $d = 10$ mm, $T_{sh,MD} = 0\,°C$, $p_c = 0.08$ mbar, $T_{sh,SD} = 40\,°C$. Below: dW data calculated from DR measurements during secondary drying as a function of drying time. (●) Mean dW of all three runs; bars, minimum and maximum of all calculated dW.

vacuum drying [164] or by 8 h of recirculated hot air (110 °C) drying down to 0.1% [165]. Figure 1.157 [164] shows that a steam-sterilized stopper, vacuum dried for 8 h, releases slightly less water to lactose than does an untreated stopper. A stopper dried for only 1 h increases the RM in 6 months of storage at 25 °C by a factor of 2.4. Figure 1.157 [164] also shows that an equilibrium is reached that, practically, does not change later. The time to reach the equilibrium depends strongly on the temperature. For a given product, the time to reach half-maximum increases from 4 days at +40 °C to 10 months at +5 °C. It is surprising that the absorption isotherms for lactose are found to be independent of temperature at +25 and +60 °C; this applies also to vancomycin at +25 and +40 °C. Figure 1.158 shows the equilibrium water content as a function of stopper treatment and amount of dry product independent of the storage temperatures of +25 and +40 °C for two different products; vancomycin is clearly more hygroscopic than lactose.

Earle *et al.* [166] showed that the RM in the product Pedvax HIB TM did not change during storage at 2–8 °C for 24 months if the stoppers were

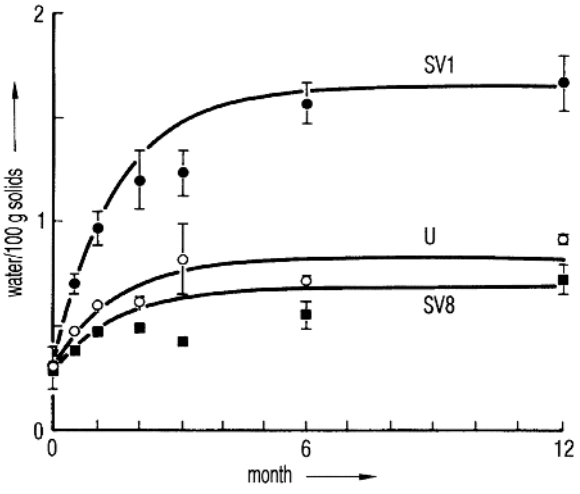

Figure 1.157 Water content of 100 mg of lactose at +25 °C as a function of time. The vials were closed with 13 mm stoppers subjected to different pretreatment: SV1, steam-sterilized; U, untreated; SV8, steam-sterilized followed by vacuum-drying for a minimum of 8 h. The lines were calculated by a model system. (See also Figure 4 from Ref. [164].)

steam-sterilized, vacuum-dried for 6 h, and finally dried at +143 °C for 4 h. If the vials were closed with stoppers that had not been dried, the RM increased in 12 months to ~5.3%. Danielson [167] warned against toxic components that could diffuse or migrate from the stopper to the product. A protective coating does not prevent the extraction of these substances, but a Teflon coating is better

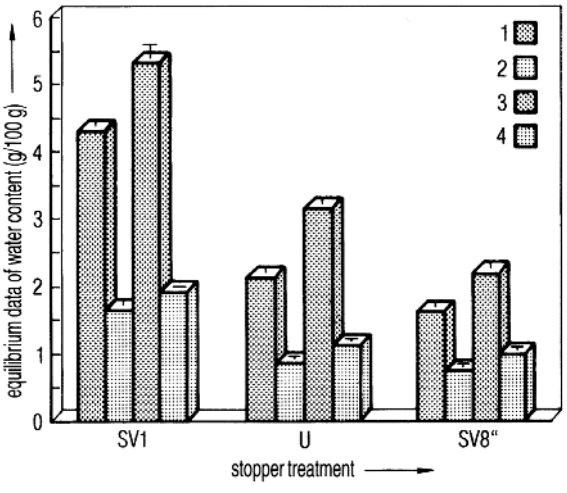

Figure 1.158 Equilibrium water content in two different freeze-dried products, each with two different amounts of product per vial. The equilibrium data are extrapolated from the +25 and +40 °C values. SV1, U, and SV8 as in Figure 1.158; 1, 25 mg of lactose; 2, 100 mg of lactose; 3, 25 mg of vancomycin; 4, 100 mg of vancomycin. (See also Figure 7 from Ref. [164].)

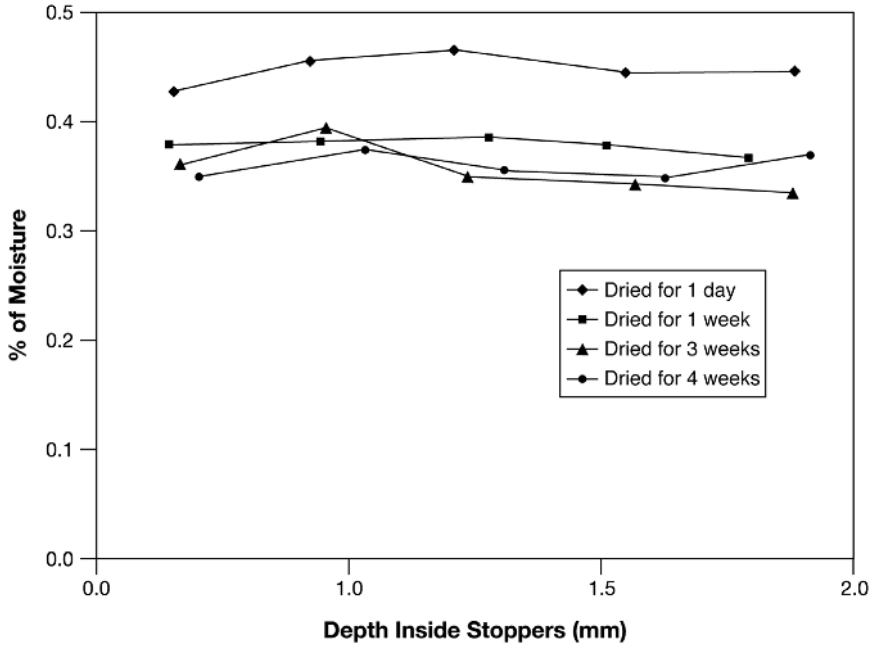

Figure 1.159 Moisture distribution inside the described rubber stoppers that were autoclaved at 121 °C for 30 min and then dried at 100 °C for different times. (See also Figure 7 from Ref. [169].)

than none. Corveleyn *et al.* [168] determined the water content of five chlorobutyl and three bromobutyl stoppers in the range of 0.85–1.49 and 1.71–1.99%, respectively, after they had been stored for 85 days at 95% RH. During sterilization, the moisture uptake was 0.82–0.9% for the chlorobutyl and 0.41–0.57% for the bromobutyl stoppers. Wang *et al.* [169] differentiated between free and bound water in stoppers. In Figure 1.159, the moisture distribution in stoppers (FM257/2, V9032, Helvoet Pharma, Pennsauken, NJ, USA) is shown after autoclaving at 121 °C for 30 min and drying at 100 °C for different times. The moisture distribution in Figure 1.159 no longer changes after 1 week of drying. The remaining amount of ~0.35%, bound to the stopper material, cannot be removed at 100 °C. The authors concluded that water that cannot be removed at 100 °C is bound in such a way that it cannot jeopardize the pharmaceutical product. Only the free water can diffuse from the stopper to the product. The moisture content is measured by the Karl Fischer method with different temperatures in the oven, 100 °C to determine the free water content and up to 300 °C to measure the free and bound water. The authors suggested developing a similar program for other stoppers, since the time for such measurements is relatively short (1 week) instead of observing the RM in a product over long times. Table 1.32 summarizes the results with the stoppers described above. Table 1.33 lists the limits of the free moisture content in two types of stoppers and for different cake weights under the assumption that a maximum RM increase of 0.5% in the product is acceptable.

Table 1.32 Moisture analysis of FM257/2, V9032 stoppers (Helvoet Pharma, Pennsauken, NJ, USA).

Oven dry	Moisture content (%) ± SA	Free moisture content (%)
No	0.52 ± 0.02	0.21
16 h	0.34 ± 0.02	0.03
1 week	0.31 ± 0.02	–

All stoppers were autoclaved for 16 min, vacuum dried for 30 min, and oven dried at 100 °C for the specified time. Table 4 from Ref. [169].

Table 1.33 Maximum moisture content of stoppers for a hypothetical product with a 0.5% moisture increase limit.

Stopper weight (g)	Cakes weight (g)	Limit for free moisture (%)
2.5	0.4	0.13
2.5	0.2	0.07
2.5	0.1	0.03
2.5	0.05	0.02
0.6	0.4	0.56
0.6	0.2	0.28
0.6	0.1	0.14
0.6	0.05	0.07

Table 3 from Ref. [169].

1.3.3 Qualities of the Dry Substances and Their Changes

During the storage of a freeze-dried product, its qualities can change under the influence of at least three conditions: residual moisture content, storage temperature, and gas mix in the packing, assuming that the freeze-drying itself has been carried out under optimum conditions and the product had the intended qualities at the end of the freeze-drying process. The changes that can be related to one or mostly to a combination of the three conditions can be divided into four groups:

1) Changes in the reconstitution with water and/or the solubility.
2) Chemical reactions in the dried product.
3) Deterioration of the biological–medical activity of the product.
4) Changes of the physical structure of the product, for example, from an amorphous to a partially or totally crystalline form.

Often changes occur that have to be accounted for as a combination of several of the four categories. In this section some typical examples are given, although some special changes are also mentioned in Chapters 3 and 4.

Liu and Langer [170] showed that BSA, ovalbumin, glucose oxidase, and β-lactoglobulin rapidly lost their solubility at 37 °C and, within 24 h, 97% became insoluble if 30% (w/w) of a buffered, physiological NaCl solution was added to the dried product. The aggregation induced by the moisture was attributed to intermolecular S–S binding. This aggregation can be minimized if the RM is optimized for a given albumin.

Zhang *et al.* [171] studied the effect of the reconstitution medium on aggregate formation in recombinant keratonocyte growth factor (KGF). Several additives reduced aggregation substantially, but similar effects were observed by adjusting the ionic strength of the reconstitution medium. Optimization of the reconstitution conditions increased the recovery of soluble active proteins; for KGF, the recovery of the soluble active proteins corresponds to the native, monomeric form. Furthermore, Zhang *et al.* [172] demonstrated that interleukin-2 (I) and RNase (II) show significant aggregation upon storage at +45 °C when pure water is used for reconstitution. The extent of aggregation can be substantially reduced if, for example, heparin or phosphates are added to the reconstitution water. Shalaev *et al.* [173] studied the acid-catalyzed inversion of amorphous sucrose to glucose and fructose at RM <0.1%. Sucrose colyophilized with, for example, citric acid undergoes acid-catalyzed inversions at 50 °C even at RH = 0.1%. The authors concluded that colyophilization of acidic substances with sucrose can produce substances capable of further reaction with other ingredients even at very low RM.

Yoshika *et al.* [174] studied the inactivation of β-galactosidase (I) during storage in relation to the water mobility by ^{17}O NMR spectroscopy. An increase in water content also produced an increase of the spin–lattice relaxation time, T_1, the inactivation being more dependent on T_1 than on the pH value. It was assumed that the water increased the mobility of the water around the enzyme, thus enhancing enzyme inactivation. The freeze-dried samples with little water also showed a greater inactivation rate than was expected from details of pH value and water mobility, this inactivation being induced by the salts used as additives for freeze-drying. Yoshika *et al.* [175] also used NMR spectroscopy but with the ^1H spin–spin relaxation time T_2. T_2 was measured on BSA and γ-globulin (BGG) as a function of hydration level. Freeze-dried BSA and BGG became sensitive to aggregation if the water content exceeded ~0.2 g/g protein. T_2 of the protein protons began to increase at low water contents and followed the increase in aggregation in time with increasing water content. For freeze-dried BGG, both the aggregation and the T_2 of the protein proton decreased at water contents >0.5 g/g protein.

The stability of moisture-sensitive drugs was studied by Vromans and Schalks [176] using amorphous vecuronium bromide. Its decomposition in a formulation depends more on the water activity a_w than on the water content. Glass-forming excipients may not only be cryoprotective but also stabilizing. Cleland *et al.* [177] found that an appropriate molar ratio of sugar to protein stabilized recombinant humanized monoclonal antibody (rhuMAb HER2) for 33 months at 40 °C. A 360: 1 molar ratio was successful in stabilizing the protein. This three- to fourfold below the normally used iso-osmotic concentrations in formulations. Souillac *et al.* [178] compared the enthalpies of freeze-dried and

physical mixtures of Rh-DNase, rh-GH, and rH-IGF-1 with mannitol, sucrose, trehalose, and dextran. For the physical mixtures, a linear relationship between the enthalpies and the percentage of protein was observed; for freeze-dried mixtures, this relationship was nonlinear. The authors concluded that direct interactions take place between the proteins and the carbohydrates in lyophilized mixtures.

Hsu *et al.* [179] demonstrated that decomposition can take place in a packaged product. It was assumed that the freeze-drying had ended with a monomolecular layer of water, which may not have been evenly distributed, but could be attached as clusters to certain locations of the molecule. This water provided optimum protection against denaturation during both drying and storage. This was demonstrated with two very different products, made by gene technology: too little water, less than one monolayer, makes *t*PA and methemoglobin physically unstable, whereas a higher water content leads to biological instability during storage.

Examples of the fourth type of changes were described by To and Flink [180] and Van Scoik and Carstensen [181]: According to To and Flink, the change from an amorphous to a crystalline phase is induced either by high storage temperatures T ($T > T_c$) or by water absorption. (*Note:* More water increases the mobility of the amorphous solid, promoting nucleation of crystals and their subsequent growth.)

Van Scoik and Carstensen [181] with their experiments differentiated between nucleation of sucrose crystals and their growth. The nucleation parameters of temperature and residual moisture were discussed and additives suggested to stop nucleation or to delay or speed it up. The influence of gases used for venting the chamber with vials or filled into the packaged bulk product is difficult to summarize. Only O_2 should be excluded in most cases. Spiess [182] suggested dry air for the storage of cauliflower and blueberry, while carrots and paprika should be stored in a gas with <0.1 mg O_2/g dry substance. Less sensitive products such as peas, green beans, and mushrooms tolerate 0.2–0.5 mg O_2/g dry substance. For drugs, viruses. or bacteria, no general recommendation can be given, since the influence of CPAs, structural additives, buffer, and so on, have to be taken into account.

The purity of gases used should also be specified, as certain impurities can have a decisive effect on storage behavior, for example, gas desorption from stoppers. Greiff and Rightsel [183] showed that influenza viruses without CPAs keep their infectivity best when stored with 1.6% RM in helium. In argon, the infectivity decreases ~10 times and in O_2 20 times faster if the average of the storage temperatures is used. Corveleyn and Remon [184] freeze-dried two different tablet formulations containing 25 mg of hydrochlorothiazide. Tablets where packed in PVC/aluminum blister packs, in PVC–poly(vinylidene chloride) (PVDC)/aluminum blister packs, closed containers with a desiccant tablet, and open containers and stored at three RHs, 45, 60, and 85%, at 60 °C. After 1 month at RH 85%, all tablets except those packed in PVDC/aluminum blister packs showed an increase from RM 2.7 to 6.8%. At a moisture content of 7.2%, one of the formulations collapsed. The increase in moisture content and decrease in mechanical strength for the PVDC/aluminum blistered tablets was much slower.

None of the packaged material used for freeze-dried tablets offered protection against moisture uptake and structural collapse.

References

1 Duckworth, R.B. (1971) Differential thermal analysis of frozen food systems: I. The determination of unfreezable water. *J. Food Technol.*, **6**, 317–327.

2 Riedel, L. (1972) Enthalpy–water content diagram for lean beef (also valid for other meats with fat content below 4%), in *Recommendations for the Processing and Handling of Frozen Foods*, 2nd edn, International Institute of Refrigeration, Paris, pp. 28–29.

3 Riedel, L. (1972), in *Recommendations for the Processing and Handling of Frozen Foods*, 2nd edn, International Institute of Refrigeration, Paris, pp. 32 and 34.

4 Steinbach, G. (1994) *Die Bedeutung des Einfriervorganges, Berechnung des Gefriervorganges, Verein Deutscher Ingenieure*, VDI-Bildungswerk, RW 1570, p. 3.

5 Oetjen, G.W. and Eilenberg, H.J. (1969) Heat transfer during freeze-drying with moved particles. International Institute of Refrigeration (Comm. X, Lausanne), pp. 19–35.

6 Sharon, Z. and Berk, Z. (1969) Freeze-drying of tomato juice and concentrate, studies of heat and mass transfer. International Institute of Refrigeration (Comm. X, Lausanne), pp. 115–122.

7 Magnussen, O.M. (1969) Measurements of heat and mass transfer during freeze-drying. International Institute of Refrigeration (Comm. X, Lausanne), pp. 65–74.

8 Gunn, R.D., Clark, J.P., and King, C.J. (1969) Mass transport in freeze-drying, basic studies and processing implications. International Institute of Refrigeration (Comm. X, Lausanne), pp. 79–98.

9 Oetjen, G.W. (1999) Industrial freeze-drying for pharmaceutical applications, in *Freeze-Drying/Lyophilization of Pharmaceuticals and Biological Products* (eds L. Rey and J.C. May), Marcel Dekker, New York, pp. 267–335 (Table 3 and Fig. 10, Pharmaceutical freeze-drying).

10 Umrath, W. (1974) Cooling bath for rapid freezing in electron microscopy. *J. Microsc.*, **101** (1), 103–105.

11 Riehle, U. (1986) Schnelleinfrieren organischer Präparate für die Elektronenmikroskopie. (Die Vitrifizierung verdünnter wässeriger Lösungen). *Chem. Ing. Tech.*, **40**, 213–218.

12 de Quervain, M.R. (1975) Crystallization of water, a review, in *Freeze-Drying and Advanced Food Technology* (eds S.A. Goldblith, L. Rey, and W.W. Rothmayr), Academic Press, New York, pp. 3–15.

13 Oetjen, G.W. (1949) Absorptionsmessungen an Lösungen von Neodymsalzen. Dissertation, Universität Göttingen, 1947. Z. Naturforsch. 4a, No. 1.

14 Dowell, L.G. and Rinfret, A.P. (1960) Low temperature forms of ice as studied by X-ray diffraction. *Nature*, **188**, 1144–1148.

15 Luyet, B. (1960) On various phase transitions occurring in aqueous solutions at low temperatures. *Ann. N. Y. Acad. Sci.*, **568**, 549–569 (Fig. 14).

16 Luyet, B. (1969) On the amount of water remaining amorphous in frozen aqueous solutions. *Biodynamica*, **10**, 277–291.

17 Shamblin, Sh.L. and Zografi, G. (1999) The effect of absorbed water on the properties of amorphous mixtures containing sucrose. *Pharm. Res.*, **16**, 1119–1124.

18 Zeng, X.M., Martin, G.P., and Marriott, C. (2001) Effects of molecular weight of polyvinylpyrrolidone on the glass transition and crystallization of co-lyophilized sucrose. *Int. J. Pharm.*, **218**, 63–73.

19 Shalaev, E.Y., Lu, Q., Shalaev, M., and Zografi, G. (2000) Acid-catalyzed inversion of sucrose in the amorphous state at very low levels. *Pharm. Res.*, **17**, 366–370.

20 Kouassi, K. and Roos, Y.H. (2001) Glass transition and water effects on sucrose version in non-crystalline carbohydrate food systems. *Food Res. Int.*, **34**, 895–901.

21 Saleki-Gerhardt, A. and Zografi, G. (1994) Non-isothermal and isothermal crystallization of sucrose from the amorphous state. *Pharm. Res.*, **11**, 1166–1173.

22 Yu, L., Milton, N., Groleau, E.G., Mishra, D.S., and Vansickle, R.E. (1999) Existence of a mannitol hydrate during freeze-drying and practical implications. *J. Pharm. Sci.*, **88**, 196–198.

23 Cannon, A. and Trappler, E.H. (2000) The influence of lyophilization on the polymorphic behavior of mannitol. *PDA J. Pharm. Sci. Technol.*, **54**, 13–22.

24 Pyne, A. and Suryanarayanan, R. (2001) Phase transitions of glycine in frozen aqueous solutions and during freeze-drying. *Pharm. Res.*, **18** (10), 1448–1454.

25 Hinrichs, W.L.J., Prinsen, M.G., and Frijlink, H.W. (2001) Inulin glasses for the stabilization of therapeutic proteins. *Int. J. Pharm.*, **215**, 163–174.

26 Davidson, P. and Sun, W.Q. (2001) Effects of sucrose/raffinose mass ratios on the stability of co-lyophilized protein during storage above T_g. *Pharm. Res.*, **18**, 474–479.

27 Fakes, M.G., Dali, M.V., Haby, Th.A., Morris, K.R., Varia, S.A., and Serajuddin, A.T.M. (2000) Moisture sorption behavior of selected bulking agents used in lyophilized products. *PDA J. Pharm. Sci. Technol.*, **54**, 144–149.

28 Thijssen, H.A.C. and Rulkens, W.H. (1969) Effect of freezing rate on rate of sublimation and flavour retention in freeze-drying. International Institute of Refrigeration (Comm. X, Lausanne), pp. 99–114.

29 Godward, J., Gunning, P., and Hills, B.P. (1999) An NMR protocol for determining ice crystal size distribution during freezing and pore size distribution during freeze-drying. *Appl. Magn. Reson.*, **17**, 537–556.

30 Reid, D.S., Lim, M.H., and McEvoy, H.M. (1983) Studies on the freezing processes in aqueous model systems. Paper 354, International Institute of Refrigeration (Comm. C1, Paris).

31 Burke, M. and Lindow, S.E. (1990) Surface properties and size of the ice nucleation of active bacteria: theoretical considerations. *Cryobiology*, **27**, 80–84.

32 Rasmussen, D. and Luyet, B. (1970) Contribution to the establishment of the temperature concentration curves of homogeneous nucleation in solutions of some cryoprotective agents. *Biodynamica*, **11** (225), 33–44.

33 Sutton, R.L. (1991) Critical cooling rates to avoid ice crystallisation in solutions of cryoprotective agents. *J. Chem. Soc., Faraday Trans.*, **87**, 101–106.

34 Correleyn, S. and Remon, J.P. (1995) The use of maltodextrin in the lyophilization of a model protein, LHD (lactate dehydrogenase). *Pharm. Res.*, **13**, 146.

35 Sutton, R.B. (1992) Critical cooling rates for aqueous cryoprotectants in the presence of sugars and polysaccharides. *Cryobiology*, **29**, 585–598.

36 Levine, H. and Slade, L. (1988) Principles of 'cryostabilisation' technology from structure/property relationship of carbohydrate/water system: a review. *Cryo Letters*, **9**, 21–63.

37 Shalaev, E.Yu. and Kaney, A.N. (1994) Study of the solid–liquid state diagram of the water– glycine–sucrose system. *Cryobiology*, **31**, 374–382.

38 Jang, J.W., Kitamura, S., and Guillory, J.K. (1995) The effect of excipients on the glass transition temperatures for FK 906 in the frozen and lyophilized state. *PDA J. Pharm. Sci. Technol.*, **49**, 166–174.

39 Gordon, M. and Taylor, J.S. (1952) Ideal copolymers and the second-order transitions of synthetic rubbers in non-crystalline copolymers. *J. Appl. Chem.*, **493**, 493–500.

40 Nicolajsen, H. and Hvidt, A. (1994) Phase behavior of the system trehalose–NaCl–water. *Cryobiology*, **31**, 199–205.

41 Carpenter, J.F., Arakawa, T., and Crowe, J.H. (1992) Interactions of stabilizing additives with proteins during freeze-thawing and freeze-drying, in *Developments in Biological Standardization*, vol. 74 (eds J.C. May and F. Brown), Karger, Basel, pp. 225–239.

42 Timasheff, S.N., Lee, J.G., Pittz, E.P., and Tweedy, N. (1976) The interaction of tubulin and other proteins with structure stabilizing solvents. *J. Colloid Interface Sci.*, **55**, 658–663.

43 Prestrelski, S.J., Arakawa, T., and Carpenter, J.F. (1993) Separation of freezing- and drying-induced denaturation of lyophilized proteins using stress-specific stabilization: II. Structural studies using infrared spectroscopy. *Arch. Biochem. Biophys.*, **303**, 465–473.

44 Carpenter, J.F., Prestrelski, S.J., Anchordogy, T.J., and Arakawa, T. (1994) Interaction of stabilizers with proteins during freezing and drying. *Formulation and Delivery of Proteins and Peptides*, ACS Symposium Series 567, American Chemical Society, pp. 134–147.

45 Rey, L. (2020) Glimpses into the realm of freeze-drying: classical issues and new ventures, in *Freeze-Drying/Lyophilization of Pharmaceutical and Biological Products* (eds L. Rey and J.C. May), Marcel Dekker, New York, pp. 1–30.

46 Meryman, H.T. (1968) The 'minimum cell volume' modes of freezing injury. *Nature*, **218**, 333 (International Institute of Refrigeration (IIR) (Comm. X), pp. 897–900, Washington, DC, 1971).

47 Pushkar, P.S. and Itkin, U.A. (1971) The study of the intercellular and extracellular crystallization of the biological objects on freezing. International Institute of Refrigeration (Comm. X, Washington, DC), pp. 861–868.

48 Nei, T. (1983) Ice particles formed in various cells. International Institute of Refrigeration (Comm. 1, Paris), pp. 429–430.

49 Cosman, M.D., Toner, M., Kandel, J., and Cravalho, E.G. (1989) An integrated cryomicroscopy system. *Cryo Letters*, **10**, 17–38.

50 De Antoni, G.L., Perez, P., Abraham, A., and Anon, M.C. (1989) Trehalose, a cryoprotectant for *Lactobacillus bulgaricus*. *Cryobiology*, **26**, 149–153.

51 Rey, L. (1962) Influence of the preliminary freezing period and adsorption phenomena in freeze-drying. Vortrag auf der 5, Gefriertrockentagung Leybold, Köln, pp. 3–19.

52 Willemer, H. (2002) Comparison between measurements of electrical resistance and cryomicroscope visualization of pharmaceutical products to be freeze-dried. ISL–FD, Lyophilization Conference, Amsterdam, October 2002.

53 MacKenzie, A.P. (1985) A current understanding of the freeze-drying of representative aqueous solutions. *Fundamentals and Applications of Freeze-Drying to Biological Materials, Drugs and Foodstuffs*, International Institute of Refrigeration, pp. 21–34.

54 Hatley, R.H.M. (1992) The effective use of differential scanning calorimetry in the optimisation of freeze-drying processes and formulations, in *Developments in Biological Standardization*, vol. 74 (eds J.C. May and F. Brown), Karger, Basel, pp. 105–122.

55 Luyet, B. and Rasmussen, D. (1968) Study by differential thermal analysis (DTA) of the temperatures of instability of rapidly cooled solutions of glycerol, ethylene glycol, sucrose and glucose. *Biodynamica*, **10** (211), 167–191.

56 Rasmussen, D. and Luyet, B. (1969) Complementary study of some non-equilibrium phase transitions in frozen solutions of glycerol, ethylene, glycol, glucose and sucrose. *Biodynamica*, **10**, 319–331.

57 Hsu, C.C., Walsh, A.J., Nguyen, H.M., Overcashier, E.D., Koning-Bastiaan, H., Bailey, R., and Nail, S.L. (1996) Design and application of a low-temperature Peltier-cooling microscope stage. *J. Pharm. Sci.*, **85**, 70–71.

58 Nunner, B. (1993) Gerichtete Erstarrung wässriger Lösungen and Zellsuspensionen. Dissertation, Rheinisch-Westfälische Technische Hochschule Aachen.

59 Dawson, P.J. and Hockley, D.J. (1992) Scanning electron microscopy (SEM) of freeze-dried preparations: relationship of morphology to freeze-drying parameters, in *Developments in Biological Standardization*, vol. 74 (eds J.C. May and F. Brown), Karger, Basel, pp. 185–192.

60 Meister, E. and Gieseler, H. (2009) Freeze-dry microscopy of protein/sugar mixtures: drying behaviour, interpretation of collapse temperature and a comparison to corresponding glass transition data. *J. Pharm. Sci.*, **98** (9), 3072–3087.

61 Gatlin, L.A. (1992) Kinetics of a phase transition in a frozen solution, in *Developments in Biological Standardization*, vol. 74 (eds J.C. May and F. Brown), Karger, Basel, pp. 93–104.

62 DeLuca, P.P. (1985) Phase transitions in frozen antibiotic solutions. International Institute of Refrigeration (Comm. C1, Tokyo), pp. 87–92.
63 Takeda, T. (1989) Crystallization and subsequent freeze-drying of cephalothin sodium by seeding method. *Yakugaku Zasshi*, **109**, 395–401.
64 Roos, Y.K.M. (1991) Thermal history and properties of frozen carbohydrate solutions. Paper 350, International Institute of Refrigeration (XVIII Congress, Montreal).
65 Talsma, H., van Steenbergen, M.J., Salemink, P.J.M., and Crommelin, D.J.A. (1991) The cryopreservation of liposomes: 1. A differential scanning calorimetry study of the thermal behavior of a liposome dispersion containing mannitol during freezing/thawing. *Pharm. Res.*, **8**, 1021–1026.
66 Williams, N.A. (1988) Differential scanning calorimetric studies on frozen cephalosporin I solutions. *Int. J. Pharm.*, **44**, 205–212.
67 Knopp, S.A., Chongprasert, S., and Nail, S.L. (1998) The relationship between the TMDSC curve of frozen sucrose solutions and collapse during freeze-drying. *J. Thermal Anal. Calorim.*, **54**, 659–672.
68 Kett, V.L. and Craig, D.Q.M. (2000) The effect of annealing on the glass transition region of sucrose solutions. Proceedings of the 28th NATAS Annual Conference on Thermal Analytical Applications, pp. 653–658.
69 Chang, L.-Q., Tang, X.-L., Pikal, M.J., Milton, N., and Thomas, L. (1999) The origin of multiple glass transitions in frozen aqueous solutions. Proceedings of the 27th NATAS Annual Conference on Thermal Analytical Applications, pp. 624–628.
70 Craig, D.C.M., Barnews, M., Royall, P.G., and Kett, V.L. (2000) An evaluation of use of modulated DSC as a means of assessing the relaxation behavior of amorphous lactose. *Pharm. Res.*, **17**, 696–700.
71 Sichina, W.J. (2000) Utilization de StepScan DSC pour l'optimisation des procedes de lyophlisation. *Spectral Analyse*, **29** (216), 35–37.
72 van Winden, E.C.A., Talsma, H., and Crommelin, D.J.A. (1998) Thermal analysis of freeze-dried liposomes–carbohydrate mixtures with modulated temperature differential scanning calorimetry (MTD-SC). *J. Pharm. Sci.*, **87**, 231–237.
73 Kett, V.L., Craig, D.Q.M., and Deutsch, D. (1999) Thermal analysis of freeze-dried formulations. Proceedings of the 27th NATAS Annual Conference on Thermal Analytical Applications, pp. 618–623.
74 Craig, D.Q.M., Barsner, M., Royall, P.G., and Kett, V.L. (2000) An evaluation of the use of modulated temperature DSC as a means of assessing the relaxation behavior of amorphous lactose. *Pharm. Res.*, **17**, 696–700.
75 Knowles, P.F., Marsh, D., and Rattle, H.W.E. (1976) *Magnetic Resonance of Biomolecules*, John Wiley & Sons, Inc., Chichester.
76 Hanafusa, N. (1992) The behavior of hydration water of protein with the protectant in the view of HNMR, in *Developments in Biological Standardization*, vol. 74 (eds J.C. May and F. Brown), Karger, Basel, pp. 241–253.
77 Nagashima, N. and Suzuki, E. (1985) Freezing curve by broad-line pulsed NMR and freeze-drying. International Institute of Refrigeration (Comm. C1, Tokyo), pp. 65–70.

78 Harz, H-.P., Weisser, H., and Liebenspacher, F. (1989) Bestimmung des Fest-Flüssiggleichgewichtes in gefrorenen Lebensmitteln mit der gepulsten Kernresonanzspektroskopie. DKV-Tagungsbericht, Hannover, pp. 741–752.

79 Girlich, D. (1992) Multikernresonanzuntersuchungen zur molekularen Dynamik wässeriger Saccharidlösungen. Dissertation, Naturwissenschaftliche Fakultät III, Biologie and vorklinische Medizin der Universität Regensburg, 1991, S. Roderer Verlag, Regensburg.

80 Kanaori, A.J. and Nosaka, A.J. (1995) Studies on human calcitinin fibrillation by proton nuclear magnetic resonance spectroscopy: characterization of the lyophilized fibril. Proceedings of the International Society of Magnetic Resonance, XIIth Meeting, Part 1, pp. 274–275 (*Bull. Magn. Reson.* 17, 1–4.

81 Yoshioka, S., Aso, Y., and Kojima, S. (1996) Determination of molecular mobility of lyophilized bovine serum albumin and gamma-globulin by solid-state 1H NMR and relation to aggregation-susceptibility. *Pharm. Res.*, **13**, 926–930.

82 Carrington, A.K., Sahagian, M.E., Goff, H.D., and Stanley, D.W. (1994) Ice crystallization temperatures of sugar/polysaccharide solutions and their relationship to thermal events during warming. *Cryo Letters*, **15**, 235–244.

83 Williams, N.A. and Gugliemo, J. (1993) Thermal mechanical analysis of frozen solutions of mannitol and some related stereoisomers: evidence of expansion during warming and correlation with vial breakage during lyophilization. *J. Parenter. Sci. Technol.*, **47**, 119–123.

84 Pearson, D.S. and Smith, G. (1998) Dielectric analysis as a tool for investigating the lyophilization of proteins. *Pharm. Sci. Technol. Today*, **1** (3), 108–117.

85 Morris, K.R., Evans, S.A., Mackenzie, A.P., Scheule, C., and Lordi, N.G. (1994) Prediction of lyophile collapse temperatures by dielectric analysis. *PDA J. Pharm. Sci. Technol.*, **48**, 318–329.

86 Smith, G., Duffy, A.P., Shen, J., and Ollliff, C.J. (1995) Dielectric relaxation spectroscopy and some applications in the pharmaceutical science. *J. Pharm. Sci.*, **84**, 1029–1044.

87 Cavatur, R.K. and Suryanarayanan, R. (1989) Characterization of frozen aqueous solutions by low temperature X-ray powder diffractometry. *Pharm. Res.*, **15**, 194–199.

88 Sane, S., Mulkerrin, M., and Hsu, Ch. (2000) Raman spectroscopic characterization of drying-induced structural changes in proteins: correlating the structural changes with long-term stability. Book of Abstracts, 219th ACS National Meeting, San Francisco, CA, March 26–30, 2000, BIOT–380. American Chemical Society, Washington, DC.

89 MacKenzie, A.P. (1992) The physico-chemical basis for the freeze-drying process, in *Developments in Biological Standardization*, vol. 74 (eds J.C. May and F. Brown), Karger, Basel, pp. 51–67.

90 Pikal, M.J. (1977) Thermal decomposition of amorphous beta-lactam antibacterials. *J. Pharm. Sci.*, **66**, 1312.

91 Pikal, M.J. *et al.* (1978) Quantitative crystallinity determinations for beta-lactam antibiotics by solution calorimetry: correlations with stability. *J. Pharm. Sci.*, **67**, 767.

92 Kovalcik, T.R. and Guillory, J.K. (1988) The stability of cyclophosphamide in lyophilized cakes: Part I. Mannitol, lactose, and sodium bicarbonate as excipients. *J. Parenter. Sci. Technol.*, **42**, 29.

93 Gatlin, L.A. (1992) Kinetics of a phase transition in a frozen solution, in *Developments in Biological Standardization*, vol. 74 (eds J.C. May and F. Brown), Karger, Basel, pp. 93–104.

94 Yarwood, R.J. and Phillips, A.J. (1989) Processing factors influencing the stability of freeze-dried sodium ethacrinate, in *Pharmaceutical Technology: Drug Stabilization* (ed. M. Rubinstein), Ellis Horwood, Chichester, pp. 40–48.

95 Koray, D.J. and Schwartz, J.B. (1989) Effects of excipients on the crystallisation of pharmaceutical compounds during lyophilization. *J. Parenter. Sci. Technol.*, **43**, 80–83.

96 De Luca, P.P., Klamat, M.S., and Koida, C. (1989) Acceleration of freeze-drying cycles of aqueous solutions of lactose and sucrose with tertiary butyl alcohol (*t*BA). *Congr. Int. Technol. Pharm.*, **1**, 439–447.

97 Kasraian, K. and De Luca, P.P. (1995) Thermal analysis of tertiary butyl alcohol–water system and its implication on freeze-drying. *Pharm. Res.*, **12**, 484–490.

98 Oesterle, J., Franks, F., and Auffret, T. (1998) The influence of tertiary butyl alcohol and volatile salts on the sublimation of ice from frozen sucrose solutions: implications for freeze drying. *Pharm. Dev. Technol.*, **3**, 175–183.

99 Wittaya-areekul, S. and Nail, S.L. (1998) Freeze-drying of *tert*-butyl alcohol/water cosolvent systems: effects of formulation and process variables on residual solvents. *J. Pharm. Sci.*, **87**, 491–495.

100 Kochs, M., Körber, Ch., Nunner, B., and Heschel, I. (1991) The influence of the freezing process on vapor transport during sublimation in vacuum-freeze-drying. *J. Heat Mass Transfer*, **34**, 2395–2408.

101 Vdi e.v. (1988) *VDI-Wärmeatlas*, 5. Auflage, p. Kb 5, VDI-Verlag, Düsseldorf.

102 Wolff, E., Gibert, H., and Rudolf, F. (1989) Vacuum freeze-drying kinetics and modeling of a liquid in a vial. *Chem. Eng. Process.*, **25**, 153–158.

103 Ybema, H., Kolkmann-Roodbeen, L., te Booy, M.P.W.M., and Vromans, H. (1995) Vial lyophilization: calculation on the rate limitation during primary drying. *Pharm. Res.*, **12**, 1260–1263.

104 Chang, B.S. and Fuscher, N.L. (1995) The development of an efficient single-step freeze-drying cycle for interleukin-1 receptor antagonist formulation. *Pharm. Res.*, **12**, 831–837.

105 Steinbach, G. (1974) Wärmeübertragung and Stofftransport bei der Gefriertrocknung. Berechnung von Gefriertrocknungsprozessen, VDI-Bildungswerk, BW 1610.

106 Steinbach, G. (1971) Equations for the heat and mass transfer in freeze-drying of porous and nonporous layers and bodies. International Institute of Refrigeration (Comm. XIII, Washington, DC), pp. 674–683.

107 Gehrke, H.-H. and Deckwer, W.-D. (1990) Gefriertrocknung von Mikroorganismen. II. Mathematische Beschreibung des Sublimationsvorganges. *Chem. Ing. Tech.*, **62** (9), 770–771.

108 Kasraian, K. and DeLuca, P.P. (1995) The effect of tertiary butyl alcohol on the resistance of the dry product layer during primary drying. *Pharm. Res.*, **12**, 491–495.

109 Jennings, T.A. (1999) *Lyophilization: Introduction and Basic Principles*, Interpharm Press, Englewood, CO, p. 314.

110 Overcashier, D.E., Patapoff, T.W., and Hsu, Ch.C. (1999) Lyophilization of protein formulations in vials: investigation of the relationship between resistance to vapor flow during primary drying and small-scale product collapse. *J. Pharm. Sci.*, **88**, 688–695.

111 Schellenz, G., Engel, J., and Rupprecht, H. (1995) Sublimation during lyophilization detected by temperature profile and X-ray technique. *Int. J. Pharm.*, **113**, 133–140.

112 Drummond, J.N. and Day, L.A. (1997) Influence of vial construction and material on performance, uniformity and morphology during freezing and freeze drying. PDA Proceedings of International Congress, Osaka, pp. 401–427.

113 Pikal, M.J. (2000) Heat and mass transfer in low pressure gases: application to freeze-drying, in *Transport Processes in Pharmaceutical Systems* (eds G.L. Amidon, P.I. Lee, and E.M. Topp), Marcel Dekker, New York, pp. 611–686.

114 Willemer, H., Spallek, M., Auchter-Krummel, P., and Heinz, J. (1998) Freezing and freeze drying of pharmaceuticals in tubing, vials with quartz-coated surfaces and resin vials. PDA Proceedings of International Congress, Basel, pp. 99–108.

115 Pikal, M.J., Roy, M.L., and Shah, S. (1984) Mass and heat transfer in vial freeze-drying pharmaceuticals: role of vial. *J. Pharm. Sci.*, **73**, 1224–1237.

116 Kobayashi, M. (1991) Vial variance of the sublimation rate in shelf freeze-drying. Paper 312, International Institute of Refrigeration, Montreal.

117 Oetjen, G.W. (1973) Vakuumtechnik, in *Ullmanns Enzyklopädie der technischen Chemie*, 4. Auflage, Band 3, Verlag Chemie, Weinheim, p. 104.

118 Searles, J.A., Carpenter, J.F., and Randolph, T.W. (2001) The ice nucleation temperature determines the primary drying rate of lyophilization for samples frozen on a temperature-controlled shelf. *PDA J. Pharm. Sci. Technol.*, **90**, 860–871.

119 Searles, J.A., Carpenter, J.F., and Randolph, T.W. (2001) Annealing to optimize the primary drying rate, reduce freezing-induced drying heterogeneity, and determine $T_{g'}$ in pharmaceutical lyophilization. *J. Pharm. Sci.*, **90**, 872–887.

120 Pikal, M.J. and Shaw, S. (1997) Intravial distribution of moisture during the secondary drying stage of freeze drying. *PDA J. Pharm. Sci. Technol.*, **51**, 17–24.

121 Pikal, M. (1991) Freeze-drying of proteins. Part I: process design. *Pharm. Technol. Int.*, **3**, 37–43.

122 Hsu, C.C., Ward, C.A., Pearlman, R., Nguyen, H.M., Yeung, D.A., and Curley, J.G. (1992) Determining the optimum residual moisture in lyophilized protein pharmaceuticals, in *Development in Biological Standardization*, vol. 74 (eds J.C. May and F. Brown), Karger, Basel, pp. 255–271.

123 Haseley, P. and Oetjen, G.W. (1999) The influence of the freezing speed on mannitol solutions during main- and desorption drying. Paper 608, International Institute of Refrigeration, XX. International Congress of Refrigeration, Sydney.

124 Kim, A.I., Akers, M.J., and Nail, S.L. (1998) The physical state of mannitol after freeze-dying: effects of mannitol concentration, freezing rate and a noncrystallizing cosolute. *J. Pharm. Sci.*, **87**, 931–935.

125 Nail, St.L. and Johnson, W. (1992) Methodology for in-process determination of residual water in freeze-dried products, in *Developments in Biological Standardization*, vol. 74 (eds J.C. May and F. Brown), Karger, Basel, pp. 137–152.

126 Willemer, H. (1992) Measurements of temperature, ice evaporation rates and residual moisture content in freeze-drying, in *Developments in Biological Standardization*, vol. 74 (eds J.C. May and F. Brown), Karger, Basel, pp. 123–136.

127 Bardat, A., Biguet, J., Chatenet, E., and Courteille, F. (1993) Moisture measurement: a new method for monitoring freeze-drying cycles. *J. Parenter. Sci. Technol.*, **47**, 293–299.

128 Willemer, H. (1993) Moderne Anlagen, in *Lyophilisation*, vol. 35 (eds D. Essig and R. Oschmann), Wissenschaftliche Verlagsgesellschaft, Stuttgart.

129 Neumann, K.H. and Oetjen, G.W. (1958) Messund Regelprobleme bei der Gefriertrocknung. First International Congress on Vacuum Technology, Namur.

130 Lentges, G., Oetjen, G.W., Willemer, H., and Wilmanns, J. (1971) Problems of measurement and control in freeze-drying down to −180°C. International Institute of Refrigeration (XIII Congress, Washington, DC), pp. 707–715.

131 Milton, N., Pikal, M.J., Roy, M.L., and Nail, S.L. (1997) Evaluation of manometric temperature measurement as a method of monitoring product temperature during lyophilization. *J. Parenter. Sci. Technol.*, **51**, 7–16.

132 Haseley, P. and Oetjen, G.W. (1998) Equipment data, thermodynamic measurements, and in-process control quality control during freeze-drying. PDA International Congress, Basel, pp. 139–150.

133 Bouldoires, J.P. (1969) Experimental study of heat and mass transfer during freeze-drying through dielectric and vapour pressure measurements, International Institute of Refrigeration (Comm. X, Lausanne), pp. 189–206.

134 Leybold, AG (1987) Vacuum Technology: Its Foundations, Formulae and Tables, Köln, 9th edn, p. 52.

135 Welch, J. (1993) Vacuum measurement in steam sterilizable lyophilizers. *J. Parenter. Sci. Technol.*, **47** (1), 29–34.

136 Connelly, J.P. and Welch, J.V. (1993) Monitor lyophilization with mass spectrometer gas analysis. *J. Parenter. Sci. Technol.*, **47**, 70–75.

137 Willemer, H. (1994) Influence of product temperature and gas composition on the lyophilisation process. International Congress, Basel, pp. 63–77.

138 Willemer, H. (1994) Water vapour pressure, its influence on the freeze-drying process and its control. 40th Annual Congress of the International Association for Pharmaceutical Technology, Abstracts, Medpharm, Stuttgart, pp. 1–67.

139 Mangold, A. (2009) Drahtlose Temperatur-Messung in der Lyophilisation: "TEMPRIS Praxisbericht in Produktionsanlagen". Das Erlangen-Seminar, March 19–20th.

140 Mangold, A. (2009) TEMPRIS, precise measurement of Tp I freeze-drying. Bologna.

141 Schneid, S. and Gieseler, H. (2008) Evaluation of a new wireless temperature remote interrogation system (TEMPRIS) to measure product temperature during freeze-drying. *AAPS PharmSciTech*. doi: 10,1208/s12249-008-9099-8

142 Hammerer, K.H. (2007) Wireless temperature-measurement as an innovative PAT- method. 2nd European Congress of Live Science Process Technology, Nuernberg, Germany, March 28.

143 Wilbur, B. (2012) Pfizer: Process Development of a Dual Syringe. Presented at CHI PepTalk Gilyos GmbH (www.gilyos.com).

144 Diels, K. and Jaeckel, R. (1962) *Vakuum Taschenbuch*, 2nd edn, Springer, Berlin, pp. 22–24.

145 MacKenzie, A.P. (1974) Collapse during freeze-drying, qualitative and quantitative aspects. *Freeze-Drying and Advanced Food Technology*, Academic Press, New York, p. 282.

146 Pikal, M.J. and Shah, S. (1990) The collapse temperature in freeze-drying: dependence on measurement methodology and rate of water removal from the glassy phase. *Int. J. Pharm.*, **62**, 165–186.

147 Thijssen, H.A.C. and Rulkens, W.H. (1969) Effect of freezing rate on rate of sublimation and flavour retention in freeze-drying. International Institute of Refrigeration (Comm. X, Lausanne), pp. 99–114.

148 Thijssen, H.A.C. and Rulkens, W.H. (1968) Retention on aromas in drying food liquids. *De Ingenieur, Chemische Techniek (Niederlande)*, **80**, 45–56.

149 Flink, J. and Karel, M. (1970) Retention of organic volatiles in freeze-dried solutions of carbohydrates. *J. Agric. Food Chem.*, **18**, 295.

150 Voilley, A., Sauvageot, F., and Simatos, D. (1971) Coefficients de volatilité rélative et retention au cours de la lyophilisation de quelques alcools, International Institute of Refrigeration, Washington, DC, pp. 639–647.

151 Flink, J. (1975) The retention of volatile components during freeze-drying: a structurally based mechanism, in *Freeze-Drying and Advanced Food Technology* (eds S.A. Goldblith, L. Rey, and W.W. Rothmayr), Academic Press, pp. 351–372.

152 Gero, L. and Smyrl, T.G. (1982) Behavior of low molecular weight organic acids during freeze-drying. *J. Food Sci.*, **47**, 954–957.

153 Seager, H., Taskis, C.B., Syrop, M., and Lee, T.J. (1985) Structures of products prepared by freeze-drying solutions containing organic solvents. *J. Parenter. Sci. Technol.*, **39**, 161–179.

154 Kahn-Wyler, A. (1987) Kaltlufttrocknung von pharmazeutischen Präparaten and gefrorenen Lösungen in der Wirbelschicht. Dissertation, Philosoph.-Nat. Fakultät der Universität Basel.

155 Labrude, P. and Rasolomana, M. (1988) Atomization of oxyhemoglobin in the presence of sucrose. Study by circular dichroism and electronic paramagnetic resonance, comparison with freeze-drying. *STP Pharma Sci.*, **4** (6), 472–480.

156 Wolff, E. and Gibert, H. (1991) La lyophilization en lit fluidise d'adsorbant, optimisation et applications. Paper 313, International Institute of Refrigeration, Montreal.

157 Mumenthaler, M. (1990) Sprühgefriertrocknung bei Atm.-Druck: Möglichkeiten and Grenzen in der pharmazeutischen Technologie and der Lebensmitteltechnologie. Dissertation, Universität Basel.

158 Webb, S. *et al.* (2002) Surface adsorption of recombinant human interferon-γ interferon lyophilized and spray-lyophilized formulations. *J. Pharm. Sci.*, **91** (6), 1474–1487.
159 May, J.C., Wheeler, R.M., Etz, N., and Del Grosso, A. (1992) Measurement of final container residual moisture in freeze-dried biological products, in *Developments in Biological Standardization*, vol. 74 (eds J.C. May and F. Brown), Karger, Basel, pp. 153–164.
160 Wekx, J.P.H. and De Kleijn, J.P. (1990) The determination of water in freeze-dried pharmaceutical products by performing the Karl Fischer titration in the glass container itself. *Drug Dev. Ind. Pharm.*, **16**, 1465–1472.
161 May, J.C., Rey, L., Del Grosso, A., Etz, N., and Wheeler, R. (2000) TG, TG/MS: applications to determination of residual moisture in pertussis vaccine and other freeze-dried biological products. Proceedings of the 28th NATAS Annual Conference on Thermal Analytical Applications, pp. 67–74.
162 Lin, T.P. and Hsu, Ch.C. (2002) Determination of residual moisture in lyophilized protein pharmaceuticals using a rapid and non-invasive method: near-infrared spectroscopy. *PDA J. Pharm. Sci. Technol.*, **56**, 196–205.
163 De Grazio, F. and Flynn, K. (1992) Lyophilization closures for protein based drugs. *J. Parenter. Sci. Technol.*, **46**, 54–61.
164 Pikal, M.J. and Shah, S. (1992) Moisture transfer from stopper to product and resulting stability implications, in *Developments in Biological Standardization*, vol. 74 (eds J.C. May and F. Brown), Karger, Basel, pp. 165–179.
165 Brinkhoff, O. (1993) Primärpackmittel für Lyophilisate, in *Lyophilisation*, vol. 35 (eds D. Essig and R. Oschmann), Wissenschaftliche Verlagsgesellschaft, Stuttgart, p. 145.
166 Earle, J.P., Bennett, P.S., Larson, K.A., and Shaw, R. (1992) The effects of stopper drying on moisture levels of haemophilus influenzae conjugate vaccine, in *Developments in Biological Standardization*, vol. 74 (eds J.C. May and F. Brown), Karger, Basel, pp. 203–210.
167 Danielson, J.W. (1992) Toxicity potential of compounds found in parenreral solutions with rubber stoppers. *J. Parenter. Sci. Technol.*, **46**, 43–47.
168 Corveleyn, S., De Smedt, S., and Remon, J.P. (1997) Moisture absorption and desorption of different rubber lyophilization closures. *Int. J. Pharm.*, **159**, 57–65.
169 Wang, Z., Frankel, B.A., and Lambert, W. (2001) Determination of moisture in rubber stoppers: effect of Karl Fischer oven temperatures. *PDA J. Pharm. Sci. Technol.*, **55**, 162–170.
170 Liu, W.R. and Langer, R. (1991) Moisture induced aggregation of lyophilized proteins in the solid state. *Biotechnol. Bioeng.*, **37**, 177–184.
171 Zhang, M.Z., Wen, J., Arakawa, T., and Orestrelsky, S.J. (1995) A new strategy for enhancing the stability of lyophilized protein: the effect of the reconstitution medium on the keratinocyte growth factor. *Pharm. Res.*, **12**, 1447–1452.
172 Zhang, M.Z., Pikal, K., Nguyen, T., Arakawa, T., and Prestrelski, S.J. (1996) The effect of reconstitution medium on the aggregation of lyophilized recombinant interleukin-2 and ribonuclease A. *Pharm. Res.*, **13**, 643–646.

173 Shalaev, E.Y., Lu, Q., Shalaeva, M., and Zografi, G. (2000) Acid-catalyzed inversion of sucrose in the amorphous state at very low levels of residual water. *Pharm. Res.*, **17**, 366–370.

174 Yoshika, S., Aso, Y., Izuutsu, K., and Terao, T. (1993) Stability of beta-galactosidase, a model protein drug, is related to water mobility as measured by oxygen-17 nuclear magnetic resonance (NMR). *Pharm. Res.*, **10**, 103–108.

175 Yoshika, S., Asu, Y., and Kojima, Sh. (1996) Determination of molecular mobility of lyophilized bovine serum albumin and gamma-globulin by solid-state 1H NMR and relation to aggregation-susceptibility. *Pharm. Res.*, **13**, 926–930.

176 Vromans, H. and Schalks, E.J.M. (1994) Comparative and predictive evaluation of the stability of different freeze dried formulations containing an amorphous, moisture-sensitive ingredient. *Drug Dev. Ind. Pharm.*, **20**, 757–768.

177 Cleland, J.L., Lam, X., Kendrick, B., Yang, J., Yang, T.H., Overcashier, D., Brooks, D., Hsu, C., and Carpenter, J.F. (2001) A specific molar ratio of stabilizer to protein is required for storage stability of a lyophilized monoclonal antibody. *J. Pharm. Sci.*, **90**, 310–321.

178 Souillac, P.O., Costantino, H.R., Middaugh, C.R., and Rytting, J.H. (2002) Investigation of protein/carbohydrate interactions in the dried state: 1. Calorimetric studies. *J. Pharm. Sci.*, **91**, 206–216.

179 Hsu, C.C., Ward, C.A., Pearlman, R., Nguyen, H.M., Yeung, D.A., and Curley, G. (1992) Determining the optimum residual moisture in lyophilized protein pharmaceuticals, in *Developments in Biological Standardization*, vol. 74 (eds J.C. May and F. Brown), Karger, Basel, pp. 255–271.

180 To, E.C. and Flink, J.M. (1978) 'Collapse', a structural transition in freeze-dried carbohydrates. *J. Food Technol.*, **13**, 583–594.

181 Van Scoik, K.G. and Carstensen, J.T. (1990) Nucleation phenomena in amorphous sucrose systems. *Int. J. Pharm.*, **58**, 185–196.

182 Spiess, W. (1974) *Verfahrensgrundlagen der Trocknung bei niedrigen Temperaturen*. VDI-Bildungswerk, BW 2229, p. 5.

183 Greiff, D. and Rightsel, W.A. (1969) Stabilities of dried suspensions of influenza virus sealed in vacuum or under different gases. *Appl. Microbiol.*, **17**, 830–835 (Table 3).

184 Corveleyn, S. and Remon, J.P. (1999) Stability of freeze-dried tablets at different relative humidities. *Drug Dev. Ind. Pharm.*, **25**, 1005–1013.